

**Assembling nanostructured connections in  
bio-electrochemical systems**

Sindhu Krishna Suravaram

Doctor of Philosophy

University of York

Chemistry

September 2016

## **Abstract**

Microbial fuel cells (MFCs) have been used in a variety of applications to date, however the power output of an MFC is its biggest limitation. The power output of an MFC can be improved by improving the electron transfer from the bacteria to the electrode. This project was interested in improving the electron transfer using gold nanoparticles.

Gold nanoparticles were incorporated in MAgarose which showed good conductive properties and when used in a bio-electrochemical cell with *Shewanella oneidensis* MR-1 as the bacteria, a current enhancement of  $\sim 29$  times was recorded when compared to plain veil. Gold macrostructures were also electrodeposited in thiolated agarose gels and used as electrodes in the bio-electrochemical cell, but the current enhancement was not very significant compared to the control and reached a saturation point over time.

Thiol group functionalised PAMAM dendrimer-protected gold nanoparticles, were attached to So surface and used as the biocatalysts in a bio-electrochemical cell. The current recorded was lower than the control. This was attributed to a weak biofilm formation on the electrode because of gold nanoparticle attachment.

The data obtained in this thesis suggests GelAuNP to be the most promising way forward of achieving a high power output from an MFC.

## Table of contents

Abstract.....	2
Table of contents .....	3
List of figures.....	10
List of tables.....	19
List of schemes .....	21
List of accompanying materials .....	23
Acknowledgements .....	24
Declaration.....	26
Chapter 1: Introduction .....	27
1 Introduction .....	28
1.1 Bio-electrochemical fuel cells.....	28
1.2 Applications of MFCs .....	30
1.3 Limitations of MFC's .....	31
1.3.1 Configuration and operational conditions .....	31
1.3.2 Electrode material .....	31
1.3.3 Choice of bacteria.....	32
1.3.4 Electron transfer.....	32
1.3.5 Other limitations .....	32
1.3.5.1 Thermodynamic factors.....	32
1.3.5.2 Mass transport.....	34
1.4 Bacterial metabolic pathways.....	35
1.4.1 Krebs cycle .....	35
1.4.2 Electron transfer from the bacterial cell membrane to the anode.....	38
1.4.2.1 Indirect electron transfer .....	38
1.4.2.2 Direct electron transfer.....	40
1.5 Improving current generation .....	43

1.5.1	Biofilm formation and stages.....	43
1.5.2	Electrode modification.....	44
1.5.3	Gold nanoparticles.....	51
1.5.3.1	Gold nanoparticle synthesis.....	51
1.5.3.2	Gold nanoparticle stabilisation.....	52
1.5.3.3	Gold nanoparticle characterisation.....	52
1.5.4	Biom mineralisation.....	53
1.6	Aims of the project.....	55
Chapter 2: Gold nanoparticles in hydrogels.....		56
2	Introduction.....	57
2.1	Hydrogels.....	57
2.1.1	Hydrogel composites.....	58
2.2	Chapter aims and content.....	59
2.3	Results and Discussion.....	59
2.3.1	Gold nanoparticle incorporation in agarose.....	59
2.3.1.1	Conductivity testing of agarose gels with gold nanoparticles.....	62
2.4	Modification of agarose (M Agarose).....	64
2.5	Characterisation of M Agarose.....	66
2.5.1	Elemental analysis.....	66
2.5.2	FTIR Spectroscopy.....	67
2.5.3	NMR spectroscopy.....	69
2.5.4	Fluorometric assay.....	70
2.5.5	T <sub>gel</sub> values.....	74
2.5.6	Viscometry.....	74
2.5.7	Control experiments.....	79
2.5.7.1	Agarose hydrolysis.....	80
2.5.7.2	Control experiments with ammonium chloride.....	80



2.6	Gold nanoparticle incorporation.....	82
2.6.1	Gold quantification .....	86
2.7	Toxicity of gold nanoparticles to <i>Shewanella oneidensis</i> MR-1 (So).....	87
2.8	Design of electrochemical set up .....	90
2.8.1	Electrode preparation .....	92
2.8.2	Preparation of bacterial culture for electrochemical set up.....	92
2.8.3	Chronoamperometric results .....	93
2.8.3.1	Chronoamperometric data .....	94
2.9	Confocal imaging of GelAuNP.....	99
2.10	Conclusions and future work.....	100
Chapter 3: Gold nanowires in hydrogels.....		102
3	Introduction.....	103
3.1	Synthesis of gold nanowires in gels.....	103
3.2	Proposed idea.....	107
3.3	Synthesis of gold nanowires in agarose .....	107
3.3.1	Synthesis of gold nanowires in hexane.....	109
3.3.2	Incorporation of nanowires in agarose gels .....	111
3.3.2.1	Conductivity testing of GelAuNW.....	115
3.3.3	Gold nanowires in thiolated agarose gels.....	119
3.3.3.1	Gold nanowire incorporation into thiolated agarose.....	121
3.4	Electrodeposition of gold nanowires in agarose gels .....	122
3.4.1	Gold nanowires in gels .....	122
3.4.2	Gold nanowires in agarose and thiolated gel .....	123
3.4.3	Gold quantification .....	127
3.4.4	Electrochemical studies.....	129
3.5	Summary and conclusions.....	132
Chapter 4: Gold nanoparticle - decorated So.....		133

4	Introduction .....	134
4.1	Interaction of gold nanoparticles with bacteria.....	134
4.1.1	Cell structures of bacteria.....	134
4.1.2	Biosynthesis of inorganic nanoparticles .....	135
4.1.3	Pre-synthesised nanoparticles.....	137
4.1.3.1	Gold nanoparticles interaction with Gram positive bacteria .....	137
4.1.3.2	Gold nanoparticles interaction with Gram negative bacteria ....	139
4.1.4	Aims of the chapter.....	142
4.2	Results and discussion.....	142
4.2.1	Synthesis of PAMAM G4 (NH <sub>2</sub> / SH) protected gold nanoparticles (DenAuNPs) .....	143
4.2.2	Characterisation of DenAuNPs.....	144
4.2.3	Incorporation of DenAuNPs into So.....	146
4.2.3.1	First method of incorporation of DenAuNPs to <i>S. oneidensis</i> ....	147
4.2.3.2	Second method of incorporation of DenAuNPs to <i>S. oneidensis</i>	151
4.3	Citrate protected gold nanoparticles (CitAuNPs).....	153
4.3.1	Synthesis of citrate protected gold nanoparticles (CitAuNPs) .....	153
4.3.2	Characterisation of citrate protected gold nanoparticles (CitAuNPs)	153
4.3.3	Incorporation of CitAuNPs into So .....	155
4.4	Electrochemical experiments.....	156
4.4.1	Chronoamperometric results .....	157
4.5	Overall comparison of electrochemical data.....	160
4.6	Summary and conclusions.....	161
	Chapter 5: Summary, conclusions and future work.....	162
5	Summary, conclusions and future work .....	163
	Chapter 6: Experimental part.....	165

6	Experimental part.....	166
6.1	Materials and methods used for synthesis and characterisation.....	166
6.2	Gold nanoparticle incorporation <sup>300-302</sup> .....	167
6.3	Synthesis of MAgarose [1] <sup>310-312</sup> .....	168
6.4	Fluorometric assay <sup>319,320</sup> .....	169
6.4.1	Calibration with ethanolamine .....	169
6.4.2	Assay with agarose and MAgarose .....	169
6.5	T <sub>gel</sub> measurements .....	170
6.6	Viscometry <sup>328,329</sup> .....	170
6.6.1	Viscosity average molecular weight determination .....	170
6.6.2	Control experiments .....	171
6.7	Control experiments .....	171
6.7.1	Agarose hydrolysis .....	171
6.7.2	Agarose with ammonium chloride and known amount of water.....	172
6.8	ICP-MS sample preparation .....	172
6.9	XPS sample preparation .....	173
6.10	Bacterial work <sup>80,99,101</sup> .....	173
6.10.1	Stock solutions.....	173
6.10.2	LB Broth.....	174
6.10.3	LB Agar .....	174
6.10.4	Agar plate with So.....	175
6.10.5	Liquid culture of So .....	175
6.10.6	Glycerol stock of So .....	175
6.10.7	Minimal media .....	175
6.10.8	Toxicity study of So with gold nanoparticles .....	176
6.11	Electrochemical experiments with So .....	176
6.11.1	Reference electrode .....	176

6.11.2	Preparation of working electrode .....	177
6.11.3	Counter electrode .....	177
6.11.4	Preparation of culture for electrochemical experiment .....	177
6.11.5	Preparing the electrochemical set up .....	177
6.12	Electrodeposition experiment to produce Auveil .....	178
6.13	Gold nanowires and ribbons incorporated in agarose gel <sup>387</sup> .....	178
6.14	Gold nanowires in hexane solution <sup>204</sup> .....	178
6.15	Synthesis of thiol functionalised agarose [2] <sup>394</sup> .....	179
6.16	Electrodeposition of gold macrostructures .....	179
6.16.1	Preparation of working electrode .....	179
6.17	Electrochemical experiment with So .....	180
6.18	Synthesis of 3-mercaptopropanoyl hydroxysuccinimide ester[3] <sup>419</sup> ..	180
6.19	Synthesis of PAMAM G4 (NH <sub>2</sub> /SH)[4] <sup>420</sup> .....	181
6.20	Synthesis of PAMAM-(NH <sub>2</sub> /SH) protected AuNP [DenAuNP] .....	181
6.21	Citrate protected gold nanoparticles [CitAuNP] <sup>180</sup> .....	182
6.22	Attachment of gold nanoparticles to So .....	182
6.22.1	First method .....	182
6.22.2	Second method .....	182
6.23	Electrochemical experimental set up .....	182
Appendices .....		183
Appendix 1 : Chapter 2 - GelAuNP .....		183
1.1	Removal of ionic species from gels using water .....	183
1.2	Conductivity data for all the gels .....	184
1.3	Electrochemical data .....	185
1.4	Fluorometric data .....	186
1.5	Viscosity data .....	187
1.7	HR-TEM images .....	189

1.7.1 Agarose with gold nanoparticles.....	189
1.7.2 MAgarose with gold nanoparticles.....	189
1.7.3 Image J processing of HR-TEM images.....	190
1.8 XPS spectra.....	190
1.9 SEM images.....	191
1.9.1 Agarose.....	191
1.9.2 MAgarose.....	191
1.10 Confocal data for long term GelAuNP with So.....	192
Appendix 2 : Chapter 3 – GelAuNW.....	193
2.1 TEM images.....	193
2.1.2 Aspartic acid and agarose nanoribbons.....	193
2.1.3 Gold nanowires in hexane.....	193
2.1.4 Gold nanowires in hexane gel.....	193
2.2 Conductivity data for all the gels.....	194
2.3 SEM images.....	194
Appendix 3 : Chapter 4 – DenAuNPs.....	196
3.1 HR-TEM images.....	196
3.1.1 First method of incorporation.....	196
3.1.2 Second method of incorporation.....	196
3.2 SEM images.....	197
3.2.1 So in media.....	197
3.2.2 So with DenAuNPs.....	197
3.3 Overall comparison of electrodes.....	198
Abbreviations.....	199
References.....	202

## List of figures

Figure 1-1: World energy consumption by fuel type from 1990-2040, quoted in Btu. Taken from ref 1 .....	28
Figure 1-2: Schematic of a two chamber microbial fuel cell. Taken from ref <sup>17</sup> .....	29
Figure 1-3: Sediment microbial fuel cell. Taken from ref <sup>43</sup> .....	30
Figure 1-4: Schematic showing the energy flux in a MFC with key points of loss. Taken from ref <sup>94</sup> .....	33
Figure 1-5: Generalised structure of bacterial cell. Adapted from ref <sup>99</sup> .....	35
Figure 1-6: Citric acid cycle in bacteria. Adapted from ref <sup>103,106</sup> .....	36
Figure 1-7: Schematic of bacterial respiration membrane process. The number of electron chain components varies with bacterial species. Taken from ref <sup>103</sup> .....	37
Figure 1-8: Schematic showing the mediated electron transfer using secondary metabolites. Two mechanisms were proposed shuttling via outer cell membrane cytochromes (red circle) and via periplasmatic or cytoplasmatic redox couples. Taken from ref <sup>95</sup> .....	39
Figure 1-9: Schematic illustration of mediated electron transfer by primary metabolite mediators. (a) via reduced terminal electron acceptors produced during anaerobic respiration, (b) oxidation of reduced fermentation products (formate and hydrogen). Taken from ref <sup>95</sup> .....	40
Figure 1-10: Schematic showing the various direct electron transfer routes. (a) Membrane bound cytochromes and (b) electronically conductive nanowires such as pili. Taken from ref <sup>95</sup> .....	41
Figure 1-11: SEM image showing a highly connected biofilm of <i>Shewanella oneidensis</i> MR-1. Taken from ref <sup>118</sup> .....	41
Figure 1-12: SEM images of bacteria (a) <i>Shewanella oneidensis</i> MR-1 and (b) <i>Pelotomaculum thermopropionicum</i> and <i>Methanothermobacter thermautotrophicus</i> , scale bar ×20k with pili or 'nanowires'. Taken from ref <sup>118</sup> ..	42
Figure 1-13: Schematic showing the 4 stages of biofilm formation, grey rectangles represent bacteria, pink halo represent the EPS and the horizontal pink squares represent human skin cells. Taken from ref <sup>121</sup> .....	43
Figure 1-14: An overview of impact of material surfaces (chemistry and topography) on the electrode characteristics and microbial electrocatalysis in bio-electrochemical systems. 2-D/3-D: two/three-dimensional; DET: direct electron	

transfer; IET: indirect electron transfer;  $k^0_{IET}$  : heterogeneous ET rate constant for abiotic reaction; PSA: projected surface area [it is the largest two-dimensional area obtained from the projection of a planar surface or a 3-D material; estimated with respect to the plane covering X and Y axes of the material]; SSA: specific surface area [it is the total surface area of electrode per unit of projected surface area or electrode volume (for 3-D architecture; often BET measurements are considered to estimate SSA)]; ESA: electroactive surface area [it is the actual surface available for electrochemical reactions (i.e. solvated, electrically connected area); cyclic voltammetry for capacitance measurement can be used to estimate ESA]. Taken from ref<sup>111</sup> ..... 44

Figure 1-15: CNT/RVC before incorporation in MFC (left) and (right) after incorporation with reddish colour showing the growth of biofilm. Adapted from ref<sup>127</sup> ..... 46

Figure 1-16: Schematic of proposed extracellular electron transfer pathway in *Shewanella oneidensis* MR-1 where ES denotes the extracellular space, P denotes the periplasm, and C denotes the cytoplasm. The silver and black spheres represent extracellular iron oxide. Taken from ref<sup>128</sup> ..... 47

Figure 1-17: Current vs Time plot of GCE (dashed line) and CNT/GCE (solid black line) as an anode in MFC with *S. oneidensis* as the bacterium run for 15 h. Taken from ref<sup>133</sup> ..... 47

Figure 1-18: Photographic images of a) the GO–agarose gel, b) GO– agarose foam and c) GCF ..... 48

Figure 1-19: UV-Vis spectrum showing the dependence of surface plasmon resonance on gold nanoparticle shape. Taken from ref<sup>194</sup> ..... 52

Figure 1-20: Gold cluster produced by *Pedomicrobium* ..... 53

Figure 1-21: TEM image of *Shewanella* algae cell covered by gold nanoparticles. Taken from ref<sup>264</sup> ..... 54

Figure 2-1: UV-Vis spectrum of agarose with (red) and without (black) gold nanoparticles ..... 61

Figure 2-2: HR-TEM images of agarose gels with gold nanoparticles. Scale bar 100 nm (left) and 5  $\mu$ m (right). The left image shows just gold nanoparticles agglomerating together to form an aggregated structure, the right image shows a gel

cube in various shades of grey with the black spots representing gold nanoparticles. .....	62
Figure 2-3: (a) Leaching of excess gold solution during gold nanoparticles incorporation into MAgarose (b) The resultant GelAuNP after leaching .....	65
Figure 2-4: FTIR spectrum of agarose and MAgarose with normalised transmittance on the y axis .....	68
Figure 2-5: Overlaid <sup>1</sup> H spectra of agarose (red) and MAgarose (blue) in d <sup>6</sup> -DMSO .....	69
Figure 2-6: Fluorescence spectrum of ethanolamine at a concentration of 0.03 mM on reaction with fluorescamine .....	71
Figure 2-7: Calibration graph of fluorescence vs concentration of ethanolamine normalised to solvent .....	71
Figure 2-8: Fluorescence spectrum of MAgarose (red) and agarose (black).....	72
Figure 2-9: Inherent viscosity vs concentration plot of agarose .....	77
Figure 2-10: Inherent viscosity vs concentration plot for MAgarose .....	78
Figure 2-11: Conductivity vs viscosity plot of control experiments with ammonium chloride using values from Table 2-13.....	81
Figure 2-12: Viscosity vs % (v/v) water added (refers to ammonium chloride experiments with known amount of water added) plot for ammonium chloride experiments.....	82
Figure 2-13: Gel obtained after reduction showing two distinct coloured bands. ..	83
Figure 2-14: HR-TEM images of purple coloured gel, scale bar 200 nm and pink coloured gel, scale bar 500 nm.....	83
Figure 2-15: Histograms showing the size distribution of gold nanoparticles in purple gel (top) and pink gel (bottom) .....	84
Figure 2-16: SEM images of agarose and MAgarose at 75k magnification with a scale bar of 100 nm in both cases .....	84
Figure 2-17: SEM image showing the line function used to calculate the width of fibres and pore sizes (left) and histogram showing the distribution in both agarose and MAgarose. ....	85
Figure 2-18: SEM images of GelAuNP, the left image was recorded under LBE and the right image was recorded under LEI. In both cases the bright spots are gold nanoparticles while the grey background is the gel network.....	85



Figure 2-19: XPS spectra of the surface of the GelAuNP .....	86
Figure 2-20: Schematic showing the incorporation of gold nanoparticles into agarose gel cylinders.....	88
Figure 2-21: Agar plate with wells to incorporate agarose gel cylinders with different gold nanoparticle concentration.....	89
Figure 2-22: Confocal images of 1 (4.2 $\mu\text{g}$ ) and 2 (8.4 $\mu\text{g}$ ) gel cylinders with different gold concentrations in brackets.....	89
Figure 2-23: Confocal imaging of gel cubes with higher gold concentrations 10 (42 $\mu\text{g}$ ) and 20 (84 $\mu\text{g}$ ).....	90
Figure 2-24: Bar chart showing the distribution of live and dead bacteria at increasing gold quantities .....	90
Figure 2-25: Schematic of carbon veil modified with MAgarose containing gold nanoparticles.....	92
Figure 2-26: Cyclic voltammogram of Ferrocene in acetonitrile with tetrabutylammonium hexafluoro phosphate (0.1 M) as supporting electrolyte.....	93
Figure 2-27: Current vs Time plot of all the controls and GelAuNP in the absence of So .....	94
Figure 2-28: Current vs time graph of Au <sup>0</sup> electrodeposition.....	95
Figure 2-29: Current vs time plot of all the controls and GelAuNP with So .....	96
Figure 2-30: 5-day experiment of GelAuNP with So .....	97
Figure 2-31: Current vs time plot of Auveil run for 5 days in the presence of So ....	98
Figure 2-32: Bar chart showing the combination of all electrochemical results.....	99
Figure 2-33: Confocal images of both carbon veil and gel surface. The top left shows live So, top right shows white field image, bottom left shows dead bacteria and bottom right shows the mixture of all three.....	100
Figure 2-34: Bar chart of number live and dead bacteria present on conductive gel .....	100
Figure 3-1: Schematic showing the incorporation of silver nanowires in agarose solution (A) and their alignment using a four electrode custom set up (B). Adapted from ref <sup>382</sup> .....	105
Figure 3-2: TEM images of microwire formation in agarose gels at 0.5% w/v with (A) 50 nm, scale bar 200 $\mu\text{m}$ (B) 100 nm, scale bar 1 mm and (C) 200 nm, scale bar 100 $\mu\text{m}$ . Adapted from ref <sup>382</sup> .....	106

Figure 3-3: UV-Vis spectrum of gold nanoribbons in agarose using aspartic acid	108
Figure 3-4: HR-TEM images of gold nanoribbons in agarose gels.....	109
Figure 3-5: UV-Vis spectrum of gold nanowires in hexane.....	110
Figure 3-6: HR-TEM image of gold nanowires in hexane. Scale bar 200 and 50 nm respectively.....	110
Figure 3-7: SEM images of (A) Agarose in water, scale bar 100 nm in both cases. (B) Agarose in hexane, scale bar 1 $\mu$ m (left) and 100 nm (right).....	112
Figure 3-8: HR-TEM images of wires in gels (GelAuNW). Scale bar 100 nm in both cases.....	113
Figure 3-9: HR-TEM images of GelAuNW in ethyl acetate (left) and the opaque area of GelAuNW in water (right). Scale bar 100 and 50 nm respectively. ....	114
Figure 3-10: TEM images of the dark band in GelAuNW in acetone (left) and water (right). Scale bar 200 nm in both cases.....	114
Figure 3-11: Schematic showing the milder solvent replacement procedure in GelAuNW in hexane.....	115
Figure 3-12: HR-TEM images of red band in GelAuNW on solvent replacement to ethanol using a milder solvent replacement procedure. Scale bar 50 and 100 nm respectively.....	115
Figure 3-13: The specially designed and arranged equipment for conductivity measurement and its dimensions. The inset is the area of the graphite block that is in contact with the gel mold.....	116
Figure 3-14: FTIR spectrum of thiolated agarose (blue) and agarose (black) .....	120
Figure 3-15: HR-TEM image of gold nanoparticles in thiolated gel with gold nanowires in ethanol. Scale bar 50 nm.....	122
Figure 3-16: Current vs time graph of electrodeposition in agarose and thiol gel at 0.5% w/v concentration.....	125
Figure 3-17: Figures showing gold macrostructures growing inside agarose thiolated gel outwards from the working electrode carbon veil .....	126
Figure 3-18: Images of carbon veil before (left) and after (middle) the electrochemical experiment. Far right image shows the middle image at low magnification .....	126
Figure 3-19: HR-TEM images of the gold macrostructures formed during electrodeposition inside agarose and thiolated gel at 0.5% w/v concentration.	

(A)Shows a dendritic morphology, scale bar 500 nm (B) Shows a grey gel structure covered by black dots indicating gold nanoparticles, scale bar 500 nm (C) Shows a trunk like nanostructure formed inside the gel, scale bar 200 nm.....	127
Figure 3-20:: An image of the calculation of area under the curve using origin and the calculated area is highlighted in grey and the value is provided on the right hand side .....	128
Figure 3-21: Current vs time graph of electrodeposited gel used as the working electrode in an electrochemical experiment .....	131
Figure 4-1: Cell structures of Gram negative and Gram positive bacteria. Adapted from ref <sup>404</sup> .....	134
Figure 4-2: Images showing the difference in cell wall nature of Gram negative(left) and Gram positive (right) bacteria. Taken from ref <sup>405</sup> .....	135
Figure 4-3: Biosynthesised gold nanoparticles by wild type So (e) and mutant So (f). The black spots around the grey oval represent gold nanoparticles. Taken from ref <sup>236</sup> .....	136
Figure 4-4: Cyclic voltammograms for(a) (1) Au-free wild-type coated on a GC electrode; Au synthesised-wild type coated onto a GC electrode in the (2) absence and (3) presence of lactate. (b) (1) Au-free mutant So and (2) Au synthesised-mutant So coated on a GC electrode. Taken from ref <sup>236</sup> .....	136
Figure 4-5: CTAB protected gold nanorods and gold nanoparticles (right) deposited on Bacillus cereus. Scale bars are 1µm, adapted from ref <sup>411</sup> .....	138
Figure 4-6: End on end assembly of bacteria and coating by gold nanospheres (lighter spots on grey background) of the bacteria. Scale bar 1 µm, adapted from ref <sup>408</sup> .....	138
Figure 4-7: Ligand structure of NP 1 and NP 2 .....	139
Figure 4-8: (Left) Aggregation and clustering of NP 1 (6nm) on surface of B. subtilis after 30 min incubation time (right) Aggregation of NP 1 (6nm) on the surface of E. Coli after 30 min incubation time. Scale bar 200 nm, adapted from ref <sup>412</sup> .....	139
Figure 4-9: B. Subtilis (left) lysed on exposure to NP 2, scale bar 200 nm. E. Coli (right) showing blebbing formation on exposure to NP 2, scale bar 50 nm. Adapted from ref <sup>412</sup> .....	140
Figure 4-10: Schematic of the idea in literature. Adapted from ref <sup>413</sup> .....	141

Figure 4-11: TEM images of MPNH <sub>2</sub> -AuNPs (e) and PAH-AuNPs (f) with So. Taken from ref <sup>413</sup> .....	142
Figure 4-12: PAMAM G2 dendrimer schematic. Each grey circle represents a nitrogen atom .....	143
Figure 4-13: UV-Vis spectrum of DenAuNPs in water .....	145
Figure 4-14: Zeta potential distribution graph of PAMAM G4 (NH <sub>2</sub> /SH) protected gold nanoparticle.....	145
Figure 4-15: HR-TEM images of DenAuNPs. Scale bar 10 and 2 nm respectively	146
Figure 4-16: HistoGram showing the size distribution of DenAuNPs.....	146
Figure 4-17: TEM images of gold nanoparticles in LB broth (left) and PBS (right). Scale bar 50 nm respectively .....	147
Figure 4-18: Images of the pellets formed from overnight cultures grown with DenAuNPs (left) and without (right) .....	148
Figure 4-19: HR-TEM imaging of So grown with DenAuNPs (left) and without (right). Scale bar 200 and 500 nm respectively.....	148
Figure 4-20: TEM imaging of So grown with DenAuNPs, showing the concentrated regions of nanoparticles forming nodes on surface of bacteria. Scale bar 200 nm in both cases.....	149
Figure 4-21: TEM images at a slightly higher gold nanoparticle concentration and their attachment to <i>S. oneidensis</i> MR-1. Scale bar 200 nm in both cases. ....	150
Figure 4-22: Proposed structural model for So nanowires. Showing that the nanowires are outer membrane (OM) and periplasmic (PP) extensions including the multiheme cytochromes responsible for extracellular electron transport. Taken from ref <sup>131</sup> .....	150
Figure 4-23: TEM images of So cells on addition of DenAuNPs after growth. Scale bar 500nm and 1 μm respectively.....	151
Figure 4-24: HR-TEM images of So with DenAuNPs added after growth and incubated for 1 h.....	152
Figure 4-25: HR-TEM imaging of So with DenAuNPs added after growth and incubated for 4 h.....	152
Figure 4-26: UV-Vis spectrum of CitAuNPs .....	154
Figure 4-27: HR-TEM images of CitAuNPs. Scale bar 50 nm in both cases.....	154
Figure 4-28: HistoGram showing the size distribution of CitAuNPs .....	155

Figure 4-29: Zeta potential graph of citrate protected gold nanoparticles .....	155
Figure 4-30: HR-TEM images of So grown in the presence of CitAuNP .....	156
Figure 4-31: Time vs Current density graph of DenAuNPs attached So. The run numbers (red and blue) indicate the number of repeats, control run (black) is with no DenAuNPs. New (pink) indicates the experiment with recently synthesised DenAuNPs.....	157
Figure 4-32: Analysis of carbon veil after chronoamperometric measurement with DenAuNPs attached to So. Scale bar 1 $\mu\text{m}$ respectively. The pillars are the carbon veil fibers. Control with no DenAuNPs (left) and with DenAuNPs (right), the bright/white spots on the right image indicate DenAuNPs on So. White arrows indicate nanowires. recorded in LABE (Low angle back scattered electron images) mode.....	158
Figure 4-33: SEM image with inset showing the nanowires of So recorded in LABE (Low angle back scattered electron images) mode with DenAuNPs.....	159
Figure 4-34: SEM images of So with DenAuNPs (left) and without(right), these were recorded in SEI (secondary electron imaging) mode where DenAuNPs were not observed.....	159
Figure 4-35: Bar chart comparing the different electrodes in this project.....	160
Figure 6-1: Current vs time plots of plain veil (left) and plain gel (right) no So ...	185
Figure 6-2: Current vs time plots of Auveil (left) and GelAuNP (right) no So .....	185
Figure 6-3: Current vs time plot of plain veil (left) and plain gel (right) with So .	186
Figure 6-4: Current vs time plot of Auveil (left) and GelAuNP (right) with So .....	186
Figure 6-5: Current vs time plot of electrodeposition of gold on plain veil.....	186
Figure 6-6: Fluorescence spectrum showing the fluorescence at different amine concentrations.....	187
Figure 6-7:HR-TEM images of agarose with gold nanoparticles. Scale bar 100 and 200 nm.....	189
Figure 6-8: HR-TEM image of bottom of GelAuNP. Scale bar 2 $\mu\text{m}$ and 200 nm. ...	189
Figure 6-9: HR-TEM images of top of GelAuNP. the right image has been stained with uranyl acetate to identify gel fibres. Scale bar 100 and 200 nm .....	189
Figure 6-10: Image J processing of counting particles automatically. (left) Original HR-TEM image, (right) Processed image by Image J .....	190
Figure 6-11: An overlay of all the XPS spectra of GelAuNP.....	190

Figure 6-12: SEM images of agarose .....	191
Figure 6-13: SEM images of MAgarose.....	191
Figure 6-14: Bar chart of live and dead bacteria for the long term chronoamperometric experiment with GelAuNP .....	192
Figure 6-15: TEM images of nanoribbons in agarose.....	193
Figure 6-16: HR-TEM images of gold nanowires in hexane. Scale bars 50 and 100nm .....	193
Figure 6-17: HR-TEM images of gold nanowires in hexane gel. Scale bars 100nm respectively.....	194
Figure 6-18: SEM images of agarose in hexane .....	195
Figure 6-19: HR-TEM images of DenAuNPs attached to So. Scale bars 10 $\mu$ m and 500 nm.....	196
Figure 6-20: HR-TEM images of DenAuNPs attached to So after growth. Scale bar 1 $\mu$ m .....	196
Figure 6-21: SEM images of So on carbon veil in media, no DenAuNPs.....	197
Figure 6-22: SEM images of DenAuNPs attached to So on carbon veil in media ...	197

## List of tables

Table 1-1: Standard reduction potentials at pH 7, 25 °C, vs. ENH of some electron transport chain molecules. Electrons may leave the system at a number of places in the electron transport chain .....	37
Table 1-2: Standard reduction potentials of electron donors and acceptors measured at pH 7 vs SHE. Taken from ref <sup>107</sup> .....	38
Table 1-3: Standard reduction potentials of endogenous secondary metabolite mediators. Taken from ref <sup>95</sup> .....	40
Table 1-4: Standard reduction potentials of DET for some bacterial strains .....	42
Table 1-5: Anode modifications to achieve high electroactive area and surface area for better biofilm formation .....	49
Table 1-6: Anode modifications by nanoparticles and their enhancements, the rows highlighted in grey represent modifications where the particles were added into the culture rather than attached to the anode.....	50
Table 2-1: Conductivity values for agarose only and agarose with gold nanoparticles .....	64
Table 2-2: Conductivity values of the gels with gold nanoparticles .....	66
Table 2-3: CHN results for agarose and aminated agarose compared to expected values. Calc – refers to expected values, Obs – refers to observed values. ....	67
Table 2-4: Table showing how the % CH can be used to calculate presence of water in agarose .....	67
Table 2-5: IR stretches of agarose and MAgarose.....	68
Table 2-6: Fluorescence values for Agarose and MAgarose .....	72
Table 2-7: The % of Nitrogen in agarose and MAgarose by fluorometric assay.....	73
Table 2-8: T <sub>gel</sub> values of agarose and MAgarose.....	74
Table 2-9: Viscosity values of agarose at different concentrations, same shear rate .....	76
Table 2-10: Intrinsic viscosity and viscosity average molecular weight of agarose	77
Table 2-11: Viscosity values of MAgarose at different concentrations, same shear rate .....	78
Table 2-12: Intrinsic viscosity and viscosity average molecular weight of agarose and MAgarose .....	79
Table 2-13: Viscosity and conductivity values for control experiments.....	81

Table 2-14: Gold content in agarose loaded with gold nanoparticles and GelAuNP by ICP-MS.....	87
Table 2-15: Modification of electrodes from literature.....	97
Table 3-1: Resistance values measured using four electrode custom set up of different diameter silver nanowires in agarose at 0.5% w/v.....	106
Table 3-2: Conductivity measurements of controls and GelAuNW in hexane and in water .....	118
Table 3-3: Showing the expected (exp) and observed (Obs) values of elemental analysis for agarose and thiolated agarose .....	120
Table 3-4: $T_{gel}$ values of agarose and thiolated agarose .....	121
Table 3-5: Conductivity data for gold nano and macro structures electrodeposited in agarose and thiolated gel at 0.5% w/v concentration.....	129
Table 4-1: Zeta potential measurements of the different charged gold nanoparticles. Adapted from ref <sup>413</sup> .....	141
Table 6-1: Volumes and concentrations used for calibration of amine to fluorescence .....	169
Table 6-2: Quantities used for fluorometric assay of gels .....	170
Table 6-3: The weights and volumes used for $T_{gel}$ recording.....	170
Table 6-4: Weights and volumes of agarose and MAgarose used for viscosity measurements .....	170
Table 6-5: Table detailing the reagents and quantities used for control experiments .....	172
Table 6-6: Detailing the quantities and reagents used to make stock solutions ...	173
Table 6-7: Conductivity values of brine gels with consecutive water washing .....	183
Table 6-8: Concentration of amine and the respective fluorescence values at 475 nm used for calibration plot.....	187
Table 6-9: Viscosity data for agarose at various concentrations.....	187
Table 6-10: Viscosity data for MAgarose at various concentrations.....	188
Table 6-11: Conductivity values for all the gels.....	194
Table 6-12: The average current generated at 27 h for all electrodes with So .....	198



## List of schemes

Scheme 2-1: Illustrating the purpose of hydrogel with gold nanoparticles, to form a conductive bridge between So and an electrode. ....	57
Scheme 2-2: Schematic of gold nanoparticle incorporation into agarose gel at 2.89 % w/v concentration .....	61
Scheme 2-3: Custom made design of equipment and its dimensions used to measure resistance of agarose gels with gold nanoparticles.....	63
Scheme 2-4: Synthesis of aminated agarose .....	65
Scheme 2-5: Reaction of fluorescamine with primary amines .....	70
Scheme 2-6: Schematic showing the control experiment to hydrolyse agarose .....	80
Scheme 2-7: Schematic of the control reaction with ammonium chloride and known amount of water.....	80
Scheme 2-8: Schematic showing the custom made 'bottomless sample vial'. The orange band represents the heat shrink tubing; the grey band represents the agarose gel cylinder.....	88
Scheme 2-9: Schematic of the three electrode electrochemical design used to record chronoamperometric data .....	91
Scheme 2-10: Ferrocene couple studied as a standard .....	93
Scheme 3-1: Schematic showing the procedure for the in situ incorporation of gold nanoribbons and nanowires in agarose gel at 0.2% w/v concentration.....	108
Scheme 3-2: Schematic showing the synthesis of gold nanowires in hexane. Adapted from ref <sup>204</sup> .....	109
Scheme 3-3: Schematic showing the custom made 'bottomless sample vial'. The orange band represents the heat shrink tubing; the grey band represents the agarose gel cube.....	1110
Scheme 3-4: Incorporation of nanowires in hexane solution from section 3.3.1 into agarose gels .....	111
Scheme 3-5: Schematic of gold nanowire incorporation in agarose gel with hexane .....	112
Scheme 3-6: Schematic showing the solvent replacement in GelAuNW in hexane. ....	113
Scheme 3-7: (A) Schematic showing the position of the gel cylinder in respect to the graphite blocks, (B) Dimensions of the gel cube (C) Dimensions of the gel cylinder in	

contact with the graphite block (D) Area of the yellow sector is removed from the area of the blue triangle to get the area of the gel in contact (segment) with the graphite block .....	117
Scheme 3-8: Schematic showing the parts of GelAuNW in water that were analysed for conductivity .....	118
Scheme 3-9: Functionalisation of agarose with thiol groups .....	119
Scheme 3-10: Schematic of three electrodes electrochemical design used to electrodeposit gold nanowires in agarose gel network .....	123
Scheme 3-11: Schematic of the three electrode electrochemical design used to record chronoamperometric data .....	130
Scheme 4-1: Synthesis of N-hydroxysuccinimide ester.....	144
Scheme 4-2: Synthesis of thiolated PAMAM G4 (NH <sub>2</sub> /SH) dendrimer .....	144
Scheme 4-3: Synthesis of PAMAM G4 (NH <sub>2</sub> /SH) protected gold nanoparticles.....	144

## List of accompanying materials

The compact disc is attached at the back of thesis and it contains

- A digital copy of the thesis
- An excel document of Raw data for
  - All the chronoamperometric data run with So
  - All the chronoamperometric data run in the absence of So
  - All the electrodeposition data for the preparation of Auveil
  - The single electrodeposition data for depAu (gel with gold macrostructures)
  - All the fluorometric data for fluorescamine assay
  - All the FTIR data for agarose, MAgarose and thiolated agarose

## **Acknowledgements**

This thesis would not be possible without the help and support of several people during the last four years. I wanted to acknowledge as many people as I can using this opportunity.

I would like to thank both my supervisors Dr. Victor Chechik and Prof. David Smith, the University of York and the Whiterose consortium for giving me the opportunity to undertake this PhD. Victor and Dave, thank you for being very understanding about my lack of knowledge regarding the multiple branches my PhD covers during my years in lab. Dave thank you very much for giving me the opportunity to be a co-author in a scientific paper. Victor thank you very much for being very patient with me in all aspects of my PhD, let it be research, reports, family or thesis.

I would like to say a very big thank you to my IPM Dr. Alison Parkin for being so supportive and empathetic regarding my electrochemical experiments and equipment issues. I have always looked forward to meeting you for a quick chat and have always left the meeting feeling more confident and positive about my PhD, so thank you very much. I wanted to say thank you to Lindsay and Hope from Alison parkin group for giving me guidance on how to get to grips with electrochemistry and bacterial work. Thank you Julia Walton for helping with all the bacterial work.

I would like to thank all the 3 workshops at the University of York. Thank you Chris for making me understand the basics and lending me a conductivity meter for recording my conductance data. Thank you Chris Mortimer for bringing my Graphite block electrode and PTFE design to life and making conductance measurements simple. Abby, thank you very much for all the glassware you have made for me including the bottomless sample vials, I always enjoyed our chats regarding designs or holidays. I would like to thank Heather for NMR, Graeme for CHN analysis, Emma for ICP-MS analysis.

I wanted to say a big thank you to all the people in lobe E002, you have made the journey of my PhD very enjoyable. You all have given me support throughout my PhD that has been invaluable. Thank you in particular to Danielle and Natalie (RED) for always listening to my questions on electrochemistry and helping me with my experiments. Thank you to Luisa, Dan, Tom and Ben for helping me with my thesis

writing and providing me with support whenever it was needed. I wanted to say thank you to present and past members of VC, you guys made the last four years very pleasant, I will definitely miss the pub lunches and long arguments with Yury.

A huge thank you to Andrew for helping me with Schlenk work and always being so nice about changing water in my dialysis when I was otherwise occupied. I always appreciated that you were there as a sounding board for all my stupid questions and ideas. I wanted to say thank you to Meg Stark and Anna Simon at the YSBL for their help in imaging my unusual samples. I would also like to thank Simon at Sheffield University for guiding me with my bacterial work.

And finally thank you to my Mom for giving me the perspective I needed in writing my thesis and helping me with my diagrams. A huge and special thank you to my husband, if you were not there to help me and pick me up in the past four years I would not be where I am today. I appreciate all the help and love that you have given me till now and for future. A mini thanks to my son for being very good during his stay in my tummy and allowing me to finish my thesis without any health problems.

## Declaration

I declare that this thesis is a presentation of original work and I am the sole author. This work has not previously been presented for an award at this or any other, University. All sources are acknowledged as References. The research presented in this thesis is to the best of my knowledge original and my own, except for the following

- Elemental analysis was carried out by Dr. Graeme McAllister
- TEM, SEM and confocal imaging was carried out by the Imaging and Cytometry team at YSBL, University of York
- Viscosity measurements were carried out by Lucia D'Andrea
- The 'graphite block' used for the measurement of conductivity of gold nanowires in gels has been published by B. O. Okesola, S. K. Suravaram, A. Parkin and D. K. Smith, *Angew. Chemie - Int. Ed.*, 2016, **55**, 183–187.<sup>1</sup>

# **Chapter 1: Introduction**

## 1 Introduction

The predicted energy consumption of the world by 2040 is 820 quadrillion Btu (British thermal unit) and the consumption by fuel type is shown in Figure 1-1.<sup>2,3</sup> The consumption by fuel type is also increasing, with a steeper increase in renewables, natural gas and coal than nuclear, showing a preference for abundant resources.

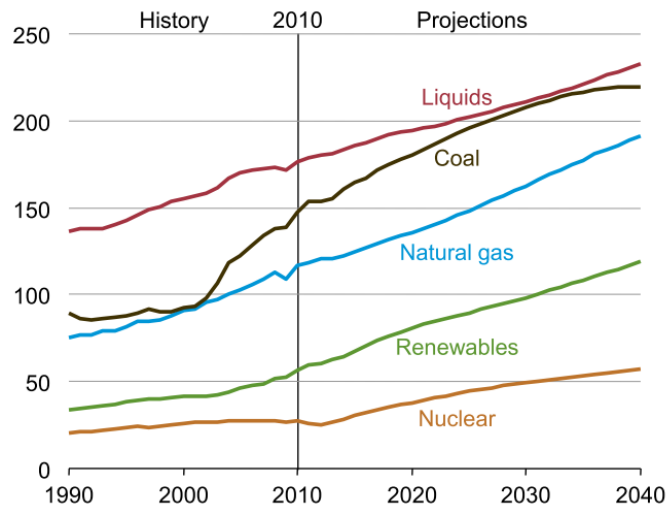


**Figure 1-1: World energy consumption by fuel type from 1990-2040, quoted in Btu. Taken from ref 1**

One of the most abundant resources is waste water, there is approximately 11 billion tonnes of waste water produced in UK per day. Waste water contains organic and human waste matter in the form of sludge, this sludge is treated anaerobically to produce bio gas to be used in combined heat and power plants to produce electricity.<sup>4</sup> Waste water treatment is energy and time intensive, an alternative to this treatment is to use microbial fuel cells to produce clean water and electricity at the same time.<sup>5</sup>

### 1.1 Bio-electrochemical fuel cells

Fuel cells convert chemical energy into electricity using a catalyst. Fuel cells utilising catalysts such as enzymes and bacteria (microbe) for converting chemical energy into electrical energy are called bio-electrochemical fuel cells.<sup>6-10</sup> A major limitation of enzymes as catalysts is that they are specific for a single reaction whereas bacteria are diverse in catalysing reactions.<sup>11-14</sup> The fuel cell with enzymes as catalyst are known as enzymatic fuel cells and fuel cells with bacteria as catalysts are known as Microbial fuel cells (MFC's), for this project only MFC's will be considered. The idea



## Chapter 1: Introduction

of MFC was first observed by Potter<sup>15</sup> where electrical energy was recorded using bacterial cultures of *Escherichia coli* and *Saccharomyces* with platinum electrodes. This was further corroborated by Cohen<sup>16</sup> when the potential of different bacterial cultures was recorded using them as electrical half cells.

MFCs in general contain an anaerobic anodic chamber, aerobic cathode chamber and a semi permeable membrane (proton exchange membrane) depending on the cell design as shown in Figure 1-2,<sup>17</sup> oxidation takes place in the anodic chamber while reduction takes place in the cathodic chamber.

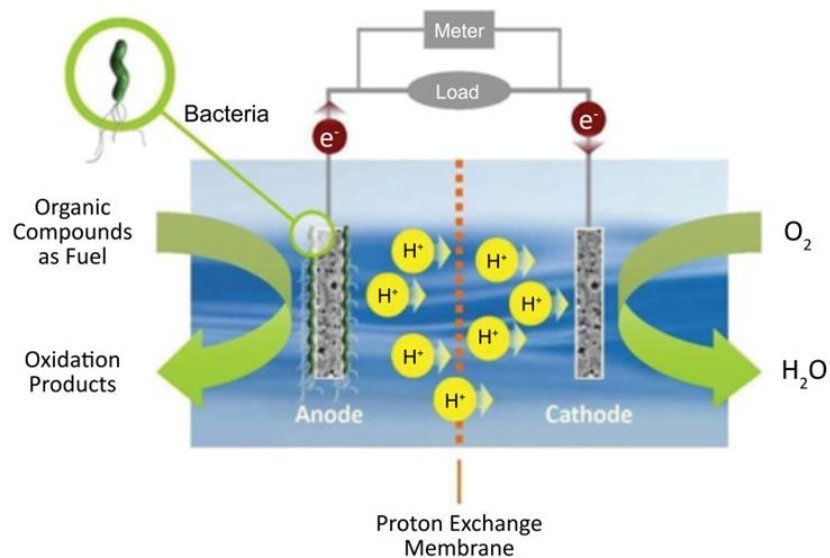


**Figure 1-2: Schematic of a two chamber microbial fuel cell. Taken from ref <sup>17</sup>**

The bacteria or enzymes present in an anodic chamber oxidise substrates such as glucose by their metabolic pathway for growth.<sup>9</sup> The electrons produced by the bacteria's metabolic pathways are transferred to the anode, by different electron transfer mechanisms dependant on the bacteria being used as the catalyst. The anodic chamber is kept anaerobic to prevent any oxygen acting as the final electron acceptor instead of the anode and the cathodic chamber is kept aerobic to facilitate reduction oxygen. The electrons flow from the positive terminal to the negative terminal via an external circuit (load or power source), whereas the protons migrate via the proton exchange membrane to form water through reduction on the cathode.<sup>18,19</sup> The presence of bacteria can be either in the anodic or the cathodic chamber dependant on the design of the MFC. If a bacterium is used at the cathode the bacterium is able to grow aerobically utilising the cathode for electrons and acting as an electron acceptor.<sup>20,21</sup>

## 1.2 Applications of MFCs

MFC's have a number of applications such as bio-sensing,<sup>22,23</sup> bioremediation,<sup>24–28</sup> metal recovery<sup>29,30</sup> and also as microbial electrolysis cells (MEC's) where an input of voltage is provided for the production of hydrogen.<sup>31–39</sup> The most important application of MFC's is in sediment microbial fuel cells (SMFC), where the sea floor contains the anode and the sea water has the cathode (Figure 1-3).<sup>40–47</sup> The Figure 1-3 shows the production of acetate from sediment organic matter fermentation and its subsequent oxidation by sediment bacteria. The oxidation of acetate leads to the production of 8 electrons that are transferred to an anode, while 8 protons migrate through the membrane to the cathode and get reduced to form water at the cathode.

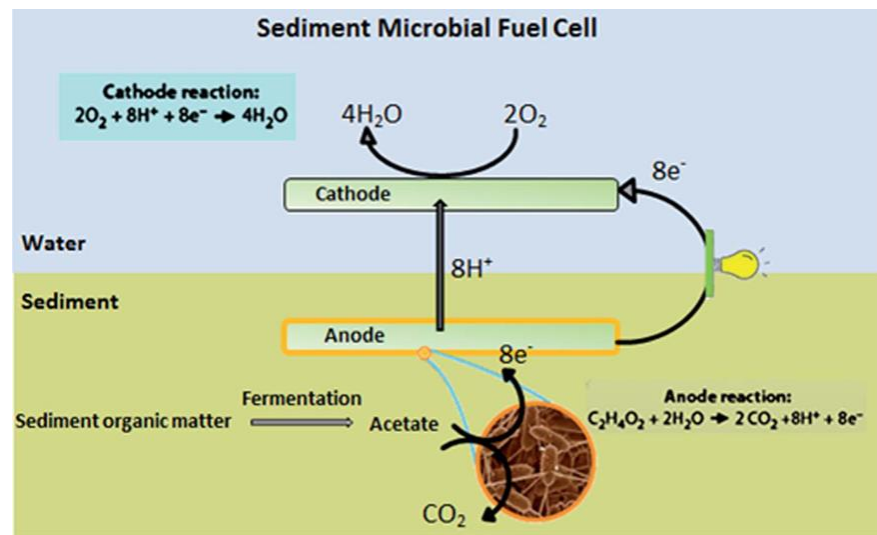


Figure 1-3: Sediment microbial fuel cell. Taken from ref <sup>43</sup>

SMFCs are the first successful examples of MFC's suitable for every day application such as the powering of a low power meteorological buoy over the long term. Tender *et al.*<sup>48</sup> have demonstrated the use of a prototype SMFC that has generated power densities of  $16 \text{ mWm}^{-2}$  (equivalent to 26 alkaline Duracell batteries per year at 298 K). The second most common application of MFCs is in waste water treatment to produce electricity and clean water.<sup>46–52</sup> The electricity generated in an MFC is dependent on the source of waste water<sup>5</sup> with the highest current density recorded at  $1000 \text{ mA}\cdot\text{m}^{-2}$  for waste water from an alcohol distillery.<sup>56</sup> Even though there are many applications of MFC's, the applicable field is quite narrow because of its low power / current generating ability. There are many limitations in a MFC and these are reviewed below.

### **1.3 Limitations of MFC's**

The performance of MFC depends on its configuration, operational conditions (pH, temperature, type of substrate and continuous or batch mode), electrode material, the bacterium used as the catalyst and electron transfer from the bacterium to the anode.<sup>57-62</sup>

#### **1.3.1 Configuration and operational conditions**

There are three different types of electrode configurations available for use two three and four electrode configurations. There are only a few examples of 4 electrode configurations, whereas predominantly three electrode configurations are used to obtain a better control on the working electrode. <sup>63</sup> The reference electrodes are usually cheap, easy to use and regenerate, such as silver / silver chloride (Ag / AgCl) or calomel electrodes.<sup>64</sup>

The choice of temperature seems to influence time scale of the MFC as it directly affects bacterial growth and in turn electron transfer. The MFC's can be run in a continuous<sup>65</sup> or batch mode depending on the configuration<sup>66</sup> such as stacked, <sup>64-68</sup> single<sup>69-74</sup> or dual chambers.<sup>49</sup> The type of substrate also influences the current generated in a MFC, the substrates that could be used are acetate, cellulose, starch, sucrose and xylose.<sup>75,76</sup> The species of bacterium used, its metabolism and pH are also important factors to consider. Bacterial growth is described by the Monod<sup>80</sup> equation similar to Michael – Menten for enzymes, where bacterial growth is dependent on substrate concentration. If the MFC is run with limited substrate material, the power output will be dependent on substrate availability for the bacterium. As the power output is directly related to the growth of bacteria, factors that influence bacterial growth become the limitations for power output.

#### **1.3.2 Electrode material**

The choice of electrode material at the anode and cathode is important in influencing the rate of electron transfer. Usually metal electrodes such as platinum,<sup>81</sup> gold, copper, silver, stainless steel, cobalt and nickel are used, however the choice of electrode material depends on its electrochemical activity, surface, cost, fouling and biocompatibility.<sup>82</sup> The use of carbon based electrode materials such as carbon foam, mesh, fibre, cloth and paper are preferred at the anode chamber of the MFC

## Chapter 1: Introduction

because of their cost, surface roughness and biocompatibility.<sup>83-86</sup> The cathode electrode material is usually platinum or the same as anode.

### 1.3.3 Choice of bacteria

There are particular species of bacteria capable of transferring electrons from their metabolism to an insoluble electron acceptor such as an electrode. Some of the electrode respiring bacteria are *Clostridium beijerinckii*, *Geobacter sulfurreducens*, *Rhodospirillum rubrum*, *Shewanella putrefaciens*, *Streptococcus lactis* and *Shewanella oneidensis*.<sup>84-87</sup>

### 1.3.4 Electron transfer

There are different ways of electron transfer from the bacteria to the anode such as direct electron transfer, mediated electron transfer or the use of nanowires. These are discussed in detail in section 1.4.2. The other electron transfer that could be a limiting factor is the catalysis at the cathode. Electrons flow from the anode to the cathode and combine with the migrated positive ions to form water or other commodities depending on the type of MFC. The reduction process at the cathode acts as an electron sink for the electrons produced at the anode.

### 1.3.5 Other limitations

Internal resistance of an MFC can arise from anode, cathode,<sup>91</sup> electrolyte resistance<sup>92</sup> and membrane resistance<sup>93</sup> and these limit the power output of a MFC. These can be reduced by increasing the anode and cathode surface area, the surface area of proton exchange membrane (PEM), the ionic strength of the electrolyte, or the pH. There are other factors that influence the current generated in a MFC such as kinetic and thermodynamic factors.

#### 1.3.5.1 Thermodynamic factors

Schroder has summarised the energy flux in a MFC, showing the loss of energy at key points during the operation of an MFC (Figure 1-4).<sup>94</sup>

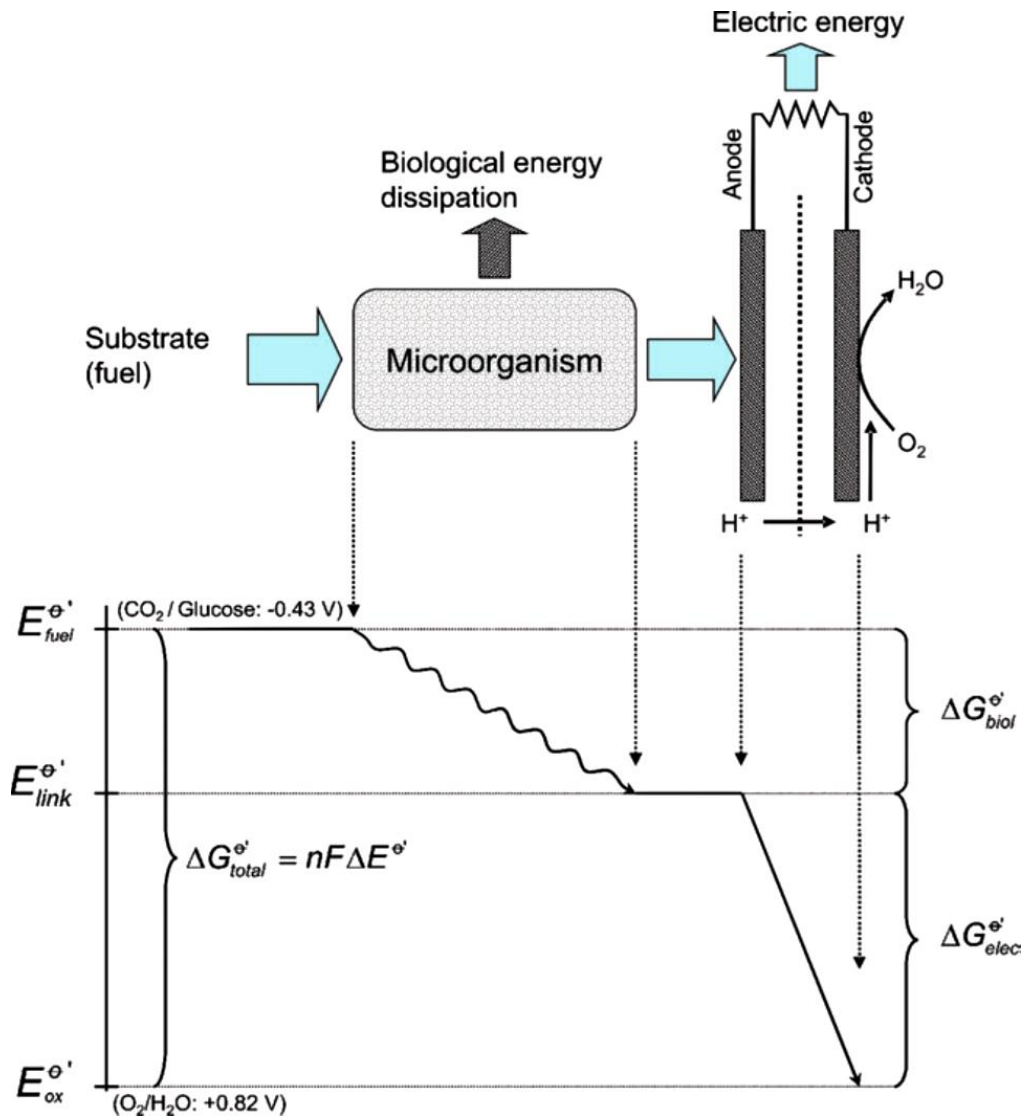


Figure 1-4: Schematic showing the energy flux in a MFC with key points of loss. Taken from ref<sup>94</sup>

In a fuel cell, the relationship is

$$\Delta G_{total}^{\theta} = nF[E^{\theta} (cathode) - E^{\theta} (anode)]$$

Where  $n$  is the moles of electrons required for the redox reaction, and  $F$  is the Faradays' constant  $96,485 \text{ C mol}^{-1}$ . In Figure 1-4, the total free energy available from the oxidation of a substrate under biological condition is given by  $\Delta G_{total}^{\theta'}$  and is determined by the potential difference  $\Delta E^{\theta'}$  between the fuel and the oxidant respective to the biological potential. In an MFC, since biological species are catalysing the redox reactions, the equation is written as<sup>95</sup>

$$\Delta G_{total}^{\theta'} = nF[E^{\theta'} (donor) - E^{\theta'} (acceptor)]$$

## Chapter 1: Introduction

Some of the free energy is lost to the bacteria for its growth and this loss can be determined by  $\Delta G_{biol}^{\theta'}$ , the total free energy obtained from the complete oxidation of substrate (taking into account the losses) is denoted by  $\Delta G_{elec}^{\theta'}$

$$\Delta G_{elec}^{\theta'} = \Delta G_{total}^{\theta'} - \Delta G_{biol}^{\theta'} \quad (1)$$

$\Delta G_{elec}^{\theta'}$  and  $\Delta G_{biol}^{\theta'}$  are related by the redox potential of the linking species and is denoted by  $E_{link_{ox}/link_{red}}^{\theta'}$

$$\Delta G_{biol}^{\theta'} = nF[E^{\theta'}(glucose, CO_2) - E^{\theta'}(link)] \quad (2)$$

$$\Delta G_{elec}^{\theta'} = nF[E^{\theta'}(link) - E_{effective}(O_2, H_2O)] \quad (3)$$

The difference in potential caused by the redox reactions taking place in between the bacteria and the anode determine the total energy obtained from a MFC. It is important to maintain a balance between  $\Delta G_{biol}^{\theta'}$  and  $\Delta G_{elec}^{\theta'}$  to sustain bacterial growth and to harvest electricity.

### 1.3.5.2 Mass transport

Mass transport plays a major role in influencing MFC performance, since the distribution of substrate species affects the electrode processes. This distribution of charges influences the rate of electron transfer processes creating a difference in potential leading to higher over potential. This is described by the Nernst equation<sup>96-98</sup> which relates the reduction potential at any point during a reaction to the standard potential in terms of concentration, activity and temperature. The Nernst equation is

$$E_{red} = E_{red}^{\theta} + \frac{RT}{zF} \ln \frac{a_{ox}}{a_{red}} \quad (4)$$

Where  $E_{red}$  is the half-cell reduction potential at the temperature of interest,  $E_{red}^{\theta}$  is the standard half-cell reduction potential, R is the universal gas constant 8.314 J K<sup>-1</sup> mol<sup>-1</sup>, T is the temperature in K, z is the moles of electrons transferred in the reaction, F is the Faradays constant, a is the activities of the reducing or oxidising agents.

## Chapter 1: Introduction

The mechanisms of electron transfer will be reviewed in detail to understand the role of bacterial metabolism and the various pathways involved for electron transfer from the bacterium to the anode.

### 1.4 Bacterial metabolic pathways

#### 1.4.1 Krebs cycle

A general bacterial cell structure consists of a number of different organelles encapsulated by cell membrane and capsule (Figure 1-5).<sup>99</sup> Most bacteria also have flagellum and nuclear material; photosynthetic lamellae are only present in photosynthetic bacteria. The cell structure of every bacterium is specific to its own species.<sup>100-102</sup>

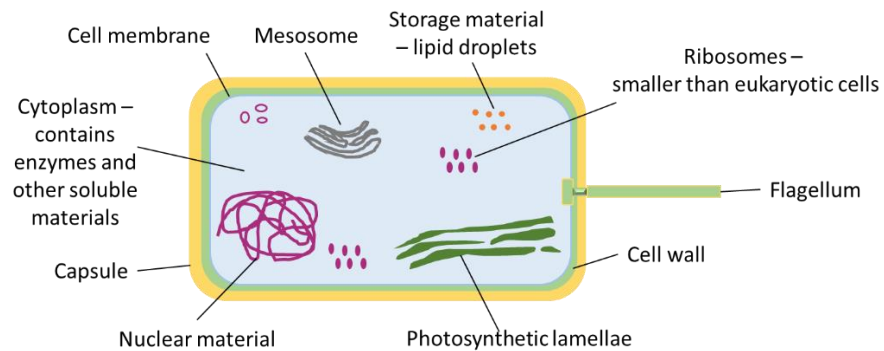


**Figure 1-5: Generalised structure of bacterial cell. Adapted from ref<sup>99</sup>**

Bacteria metabolise carbohydrates, lipids and proteins through glycolysis to produce acetyl unit of Acetyl-CoA which forms part of the Citric Acid Cycle / Krebs Cycle (Figure 1-6).<sup>103-105</sup> This cycle is used to oxidise pyruvate formed in glycolysis to carbon dioxide and water.

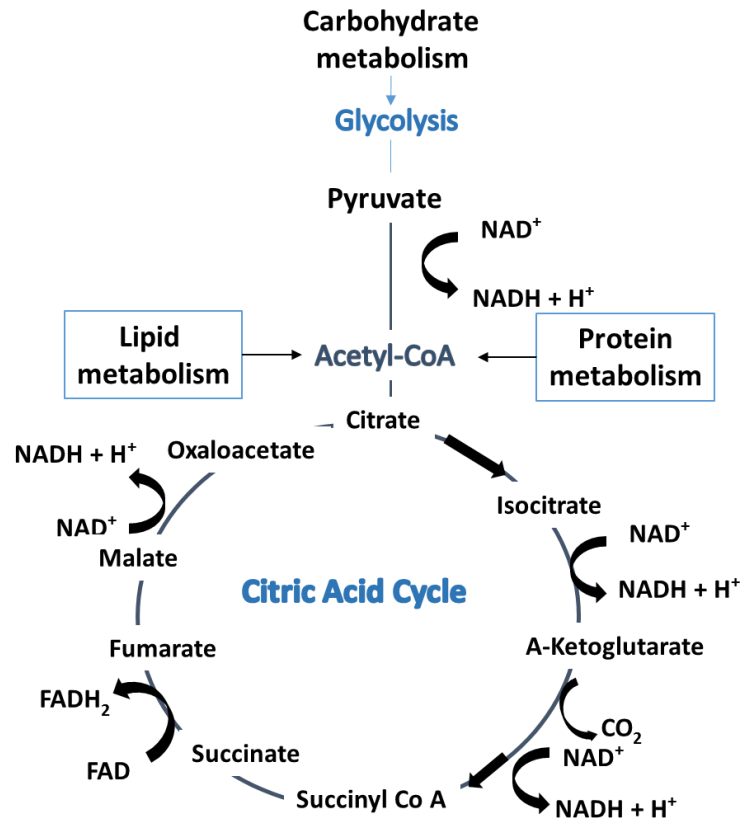


**Figure 1-6: Citric acid cycle in bacteria.** Adapted from ref <sup>103,106</sup>

Acetyl-CoA feeds into the citric acid cycle, where various oxidation reactions reduce  $\text{NAD}^+$  and  $\text{FAD}$  to their electron carrier forms  $\text{NADH}$  and  $\text{FADH}_2$ . These  $\text{NADH}$  and  $\text{FADH}_2$  transfer electrons from the cytoplasm to the cell membrane of a bacteria.

A cell membrane contains a multitude of enzymes and proteins which form part of an electron transport chain for bacterial ATP synthesis. Adenosine triphosphate (ATP) is synthesised using oxidative or photophosphorylation in both eukaryotic (animal and plant) and prokaryotic (archaea and bacterial) cells. If phosphorylation is driven by light, as in plant and photosynthetic prokaryotic cells it is known as photophosphorylation, if it is driven by the oxidation of organic and inorganic compounds it is known as oxidative phosphorylation.<sup>107</sup> The location for oxidative phosphorylation in bacterial cells, is in the inner membranes and ATP synthesis is linked to the electron transport chain of respiration.



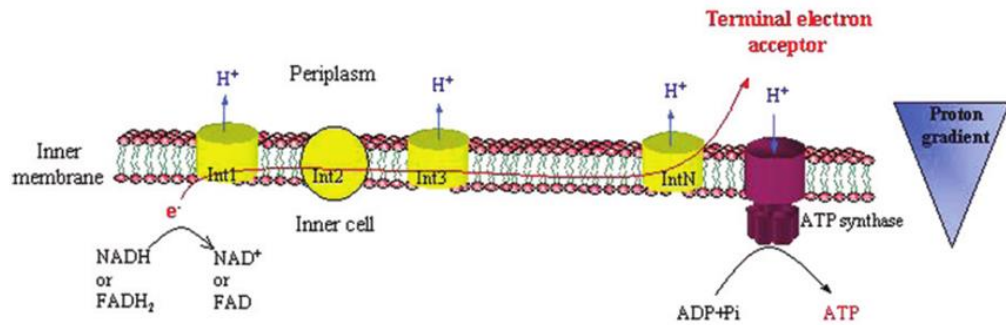


**Figure 1-7: Schematic of bacterial respiration membrane process. The number of electron chain components varies with bacterial species. Taken from ref <sup>103</sup>**

The cell membrane of a bacteria contains intermediaries that shuttle electrons through and pump out protons through reduction, creating a proton gradient across the membrane (Figure 1-7). ATP synthase transmembrane protein utilises the proton gradient energy to phosphorylate ADP to produce ATP.<sup>107</sup> 10 ATP molecules are produced per one glucose molecule. The electrons are gained by a terminal electron acceptor such as oxygen if it is aerobic respiration or an inorganic acceptor such as nitrate, sulphate and carbonate in anaerobic respiration.<sup>108</sup> The position of the last intermediary in the chain and the terminal electron acceptor is different for every bacterium. In Table 1-1, the standard reduction potentials are provided for some of the intermediaries in an electron transport chain; cytochrome and ubiquinone are membrane proteins.

**Table 1-1: Standard reduction potentials at pH 7, 25 °C, vs. ENH of some electron transport chain molecules. Electrons may leave the system at a number of places in the electron transport chain**

Name	E <sup>0</sup> / V
NAD <sup>+</sup> / NADH + H <sup>+</sup>	-0.32
FAD <sup>+</sup> / FADH <sub>2</sub>	-0.22
Cytochrome b (+3) / Cytochrome b (+2)	0.07
Ubiquinone (ox) / Ubiquinone (red)	0.10
Cytochrome c (+3) / Cytochrome c (+2)	0.22
Fe <sup>3+</sup> / Fe <sup>2+</sup>	0.77
1/2O <sub>2</sub> + H <sup>+</sup> / H <sub>2</sub> O	0.82

Bacteria are able to use the anode as the terminal electron acceptor in the MFCs. Depending on the bacterium, the potentials at which electrons may be released to

the anode changes. The reduction potential of a donor present in the transport chain is more negative than the terminal acceptor, which has a much more positive reduction potential (Table 1-2).<sup>107</sup>

**Table 1-2: Standard reduction potentials of electron donors and acceptors measured at pH 7 vs SHE. Taken from ref<sup>107</sup>**

<b>Redox couple</b>	<b>E° /V</b>
<b>CO<sub>2</sub>/Glucose</b>	-0.43
<b>CO<sub>2</sub>/Formate</b>	-0.43
<b>2H<sup>+</sup>/H<sub>2</sub></b>	-0.42
<b>CO<sub>2</sub>/Acetate</b>	-0.28
<b>CO<sub>2</sub>/CH<sub>4</sub></b>	-0.24
<b>SO<sub>4</sub><sup>2-</sup>/HS<sup>-</sup></b>	-0.22
<b>Pyruvate/lactate</b>	-0.19
<b>Fumarate/succinate</b>	+0.33
<b>NO<sub>3</sub><sup>-</sup>/NO<sub>2</sub><sup>-</sup></b>	+0.43
<b>MnO<sub>2</sub>/Mn<sup>3+</sup></b>	+0.60
<b>Fe<sup>3+</sup>/Fe<sup>2+</sup></b>	+0.77
<b>1/2O<sub>2</sub>/H<sub>2</sub>O</b>	+0.82
<b>1/2O<sub>2</sub>/H<sub>2</sub>O</b>	+0.51

The pathways involved in transferring electrons from the bacterial membrane to the anode will be reviewed.

#### **1.4.2 Electron transfer from the bacterial cell membrane to the anode**

Electron transfer mechanisms in biology and chemistry have been established by Marcus<sup>109,110</sup> and are dependent on redox centre separations, driving force such as the potential difference between the redox centres and their reorganisation energy. There are two main electron transfer pathways from the cell membrane to the anode; direct and indirect electron transfer.<sup>111,112</sup>

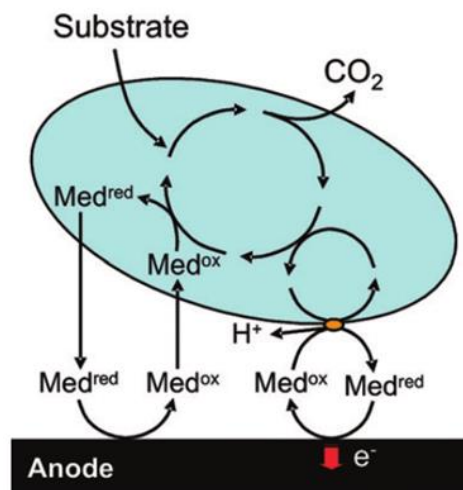
##### **1.4.2.1 Indirect electron transfer**

The use of mediators to transport electrons from the membrane to the electrode was recorded by Davis and Yarbrough.<sup>113</sup> Indirect electron transfer involves the use of mediators that are exogenous (artificial) or endogenous mediators. Exogenous

## Chapter 1: Introduction

mediators are usually organic or inorganic substances such as phenazines,<sup>114</sup> quinones<sup>115</sup> and phenoxazines. The disadvantage in using these as the mediators, is the need to maintain their concentration, whereas endogenous mediators are secreted by the microorganism during its metabolism.<sup>116</sup>

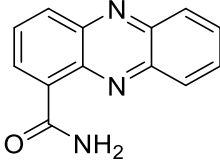
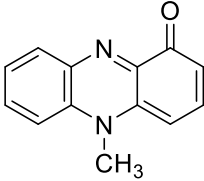
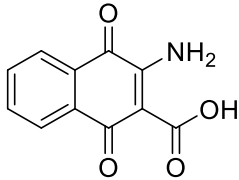
There are two types of endogenous mediators based on the bacterial metabolism; secondary and primary. Primary metabolites are produced by the primary metabolism of the bacteria and are related to bacterial growth, respiration and ATP synthesis. Secondary metabolites are not related to primary metabolism, usually are secreted for defence, antibiotics and intracellular communication.<sup>99</sup> Secondary metabolite mediators are able to shuttle between reduced and oxidised states improving the reusability of them as mediators (Figure 1-8).<sup>95</sup>



**Figure 1-8: Schematic showing the mediated electron transfer using secondary metabolites. Two mechanisms were proposed shuttling via outer cell membrane cytochromes (red circle) and via periplasmatic or cytoplasmatic redox couples. Taken from ref<sup>95</sup>**

Some of the secondary metabolite mediators are phenazine-1-carboxamide, Pyocyanine (phenazines) and 2-amino-3-carboxy-1,4-naphthoquinone (ACNQ) (Table 1-3).

**Table 1-3: Standard reduction potentials of endogenous secondary metabolite mediators.**  
Taken from ref <sup>95</sup>

Mediator		Redox potential. $E^\circ$ / V
Phenazine-1-carboxamide		-0.115
Pyocyanine (phenazines)		-0.030
2-amino-3-carboxy-1,4-naphthoquinone (ACNQ)		-0.071

Primary metabolite mediators are produced under anaerobic conditions by anaerobic respiration and fermentation. During fermentation, metabolites such as hydrogen, ethanol or formate are produced which act as mediators (Figure 1-9).

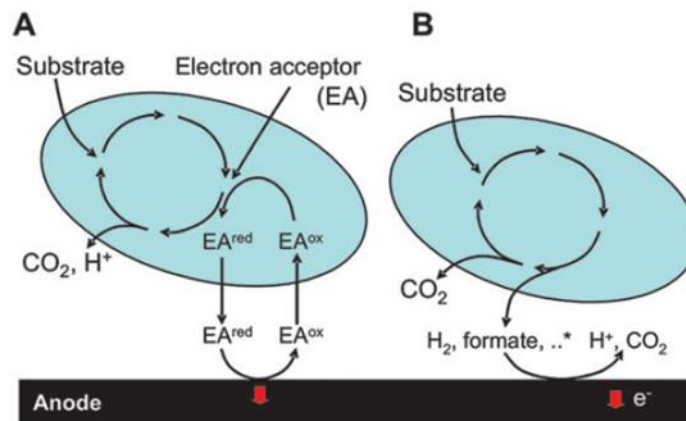


**Figure 1-9:** Schematic illustration of mediated electron transfer by primary metabolite mediators. (a) via reduced terminal electron acceptors produced during anaerobic respiration, (b) oxidation of reduced fermentation products (formate and hydrogen). Taken from ref <sup>95</sup>

#### 1.4.2.2 Direct electron transfer

In direct electron transfer (DET) the bacteria is connected to the electrode by membrane-bound proteins, heme proteins or cytochromes that are capable of acting as electron transfer relays units. These are capable of transferring electrons to

## Chapter 1: Introduction

acceptors such as electrodes, limiting the current generated in the MFC to the layer of biofilm in direct contact with the electrode (Figure 1-10).

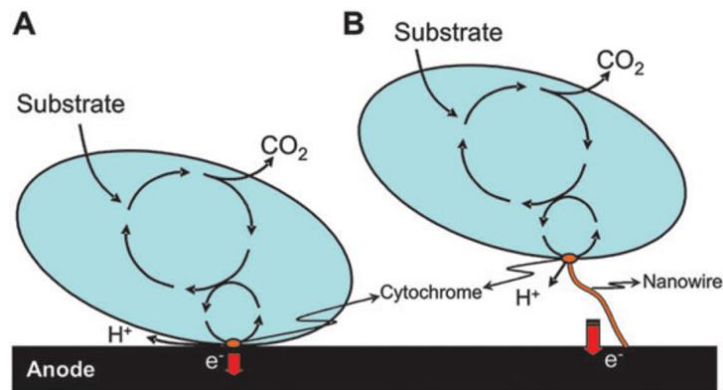


**Figure 1-10: Schematic showing the various direct electron transfer routes. (a) Membrane bound cytochromes and (b) electronically conductive nanowires such as pili. Taken from ref 95**

Some bacteria have conductive pili (nanowires) which are connected to the membrane-bound proteins, but allow bacteria to access electrodes that are not directly in physical contact. These pili also create a highly connected biofilm that is capable of generating high current densities.<sup>117</sup>



**Figure 1-11: SEM image showing a highly connected biofilm of *Shewanella oneidensis* MR-1. Taken from ref<sup>118</sup>**

Pili or 'nanowires' generated by *Shewanella oneidensis* MR-1, *Pelotomaculum thermopropionicum* and *Methanothermobacter thermautotrophicus* for electron transfer to an anode.

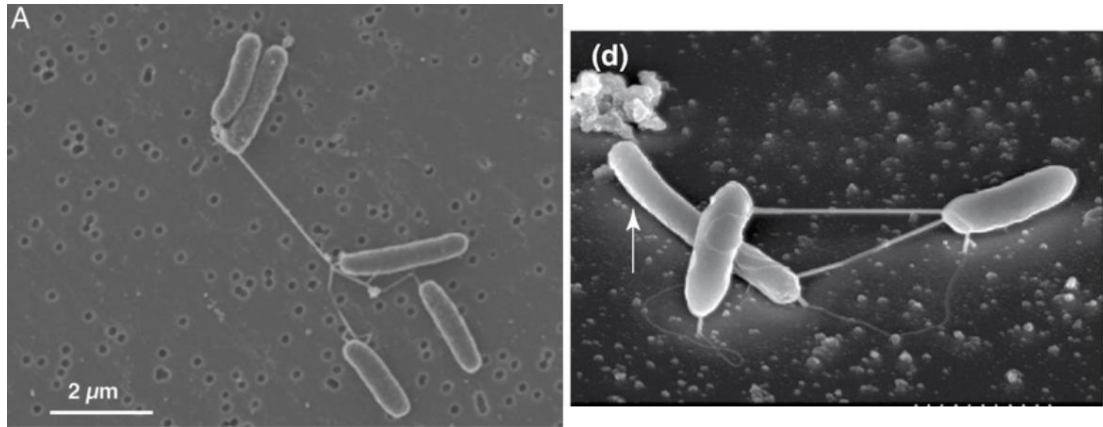


**Figure 1-12: SEM images of bacteria (a) *Shewanella oneidensis* MR-1 and (b) *Pelotomaculum thermopropionicum* and *Methanothermobacter thermautotrophicus*, scale bar  $\times 20k$  with pili or 'nanowires'. Taken from ref <sup>118</sup>**

Some standard reduction potentials ( $E^\ominus$ ) were measured for the DET mechanism in different bacterial strains as shown in Table 1-4.

**Table 1-4: Standard reduction potentials of DET for some bacterial strains**

Bacterial strain	$E^\ominus / V$
<b><i>Shewanella putrefaciens</i> IR-1</b>	+0.01
<b><i>Shewanella putrefaciens</i> MR-1</b>	-0.02
<b><i>Shewanella putrefaciens</i> SR-1</b>	-0.01
<b><i>Acromonas hydrophila</i> PA 3</b>	0
<b><i>Clostridium sp. EG 3</i></b>	0

The values in Table 1-4 are assumptions that at this potential these bacterial strains will transfer electrons via their outer membrane cytochromes to an anode. This is because these potential values do not account for concentration differences in reduced or oxidised species involved in electron transfer as per the Nernst equation. An improvement in electron transfer would increase the current generating ability and consequently the power output of a MFC. Addressing any of the limitations mentioned in section 1.3 would have the potential of increasing power output. There are many literature articles that address changes in configuration, operation, substrate and the choice of bacterium to improve current generation or power output. There are only a few articles that are focussed on improving the electron transfer from the bacterium to the anode in a MFC and these will be reviewed in detail.

## 1.5 Improving current generation

### 1.5.1 Biofilm formation and stages

Since the current generated in a MFC is related to bacterial growth, it is important to understand how bacteria grow and form an electroactive biofilm on an electrode. Biofilm is defined as a 'An extracellular polymeric substance (EPS) encased, surface adhering microbial community'<sup>67</sup>. It is formed in 4 different stages<sup>119-121</sup> (Figure 1-13), (i) reversible – irreversible attachment of bacteria to a surface. This attachment depends on a number of factors such as Brownian motion, gravitational forces, attractive or repelling forces which are dependent on pH, ionic strength, temperature. The bacterial cell surface properties and the surface properties to which to attach influence adhesion. The adhesion is reversible and depends on nutrient availability and shear forces, some bacteria use pili to attach to a surface.

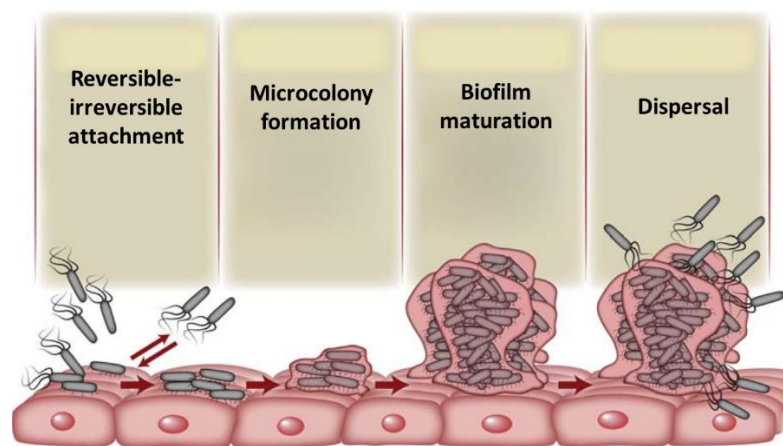


**Figure 1-13: Schematic showing the 4 stages of biofilm formation, grey rectangles represent bacteria, pink halo represent the EPS and the horizontal pink squares represent human skin cells. Taken from ref <sup>121</sup>**

The second stage involves microcolony formation, on attachment to a surface the secretion of the extracellular matrix is triggered within the bacterial metabolism. Extracellular DNA is released by controlled cell death that initiates cell to cell contact and maintains bacterial adhesion.<sup>122</sup> The third stage is biofilm maturation, the bacteria within the biofilm exchange enzymes, metabolic products and continue to grow. The fourth stage is dispersal, this is when bacteria become sensitive to change in pH, oxygen content, nutrient availability and increase in stress due to changes in the environment. Bacteria secrete enzymes that break down the EPS leading to dispersal. Dispersal can be caused by the presence of metal nanoparticles, toxic byproduct or any other physiological changes.



## Chapter 1: Introduction

In a MFC all the bacteria used are able to use MET and DET to transfer electrons from bacterial membrane to anode. The presence of a biofilm will influence the rate of electron transfer as it determines which MET or DET the bacteria can use to transport electrons. All the biofilms in MFC are known to be electroactive because of this electron transferring capability.<sup>119-121</sup>

### 1.5.2 Electrode modification

Current generation of a MFC can be improved by modifying the surface of the anode by using electrodes with higher specific areas (porosity) to improve biofilm formation to increase MET or DET depending on the bacterium and also by improving the conductivity of the electrode.<sup>124</sup> Modification of the anode surface can create an impact from single cell bacterium level to process level, an excellent review by Guo *et al.*<sup>111</sup> has summarised the various parameters that will change depending on the modification (Figure 1-14).

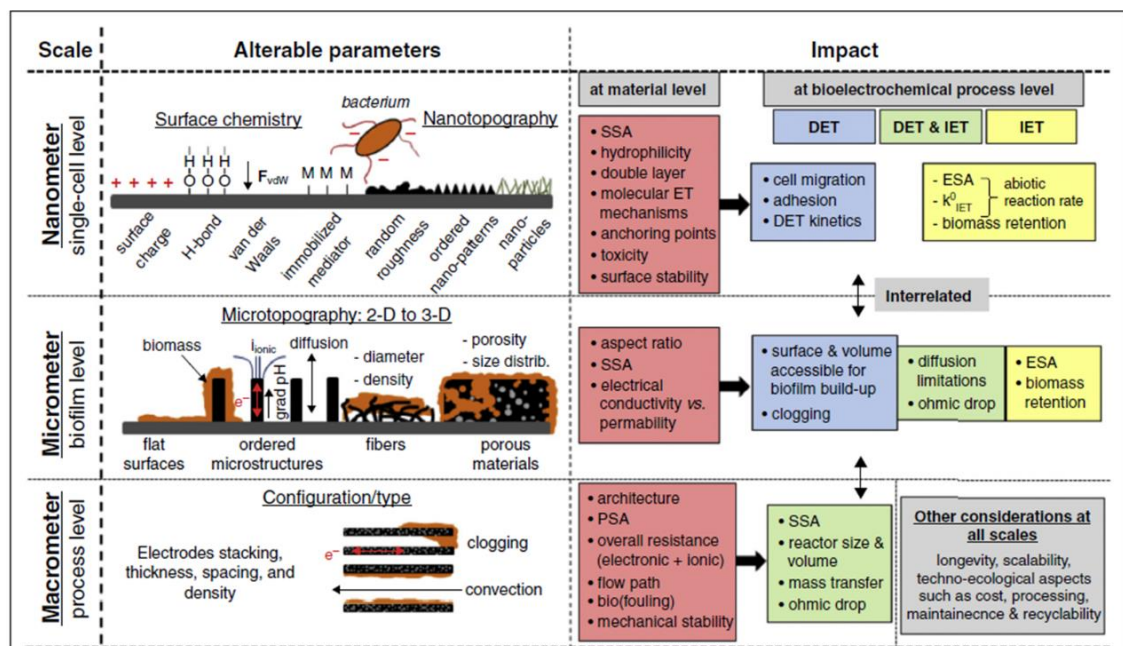


**Figure 1-14: An overview of impact of material surfaces (chemistry and topography) on the electrode characteristics and microbial electrocatalysis in bio-electrochemical systems. 2-D/3-D: two/three-dimensional; DET: direct electron transfer; IET: indirect electron transfer;  $k^0_{IET}$ : heterogeneous ET rate constant for abiotic reaction; PSA: projected surface area [it is the largest two-dimensional area obtained from the projection of a planar surface or a 3-D material; estimated with respect to the plane covering X and Y axes of the material]; SSA: specific surface area [it is the total surface area of electrode per unit of projected surface area or electrode volume (for 3-D architecture; often BET measurements are considered to estimate SSA)]; ESA: electroactive surface area [it is the actual surface available for electrochemical reactions (i.e. solvated, electrically connected area)]; cyclic voltammetry for capacitance measurement can be used to estimate ESA]. Taken from ref <sup>111</sup>**



## Chapter 1: Introduction

Figure 1-14 summarises the complexity of electrode catalysis involved in a MFC and how a single change in electrode surface can lead complementary changes at a process and configuration level. All the changes seem to influence the adhesion of bacteria and bacterial biofilm formation on the electrode.

At the nanometer level, a change in surface charge of the electrode can drive bacterial adhesion to the electrode surface leading to better biofilm formation. Positive charge is known to increase biofilm formation as bacterial surfaces are negatively charged. Surface property of an electrode such as hydrophilicity is also known to increase bacterial adhesion to electrode. By changing the surface roughness of an electrode by modification can also improve bacterial adhesion.

At the micrometre scale, increasing the porosity of the electrode can increase biofilm attachment and also minimise mass transport issues of substrate and ion diffusion. At the macrometer scale, having a flow reactor would allow for removal of side reaction products more quickly than a stationary reactor design. The distance between electrode will reduce internal resistance, driving bacterial biofilm formation.

In the early stages of MFC power improvement, most of the MFC anodes took part in electron transfer reactions via MET using metabolites as mediators or exogenous mediator. In the current MFCs predominantly DET is being used as the main electron transfer pathway, and is being targeted as the point of improvement for catalysis.

126

Most electrode modifications are based on using cheap, easy to source materials such as carbon-based electrodes and modifying them to achieve better electrocatalysis. This is because even though carbon is biocompatible and cheap, its electrocatalytic ability for bio-electrochemical reactions is low. The other advantage of using carbon based materials as electrodes is that, they are available in various topographies such as flat, porous, fibrous structures that can maximise surface area, diffusion of substrate and create 2 to 3-dimensional electrode surfaces that can be further modified to improve electron transfer.<sup>85,83</sup>

The anode in a MFC can be modified by incorporating materials that have faster electron-transfer rates, low resistance and those that minimise kinetic effects. Some

## Chapter 1: Introduction

of the modifications and their respective enhancements will be reviewed in detail below.

Carbon nanotubes were grown on reticulated vitreous carbon CNT / RVC (carbon combined with glass and ceramics in a foam structure with high surface area and low electrical and thermal resistance) by Flexer *et al.*<sup>127</sup> This was used as an anode in an MFC reactor with mixed microbial communities sourced from the sediment of a lake at the University of Queensland. An enhancement in current density from 2.3 mA m<sup>-2</sup> for the control (RVC) to 6.8 mA m<sup>-2</sup> (CNT/RVC) was observed, this was attributed to highly porous surface area of the CNT/RVC that minimises mass transport issue and maximises biofilm formation (Figure 1-15).<sup>127</sup>

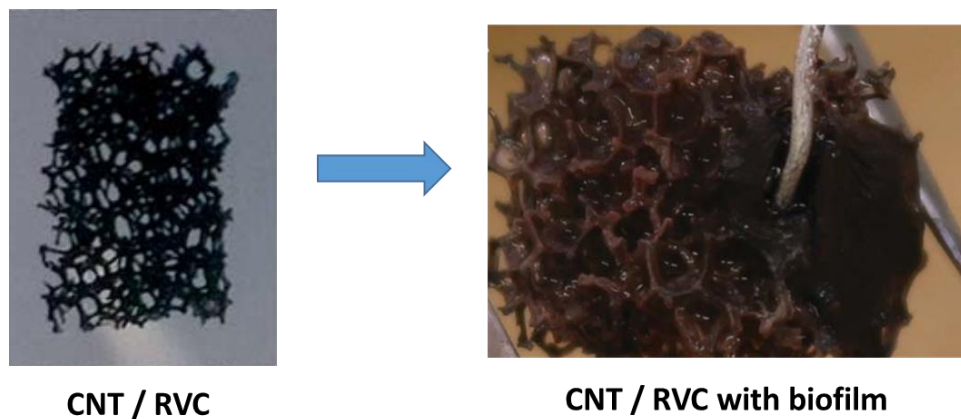


**Figure 1-15: CNT/RVC before incorporation in MFC (left) and (right) after incorporation with reddish colour showing the growth of biofilm. Adapted from ref<sup>127</sup>**

*Shewanella oneidensis* MR-1 (So) has one of the best completely understood electron transfer pathways, it uses c-type cytochromes (proteins) that shuttle electrons from cytoplasmic and inner membrane to the outside of the cell during anaerobic respiration. The major components of the So electron transfer pathway are inner membrane tetraheme cytochrome CymA, a periplasmic decaheme cytochrome MtrA, outer membrane decaheme cytochromes OmcA and MtrC, and an outer membrane  $\beta$ -barrel protein MtrB. This pathway is proposed to move electrons from the intracellular quinol pool to extracellular electrodes (Figure 1-16).<sup>128-132</sup>

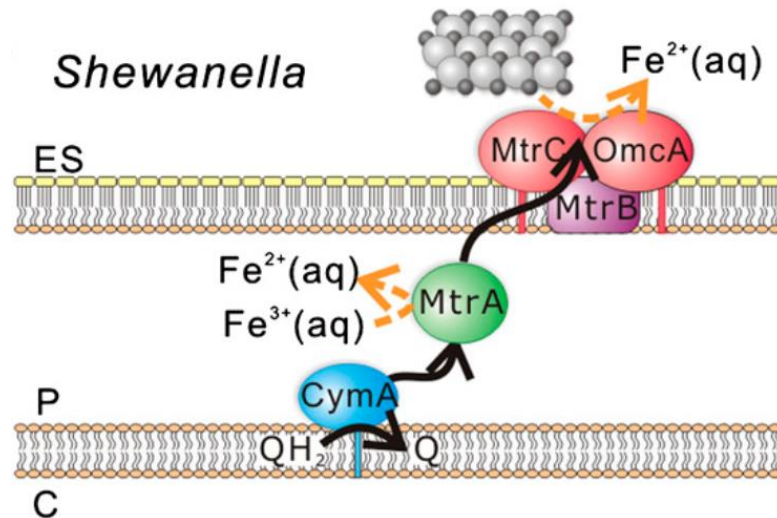


**Figure 1-16: Schematic of proposed extracellular electron transfer pathway in *Shewanella oneidensis* MR-1** where ES denotes the extracellular space, P denotes the periplasm, and C denotes the cytoplasm. The silver and black spheres represent extracellular iron oxide. Taken from ref<sup>128</sup>

Peng et al.,<sup>133</sup> were interested in enhancing the electron transfer of outer membrane bound Cytochrome *c* in *So*. They deposited carbon nanotubes on a glassy carbon electrode (GCE) and used it as an anode in an MFC. *So* was used as the bacterium with Luria-Bertani and phosphate buffer as solution. A current density enhancement of ~ 82 times was observed from bare GCE ( $0.117 \mu\text{A cm}^{-2}$ ) to CNT/GCE ( $9.70 \mu\text{A cm}^{-2}$ ).

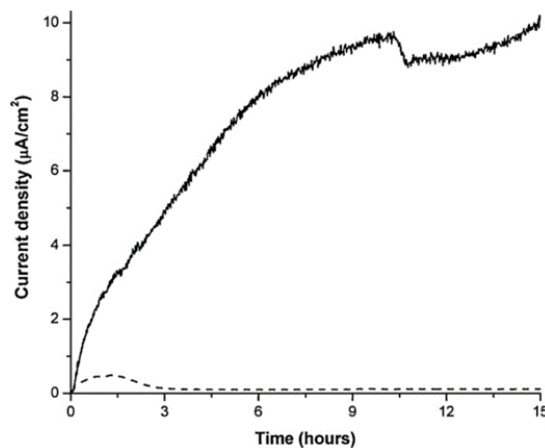


**Figure 1-17: Current vs Time plot of GCE (dashed line) and CNT/GCE (solid black line) as an anode in MFC with *So* as the bacterium run for 15 h.** Taken from ref<sup>133</sup>

This enhancement was attributed to the successful improvement in rate of electron transfer from Cytochrome *c* to the electrode. However, the MFC was run only for 15 h and it can be seen from Figure 1-17 that the current density is still increasing at 15 h, the MFC should have been run for a longer time to see how the current density

## Chapter 1: Introduction

changes over long term operation. During long term operation, there will be a build-up of dead cells and other metabolic side products that can lead to increased resistance and current decrease.

Yang *et al.*<sup>134</sup> have synthesised a composite containing chemically exfoliated graphene oxide (GO), graphene containing foam (GCF), agarose and stainless steel mesh (SSM). A GCF was prepared by freeze drying and pyrolysis of GO – agarose gel which is embedded with SSM and graphene (Figure 1-18). This produced a GCF structure that had higher 3-dimensional surface area and conductivity because of the presence of SSM and graphene. They were interested in improving the power density of a MFC with this composite.

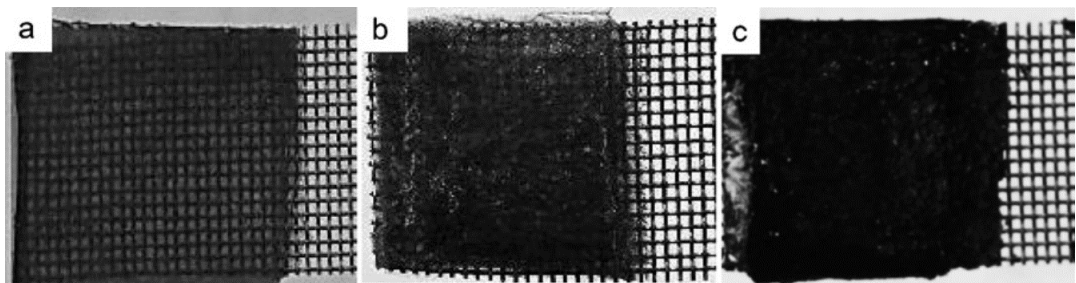


**Figure 1-18: Photographic images of a) the GO-agarose gel, b) GO- agarose foam and c) GCF**

The GCF was used as an anode in a MFC with *Shewanella putrefaciens* as the bacterium and a power density enhancement  $\sim 4$  times was observed with GCF ( $786 \text{ mW m}^{-2}$ ) compared to commercially available carbon cloth ( $190 \text{ mWm}^{-2}$ ). This enhancement was also attributed to the anode having a microporous structure for better biofilm formation. Some other modifications are outline in Table 1-5.

**Table 1-5: Anode modifications to achieve high electroactive area and surface area for better biofilm formation**

<b>Anode material</b>	<b>Modification</b>	<b>Culture in MFC</b>	<b>Enhancement</b>	<b>Reference</b>
<b>Carbon cloth</b>	Amino pyrazine reduced graphene oxide	Waste water in Phosphate buffer solution	2	<sup>135</sup> (2016)
<b>2 D planar graphene</b>	3D microporous graphene	<i>Geobacter sulfurreducens</i> with sodium acetate as carbon source	3.3	<sup>136</sup> (2016)
<b>Carbon paper</b>	Polypyrrole nanotubes	<i>Shewanella oneidensis MR-1</i> with sodium lactate as carbon source	6	<sup>137</sup> (2015)
<b>Graphite felt</b>	Polypyrrole hydrogel with carbon nanotubes	Waste water with sodium acetate as carbon source	2	<sup>138</sup> (2015)

All the modifications outlined in Table 1-5 have shown that a there is direct correlation between biofilm formation and current generation. They also emphasise the importance of having a large surface area of anode to maximise biofilm formation to improve electron transfer and diffusion of ions.

The anode can also be modified using nanoparticles improve their conductivity without any biocompatibility issues. Incorporating nanoparticles on an anode by adsorption on its surface, can increase the rate of electron transfer by increasing the conductivity of the anode. The nanoparticles can facilitate electron-transfer by acting as electron sinks and reducing the distance between bacteria and the anode. There are examples in literature where metal nanoparticles have taken part in electron transfer reactions by acting as electron mediators for electron transfer from solutions to electrodes.<sup>139-143</sup> The high surface area to volume ratio of nanoparticles enables them to carry electrons on their surface for electron transfer. The charges on the nanoparticle surface and the electrode surface creates a potential difference facilitating electron transfer. A similar mechanism must be used for electron transfer from the bacterial respiration chain to nanoparticle surface.

## Chapter 1: Introduction

Some of the modifications of the anode to incorporate nanoparticles are detailed below (Table 1-6).

**Table 1-6: Anode modifications by nanoparticles and their enhancements, the rows highlighted in grey represent modifications where the particles were added into the culture rather than attached to the anode.**

<b>Anode material</b>	<b>Modification</b>	<b>Culture in MFC</b>	<b>Enhancement</b>	<b>Reference</b>
<b>Indium tin oxide</b>	Antimony doped tin oxide nanoparticles	<i>Shewanella loihica</i> PV-4 with sodium lactate as carbon source	115	<sup>144</sup> (2015)
<b>Glassy carbon</b>	Fe <sub>3</sub> O <sub>4</sub> /Au nanocomposites	<i>Shewanella oneidensis MR-1</i> with sodium lactate as carbon source	22	<sup>145</sup> (2010)
<b>Carbon paper</b>	Graphene / gold nanocomposites	<i>Shewanella oneidensis MR-1</i> with sodium lactate as carbon source	4	<sup>146</sup> (2015)
<b>Graphite disk</b>	Palladium nanoparticles	<i>Shewanella oneidensis MR-1</i> with sodium lactate as carbon source	2.4	<sup>147</sup> (2011)
<b>Graphite disk</b>	Gold nanoparticles	<i>Shewanella oneidensis MR-1</i> with sodium lactate as carbon source	20	<sup>147</sup> (2011)
<b>Carbon paper</b>	Gold nanoparticles	Waste water with sodium acetate as carbon source	1.88	<sup>148</sup> (2014)

Table 1-6 proves that modification of the anode or culture by nanoparticles can influence current generation and by comparing the enhancements from Table 1-5 nanoparticle modification has a higher enhancement. The choice of nanoparticles is determined by cost, biocompatibility, detection and stability in an MFC. It is also important to consider the method of adsorbing nanoparticles onto the surface of anode or the culture.

### 1.5.3 Gold nanoparticles

#### 1.5.3.1 Gold nanoparticle synthesis

Gold is considered as a metal for modifying an anode because of its inertness, cost and also ease of preparation of gold nanoparticles. In terms of synthesis, gold nanoparticle synthesis<sup>149-172</sup> has been well documented. There are a number of different methods for producing gold nanoparticles such as chemical reduction, electrochemical reduction and photo-chemical reduction.<sup>173</sup> The most common method of gold nanoparticle synthesis is by addition of a reducing agent to a solution of a Au (III) salt. Gold nanoparticles are formed when Au (III) is reduced to Au (0) forming agglomerates (particles which are stabilized by a ligand or by a reducing agent acting as a ligand).

There are many types of ligand that can be used to synthesise gold nanoparticles such as phosphines,<sup>174</sup> thiol-containing molecules<sup>175</sup> and highly branched supporting structures such as dendrimers.<sup>176</sup> The properties of nanoparticles change depending on the ligand surrounding them, if the ligand is hydrophilic in nature the nanoparticles will be water soluble and if the ligand is hydrophobic in nature the nanoparticles will be water insoluble.<sup>177</sup>

Michael Faraday<sup>178</sup> reported the first synthesis of gold nanoparticles using phosphorus as a reducing agent in carbon disulfide to form a gold film on glass. This was followed by Turkevich<sup>179</sup> and Frens<sup>180</sup> using citrate as a reducing agent and ligand to produce gold nanoparticles. Brust<sup>181</sup> developed a two phase synthesis using tetraoctylammoniumbromide as a phase transfer reagent which transfers the Au salt to toluene and reduces it using sodium borohydride and dodecanethiol. There are other ways of synthesizing gold nanoparticles with a specific functionalisation as the target.

Gold nanoparticles are increasingly being used in a number of areas with specific applications in biology for cell labelling, drug design, as transfection agents and photovoltaic as they are simple to synthesise and functionalize with biocompatible ligands.<sup>182-185</sup> Gold nanoparticles can also be synthesised in templates which is covered in detail in Chapters-1& 2.

### 1.5.3.2 Gold nanoparticle stabilisation

Gold nanoparticles tend to coalesce because of Van der Waals and dispersion forces acting between the gold nanoparticles. The stability of particles is described by DLVO (Derjaguin-Landau-Verwey-Overbeek) theory and it states that the balance of both Van der Waals and dispersion forces are responsible for particle stability and the particles are covered by an electrical diffuse layer. The particles diffuse layer is dependent on solutions properties such as pH and ionic strength. The particles are capped by ligands that provide steric or electrostatic repulsion, preventing particle aggregation.<sup>186-189</sup>

### 1.5.3.3 Gold nanoparticle characterisation

Gold nanoparticles can be characterised using multiple techniques.<sup>154-156</sup> Gold nanoparticles can be detected using their unique surface plasmon resonance which is dependent on size, shape, surrounding environment and solvent of the nanoparticle (Figure 1-19).<sup>157-167</sup>

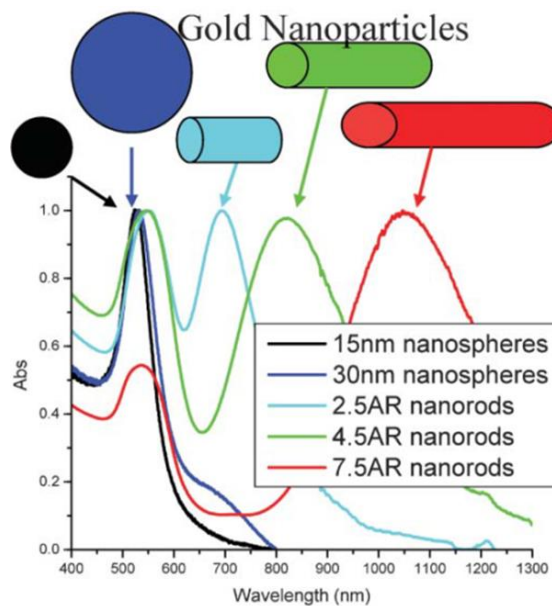


**Figure 1-19: UV-Vis spectrum showing the dependence of surface plasmon resonance on gold nanoparticle shape. Taken from ref <sup>194</sup>**

They are also detected by Surface Enhanced Raman Spectroscopy (SERS),<sup>202-205</sup> XPS,<sup>206-208</sup> TEM,<sup>175,176</sup> SEM,<sup>210-213</sup> DLS,<sup>181-185</sup> EDX<sup>186-189</sup> and their surface charge can also be determined by Zeta potential.<sup>190-193</sup> Gold was already shown to be biocompatible<sup>194-203</sup> and to be easily incorporated into an anode<sup>237-241</sup> or bio-electrochemical system.<sup>233,242</sup>



## Chapter 1: Introduction

The bacteria capable of producing high current densities seem to be *Shewanella oneidensis* MR-1(So) and *Geobacter sulfurreducens* from the tables of modifications and also from literature. Both species are dissimilatory metal reducing bacteria, capable of using a range of metal electrodes as the terminal electron acceptors in their respiration. <sup>243-247</sup> *Shewanella oneidensis* MR-1 was well known to reduce metal salts to their nanoparticle equivalents through its respiration<sup>214-216</sup> and has a multitude of membrane proteins, flavins, quinones and nanowires capable of electron transfer from its membrane to an anode.<sup>217-227</sup> The production of nanoparticles by bacteria is reviewed below.

### 1.5.4 Biomineralisation

Biomineralisation is a process where a microorganism produces or accumulates minerals or metals using its metabolism. There are three main reasons for this phenomenon, they are chemolithotrophy for energy production where the minerals or metals are used as reduced equivalents for its respiration followed by the use of these particles for special functions such as the formation of shells and detoxification for survival in toxic environments.<sup>262</sup>

S. Mann<sup>263</sup> reported the first case of biomineralization of gold in 1992, by *Pedomicrobium* bacteria's synthesis of 24 carat gold nanofibers and clusters. The image below shows the cluster produced by the bacterium.

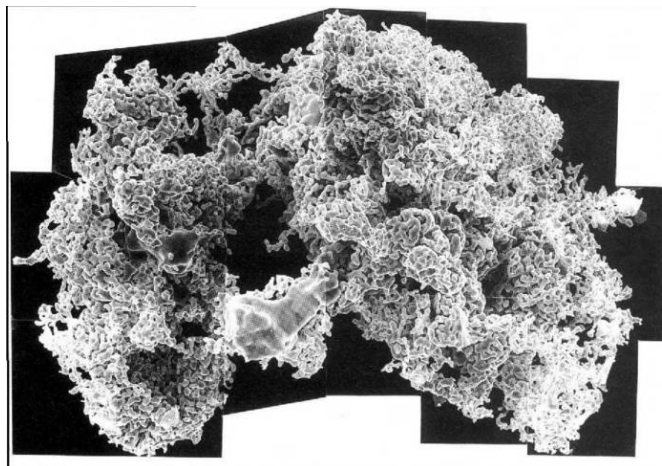


**Figure 1-20: Gold cluster produced by Pedomicrobium**

Biomineralisation is not specific only to gold, there have been a number of cases reported of biomineralisation of copper, platinum, silver and other metals.<sup>262</sup>

## Chapter 1: Introduction

*Shewanella algae* and *Bacillus subtilis* are two strains of bacteria of particular interest as they are metal reducing bacteria and are currently being used in MFC's as biocatalysts; these bacteria have also been shown to have gold mineralization capability.<sup>264,265</sup> The Figure 1-21 below shows gold mineralization by *Shewanella algae*, where the gold nanoparticles are indicated as the dark spots on the dark grey background of the bacteria.

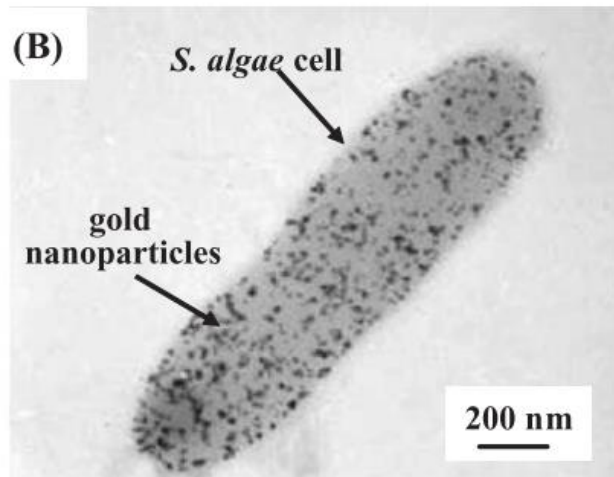


**Figure 1-21: TEM image of *Shewanella algae* cell covered by gold nanoparticles. Taken from ref<sup>264</sup>**

## **1.6 Aims of the project**

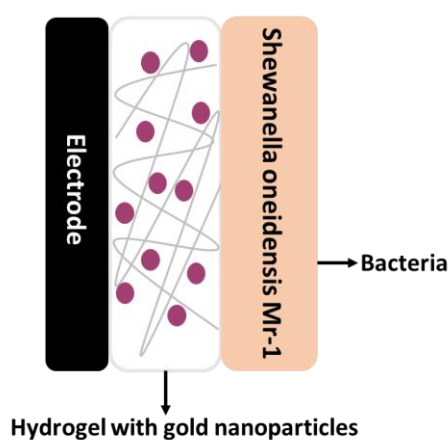
*Shewanella oneidensis* MR-1 and gold nanoparticles have shown potential to be used in a MFC to increase its current generation ability and power output. The original aim of the project was to increase electron transfer from the bacterium to an anode. So was chosen as the bacterium to investigate and gold nanoparticles are chosen as the modification to improve electron transfer between So and an anode in an MFC.

Gold nanoparticles will be incorporated into an MFC by synthesis of a hydrogel / gold nanoparticle composite electrode, hydrogel / gold nanowire composite electrode and attachment of biocompatible gold nanoparticles to So. These composites and nanoparticle-attached So will be investigated for their electrocatalytic ability by incorporating them in a bio-electrochemical cell and measuring their current response over time to measure the enhancement. Finally, the interaction between So and gold nanoparticles will be investigated using imaging techniques for the electrodes.

# **Chapter 2: Gold nanoparticles in hydrogels**

## 2 Introduction

The aim of this chapter was to create a hydrogel containing gold nanoparticles that would act as a conductive bridge in between So and an electrode (Scheme 2-1). The encapsulation of gold nanoparticles into a hydrogel should provide a porous structure for biofilm formation and increase the electroactive surface area available for electron transfer from So to the electrode. The use of hydrogels should also minimise the amount of gold used, by anchoring the gold nanoparticles to form a conductive pathway and making the gel and nanoparticle composite economically viable.



**Scheme 2-1:** Illustrating the purpose of a hydrogel with gold nanoparticles, to form a conductive bridge between So and an electrode.

### 2.1 Hydrogels

Gels consist of gelator molecules and solvents, the gelator molecules assemble into fibres, fibrils and bundles trapping the solvent molecules and restricting their flow.<sup>266–268</sup> The gelator molecules can be amino acids, peptides or naturally available polysaccharide polymers such as gelatin, agarose, carrageenan or alginate.<sup>269</sup> Synthetic polymers such as poly(vinyl alcohol), poly(ethyleneimine) and poly-N-isopropylacrylamide have also been used to form hydrogels.

The solvent molecules can also be either an organic solvent (organogels) or water (hydrogels). The mechanism of trapping the solvent molecules, by forming a cross-linking network can be via physical or chemical cross-linking, both lead to formation of fibres, fibrils and bundles. The name given to a gel is entirely dependent on the gelator molecule, the solvent and the gelation mechanism of cross-linking. For the purposes of this project only hydrogels will be considered.

## Chapter 2: Gold nanoparticles in hydrogels

Hydrogels retain a large quantity of water making them 'wet' and suitable for a number of biomedical applications such as drug delivery<sup>270</sup> and tissue engineering.<sup>271</sup> Hydrogels can be prepared via a supramolecular process using non-covalent interactions such as hydrogen bonding, electrostatic interactions and  $\pi$ - $\pi$  stacking or covalent bonds.<sup>267</sup> Some hydrogels respond to external stimuli and undergo a gel to liquid to gel transition, the stimuli can be temperature, pH, light, sonication or a change in solvent.

### 2.1.1 Hydrogel composites

Hydrogel composites can be prepared by the incorporation of either conductive gels or nanoparticles into non-conductive or conductive hydrogels. There are a number of examples of conductive gel and hydrogel composites in the literature that are used for biomedical applications.<sup>272-274</sup> Carbon nanoparticles, carbon nanotubes and metal nanoparticles have also been incorporated into hydrogels and have led to materials with biomedical applications.<sup>275-278,279</sup>

There are a number of examples in literature for the incorporation of metal nanoparticles into hydrogels, with the majority of the hydrogels being supramolecular<sup>280-287,288</sup> in nature, with few being polymeric and based on naturally occurring polysaccharides.<sup>150,166,202</sup> The use of naturally occurring polymer polysaccharides as hydrogels was chosen, to improve the economic viability of the project.

The literature was reviewed to identify if incorporation of gold nanoparticles into natural polymer-based hydrogels can be carried out with relative ease and if the hydrogel nanoparticle composite is conductive and suitable for application in a bio-electrochemical system.

There were no examples of hydrogels with metal nanoparticles being used in bio electrochemical systems reported in the literature to the best of our knowledge. However, carbon nanotube and hydrogel composites,<sup>289</sup> conductive polymers and hydrogel composites<sup>290,291</sup> have been used to improve electron transfer.

Liu *et al.*<sup>289</sup> have electrodeposited carbon nanotubes (CNT) and chitosan solution onto a carbon paper to obtain a chitosan / CNT composite. They were interested in improving the electron transfer efficiency in a bio-electrochemical system. The

## Chapter 2: Gold nanoparticles in hydrogels

chitosan / CNT composite was used as an anode in a dual chamber fuel cell that was inoculated with activated sludge from a waste water facility. Chronoamperometric measurements were recorded to understand the influence of the chitosan / CNT composite on the current generated compared to a control (just carbon paper). The current density of the chitosan / CNT composite was  $500 \text{ mA/m}^{-2}$  whereas the control was  $150 \text{ mA/m}^{-2}$ , proving that the composite does improve electron transfer leading to high current generation. This work proves that the use of hydrogel composites as anodes in bio-electrochemical systems is a viable hypothesis. The use of gold nanoparticles to improve electron transfer in bio-electrochemical systems has already been reviewed in Chapter 1 section 1.5.2.

There were two main ways of incorporating nanoparticles into hydrogels; one is to diffuse a solution of pre-formed nanoparticles into the hydrogel (dependent on hydrogel pore size and nanoparticle size) and the other was to use the gel structure itself as the stabilising/reducing agent for the formation of nanoparticles.<sup>287,292</sup> A mixture of above methods will be used to synthesise hydrogels containing gold nanoparticles.

### **2.2 Chapter aims and content**

In this chapter the synthesis of agarose gels containing gold nanoparticles will be discussed. The resultant gels with gold nanoparticles will be incorporated into a bio-electrochemical cell and the effect on current generation will be investigated. The gel with gold nanoparticles will be analysed by confocal microscopy after the bio-electrochemical study to understand biofilm formation by *S. aureus* on the electrodes.

### **2.3 Results and Discussion**

#### **2.3.1 Gold nanoparticle incorporation in agarose**

Agarose was chosen as the hydrogel to investigate as a hydrogel gold nanoparticle composite. Agarose is a non-ionic polysaccharide capable of absorbing ~99 % water to form a hydrogel.<sup>293,294</sup> Agarose is the neutral part of agar and is used for electrophoresis due to its high electro-osmosis compared to agar. It was traditionally extracted from the cell walls of red algae.<sup>295</sup>

## Chapter 2: Gold nanoparticles in hydrogels

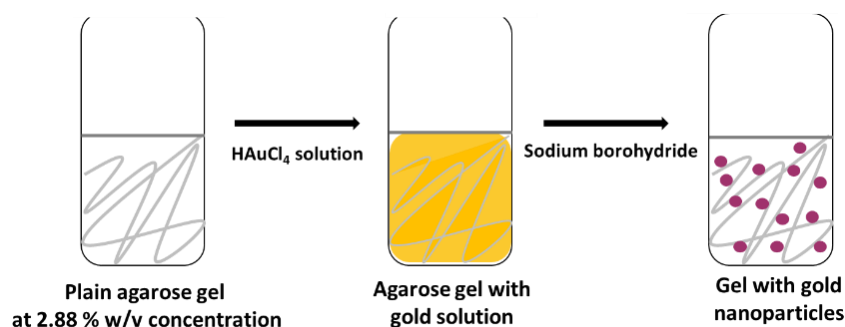
Agarose was chosen because of its thermo-responsive properties as it allows the gels to be moulded and reshaped as required. Its neutral nature makes it biocompatible and suitable as a substrate for human / bacterial cell growth. Its repeating unit has exposed hydroxyl groups<sup>296</sup> that allow for modification making it versatile for a number of applications and improvements.<sup>276,297</sup> Agarose consists of *D*-galactose and 3, 6-anhydro-*L*-galactopyranose linked by glycosidic bonds.<sup>293</sup> The agarose used in this project was obtained from Sigma and melts at ~85 °C and forms a gel at ~37 °C.

There are a number of examples of agarose with gold nanoparticles in the literature with one of them making a conductive hydrogel nanoparticle composite. <sup>298-300</sup> However these literature examples did not extend to testing the composites in a bio-electrochemical system.

Gold nanoparticles were incorporated into agarose using a similar method as described by Mohan *et al.* <sup>300-302</sup> It consisted of preparing an agarose gel at 2.88% w/v and diffusing a solution of chloroauric acid on top of the gel. Excess gold solution was removed and sodium borohydride was added to reduce Au<sup>3+</sup> to Au<sup>0</sup> (Scheme 2-2). The success of the reduction was evidenced by a colour change of the gel from yellow to purple as observed and described in the literature.<sup>299</sup> During the reduction any excess gold solution in the agarose gel leached out as black solution leaving agarose gel with gold nanoparticles behind. The obtained gels with gold nanoparticles were washed extensively in three changes of water to remove any ionic species. A control experiment with agarose gels containing brine solution was washed for the same time to prove the validity of the removal of ions (appendix).



## Chapter 2: Gold nanoparticles in hydrogels



**Scheme 2-2: Schematic of gold nanoparticle incorporation into agarose gel at 2.88 % w/v concentration**

The concentration of gold solution added on top of the agarose gel was  $\sim 250$  mM as per Faucher *et al.*,<sup>300</sup> since they observed a significant drop in resistance when agarose gel slabs were exposed to gold solutions at concentrations 200- 600 mM.

The agarose gel was analysed by UV-Vis spectroscopy to confirm that the colour change was due to the presence of gold nanoparticles (Figure 2-1). The spectrum showed a distinctive plasmon peak at  $\sim 550$  nm indicative of nanoparticles, compared to just agarose which has no significant absorption peaks. This further proves the presence of nanoparticles in the agarose gel.

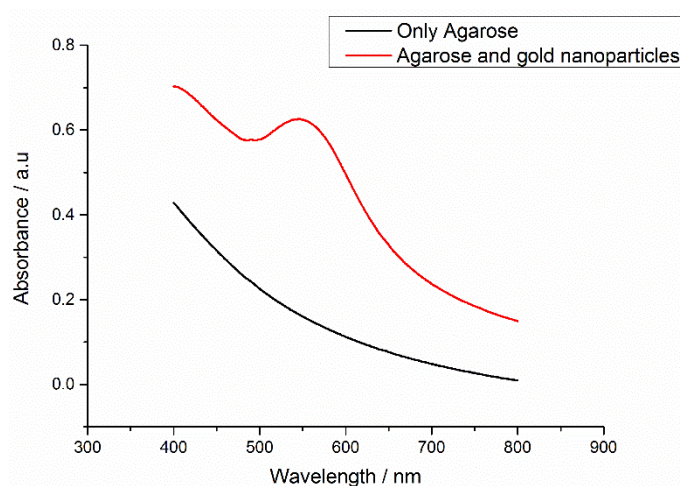


**Figure 2-1: UV-Vis spectrum of agarose with (red) and without (black) gold nanoparticles**

The agarose gels with gold nanoparticles were also analysed by TEM to identify the shape and position of the gold nanoparticles in respect to the agarose gel fibres (Figure 2-2). The images show a mixture of gold nanoparticles surrounded by gel structure as well as aggregates of gold nanoparticles forming long continuous structures within the gel.

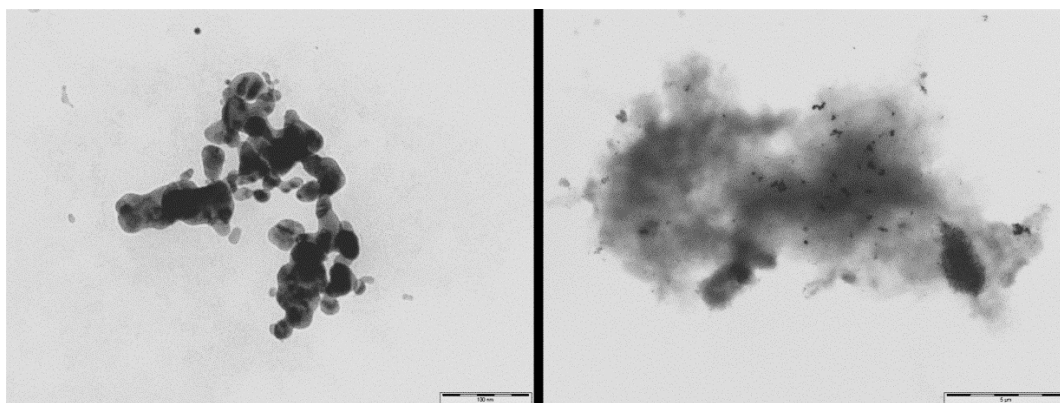
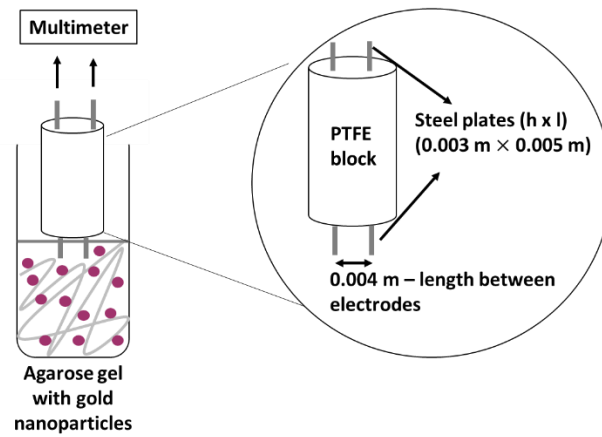


**Figure 2-2: HR-TEM images of agarose gels with gold nanoparticles. Scale bar 100 nm (left) and 5  $\mu\text{m}$  (right). The left image shows just gold nanoparticles agglomerating together to form an aggregated structure, the right image shows a gel cube in various shades of grey with the black spots representing gold nanoparticles.**

It was evident from the TEM images that the gold nanoparticles are not distributed along the gel fibres, but are instead localised to the water pockets within the agarose gel structure. This was similar to the behaviour observed by Faucher *et al.*<sup>300</sup> where the gold nanoparticles aggregate in the water pockets saturating the gel structure. This would lead to the use of large amounts of gold and mechanical instability as high gold nanoparticle concentration would cause brittleness in gel structure.<sup>274,303</sup> The conductivity of these gels was tested to see if the presence of the nanoparticles had any influence on how conductive the gels were compared to their absence.

### **2.3.1.1 Conductivity testing of agarose gels with gold nanoparticles**

A 'custom made' design consisting of a cylindrical PTFE block with two identical steel plates attached to it was used to measure the conductivity of these agarose gels with gold nanoparticles. The steel plates were pierced into the gel cylinders and the resistance was recorded using a multimeter.



**Scheme 2-3: Custom made design of equipment and its dimensions used to measure resistance of agarose gels with gold nanoparticles**

The resistance measurements were converted to resistivity using the length between the electrodes and the cross sectional area of the gel cylinder in contact with the steel electrodes. Resistance and resistivity are related by the equation below

$$\rho = R \frac{A}{l} \quad (5)$$

R is resistance / $\Omega$ ,  $\rho$  is resistivity /  $\Omega \text{ m}^{-1}$ , A is the cross sectional area perpendicular to the direction of the current /  $\text{m}^2$ , l is the length in between the electrodes / m. The cross sectional area A was calculated using dimensions shown in Scheme 2-3 and was found to be  $0.0015 \text{ m}^2$  (length  $\times$  height).

Resistance was converted to resistivity using equation (5) as below

$$\rho = R \frac{(0.0015 \text{ m}^2)}{(0.004 \text{ m})}$$

Conductivity ( $\sigma$  /  $\text{S m}^{-1}$ ) is the reciprocal of resistivity and was calculated as such

$$\sigma = \frac{1}{\rho} \quad (6)$$

The controls (no nanoparticles) and samples were measured a minimum of 3 times and an average value was used for analysis (Table 2-1).

**Table 2-1: Conductivity values for agarose only and agarose with gold nanoparticles**

<b>Name</b>	<b>Conductivity / Sm<sup>-1</sup></b>	<b>Volume of gel / ml</b>	<b>Gel Concentration / % w/v</b>
<b>Agarose only</b>	$5.39 \times 10^{-7} \pm 7.92 \times 10^{-9}$	0.30	2.88
<b>Agarose with gold nanoparticles</b>	$1.66 \times 10^{-5} \pm 1.94 \times 10^{-7}$	0.30	2.88

It was seen from the conductivity data that the presence of gold nanoparticles in an agarose gel does increase the conductivity ~30 times compared to no nanoparticles. However, this increase is not sufficient to be applicable in a bio electrochemical system and the distribution of gold nanoparticles within the agarose gel structure has to be improved to reduce the use of gold and increase conductivity.

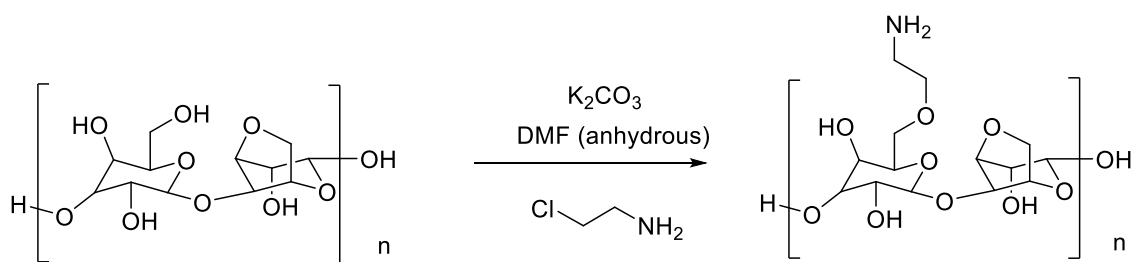
#### **2.4 Modification of agarose (MAgarose)**

The presence of gold affinity groups along the gel fibres would allow for the control of gold nanoparticles distribution through the gel network, allowing to decrease the amount of gold content while increasing conductivity.

Amine groups were known to stabilise gold nanoparticle formation by a combination of Van der Waals and Au-N interactions which are labile in nature.<sup>157,304–309</sup> Incorporating these groups into agarose should provide the control of gold nanoparticle distribution.

A simple literature method was followed where agarose (1 eq) was dissolved in DMF and reacted with potassium carbonate (1.5 eq)<sup>310–312</sup> and 2-chloroethylamine hydrochloride (1.5 eq) at 85 °C in an overnight reaction (Scheme 2-4).<sup>313</sup> DMF was chosen as the solvent as agarose was still in solution and did not form a gel even at room temperature.<sup>314</sup>

## Chapter 2: Gold nanoparticles in hydrogels



**Scheme 2-4: Synthesis of aminated agarose**

The mechanism was thought to involve the formation of ethyleneimine which was ring opened by the free hydroxyl group on agarose structure, leading to an amine incorporation.<sup>315,316</sup> The product was quenched with hydrochloric acid to remove any free aziridine groups and dialysed extensively for three days with three changes of water.

Gold nanoparticles were incorporated in the MAgarose (2.88 % w/v gel concentration) as per section 2.3.1, and these gels will be referred to as GelAuNP throughout the project. During gold nanoparticle incorporation, on addition of sodium borohydride solution to the gel, the gel started leaching out black solution of excess gold (Figure 2-3).

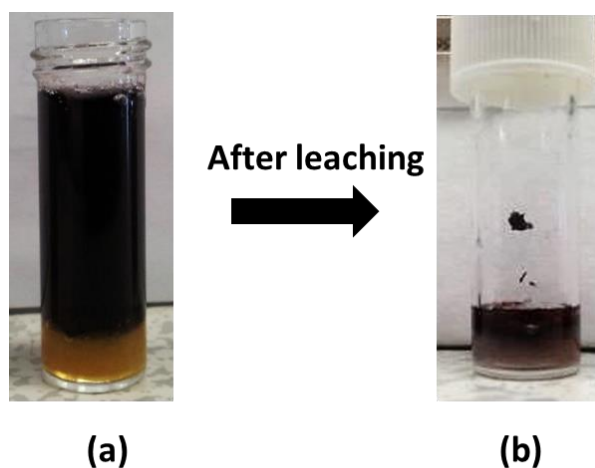


**Figure 2-3: (a) Leaching of excess gold solution during gold nanoparticles incorporation into MAgarose (b) The resultant GelAuNP after leaching**

## Chapter 2: Gold nanoparticles in hydrogels

The conductivity of GelAuNP was also measured in the same way as in sect 2.3.1.1 (Table 2-1).

**Table 2-2: Conductivity values of the gels with gold nanoparticles**

<b>Name</b>	<b>Conductivity / <math>\text{Sm}^{-1}</math></b>	<b>Volume of gel / ml</b>	<b>Gel Concentration / % w/v</b>
<b>Agarose only</b>	$5.39 \times 10^{-7} \pm 7.92 \times 10^{-9}$	0.30	2.88
<b>Agarose with gold nanoparticles</b>	$1.66 \times 10^{-5} \pm 1.94 \times 10^{-7}$	0.30	2.88
<b>GelAuNP</b>	$7.27 \times 10^{-3} \pm 2.05 \times 10^{-4}$	0.30	2.88

The conductivity of GelAuNP was  $\sim 13500$  times higher than the control with no nanoparticles, this was significantly higher than agarose with gold nanoparticles. GelAuNP was also  $\sim 400$  times more conductive than agarose with gold nanoparticles, both these observations prove that modification of agarose produces gel structure capable of forming a conductive gel when gold nanoparticles are incorporated.

### 2.5 Characterisation of MAgarose

As commercially available agarose is hygroscopic, MAgarose was lyophilised and extensively dried under vacuum to remove any residual water and used for subsequent characterisations.

#### 2.5.1 Elemental analysis

Elemental analysis was performed on both agarose and MAgarose to detect nitrogen presence in MAgarose, but no nitrogen content was detected in MAgarose (Table 2-3). Since nitrogen was not detected by CHN analysis, the calculated values of %CHN for MAgarose were assumed to be the same as agarose.

**Table 2-3: CHN results for agarose and aminated agarose compared to expected values. Calc - refers to expected values, Obs - refers to observed values.**

Name	C %		H %		N %		Rest %	
	Calc	Obs	Calc	Obs	Calc	Obs	Calc	Obs
<b>Agarose</b>	47.06	46.86	5.92	6.06	-	-	47.01	47.09
<b>MAgarose</b>	47.06	45.43	5.92	6.14	4.01	-	47.01	48.43

The observed values for the %CHN do not compare to the expected values, this is because of the agarose and MAgarose gels hygroscopic properties. The values could not be improved on extensive drying under vacuum or by extensive drying with minimal heating (50 °C) under vacuum for a minimum of three days.

The % CHN found experimentally and the % CHN calculated can be used to determine the % of water in MAgarose. The presence of water was found to be ~3.47 %, which was quite high. The values used for this calculation are provided below (Table 2-4). The calculated values were optimised by least square fitting model to the experimental value. This gave a result of ~ 1.5:1 agarose to water in molar ratio.

**Table 2-4: Table showing how the % CH can be used to calculate presence of water in agarose**

Name	%C	%H
<b>Calculated for one molecule of water</b>	45.43	6.11
<b>Found experimentally</b>	45.43	6.14

By comparing the values of Table 2-3 to the values in Table 2-4, the number of water molecules is ca~ 0.6 per repeat unit, which equates to the sample having very little water which is impossible to incorporate under synthetic conditions.

An alternative method of characterising the presence of nitrogen in MAgarose was attempted using techniques such as FTIR and NMR.

### 2.5.2 FTIR Spectroscopy

Lyophilised MAgarose and agarose were analysed by FTIR spectroscopy to identify common functional groups within agarose and MAgarose such as O-H, C-O and C-H,

in addition to the N-H stretch / bend and C-N stretch in MAgarose (Figure 2-4). The spectra were compared to agarose FTIR available from the Sigma website and literature.<sup>314</sup>

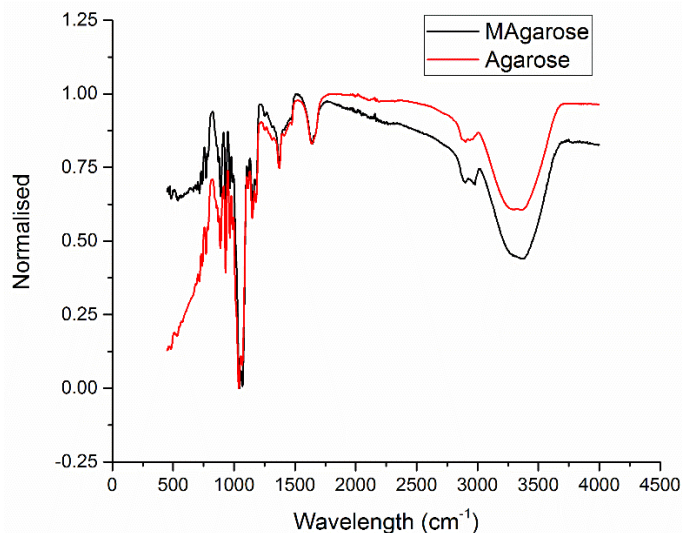


**Figure 2-4: FTIR spectrum of agarose and MAgarose with normalised transmittance on the y axis**

FTIR spectrum of agarose compares well with literature values, displaying the characteristic peaks for O-H stretch of the hydroxyl groups and C-H stretches for CH and CH<sub>2</sub> groups present within agarose (Table 2-5).<sup>317</sup> The C-O stretches were also identified for the glycosidic linkage of the galactose units.<sup>314</sup> The stretch at ~1640 cm<sup>-1</sup> is observed in literature and also in FTIR spectrum provided by Sigma for agarose and MAgarose and in both cases was attributed to residual bound water.<sup>314</sup> In their respective FTIR spectra the peak positions and splitting patterns are almost identical for both agarose and MAgarose.

**Table 2-5: IR stretches of agarose and MAgarose**

IR stretches	Agarose / cm <sup>-1</sup>	MAgarose / cm <sup>-1</sup>
$\nu$ (O-H) H- bonded	3360	3375
$\nu$ (C-H) stretch	2942	2974
$\nu$ (H-O-H) bound water	1638	1644
$\nu$ (N-H) bend	-	1644
$\nu$ (C-H) rock	1372	1372
$\nu$ (C-O) stretch	1066	1068
$\nu$ (C-N) stretch	-	1068



The stretches associated with N-H and O-H are usually broad and since both agarose and MAgarose have a large number of O-H groups was not possible to identify the N-H stretch exclusively. The C-N stretch overlaps with C-O making interpretation of nitrogen presence within MAgarose inconclusive and concluding that the FTIR spectra of both agarose and MAgarose are identical in appearance. FTIR spectroscopy does not provide any evidence of amine incorporation into agarose.

### 2.5.3 NMR spectroscopy

NMR spectra were also recorded in  $d^6$ -DMSO for agarose and MAgarose to identify the extra protons in MAgarose compared to agarose. An overlaid  $^1\text{H}$  spectra shows the similarity of peak position and the splitting pattern (Figure 2-5). Both the spectra show peaks corresponding to the various CH's and CH<sub>2</sub>'s present within the monomer repeating units of agarose. The CH's were expected at  $\sim 3$  ppm and the protons near quaternary carbons flanked by an oxygen and a hydroxyl group to be at  $\sim 5$  ppm. The appearance of the agarose  $^1\text{H}$  spectrum compared well with literature spectrum. The literature spectrum was recorded at  $80^\circ\text{C}$  and had better resolution.<sup>318</sup>

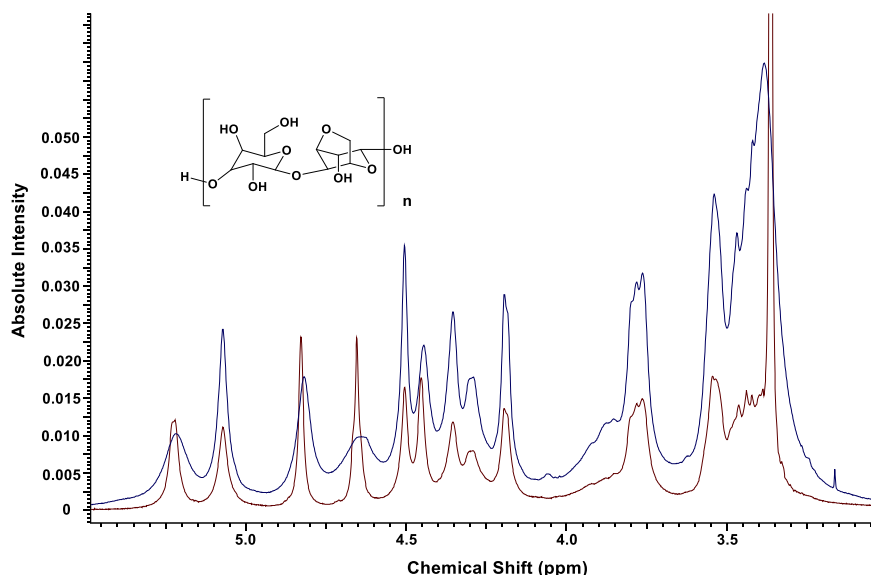


**Figure 2-5: Overlaid  $^1\text{H}$  spectra of agarose (red) and MAgarose (blue) in  $d^6$ -DMSO**

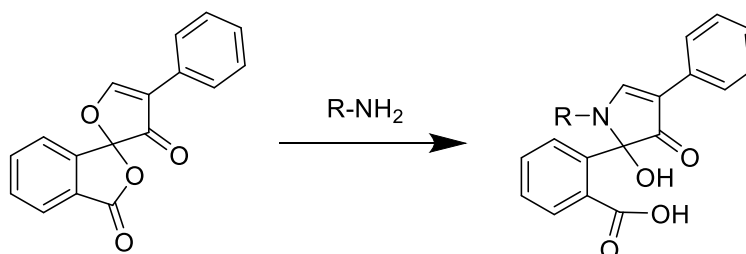
Both the spectra show residual water peaks at  $\sim 3.35$  ppm. On integration of the agarose spectrum the expected protons were found, but in the case of MAgarose only two extra protons were observed, where four extra protons from the two extra CH<sub>2</sub>'s were expected. The same conclusion as with FTIR spectroscopy was reached, the  $^1\text{H}$  spectra are identical for both agarose and MAgarose. Simple analytical

methods were also investigated to identify if the amination of agarose was successful and also to elucidate the structure of MAgarose.

Since elemental analysis, FTIR or NMR were unable to prove the presence of nitrogen a more sensitive technique such as fluorescence was used. Elemental analysis had an accuracy of  $\pm 0.15\%$  which was quite high, but fluorescence was expected to be more sensitive.

#### 2.5.4 Fluorometric assay

The sensitivity of fluorescence detection is dependent on the instrument and the fluorescence of the fluorophore being investigated. To investigate using fluorescence technique, a simple fluorometric assay involving fluorescamine was attempted (Scheme 2-5).<sup>319,320</sup> Fluorescamine reacts selectively with primary amines to form a product that is fluorescent at 475 nm while fluorescamine on its own is non-fluorescent, it can detect the presence of nitrogen to picomole values.<sup>321</sup> MAgarose should react with fluorescamine to give a fluorescent product, while the same assay with agarose should give a non-fluorescent product, proving the success of the amination reaction and the presence of nitrogen in MAgarose.



**Scheme 2-5: Reaction of fluorescamine with primary amines**

A series of known concentrations of ethanolamine (primary amine) was reacted with fluorescamine in a solution of DMSO with 2% water to plot a calibration graph of fluorescence vs concentration of amine. DMSO with 2% water was chosen as the solvent, as both agarose and MAgarose are soluble in this solution at room temperature with no gelation and it had the right pH for fluorometric assay.<sup>322</sup>

Fluorescence emission spectra were recorded between 400-750 nm with excitation at 390 nm and the baseline for each fluorescence measurement was corrected manually to account for the difference in baseline starting points. The fluorescence spectrum obtained at a concentration of 0.03 mM was provided below (Figure 2-6).

## Chapter 2: Gold nanoparticles in hydrogels

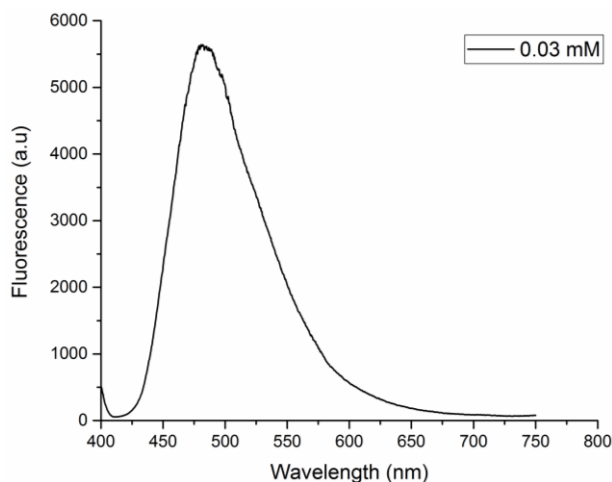


**Figure 2-6: Fluorescence spectrum of ethanolamine at a concentration of 0.03 mM on reaction with fluorescamine**

The fluorescence at 475 nm was recorded for the different ethanolamine concentrations and a calibration graph was plotted (Figure 2-7). The intercept was set through the origin, as the data was normalised to 0 mM.

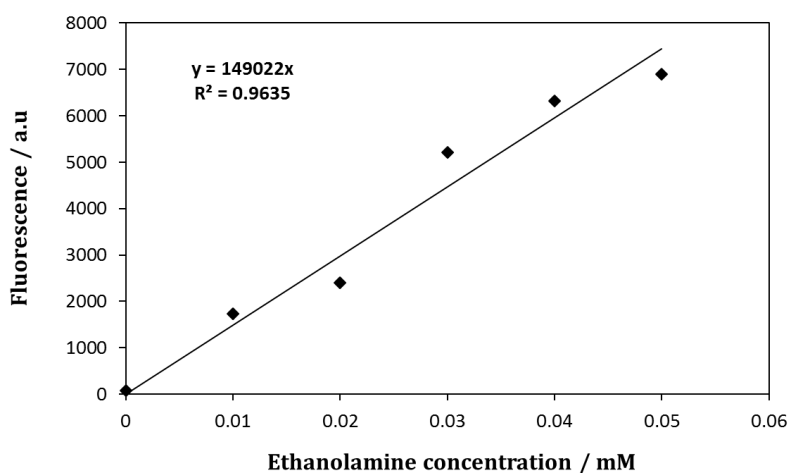


**Figure 2-7: Calibration graph of fluorescence vs concentration of ethanolamine normalised to solvent**

Linear regression was carried out on the data to obtain a calibration graph. The calibration graph was used to calculate the concentration of amine in both agarose and MAgarose. The fluorometric assay was carried out by soaking a known amount of agarose and MAgarose gels in a solution of fluorescamine and recording their fluorescence spectra after 20 min (Figure 2-8). This method provides a quantitative way of determining the presence of nitrogen in agarose and MAgarose. The spectrum shows that agarose has significant fluorescence, but MAgarose has considerably higher fluorescence. Since commercially available agarose was used

## Chapter 2: Gold nanoparticles in hydrogels

throughout the project, there might have been some amine in natural agarose that lead to this fluorescence.

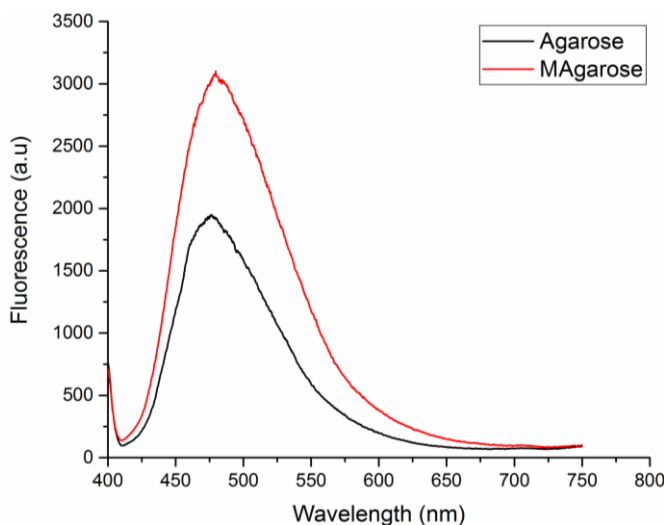


**Figure 2-8: Fluorescence spectrum of MAgarose (red) and agarose (black)**

The fluorescence at 475 nm was recorded for both agarose and MAgarose and using the calibration graph (Figure 2-7) the concentration of amine was determined.

**Table 2-6: Fluorescence values for Agarose and MAgarose**

Name of gel	Fluorescence at 475 nm	Concentration of amine / mM
Agarose	1824	$1.22 \times 10^{-2}$
MAgarose	2879	$1.93 \times 10^{-2}$

The % of nitrogen was calculated following the procedure described below with a few assumptions

- MAgarose repeating unit has a molecular weight (mol.wt) of  $306.27 \text{ g mol}^{-1}$
- The mol. wt of agarose is  $120,000 \text{ g mol}^{-1}$
- The number of repeating units ( $\frac{\text{mol.wt of agarose}}{\text{mol.wt of repeat unit}}$ ) are 391.8

$$\text{The expected moles of amine} = \frac{\text{Gel weight used for fluorometric assay}}{\text{Molecular weight of repeating unit}} \quad (7)$$

$$\text{The expected moles of amine} = \frac{1.55 \times 10^{-3} \text{ g}}{306.27 \text{ g mol}^{-1}} = 5.06 \times 10^{-6} \text{ mol}$$

$$\text{The observed moles of amine} = \frac{\text{Concentration of amine} \times \text{volume of solution}}{1000} \quad (8)$$

## Chapter 2: Gold nanoparticles in hydrogels

$$\text{The observed moles of amine} = \frac{1.95 \times 10^{-5} \text{ M} \times 1 \text{ ml}}{1000} = 1.93 \times 10^{-8} \text{ mol}$$

$$\text{The \% yield} = \frac{\text{Observed moles}}{\text{Expected moles}} = \frac{1.95 \times 10^{-8}}{5.06 \times 10^{-6}} \times 100 = 0.39 \%$$

$$\text{The number (no.) of amine groups} = \frac{\% \text{yield}}{100} \times \text{no. of repeating units} \quad (9)$$

$$\text{The no. of amine groups} = \frac{0.39}{100} \times 391.8 = 1.51 \text{ amine groups}$$

$$\text{The \% nitrogen} = \frac{\text{Mol. wt of nitrogen} \times \text{No. of amine groups}}{\text{Mol. wt of agarose}} \times 100 \quad (10)$$

$$\text{The \% nitrogen} = \frac{14 \text{ g mol}^{-1} \times 1.51}{120,000} \times 100 = 0.018\%$$

This proves that there is nitrogen present in MAgarose by fluorometric assay, agarose fluorescence was also analysed using equations 7-10, assuming that there is nitrogen presence and making the same assumptions about mol.wt and repeating units. The values obtained are summarised in a table below (Table 2-7).

**Table 2-7: The % of Nitrogen in agarose and MAgarose by fluorometric assay**

Name	Expected moles /mol	Observed moles / mol	% Yield	% Nitrogen
<b>MAgarose</b>	$5.06 \times 10^{-6}$	$1.93 \times 10^{-8}$	0.39	0.018
<b>Agarose</b>	$9.73 \times 10^{-6}$	$1.22 \times 10^{-8}$	0.13	0.006

Even though there was nitrogen content detected in commercially available agarose, the MAgarose had ~ 3 times more nitrogen content than agarose. But from Figure 2-8, the fluorescence of MAgarose was only slightly higher than agarose, this was because even though the fluorescence of agarose was only little lower than MAgarose the moles of agarose dissolved in solution was ~2 times more than MAgarose. It could be that, because the % of nitrogen detected was low elemental analysis, NMR and FTIR could not show any nitrogen presence or difference in the MAgarose structure compared to agarose.

### 2.5.5 $T_{gel}$ values

When a gelator is dissolved in water, it forms chains by interlocking on itself called a 'sol', this is the first stage of gel formation. When the process continues forming more interlocking chains until a three-dimensional network is formed, the chains become insoluble forming a 'gel'.<sup>323</sup> This process of interlocking depending on the gelator and can be controlled by temperature, pH, sonication or by solvent. For a gelator such as agarose this is controlled by temperature. The temperature at which agarose reverts to being a 'sol' is called the gel transition temperature and this on comparison would show that the structures of MAgarose and agarose are different. Both agarose and MAgarose were tested for their  $T_{gel}$ , temperatures using a temperature controlled oil bath (Table 2-8).

**Table 2-8:  $T_{gel}$  values of agarose and MAgarose**

Name	Gel concentration % (w/v)	Gel volume / ml	Temperature / °C
Agarose	2.88	0.30	97.8 - 100.1
MAgarose	2.88	0.30	80.1 - 82.7

The  $T_{gel}$  of the MAgarose was  $\sim 17$  °C lower than agarose, indicating that it has physical properties different to agarose. Since the  $T_{gel}$  value was lower it could be said that compared to agarose, MAgarose reverts to being a 'sol' with much less temperature stimulus than agarose concluding that the gel strength was lower for MAgarose than agarose. Since FTIR and NMR suggest the structure of MAgarose to be identical to agarose, the difference in physical properties can be linked to their molecular weight. Viscometry was used to determine if the molecular weight of MAgarose and agarose was different.

### 2.5.6 Viscometry

If agarose was partially hydrolysed during the synthesis of MAgarose, then the molecular weight of MAgarose would be lower than agarose. In general, molecular weight of polymers can be determined using techniques such as size exclusion chromatography, sedimentation and diffusion. A number average molecular weight

## Chapter 2: Gold nanoparticles in hydrogels

can be determined, as each polymer chain is polymerised to a certain degree and has a certain mass. The number average molecular weight of polymers is quoted as

$$M_n = \frac{\sum N_i M_i}{\sum N_i}$$

Where  $M_n$  – is the number average molecular weight,  $M_i$  – is the molecular weight of a chain,  $N_i$  – is the number of chains with that particular molecular weight.<sup>324</sup>

Viscosity average molecular weight can also be calculated by comparing the viscosity of agarose and MAgarose. This can prove that agarose and MAgarose have different physical properties and are different in structure

Intrinsic viscosity and viscosity average molecular weight are related by Mark-Houwink equation<sup>325-327</sup>

$$[\eta] = KM^\alpha \quad (11)$$

$[\eta]$  represents intrinsic viscosity,  $K$  and  $\alpha$  are constants specific to polymer, solvent and temperature.  $K$  and  $\alpha$  can be determined for a specific polymer by measuring the polymers viscosities over a range of molecular weights (determined using absolute techniques such as size exclusion chromatography, sedimentation and diffusion) and fitting the data to a straight line as in equation (6)<sup>328,329</sup>

$$\log [\eta] = \log K + \alpha \log M \quad (12)$$

The value of  $\alpha$  gives an indication of the type of polymer present in a particular solvent, so  $0.5 < \alpha < 0.8$  for flexible random coils in good solvent,  $0.8 < \alpha < 1.0$  for inherently stiff molecules such as DNA and  $1.0 < \alpha < 1.7$  for highly extended chains such as polyelectrolytes in low concentrations.<sup>327,330</sup>

Rochas and Lahaye have established the constants  $K$  and  $\alpha$  for agarose in a solution of sodium thiocyanate at a concentration of 0.75 M and found them to be 0.07 and 0.72 respectively.<sup>322</sup> The Mark-Houwink equation for agarose is shown below as equation (13)

$$[\eta] = 0.07M^{0.72} \quad (13)$$

## Chapter 2: Gold nanoparticles in hydrogels

$[\eta]$  can be calculated using mathematical equations such as Huggins or Kraemer using the viscosities of polymer at different dilute concentrations.<sup>331,332</sup> The Huggins equation (14) and Kraemer equation (15) when plotted as a straight line graph give the intercept of the slope as the intrinsic viscosity.

$$\frac{\eta_{sp}}{c} = [\eta] + k_H[\eta]^2 c \quad (14)$$

$\eta_{sp}$  is specific viscosity,  $k_H$  is the Huggins constant and  $c$  is the concentration/gml<sup>-1</sup>.  $\frac{\eta_{sp}}{c}$  is also referred to as reduced viscosity.

$$\frac{\ln \eta_{rel}}{c} = [\eta] + k_K[\eta]^2 c \quad (15)$$

$\eta_{rel}$  is relative viscosity,  $k_K$  is the Kraemer constant and  $c$  is the concentration / gml<sup>-1</sup>.  $\frac{\ln \eta_{rel}}{c}$  is also referred to as inherent viscosity.

$$\text{Where } \eta_{sp} = \eta_{rel} - 1 = \frac{\eta}{\eta_0} - 1 \quad (16)$$

$\eta$  is the measured viscosity of the polymer solution and  $\eta_0$  is the viscosity of pure solution. The equations (11) – (16)<sup>329,330,333–336</sup> were used to determine the viscosity average molecular weight of agarose and MAgarose in solution of sodium thiocyanate at 0.75 M. The viscosity of sodium thiocyanate solution of concentration 0.75 M was found to be 0.7713 cP. The viscosity of agarose and MAgarose was measured at different concentrations using Brookfield rotational rheometer at a shear rate ramp at 30 °C. Agarose shows a ‘non-Newtonian’ type behaviour where the viscosity observed is dependent on shear rate comparing well with literature.<sup>337,338,339</sup> The viscosities used for analysis were collected at the same shear rate for agarose (Table 2-9).

**Table 2-9: Viscosity values of agarose at different concentrations, same shear rate**

Agarose		
$c / \text{gml}^{-1}$	$\eta / \text{cP}$	$\frac{\ln \eta_{rel}}{c}$
$8.45 \times 10^{-03}$	$1.70 \times 10^1$	$3.66 \times 10^2$
$1.86 \times 10^{-02}$	$8.32 \times 10^1$	$2.52 \times 10^2$



$1.06 \times 10^{-02}$	$3.00 \times 10^1$	$3.45 \times 10^2$
$1.46 \times 10^{-02}$	$3.90 \times 10^1$	$2.69 \times 10^2$
$1.27 \times 10^{-02}$	$3.16 \times 10^1$	$2.92 \times 10^2$

The values in Table 2-9 and equation (15) were used to plot a straight line with the intercept as  $[\eta]$  (Figure 2-9). Equation (15) was chosen to plot the graph as this relationship showed a better linear regression fit than equation (14) and also to minimise the dependence of viscosity on concentration even at small concentration values.<sup>333,334</sup> The intercept was found to be 461.26 cP, and was used to calculate the viscosity average molecular weight using equation (11).

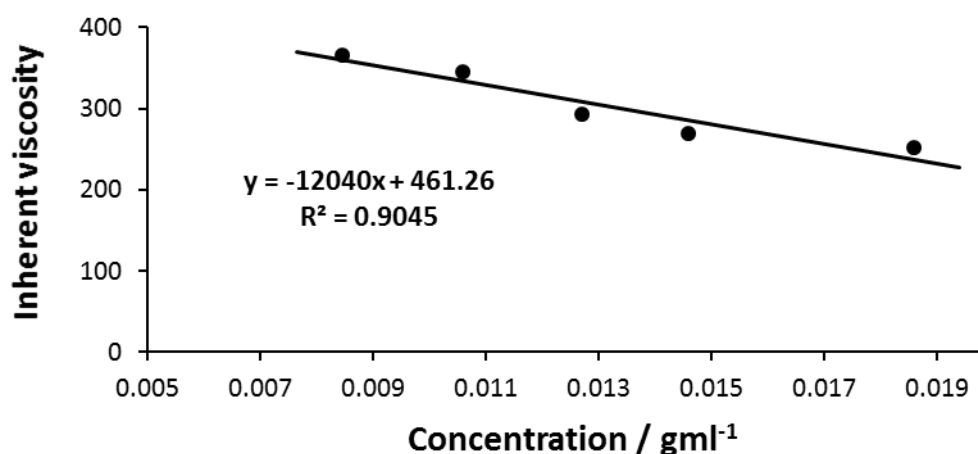


Figure 2-9: Inherent viscosity vs concentration plot of agarose

The viscosity average molecular weight calculated in Table 2-10 compared well with literature values.<sup>340-342</sup> In one instance<sup>342</sup> the viscosity average molecular weight was slightly higher than the value quoted in the literature, this could be due to the use of different commercially available grades of agarose and the method of viscosity measurements.

Table 2-10: Intrinsic viscosity and viscosity average molecular weight of agarose

Intrinsic viscosity / mlg <sup>-1</sup>	Viscosity average molecular weight
$4.61 \times 10^2$	$2.01 \times 10^5$

Similarly, the viscosity average molecular weight of MAgarose was also determined. However, the viscosity values obtained for MAgarose showed a 'Newtonian type' behaviour where the viscosity was not dependent on shear rate. To keep consistency, the viscosity values obtained at low shear rate were used for analysis for MAgarose (Table 2-11).

**Table 2-11: Viscosity values of MAgarose at different concentrations, same shear rate**

<b>MAgarose</b>		
$c / \text{gml}^{-1}$	$\eta / \text{cP}$	$\frac{\ln \eta_{rel}}{c}$
$1.96 \times 10^2$	3.42	$7.62 \times 10^1$
$3.47 \times 10^2$	9.39	$7.20 \times 10^1$
$6.51 \times 10^2$	$8.07 \times 10^1$	$7.14 \times 10^1$
$8.90 \times 10^2$	$1.04 \times 10^2$	$5.52 \times 10^1$
$5.00 \times 10^2$	$1.93 \times 10^2$	$6.44 \times 10^1$

The values in Table 2-11 and equation (9) were used to plot a straight line with the intercept as  $[\eta]$  (Figure 2-10). The intercept was found to be 81.388 cP, and was used to calculate the viscosity average molecular weight using equation (11).

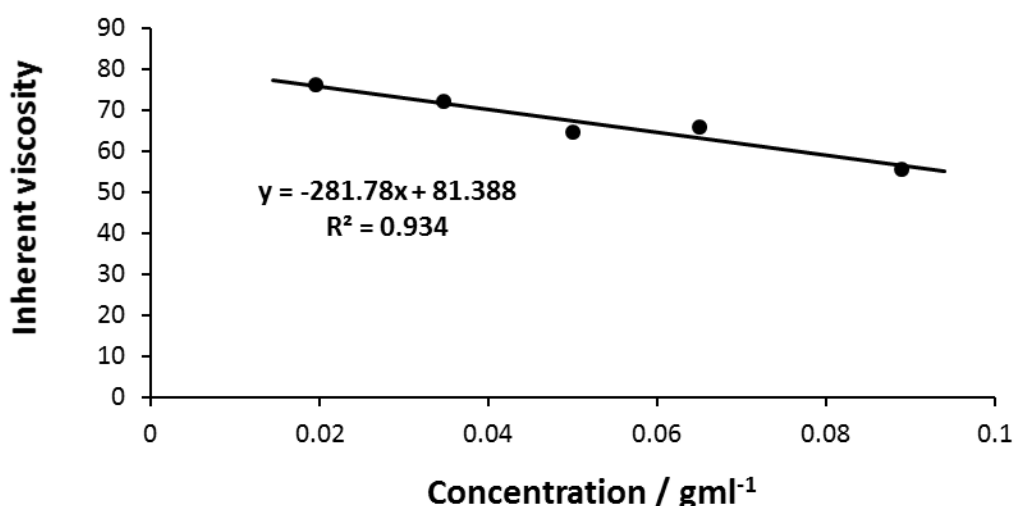


**Figure 2-10: Inherent viscosity vs concentration plot for MAgarose**

It is immediately apparent that the intrinsic viscosity of MAgarose is much lower than agarose, almost  $\sim 5.6$  times lower. It was also apparent that a much higher concentration of MAgarose had to be used to record viscosity values at an

observable range similar to agarose. Both the intrinsic viscosity values and the viscosity average molecular weights of agarose and MAgarose were summarised in the table below (Table 2-12).

**Table 2-12: Intrinsic viscosity and viscosity average molecular weight of agarose and MAgarose**

<b>Name of gel</b>	<b>Intrinsic viscosity / mlg<sup>-1</sup></b>	<b>Viscosity average molecular weight</b>
<b>MAgarose</b>	$8.14 \times 10^1$	$1.81 \times 10^4$
<b>Agarose</b>	$4.61 \times 10^2$	$2.01 \times 10^5$

There is a significant difference in the viscosity average molecular weight of MAgarose compared to agarose with MAgarose having a value  $\sim 11$  times smaller than agarose. This further corroborates the behaviours of both gels as either Newtonian or non-Newtonian and also MAgarose forming a less viscous solution even at a much higher concentration than agarose (Table 2-11). This could be because of the synthetic conditions involved in the preparation of MAgarose, as MAgarose is exposed to alkali conditions at high temperatures and the presence of water (hygroscopic nature of agarose and MAgarose), these might be affecting the viscosity nature of agarose by hydrolysing it.<sup>343</sup>

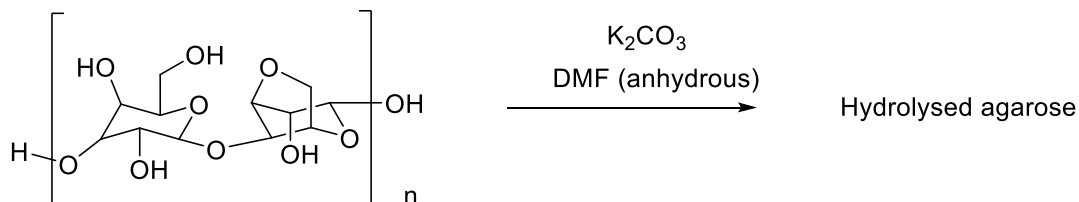
However, Viscometry proves that there is a difference in physical properties and gel strength between agarose and MAgarose. Some control experiments were carried out to identify a pattern between hydrolysis, viscosity and conductivity, since a gel with low viscosity (MAgarose) seems to form the most conductive gel with gold nanoparticles (GelAuNP).

### **2.5.7 Control experiments**

From Viscometry measurements it was proven that MAgarose and agarose structures and physical properties are different, this was attributed the presence of water in agarose during the synthetic procedure of MAgarose leading to hydrolysis of agarose. To identify the extent of agarose hydrolysis to form MAgarose, control experiments with the addition of different amounts of water were attempted.

### 2.5.7.1 Agarose hydrolysis

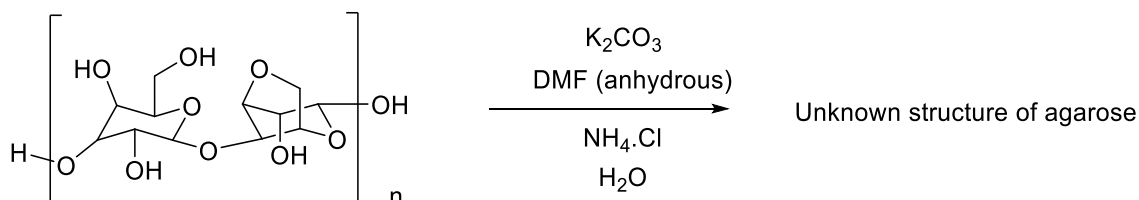
A control experiment using only agarose and potassium carbonate was carried out in the absence of 2-chloroethylamine to hydrolyse agarose under mildly alkaline conditions (Scheme 2-6), the equivalence between base and agarose was same as in section 2.4. The obtained gel was lyophilised and used for subsequent analysis.



**Scheme 2-6: Schematic showing the control experiment to hydrolyse agarose**

### 2.5.7.2 Control experiments with ammonium chloride

Control experiments using agarose, potassium carbonate, ammonium chloride and addition of different amount of water was carried out, to understand the role of 2-chloroethylamine in the preparation of MAgarose under partial hydrolysis (Scheme 2-7). The equivalence between base, agarose and amine was the same as 2.4 and the obtained gel was lyophilised and used for subsequent analysis.



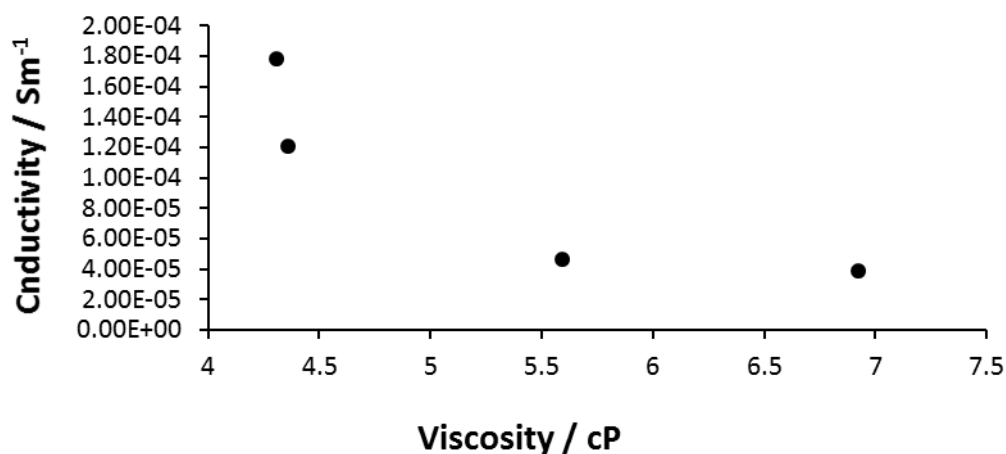
**Scheme 2-7: Schematic of the control reaction with ammonium chloride and known amount of water**

The viscosity and the conductivity of these control gels was investigated in a similar way to sections 2.5.6 and 2.3.1.1. The values are summarised in a table below (Table 2-13), conductivity measurements for one of the control gels with 0.1 % (v/v) water was not recorded, but the values available were used to plot a graph of viscosity vs conductivity for ammonium chloride reactions. This should give an indication of whether viscosity affects conductivity and also if the structure of MAgarose resembles partially hydrolysed agarose (Figure 2-11).

**Table 2-13: Viscosity and conductivity values for control experiments**

Name	% (v/v) Water	Viscosity / cP	Conductivity / $\text{Sm}^{-1}$
<b>Hydrolysed agarose (2.5.7.1)</b>	0	$1.43 \times 10^1$	$5.81 \times 10^{-5}$
<b>Ammonium chloride with known amount of water (2.5.7.2)</b>	0	4.31	$1.78 \times 10^{-4}$
	0.05	4.36	$1.21 \times 10^{-4}$
	0.10	4.68	-----
	0.50	5.59	$4.61 \times 10^{-5}$
	1.00	6.92	$3.88 \times 10^{-5}$

The viscosity of completely hydrolysed agarose was much higher and the conductivity was lower, compared to the experiments where ammonium chloride and known amount of water were used, this proves that MAgarose is not completely hydrolysed agarose. The viscosity values for ammonium chloride experiments were slightly closer to the value obtained for MAgarose (Table 2-11) however only 0 and 0.05 % (v/v) seem to have high conductivity values with low viscosity values.

**Figure 2-11: Conductivity vs viscosity plot of control experiments with ammonium chloride using values from Table 2-13**

From Figure 2-11, it is apparent that as viscosity increases the conductivity decreases, this supports the previous found pattern between agarose and MAgarose. A plot of viscosity vs ammonium chloride with known amounts of % (v/v) water added was also considered to identify if the reason MAgarose has a lower viscosity,

is because of the presence of minute amount of water during the synthesis of MAgarose (Figure 2-12).

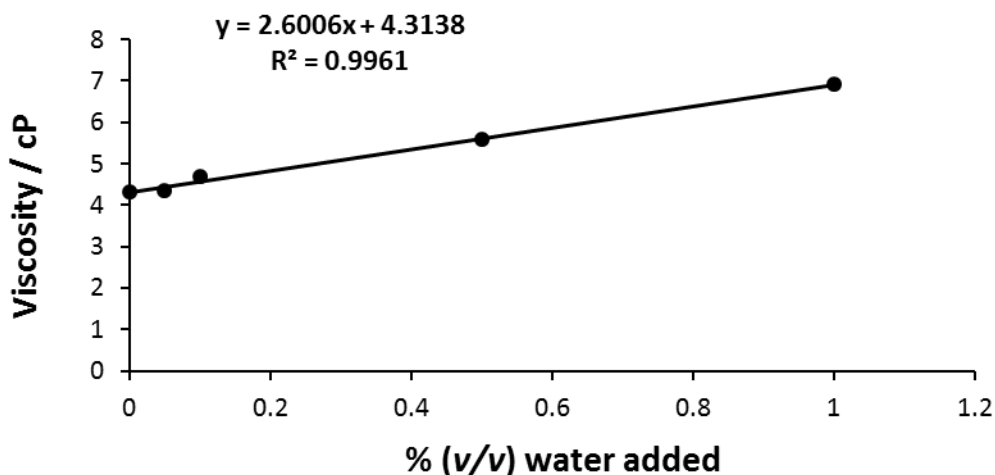


**Figure 2-12: Viscosity vs % (v/v) water added (refers to ammonium chloride experiments with known amount of water added) plot for ammonium chloride experiments**

The plot shows a linear relationship between viscosity and the % (v/v) water added in the control experiments, this further corroborates the presence of water during the synthesis of MAgarose. The viscosity of MAgarose was in the 3 – 4 cP range (for the same gelator concentration), this corresponds to the lowest % (v/v) water addition. Figure 2-11 correlates the lowest viscosity values to highest conductivity in the presence of ammonium chloride with known amounts of water. Both of these observations prove that MAgarose is partially hydrolysed agarose with some amine group incorporation and these control experiments support both the viscosity measurements and the results of fluorometric assay.

The GelAuNP was investigated for its applicability in a bio-electrochemical system without knowing its structure.

## **2.6 Gold nanoparticle incorporation**

After incorporation of gold nanoparticles into GelAuNP, the gel formed two distinct bands of colours purple and pink. The purple colour was at the top near the meniscus of the gel, while the pink colour was at the bottom (Figure 2-13).



**Figure 2-13: Gel obtained after reduction showing two distinct coloured bands.**

The bands were analysed by HR-TEM to get an understanding of the nanoparticle size distribution and their position relative to the agarose fibres (Figure 2-14).

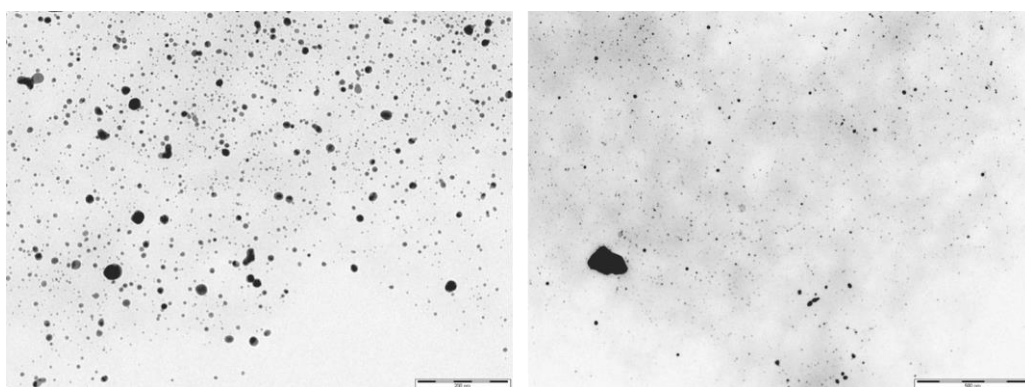


**Figure 2-14: HR-TEM images of purple coloured gel, scale bar 200 nm and pink coloured gel, scale bar 500 nm**

The TEM images show well distributed gold nanoparticles within the gel structure, the gold nanoparticles were also analysed by Image J software to get a distribution of nanoparticle size (Figure 2-15). The top of the gel contained large nanoparticles of average size  $\sim 6$  nm and the bottom part pink gel had an average  $\sim 2$  nm size gold nanoparticles. The difference in sizes across the GelAuNP could be because of a difference in pore size of the gel where the upper part of the gel is blocked by the formation of large gold nanoparticles which leads to restricted borohydride solution diffusion to the bottom part of the gel. So the bottom part of the gel has smaller nanoparticle formation.

## Chapter 2: Gold nanoparticles in hydrogels

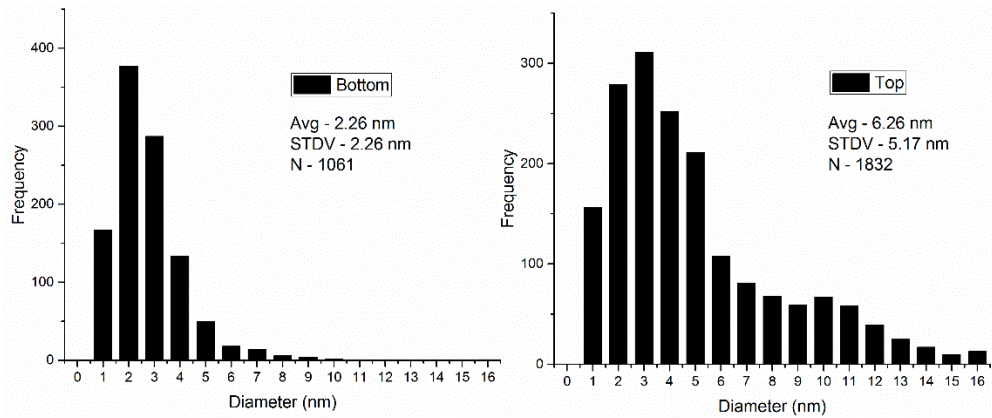


**Figure 2-15: Histograms showing the size distribution of gold nanoparticles in purple gel (top) and pink gel (bottom)**

To get an idea of the pore sizes in both agarose and MAgarose SEM was used to analyse lyophilised gels (Figure 2-16), the SEM images of agarose compare well with literature.<sup>344</sup>

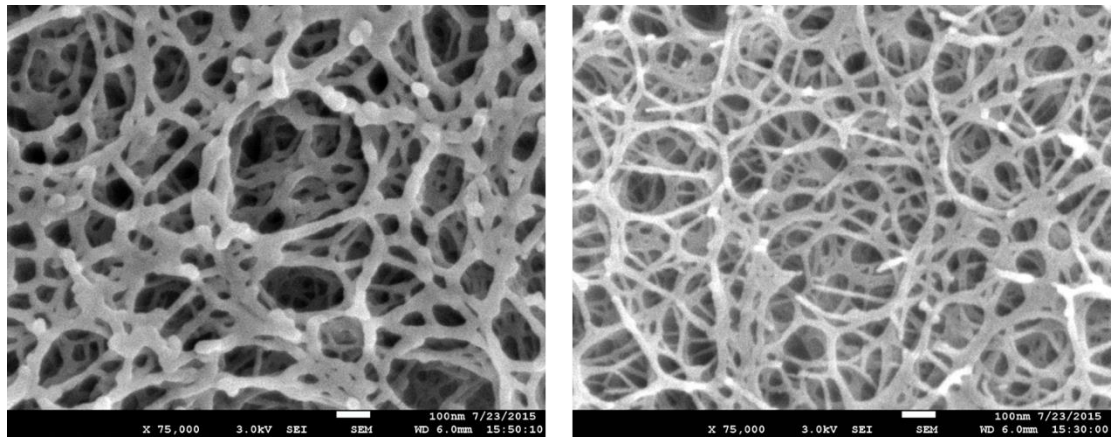


**Figure 2-16: SEM images of agarose and MAgarose at 75k magnification with a scale bar of 100 nm in both cases**

The pore sizes and fiber widths of both agarose and MAgarose gels were compared at same magnification and gel concentration to get a qualitative understanding. The images were analysed in Image J software using the line function to measure both the pore size and also the fiber width (Figure 2-17).



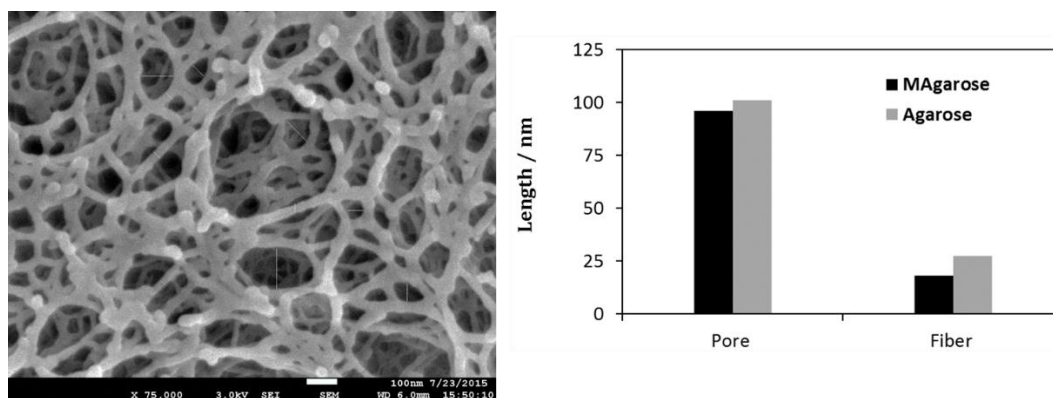


**Figure 2-17: SEM image showing the line function used to calculate the width of fibres and pore sizes (left) and histogram showing the distribution in both agarose and MAgarose.**

By comparison it is seen that in the case of MAgarose gel both the pore and the fibre widths are smaller than agarose. This could be a reason for its low  $T_{gel}$  value and also for the different gold nanoparticle distribution. SEM images of GelAuNP were also analysed to see the distribution of gold nanoparticles across the gel structure, but because of the nanoparticle presence it was hard to get good resolution on the images (Figure 2-18). The images show gold nanoparticle distribution throughout the gel structure.

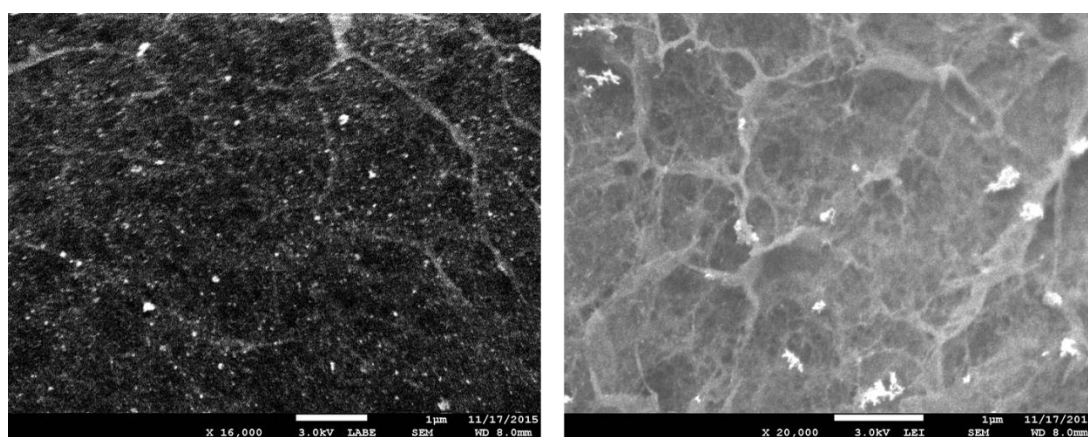


**Figure 2-18: SEM images of GelAuNP, the left image was recorded under LAGE and the right image was recorded under LEI. In both cases the bright spots are gold nanoparticles while the grey background is the gel network**

Three different surfaces of the GelAuNP were selected and analysed by XPS, to identify the species of gold present within the gel structure (Figure 2-19).

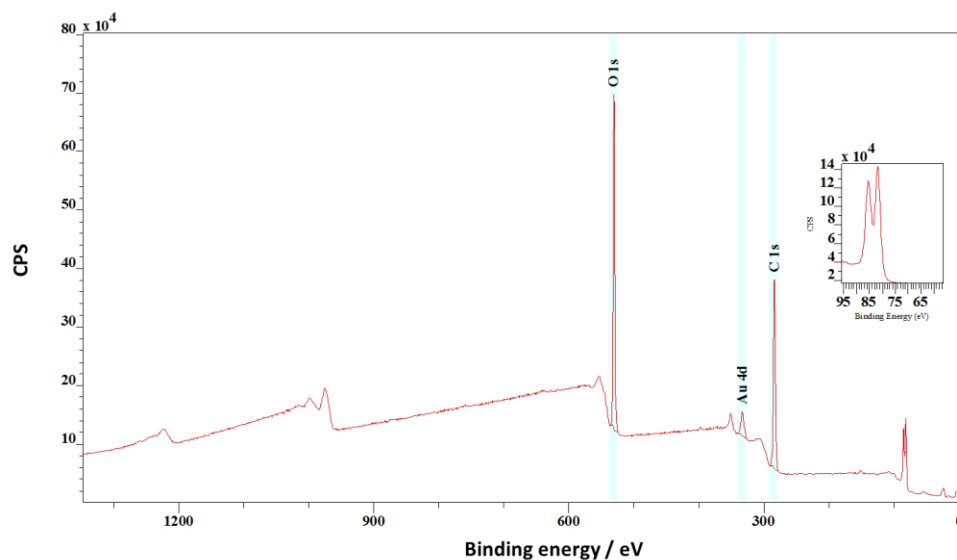


**Figure 2-19: XPS spectra of the surface of the GelAuNP**

The XPS spectra were analysed by software CasaXPS provided by Newcastle University, it automatically detected the presence of oxygen, carbon and gold in GelAuNP. Gold has Au  $4f_{7/2}$  and  $4f_{5/2}$  region with a well-known spin orbit coupling of  $\sim 3.7$  eV,<sup>206</sup> this was observed for GelAuNP across all three surfaces. The Au  $4f_{7/2}$  binding energy peak is used as a reference to identify the type of gold species present, in general a binding energy lower than 84.0 eV was attributed to Au<sup>0</sup> and a binding energy higher than 85.6 eV was attributed to Au<sup>+</sup> and Au<sup>3+</sup> ions.<sup>206,207,345,346</sup> For GelAuNP a binding energy of 83.0 eV to 77.9 eV for Au  $4f_{7/2}$  was observed across the three surfaces, this proves the presence of Au<sup>0</sup> in the GelAuNP.

### 2.6.1 Gold quantification

To use GelAuNP in bio-electrochemical systems, it must contain the minimal amount of gold to make it affordable and viable to use in scaled up systems. The gold content in GelAuNP was quantified using ICP-MS. Digestion of GelAuNP to form a solution of gold ions was carried out using a ‘trial and error method’. The method involved the digestion of agarose structure using piranha solution followed by the digestion of gold nanoparticles by aqua regia.

To validate the method, a control of agarose with known amount of gold was analysed parallel to GelAuNP with the same method of digestion. The sample was submitted for analysis by ICP-MS and the values are provided in the Table 2-14 below.

**Table 2-14: Gold content in agarose loaded with gold nanoparticles and GelAuNP by ICP-MS**

<b>Name of gel</b>	<b>Weight of gel / mg</b>	<b>Expected gold weight / mg</b>	<b>Observed gold weight / mg</b>
<b>Agarose loaded with gold nanoparticles</b>	11.84	2.90	2.54
<b>GelAuNP</b>	9.60	5.80	0.56

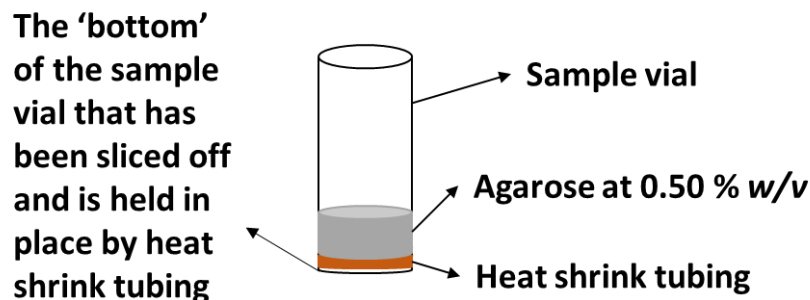
Comparing the expected and the observed values for gold content in agarose loaded with gold nanoparticles there was ~ 88% recovered, this makes a loss of ~ 12%. Therefore, the gold content in GelAuNP was estimated as 0.56 mg  $\pm$  0.7mg, This was much lower than expected, but the loss could be because of the leaching of excess gold solution during gold nanoparticle incorporation (Figure 2-3) but it makes GelAuNP a viable option to use in a bio-electrochemical system as no further leaching was observed.

The next step was to test the toxicity of gold nanoparticles to *So* when incorporated in gels.

## **2.7 Toxicity of gold nanoparticles to *Shewanella oneidensis* MR-1 (*So*)**

The toxicity of gold nanoparticles to *Shewanella oneidensis* MR-1 was investigated by a simple experiment.

4 sterile gel cylinders (0.30 ml each) of agarose at 0.5 % w/v concentration were prepared using a custom made 'bottomless sample vial's. This was a 2 ml sample vial with the bottom part sliced off to give a very thin glass bottom that fits to complete the sample vial (reminiscent of a bottomless cake tin). The glass bottom has to be very thin to make the removal of the gel easier without any squashing. The two parts were held together using a heat shrink tubing specific to the vials diameter, this allows the gel to be moulded in the vial. Once the gel has set, the heat shrink tubing was removed to get the bottom off and the gel cylinder was removed (Scheme 2-8).



**Scheme 2-8: Schematic showing the custom made 'bottomless sample vial'. The orange band represents the heat shrink tubing; the grey band represents the agarose gel cylinder.**

Gold nanoparticles were incorporated into these sterile gels in a similar way as to sect 2.3.1. These sterile gels were washed in sterile water extensively for two days to remove excess gold and borohydride ions. An excess of LB medium was added to these gels and allowed to diffuse through for two days with fresh LB solution changes carried out three times a day (Figure 2-20).

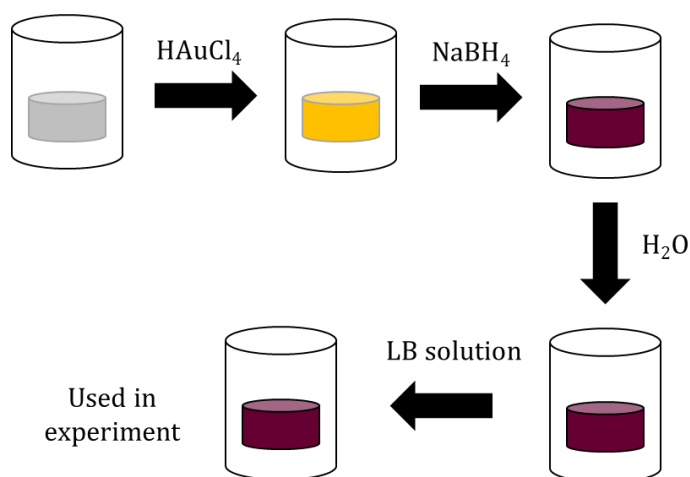


**Figure 2-20: Schematic showing the incorporation of gold nanoparticles into agarose gel cylinders**

An LB agar plate with four wells was prepared and the gel cylinders with gold nanoparticles were placed into the wells. Liquid culture (1 ml) of *Shewanella oneidensis* MR-1 was poured on top of the wells and spread using a spreader. This was placed in an incubator at 25 °C to grow the cells for three days (Figure 2-21). The gold concentration was based on the volume of solution added to each cylinder, this was converted to mass in  $\mu\text{g}$  and is quoted from here on.

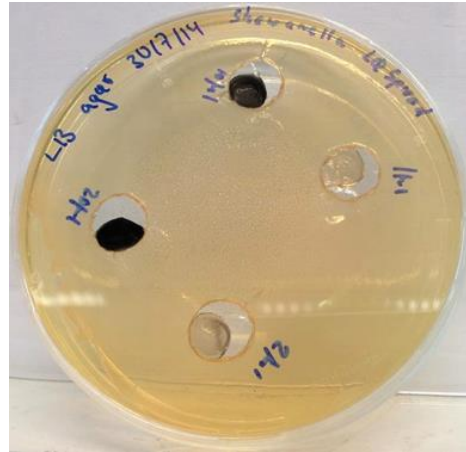


**Figure 2-21: Agar plate with wells to incorporate agarose gel cylinders with different gold nanoparticle concentration**

The 4 different gel cylinders had shrunk in size after the growth of *Shewanella oneidensis* MR-1 and a pink sheen was apparent on the surface of the gold nanoparticle gel cylinders. The surfaces of the 4 different gel cylinders were analysed by confocal microscopy, to identify the live and dead bacteria present at different gold concentrations at the end of growth time (Figure 2-22).

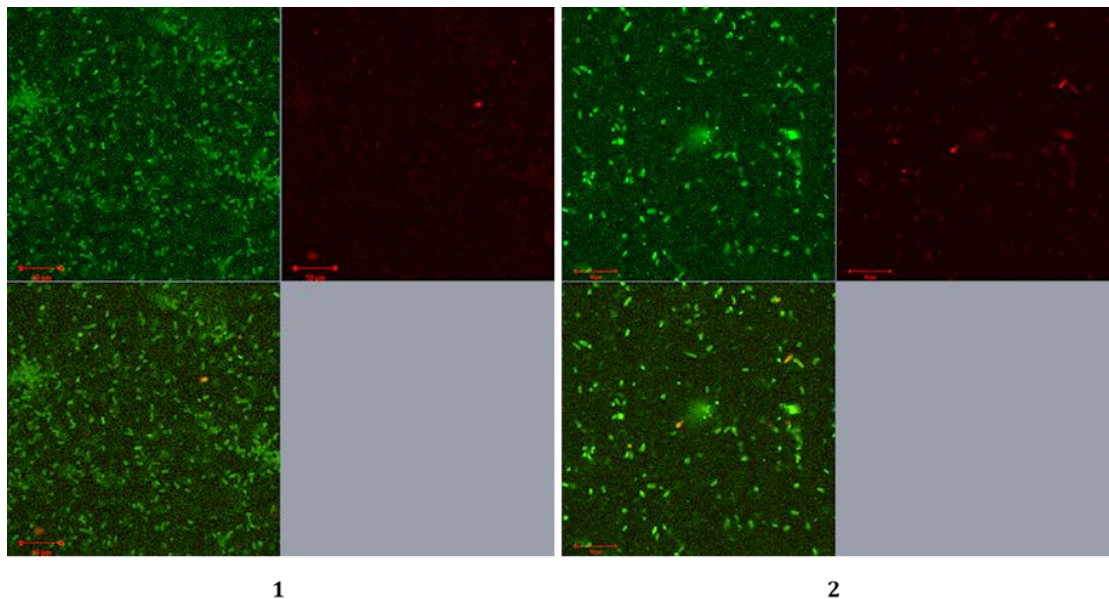


**Figure 2-22: Confocal images of 1 (4.2  $\mu\text{g}$ ) and 2 (8.4  $\mu\text{g}$ ) gel cylinders with different gold concentrations in brackets**

The confocal images show a set of four images, top left image indicates the presence of live bacteria stained by Syto 9, top right the presence of dead bacteria stained by propidium iodide. The bottom images, left shows the mixture of both live and dead bacteria, and the right shows the white field image with no fluorescence.

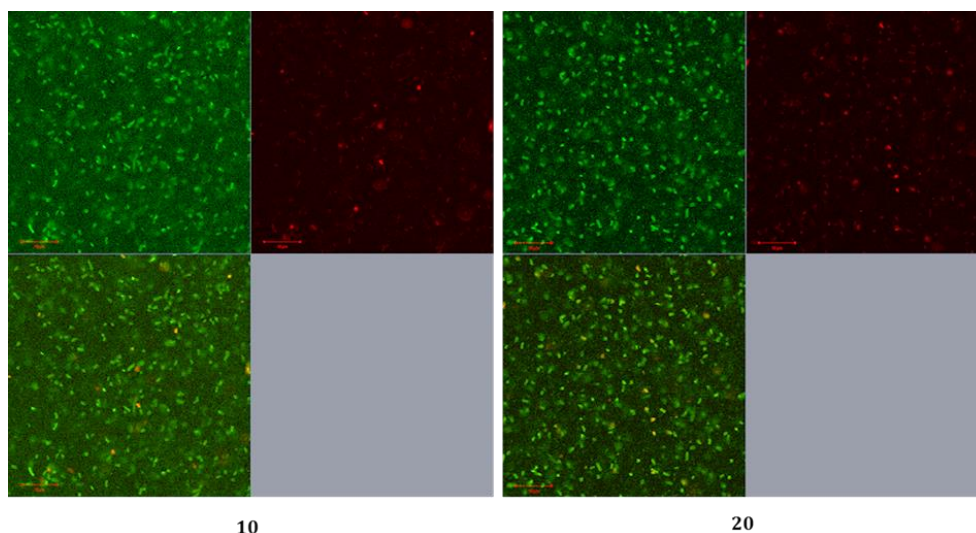


**Figure 2-23: Confocal imaging of gel cubes with higher gold concentrations 10 (42  $\mu\text{g}$ ) and 20 (84  $\mu\text{g}$ ).**

In the case of low and high gold concentrations, the gel cylinders have a higher number of live bacteria than dead bacteria (Figure 2-24). Since Styro 9 stains all bacteria in green and propidium iodide stains only the dead bacteria red, the number of dead bacteria was removed from the live stain to get the true number of live bacteria in all the images. These images show that *So* was capable of growing in the presence of gold nanoparticles incorporated into gels at different gold quantities.

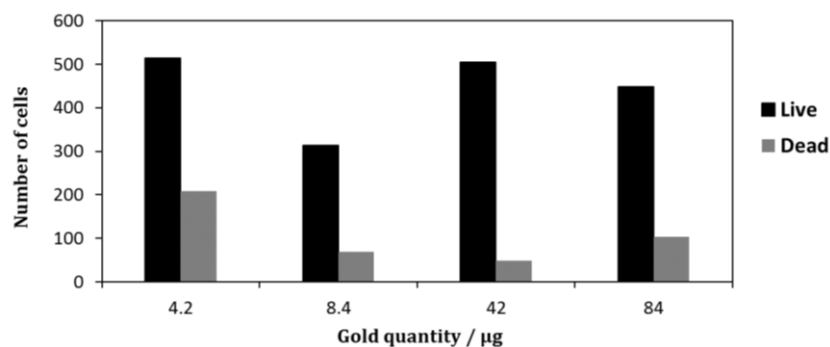


**Figure 2-24: Bar chart showing the distribution of live and dead bacteria at increasing gold quantities**

Based on these observations, GelAuNP was investigated for its capability to support the growth of *So* and also its current generating ability when used as a modified electrode in a bio-electrochemical system.

## 2.8 Design of electrochemical set up

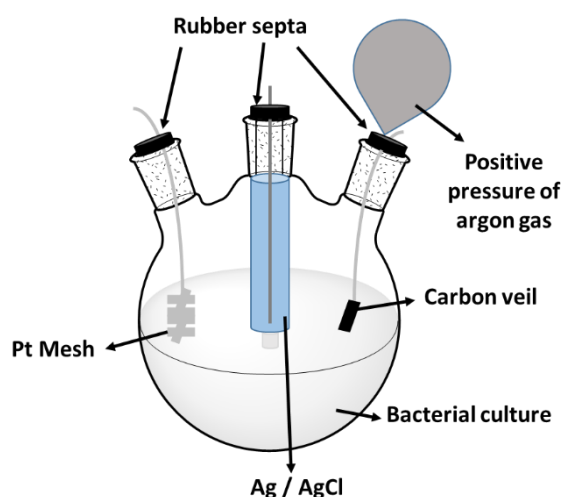
A three electrode cell was designed that would minimise oxygen presence, be easy to sterilise and would also allow a gas inlet for argon (Scheme 2-9). Three electrode



## Chapter 2: Gold nanoparticles in hydrogels

cells were increasingly being used to monitor current generation over a long period of time. By using a reference electrode, the potential of the working electrode can be maintained at a fixed value and would enable the study of anodic reactions, it would also allow for variation of potential as required.<sup>347-349</sup> Three electrode cells are also good at minimising the internal resistance of the MFC by reducing the distance between electrodes.

From literature, there were a number of different experiments that could be used to understand bacterial behaviour, electron transfer mechanisms and the rate of electron transfer.<sup>63</sup> The main aim was to study the change in current production at constant potential. Chronoamperometric experiments would satisfy this aim and would provide a simple way of studying the effect of the modified electrode on bacterial growth and current generation.<sup>133,349,350</sup>



**Scheme 2-9: Schematic of the three electrode electrochemical design used to record chronoamperometric data**

The choice to study *So* has been justified in Chapter 1 section 1.5.4. *So* is capable of growing<sup>245,351</sup> and attaching to an electrode at a range of negative to positive potentials.<sup>77,254,256,352-354</sup> Literature suggest the use of a positive potential as it drives bacterial adherence to the electrode, 0.2 V vs Ag/AgCl was chosen as the potential for chronoamperometric experiments as it was observed that an increase in extracellular electron transfer associated with Mtr and OmCA in *So* heme proteins was highest at this potential.<sup>352</sup>

Carbon based electrodes were most commonly used to investigate MFCs as they are cheap, biocompatible, have low resistance and are also resistant to corrosion.<sup>83,84,86</sup>

A carbon veil from TFP was used as the working electrode in the bio-electrochemical cell. It is a 2 D electrode with planar diffusion, made with recycled carbon fibres and it has good porosity for strong biofilm formation and imaging solutions.<sup>112</sup> A single sheet of carbon veil with carbon content of 10 gm<sup>-2</sup> was used for all experiments to maintain repeatability. Platinum mesh was chosen as the counter electrode to achieve maximum surface area for the electrochemical study.

### 2.8.1 Electrode preparation

The carbon veil was modified by depositing the conductive gel (section 2.3.1) on top using a 'bottomless vial' described in section 2.7 (Figure 2-25). The gel was washed extensively in water to remove any unreacted H<sub>2</sub>AuCl<sub>4</sub> and sodium borohydride.

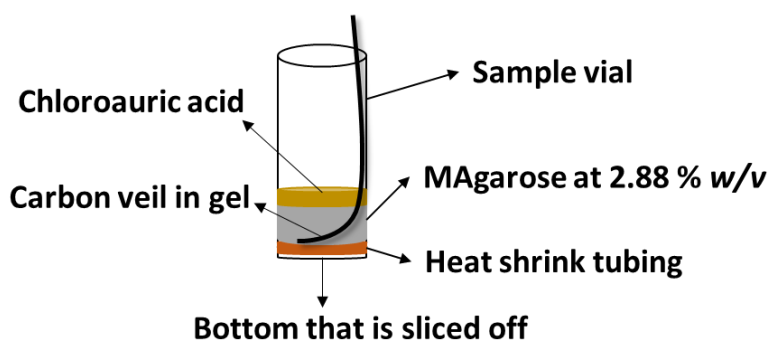


**Figure 2-25: Schematic of carbon veil modified with MAgarose containing gold nanoparticles.**

The electrode was sterilised with ethanol before use and incorporated into the three electrode cell as the working electrode. The next step was to decide on cell culture media and its preparation.

### 2.8.2 Preparation of bacterial culture for electrochemical set up

Minimal media was chosen as the medium to use during the chronoamperometric experiments. So grows slowly over a long period of time in minimal media enabling the study of how the GelAuNP affects the current generation. So was grown in LB medium overnight at 25 °C with shaking and 1 ml of this culture was used to obtain a 25 ml minimal media culture containing So at an OD<sub>600</sub> of 0.03.

The same starting OD<sub>600</sub> was used for all the experiments. By starting with a low OD<sub>600</sub> the development of a biofilm and also the effect on current generation can be studied gradually over a long time.



### 2.8.3 Chronoamperometric results

Since chronoamperometric experiments were run for long time periods, the reference electrode was regularly checked before every chronoamperometric run using a solution of ferrocene as a standard to avoid contamination of the electrode.



#### Scheme 2-10: Ferrocene couple studied as a standard

Ferrocene undergoes reversible one electron oxidation (Scheme 2-10) to produce a cyclic voltammogram (CV) with well separated anodic and cathodic peaks in non-aqueous solvents.<sup>355</sup> A reference electrode of Ag / AgCl, working and counter electrodes of carbon rod were used to record the CV with ferrocene in acetonitrile and tetrabutylammonium hexafluorophosphate (Figure 2-26).

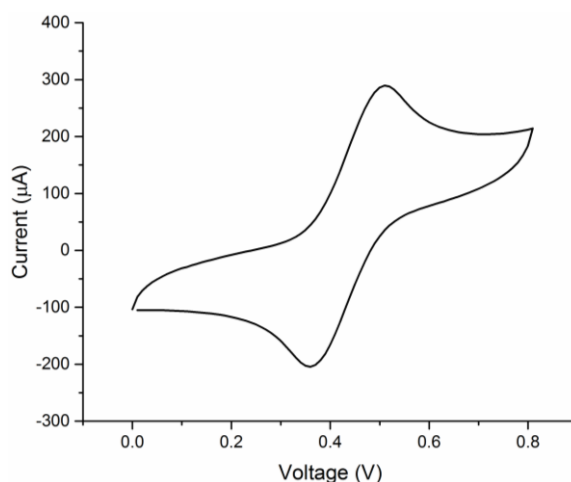


**Figure 2-26: Cyclic voltammogram of Ferrocene in acetonitrile with tetrabutylammonium hexafluoro phosphate (0.1 M) as supporting electrolyte**

In an ideal experiment, for a reversible one electron redox reaction the peak separation between the anodic and cathodic peaks  $\sim 0.059$  V.<sup>356</sup> In the case of Figure 2-26 it was always found to be within the range of 0.13 – 0.16 V, this is reasonable as the peak separation is dependent on electron transfer rates, electrode material, solvent and diffusion of ions.<sup>355–357</sup> If the peak separation was outside this range, the electrode was regenerated. Once this check was performed the electrodes were rinsed with acetonitrile and ethanol extensively and used for bio-electrochemical cells.

### 2.8.3.1 Chronoamperometric data

The carbon veil was sterilised using ethanol and dried before using in the set up. The chronoamperometric experiments were run for  $\sim 27$ h, with a poised potential of 0.2 V vs. Ag/AgCl at 30 °C. Initially the chronoamperometric experiments were run in the absence of So to understand the range of currents that could be produced. Each control and GelAuNP was run 3 times and an average of the runs was compared. Since it is not possible to estimate the area of carbon veil not covered by GelAuNP, all the data were compared as current rather than current density and similar surface areas of the electrode were used in the range of 1.2 – 1.6 cm<sup>2</sup>.

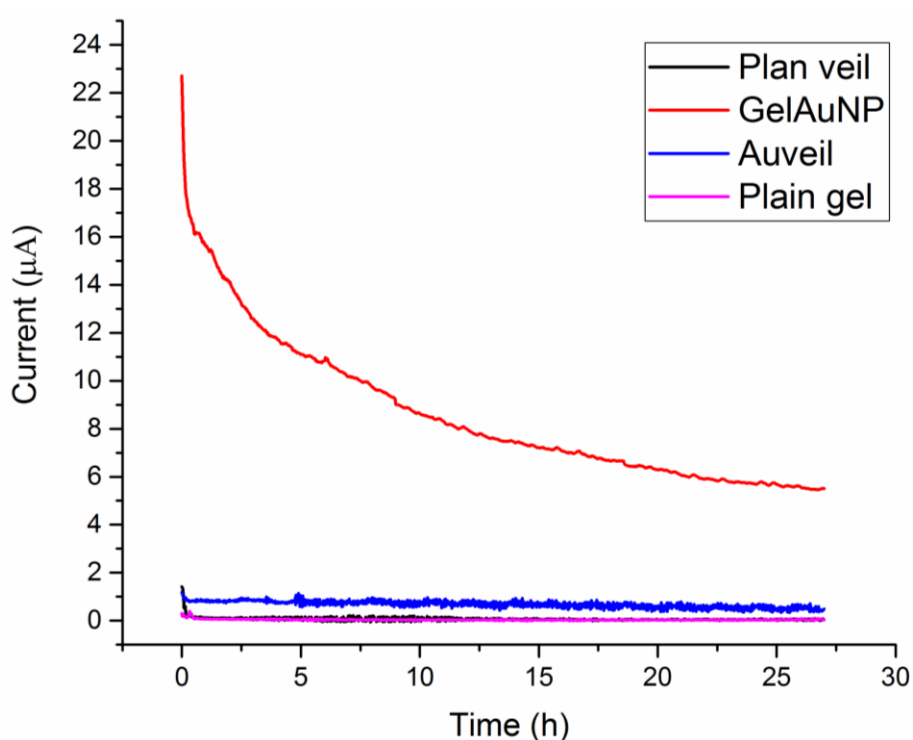


**Figure 2-27: Current vs Time plot of all the controls and GelAuNP in the absence of So**

It is apparent from Figure 2-27, that the GelAuNP started with the highest current at  $\sim 23$   $\mu$ A, while all the controls had current ranges of  $\sim 0.5 - 1.5$   $\mu$ A, this was attributed to the GelAuNP being the most conductive of all the electrodes and having a higher charging current. The graphs recorded for carbon veil were quite noisy reflecting the porosity of the carbon veil. The currents recorded for plain gel in the absence of gold nanoparticles was small  $\sim 0.034$   $\mu$ A. This could be because of an insulating effect of the gel, where it blocks a part of the veil exposed to solution. It is important to note that the current generated in the absence of So decreases over time for all the controls.

## Chapter 2: Gold nanoparticles in hydrogels

A control experiment with Au<sup>0</sup> deposited carbon veil was also performed and labelled as Auveil in Figure 2-27. The Auveil electrode was prepared by electrodeposition of gold on the carbon veil using the same three electrode set up as in section 2.8. The working electrode was carbon veil, counter electrode was platinum mesh and the reference electrode was Ag / AgCl. A solution of chloroauric acid (5mg) dissolved in 100 mM sodium acetate (1ml) was used as the electrolyte. Chronoamperometric detection experiment was run at -0.6 V vs Ag/ AgCl (Figure 2-28) till the solution of gold turned colourless.

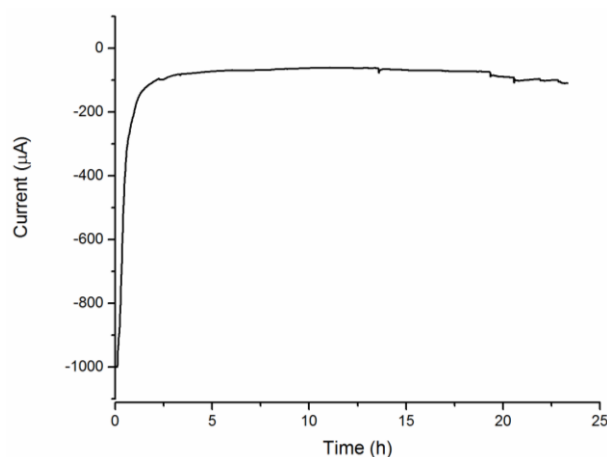


**Figure 2-28: Current vs time graph of Au<sup>0</sup> electrodeposition**

The shape of the curve in Figure 2-28 corresponds well to literature where initially double layer charging occurs followed by nucleation and growth of gold nuclei ( $\sim -1000 \mu\text{A}$ ) and then reduction proceeds which will be limited by the concentration of gold near the electrode ( $\sim -100 \mu\text{A}$ ).<sup>358</sup> The current generated when the Au deposited veil was used in Figure 2-27 experiments was  $\sim 0.49 \mu\text{A}$  which was higher than plain veil ( $\sim 0.033$ ) or plain gel ( $\sim 0.034$ ) (Figure 2-27). These results were compared to the same electrodes in the presence of So.

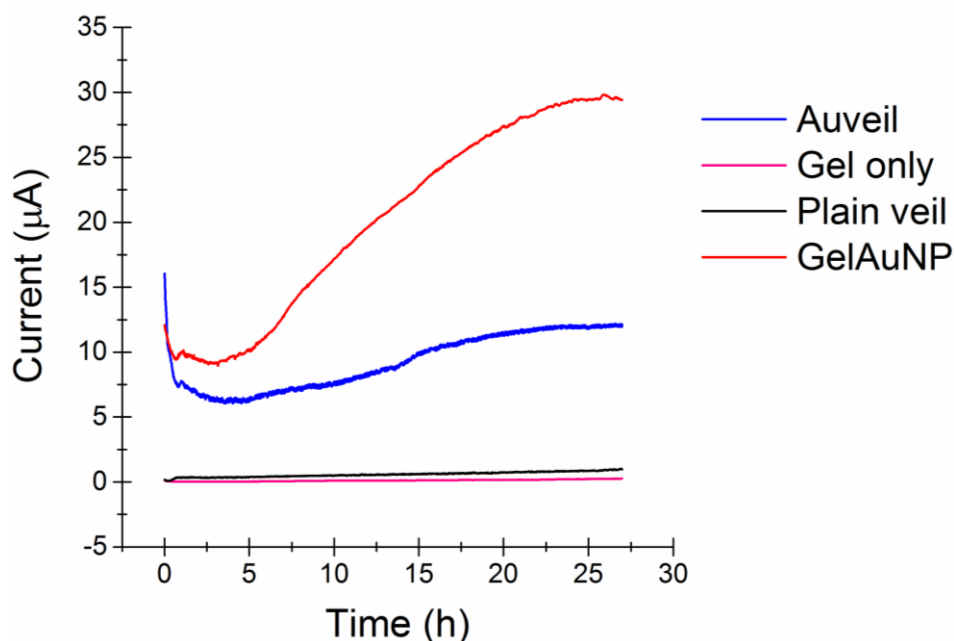


**Figure 2-29: Current vs time plot of all the controls and GelAuNP with So**

From Figure 2-29, it is apparent that the shape of the plot is different to Figure 2-27 in that current generation increases with time for all the electrodes. This shape corresponds well with literature where similar chronoamperometric experiments were recorded in the presence of bacteria,<sup>132,144,251,257,359,360,289</sup> the shape shows initially a slow increase in current, followed by a rapid increase in current production.

This shape was also complementary to the growth of So as the current produced is dependent on So growth and biofilm formation on the working electrode. The shape follows the general trend of bacterial growth depicting the lag phase (initial acclimatisation to environment) and the exponential phase (rapid growth).<sup>80</sup> The GelAuNP seems to produce a higher current than all the electrodes tested till now in the range of ~26 – 30  $\mu\text{A}$ . Auveil also produces high current at ~11- 12  $\mu\text{A}$ , this could be due to the presence of gold which increases the rate of electron transfer. The current generated by plain veil and plain gel are almost negligible at 1-2  $\mu\text{A}$ .

From comparison it was seen that the enhancement between commercially available carbon veil and GelAuNP was ~ 29 times higher which also higher than some reports in the literature (Table 2-1).<sup>138,146,147</sup>

**Table 2-15: Modification of electrodes from literature**

Electrode material	Modification	Magnitude of increase	Authors	Year
Graphite felt	Polypyrrole hydrogel and carbon nanotubes	1.3	Tang et al. <sup>138</sup>	2015
Carbon paper	Graphene and gold	5	Zhao et al. <sup>146</sup>	2015
Graphite disks	Au / Pd nanoparticles	2-20	Fan et al. <sup>147</sup>	2011

The table shows the different modifications from literature where a significant enhancement in current production was observed.

This proves that there is an improvement in electron transfer in between the GelAuNP and So in the electrochemical system. To identify if the current continues to increase over time, a single chronoamperometric experiment was run for ~ 6 days (Figure 2-30).

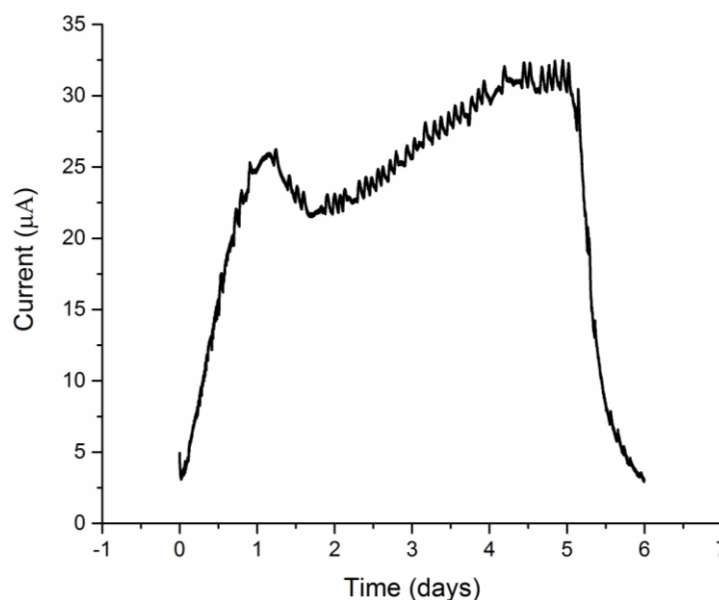
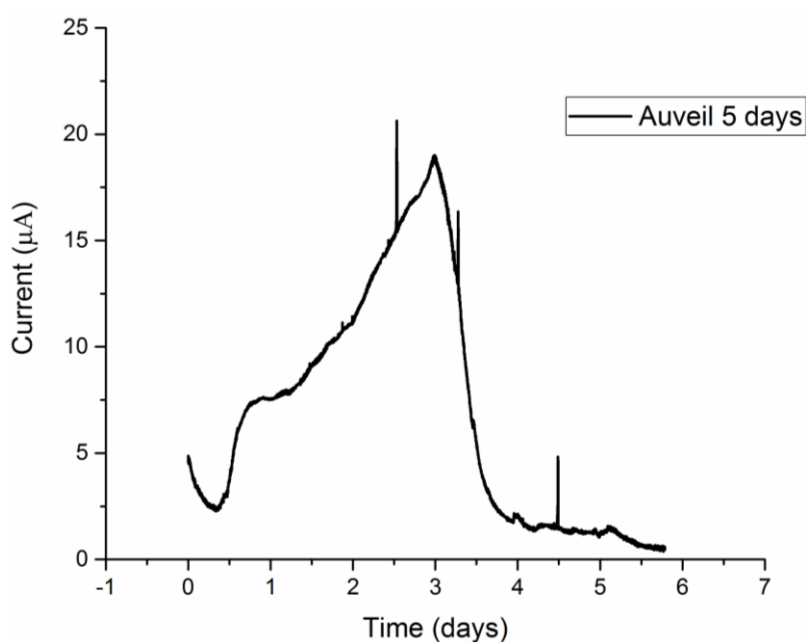
**Figure 2-30: 5-day experiment of GelAuNP with So**

Figure 2-30 shows two significant points where the current spikes, this could be because of biofilm formation and slow bacterial growth. After ~5 days the current generation decreases, this could be because of bacterial growth being limited by nutrient depletion.

## Chapter 2: Gold nanoparticles in hydrogels

A control experiment was also conducted using Auveil for a 5 day run in the presence of So to prove that the presence of gel does influence continuous running of the electrochemical cell (Figure 2-31). It was seen from Figure 2-31, that the current generation started to drop at  $\sim 3$  days which is 2 days earlier than GelAuNP. However, this plot also shows two significant spikes in current generation over time further proving that the increase in current was due to bacterial growth and biofilm formation.



**Figure 2-31: Current vs time plot of Auveil run for 5 days in the presence of So**

Figure 2-31 also proves that the presence of gel in GelAuNP increases the viability of So prolonging its growth for a longer time period than in the absence of gel.

A cumulative bar chart was plotted to understand the significance of modification (Figure 2-32). The current at 27 h was averaged across the triplicate experiments.

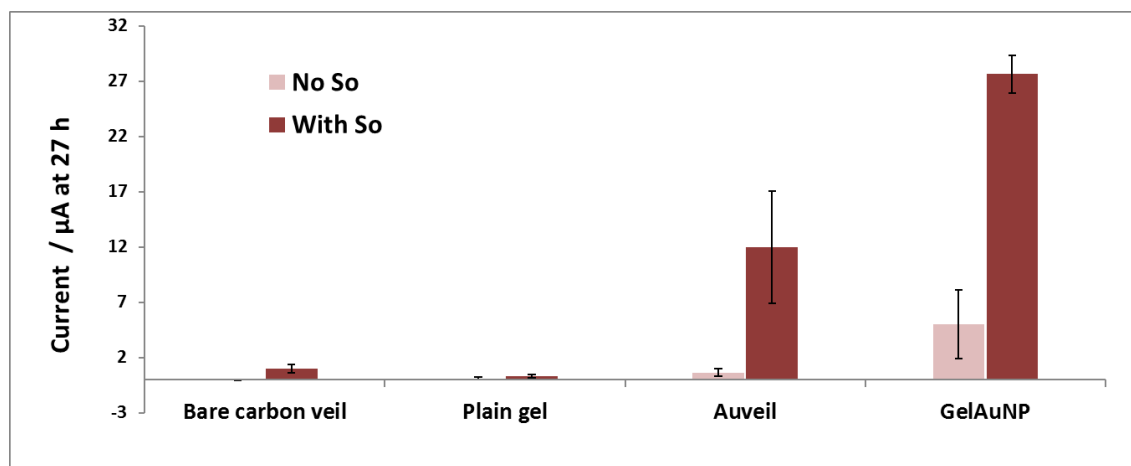


**Figure 2-32: Bar chart showing the combination of all electrochemical results**

The bar chart gives a good indication of enhancement of current across the controls and the experiments with different electrodes. It also identifies GelAuNP as the best electrode of all of them. To understand its influence on bacterial growth, analysis of the GelAuNP after the experiment was performed.

## 2.9 Confocal imaging of GelAuNP

The GelAuNP from one of the chronoamperometric experiments performed in the presence of So was analysed by confocal imaging to identify the presence of live and dead bacteria. Two different positions on the gel were stained, the top of the gel surface and the bottom where the veil is.

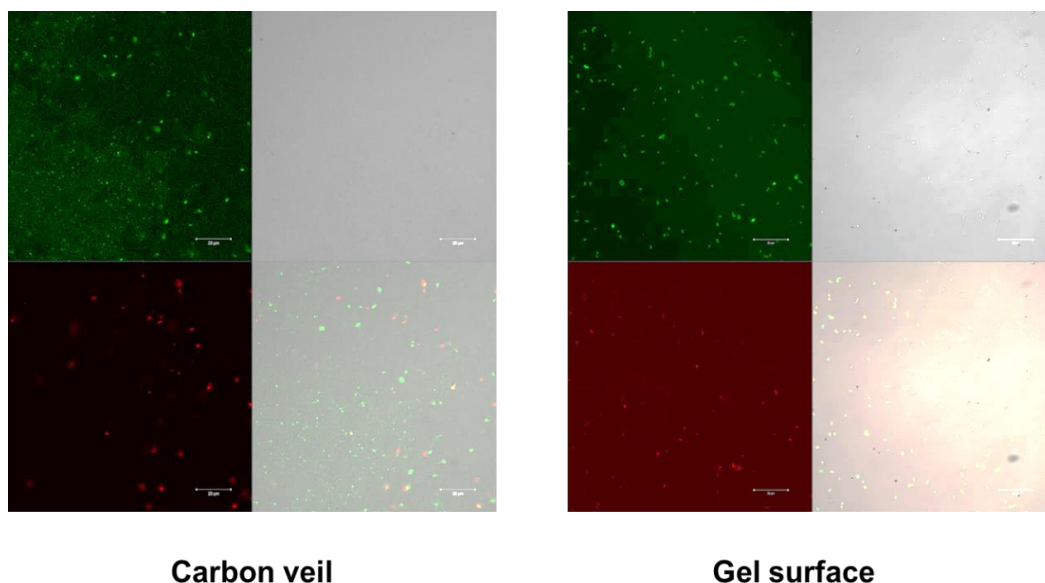


**Figure 2-33: Confocal images of both carbon veil and gel surface. The top left shows live *So*, top right shows white field image, bottom left shows dead bacteria and bottom right shows the mixture of all three.**

The images show a mixture of both live and dead bacteria present in both cases. These images were analysed by Image J to quantify the number of live and dead bacteria (Figure 2-34).

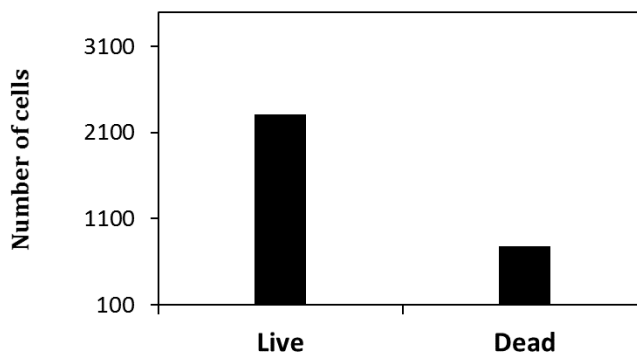


**Figure 2-34: Bar chart of number live and dead bacteria present on conductive gel**

The bar chart indicates that the amount of gold in GelAuNP is not very toxic to *So* and that it is able to grow in the presence of it.

## 2.10 Conclusions and future work

Amine functionalisation (MAGarose) of agarose was attempted but the presence of nitrogen was not detected by NMR, IR or by CHN analysis. A Fluorometric assay seemed to provide a qualitative comparison for nitrogen detection. Viscometry provided suitable evidence in viscosity average molecular weight that agarose and MAGarose were different. The structure of MAGarose was elucidated with control



## Chapter 2: Gold nanoparticles in hydrogels

experiments to be partially hydrolysed agarose with some amine incorporation proving that the presence of water during synthesis to be a crucial factor. MAgarose was found to be capable of supporting gold nanoparticle formation and forming GelAuNP which was  $\sim 1400$  times more conductive than the respective control.

A simple toxicity test of gold nanoparticles to So was performed and it was found that the relation between an increase in gold concentration and the number of dead cells varied. GelAuNP was used as electrode in three electrode electrochemical cell containing So as the catalyst. On comparison of similar surface areas an enhancement of  $\sim 29$  times was observed compared to commercially available carbon veil. The influence on current generated, over long period of time was investigated and the presence of gel in GelAuNP seem to be a crucial factor.

Confocal imaging of the GelAuNP has shown promising results of a higher number of live So than dead, indicating that gold nanoparticles in the gel have relatively low toxicity.

The operation of the electrochemical cell for longer than 3 days must be investigated. At the end of the long-term operation, the stability of the GelAuNP and the toxicity of the GelAuNP to So needs to be studied. The gold content in GelAuNP after the long term experiment must be analysed by ICP-MS. This is to understand if any gold has leached into the cell because of MAgarose degradation by So. In conclusion, even though a current enhancement of  $\sim 29$  times was observed, on long term operation this enhancement could change and this has to be investigated.

The other investigation to undertake is the scale up of the electrochemical cell and how the current enhancement changes because of the scale up.

# **Chapter 3: Gold nanowires in hydrogels**

### 3 Introduction

In Chapter -2, the incorporation of GelAuNP as an anode in a bio-electrochemical system has led to an increase in current generation and an improvement in electron transfer from So to the anode compared to the respective control (plain veil). To improve this further, incorporation of gold nanowires in gels as an alternative to gold nanoparticles was considered. Metal nanowires,<sup>361-363</sup> conducting polymer nanowires,<sup>364-366</sup> conductive adhesives with metal nanowires<sup>367-369</sup> and biologically produced bacterial nanowires<sup>260,370,371</sup> have shown promise in electron transfer. Gold nanowires are capable of forming continuous electron transfer pathways.

The incorporation of gold nanowires into hydrogels should create a conductive hydrogel capable of improving electron transfer from So to anode, the nanowires in the gel should bridge the gel structure using their one-dimensional structure. Nanowires require a lower metal content than nanoparticles, reducing the use of noble metal and increasing the economic viability.<sup>372</sup> A similar result to Chapter 2 was expected, where the presence of nanowires increases the current produced when incorporated in a bio-electrochemical cell. To date, there has not been an example reported in the literature where gold nanowires incorporated into hydrogels have been used as an anode in a bio-electrochemical system.

The literature was reviewed to understand if gold nanowires can be incorporated into hydrogels to increase conductance. If these nanowire gels can be synthesised with relative ease, are biocompatible for use in bio-electrochemical systems and have economic viability, they would prove to be quite applicable.

#### 3.1 Synthesis of gold nanowires in gels

There are two ways of incorporating nanostructures in gels as introduced in Chapter 1 section 1.5.3; one is by the synthesis of nanostructures using the gel itself as a reducing agent or by diffusing a solution of pre-formed gold nanostructures into the gel.<sup>373</sup> The latter method has a drawback in that, the nanostructures' size has to be smaller than the gels' pore size to prevent blocking of the gel.<sup>292</sup>

With nanowires, there are multiple approaches in the literature for their incorporation in gels. Template-based synthesis was used predominantly where structures with linear nanosized pores are used as the support for nanowire

### Chapter 3: Gold nanowires in hydrogels

formation. The template is usually removed to leave just the nanowires while some use the combination together for applications such as photovoltaic cells<sup>374</sup> and sensory devices.<sup>375</sup> In template-based syntheses, materials such as anodised aluminium oxide (AAO),<sup>376</sup> silica gels,<sup>377</sup> track-etched templates, carbon nanotubes, polycarbonate films and biological templates such as DNA were used.<sup>378-380</sup> In most template-based syntheses electrodeposition, ultrasound, dielectrophoretic assembly and hydrothermal vessels are used as the method of preparation.<sup>379,381-383</sup> Nanoparticles can also be self-assembled into nanowires using non-template methods.<sup>384,385</sup> A lot of research has also been conducted for the growth of crystals in gels with gels being silica, polyacrylamide, gelatin, agar and clay.<sup>373</sup>

Paunov *et al.*<sup>382</sup> have synthesised silver nanowires in agarose gels using a dielectrophoretic assembly. Their method involved the addition of silver nanowires to a hot agarose solution and their dispersion through ultrasound. An aliquot of this dispersion is suspended in between four electrodes of a custom made cell with temperature control and an AC field is applied. This aligns the nanowires to form a connection with the electrodes to form microwires, the temperature of the cell is dropped to room temperature for the formation of agarose gel. This gel formation fixes the nanowires in position and the AC field is removed (Figure 3-1). This was termed as a 'novel method' since previously in the absence of gel, the wires lose their alignment on removal of the AC field in solution.

### Chapter 3: Gold nanowires in hydrogels

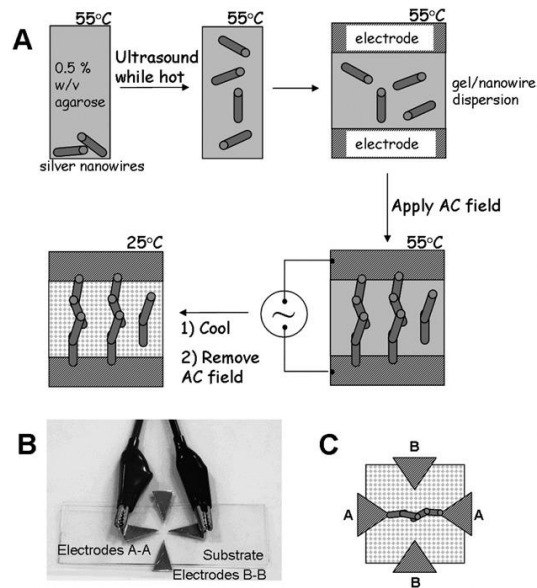


**Figure 3-1: Schematic showing the incorporation of silver nanowires in agarose solution (A) and their alignment using a four electrode custom set up (B). Adapted from ref <sup>382</sup>**

Agarose gels at 0.5% w/v were used throughout as this provided the best concentration for dielectrophoretic assembly of wire and a range of 50, 100 and 200 nm diameter silver wires of length 40-50  $\mu\text{m}$  were investigated. The cell consisted of two copper electrodes with a 4 mm gap in between them. The voltage applied for microwire formation was found to be dependent on the wire diameter with the 50 nm requiring 250-300  $\text{V cm}^{-1}$ , 100 nm requiring 500-600  $\text{V cm}^{-1}$  and 200 nm requiring 350-400  $\text{V cm}^{-1}$ .

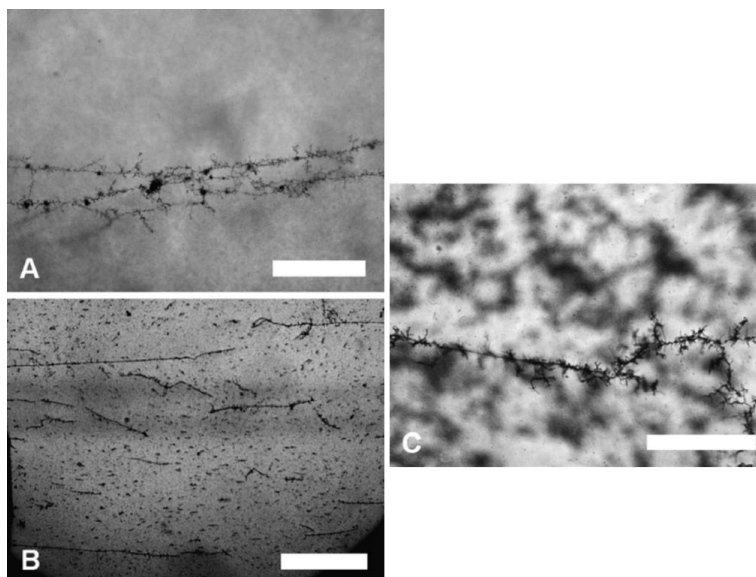


**Figure 3-2: TEM images of microwire formation in agarose gels at 0.5% w/v with (A) 50 nm, scale bar 200  $\mu\text{m}$  (B) 100 nm, scale bar 1 mm and (C) 200 nm, scale bar 100  $\mu\text{m}$ . Adapted from ref<sup>382</sup>**

In the case of 50 and 200 nm diameter wires, by increasing the AC field application time, branching of the wires within the gel was observed by optical microscopy (Figure 3-2). The TEM images also show a general alignment of wires through the gel parallel to the electrode position. The four electrode set up was also used to record the resistance of the wires parallel and perpendicular to their growth in gels. There was no relationship found between the diameter of the wire and the resistance of the gel, but the resistance of the gel with wire was lower than the gel with no wires (Table 3-1).

**Table 3-1: Resistance values measured using four electrode custom set up of different diameter silver nanowires in agarose at 0.5% w/v.**

Diameter of wire / nm	Volume of gel / $\mu\text{l}$	Resistance / $\text{k}\Omega \text{ cm}^{-1}$
<b>0 (Control)</b>	200	1000
<b>50</b>	200	3.5-5.8
<b>100</b>	200	0.9-1.4
<b>200</b>	200	2.8-3.5

The absence of the relationship between resistance and wire diameter was attributed to the formation of wires from aggregated nanowire dispersion than individual nanowires. The limitation of this method is that on continued application of an AC field, the gel becomes dry (solvent evaporation) and cracks leading to

collapse of the gel structure and the wires. This work is a good example to prove that the presence of nanowires in agarose gels can increase the conductance of a gel compared to a gel with no nanowires.

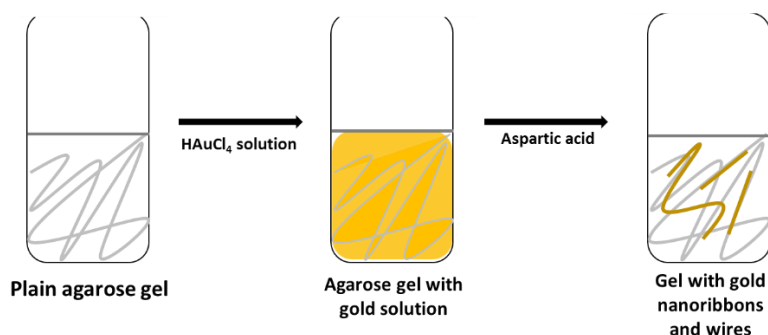
There was one other example in the literature where Thai *et al.*<sup>386</sup> have synthesised nanowire capacitors which have a gold core on which  $\delta$  -  $\text{MnO}_2$  is electrodeposited. The entire  $\text{Au@}\delta$  -  $\text{MnO}_2$  is encapsulated in a poly (methyl methacrylate) PMMA gel electrolyte. The capacitor was able to cycle reversibly for 200,000 cycles and retain its charge transferring capability at 95 %. The enhanced reversibility was attributed to the encapsulation of the wires in the gel electrolyte. This is another example where the presence of a gel increases the stability of the nanowires to corrosion and dissolution.

### **3.2 Proposed idea**

The synthesis of gold nanowires in agarose gel will be investigated using a combination of methods described above. The stability of the incorporated wires in gel and the conductivity of these nanowire gels (GelAuNW) will be analysed. If the gels are stable, their incorporation into a bio-electrochemical cell will be investigated.

### **3.3 Synthesis of gold nanowires in agarose**

A simple method of using an agarose network as the host matrix with aspartic acid as a reducing agent was utilised for this purpose. The method involved the addition of gold chloride solution to a preformed agarose gel cube at 0.2% w/v concentration, followed by the addition of aspartic acid solution to reduce  $\text{Au}^{3+}$  to  $\text{Au}^0$ .



**Scheme 3-1: Schematic showing the procedure for the in situ incorporation of gold nanoribbons and nanowires in agarose gel at 0.2% w/v concentration**

The concentrations and equivalence of gold chloride to aspartic acid was as per literature instructions, in solution, these equivalences produce gold nanoribbons.<sup>387</sup> The gels were characterised by UV-Vis spectroscopy that showed a surface plasmon resonance peak at  $\sim 550$  nm indicative of nanoribbons (Figure 3-3).<sup>387,388</sup>

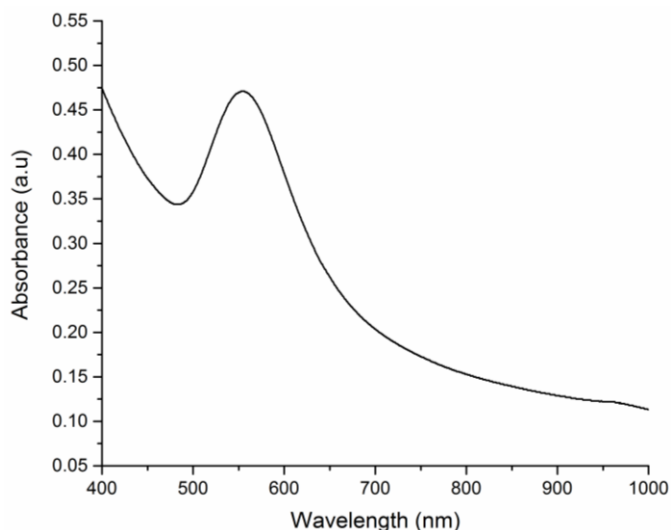


**Figure 3-3: UV-Vis spectrum of gold nanoribbons in agarose using aspartic acid**

The gels were also analysed by HR-TEM to investigate if the incorporation was successful and if the nanoribbons were distributed throughout the agarose gel. The HR-TEM images proved the reaction to be successful as the nanoribbons were distributed through the agarose gel network (Figure 3-4). The nanoribbons look similar to the ones produced in solution, reported in literature.<sup>387</sup>



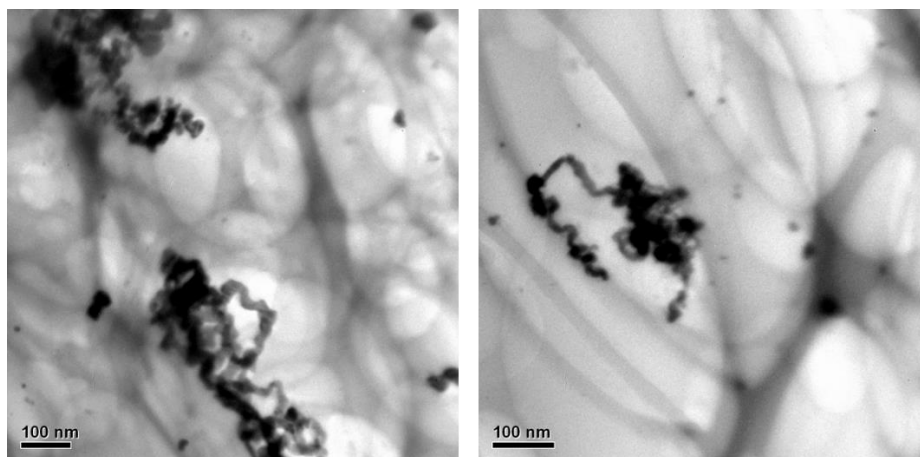
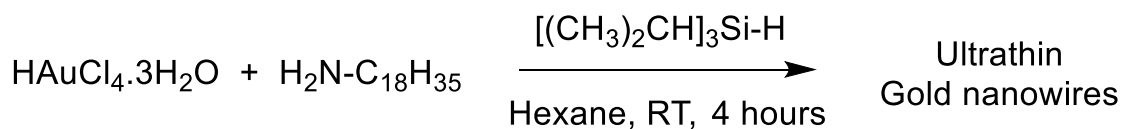


**Figure 3-4: HR-TEM images of gold nanoribbons in agarose gels**

Most of the nanoribbons seem to be twisted in on themselves, they are not very well spread out along the gel fibers. The images also show a lot of nanoparticles rather than nanoribbons; indicating that not all of them have aged to ribbons. To improve the ratio of nanowires or nanoribbons to nanoparticles and also to get a better distribution of nanowires or ribbons through the gel, an alternative approach was pursued.

### 3.3.1 Synthesis of gold nanowires in hexane

Gold nanowires were synthesised in hexane using a literature method involving the addition of triisopropylsilane to a mixture of gold chloride and oleylamine (Scheme 3-2). The resulting mixture was incubated at 30 °C for four hours undisturbed, to obtain oleylamine protected gold nanowires in a black solution.<sup>204</sup> In this reaction, triisopropylsilane acts as a reducing agent while oleylamine stabilises nanowire formation as well as acting as a template for its directional growth.<sup>389</sup> The gold nanowires were used with no further purification as per literature.<sup>204</sup>



**Scheme 3-2: Schematic showing the synthesis of gold nanowires in hexane. Adapted from ref<sup>204</sup>**

The gold nanowires were stable in solution without any aggregation for ~ 4 months and were used immediately after synthesis. The gold nanowires in solution were characterised by UV-Vis Spectroscopy to find the a plasmon resonance shoulder at ~ 500 nm indicative of nanowires (Figure 3-5).<sup>389,390,391</sup>

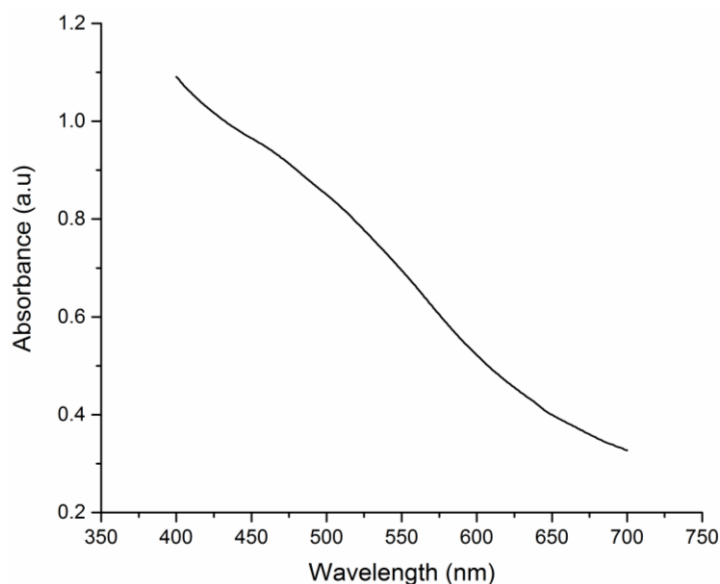


**Figure 3-5: UV-Vis spectrum of gold nanowires in hexane**

The as prepared gold nanowires were also characterised by HR-TEM to observe their dimensions in terms of diameter and length (Figure 3-6). The HR-TEM images look similar to the literature used for their synthesis, showing very long and very thin wires of ca. < 2nm in diameter.<sup>204</sup> It was not possible to measure the diameter accurately due to the wires being very thin, but manual measurements of wires were recorded to get an average value. The wires in solution showed a good distribution along with some nanoparticles that have still to form wires.

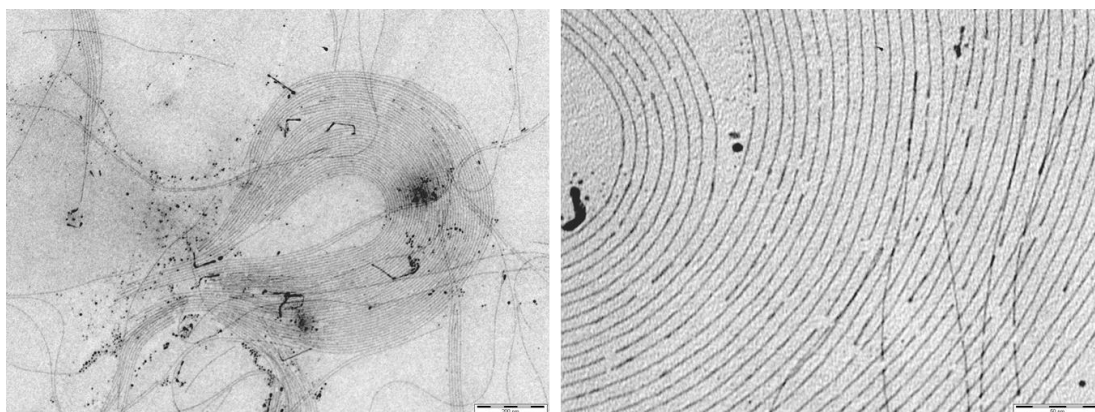
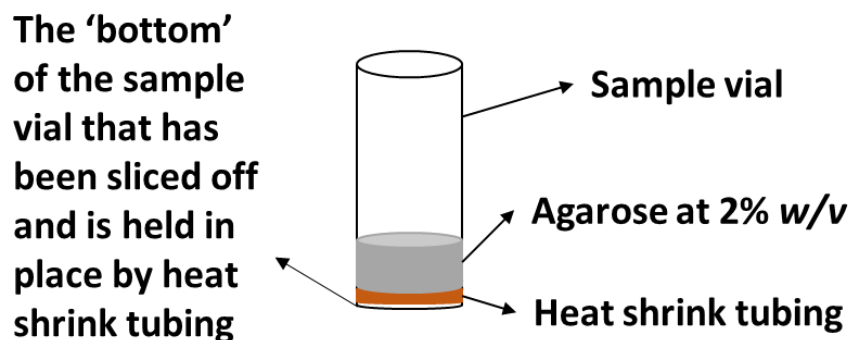


**Figure 3-6: HR-TEM image of gold nanowires in hexane. Scale bar 200 and 50 nm respectively.**

The bundling of the nanowires to form parallel aligned networks was similar to the behaviour observed by Feng *et al.*<sup>204</sup>

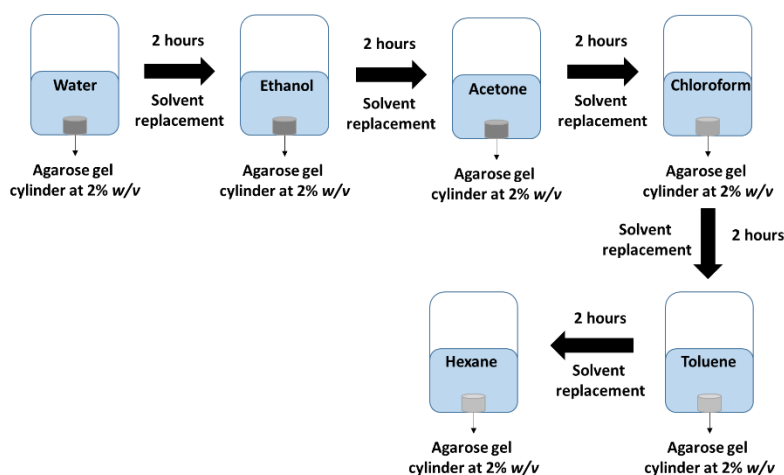
### 3.3.2 Incorporation of nanowires in agarose gels

An agarose gel in water at 2 % w/v concentration was prepared using a custom made 'bottomless sample vial' (section), once the gel has set, the heat shrink tubing was removed to get the bottom off and the gel cylinder was removed (Scheme 2-8).



**Scheme 3-3: Schematic showing the custom made 'bottomless sample vial'. The orange band represents the heat shrink tubing; the grey band represents the agarose gel cylinder.**

The resultant gel cylinder had solvent (water) consecutively replaced for 2 hours each with increasingly non-polar solvents such as ethanol, acetone, chloroform, toluene and hexane (Scheme 3-4). As the solvents get increasingly non-polar the gel cylinder gets progressively transparent, this could be due to the refractive index of the gel fibres getting closer to the respective solvents.



**Scheme 3-4: Incorporation of nanowires in hexane solution from section 3.3.1 into agarose gels**

The agarose gels in water and after solvent replacement in hexane were characterised using SEM (Figure 3-7). The images show a distinct difference in gel structure hydrated by water and by hexane, the gel fibres hydrated by water had well defined pores and a porous fibre network with well defined fibre diameters.

## Chapter 3: Gold nanowires in hydrogels

The gel in hexane was quite rough in structure and had very little pores or porous fibre network, it also looked to be folding in on itself which could be because of the volatility of hexane compared to water.

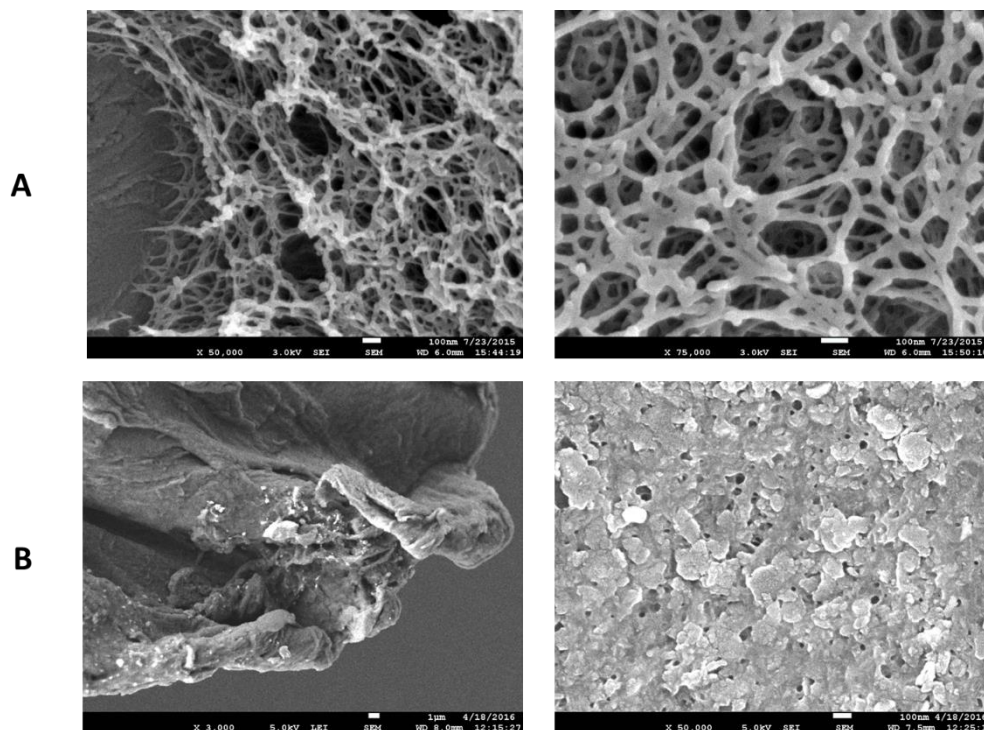
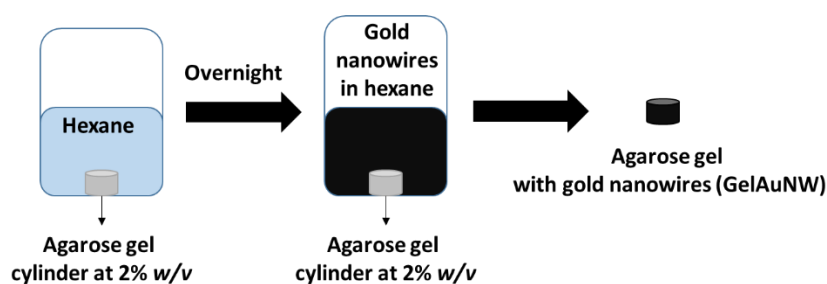


**Figure 3-7: SEM images of (A) Agarose in water, scale bar 100 nm in both cases. (B) Agarose in hexane, scale bar 1 $\mu$ m (left) and 100 nm (right)**

Once the solvent in the gel was replaced by hexane, the gel cylinder was placed overnight in gold nanowire solution prepared in section 3.3.1 to obtain a black coloured gel cylinder (GelAuNW) (Scheme 3-5).



**Scheme 3-5: Schematic of gold nanowire incorporation in agarose gel with hexane**

The resultant gel with gold nanowires (GelAuNW) were stable in the nanowire solution (sect 3.3.1) for  $\sim$  6 months, but if removed from solution and exposed to air, the gel dries out very quickly leading to a collapsed structure. The gel cylinders with nanowires were also analysed by HR-TEM to see if the incorporation was successful (Figure 3-8). The images show gold nanowires similar to Figure 3-6, with

long and thin nanowires with some gold nanoparticles and similar bundling of nanowires.

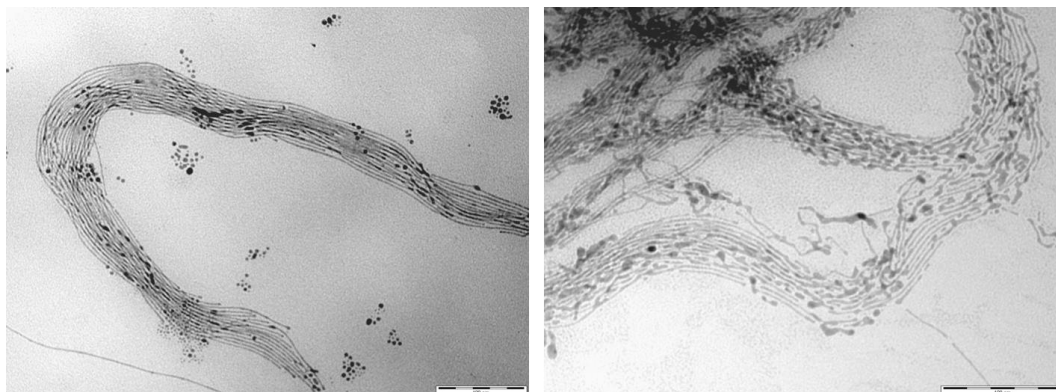
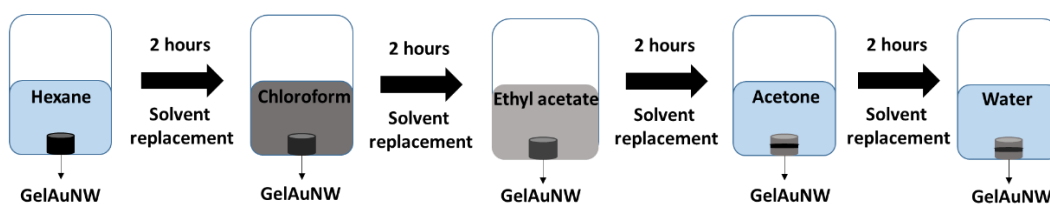


**Figure 3-8: HR-TEM images of wires in gels (GelAuNW). Scale bar 100 nm in both cases.**

Since these nanowires are incorporated in agarose gels with hexane as a solvent, they are unsuitable for use in biological systems. To improve their suitability, for biological applications, another solvent replacement back to more polar solvents was attempted. To achieve this, GelAuNW was soaked in increasingly polar solvents such as chloroform, ethyl acetate, ethanol and water for 2 h each (Scheme 3-6). As soon as the GelAuNW was placed in chloroform the GelAuNW started leaching the black nanowire solution and this continued until acetone was used in the solvent replacement procedure. Once GelAuNW was soaked in acetone a much darker band in the middle of the GelAuNW was observed which stayed even on complete solvent replacement to water. The GelAuNW cylinder seemed to lose their black colour and become increasingly opaque, except for the dark band.



**Scheme 3-6: Schematic showing the solvent replacement in GelAuNW in hexane.**

The dark band in the middle and the opaque areas of the GelAuNW were analysed by HR-TEM to see which nanostructures were giving rise to the colour changes and to understand if the wires were still stable inside the GelAuNW even on solvent replacement (Figure 3-9) and (Figure 3-10). The opaque part of the gels seemed to have gold nanoparticles with few broken nanowires whereas the dark band seemed



### Chapter 3: Gold nanowires in hydrogels

to have a larger proportion of broken nanowires than nanoparticles, this could be the reason for the darker colour in the band than the opaque sections of the gel.

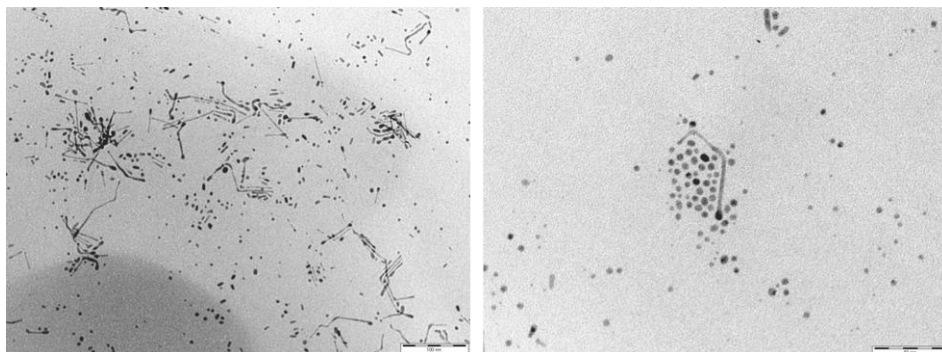


**Figure 3-9: HR-TEM images of GelAuNW in ethyl acetate (left) and the opaque area of GelAuNW in water (right). Scale bar 100 and 50 nm respectively.**

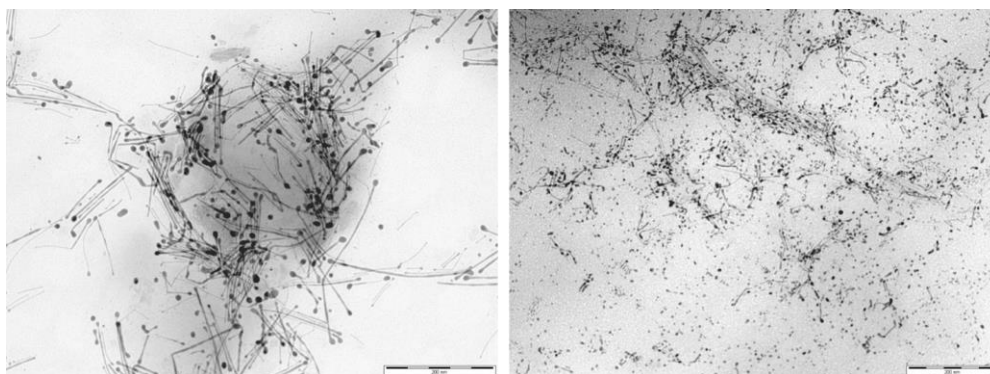


**Figure 3-10: TEM images of the dark band in GelAuNW in acetone (left) and water (right). Scale bar 200 nm in both cases.**

To prevent the AuNWs in GelAuNW breaking into gold nanoparticles, a milder solvent replacement procedure was attempted. The solvent was replaced in increasing polarity over 5 different solvents as shown in Figure 3-11, on using ethanol as the solvent a red band in the middle of the GelAuNW was observed.

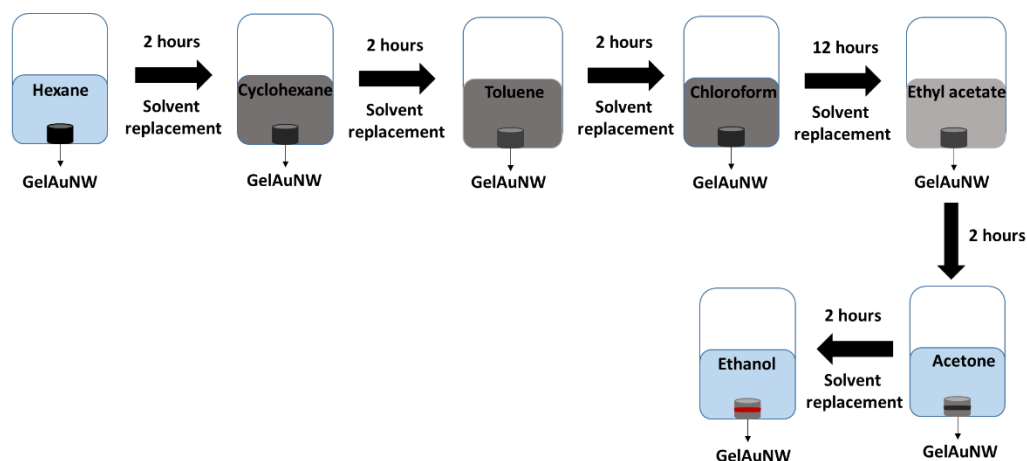


**Figure 3-11: Schematic showing the milder solvent replacement procedure in GelAuNW in hexane**

The red band was analysed by HR-TEM to identify if the colour was due to nanowires or nanoparticles (Figure 3-12). The HR-TEM images show only gold nanoparticles, no nanowires were observed, proving that the red colour in the gel cylinder was due to nanoparticles. These images also prove that the nanowires are not stable in gel cylinders once the solvent has been replaced to polar solvents. The nanoparticles continue to leach out of the gel, till an opaque gel with no colour was obtained.

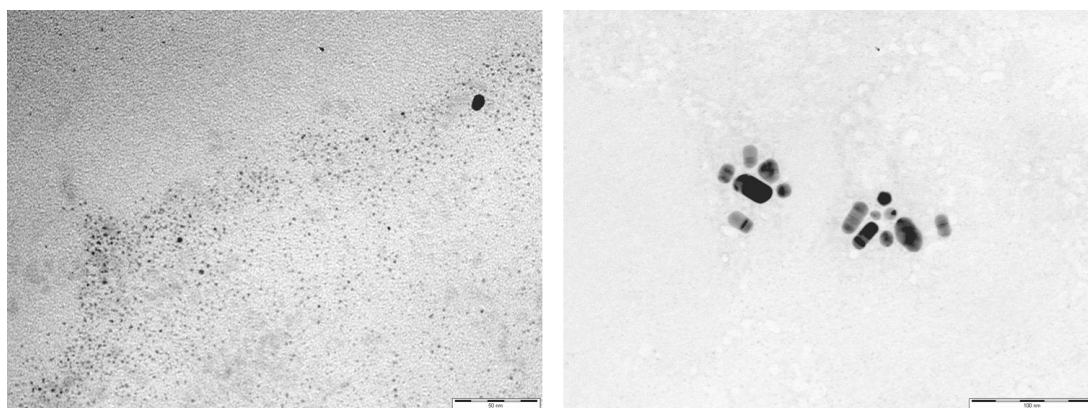


**Figure 3-12: HR-TEM images of red band in GelAuNW on solvent replacement to ethanol using a milder solvent replacement procedure. Scale bar 50 and 100 nm respectively.**

This was unfortunate as the requirement was for nanowire incorporation into agarose gels. The conductivity of these gels was tested to see if the presence of either the nanowires (GelAuNW) or the nanoparticles had any influence on how conductive the gels were compared to their absence.

### 3.3.2.1 Conductivity testing of GelAuNW

A 'custom made' design consisting of identical graphite blocks attached to a glass slide was used to measure the conductivity of these GelAuNW (Figure 3-13). The gel

cube was placed on top of the graphite blocks and the conductance measurement was recorded using a conductivity meter.

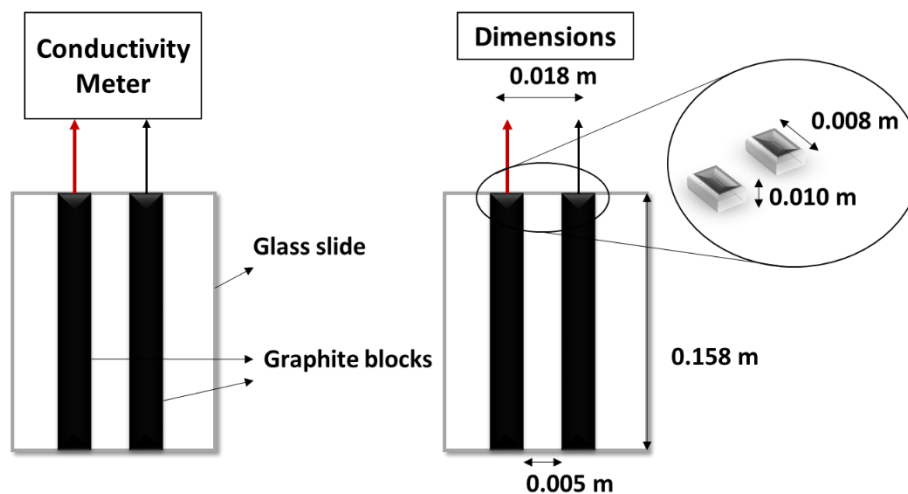


**Figure 3-13: The specially designed and arranged equipment for conductivity measurement and its dimensions. The inset is the area of the graphite block that is in contact with the gel mold.**

The conductance measurements were converted to conductivity using the length between the electrodes and the cross sectional area of the gel cube in contact with the graphite block. The dimensions used to convert conductance into conductivity are detailed below (Figure 3-13).

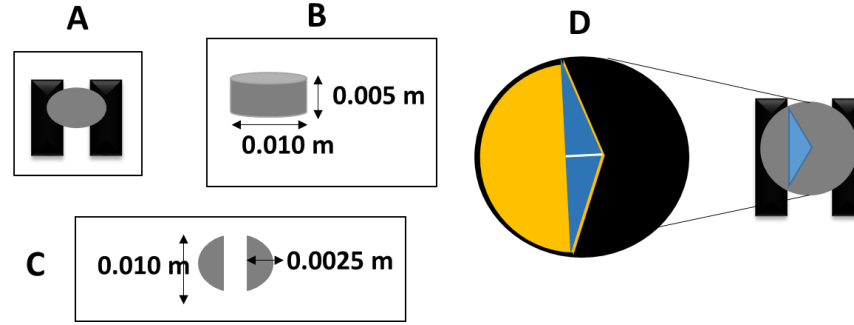
Conductance and conductivity are related by the equation below

$$G = \sigma \frac{A}{l} \quad (17)$$

$G$  is conductance / S,  $\sigma$  is conductivity / S m<sup>-1</sup>,  $A$  is the cross sectional area perpendicular to the direction of the current / m<sup>2</sup>,  $l$  is the length in between the electrodes / m.

The cross sectional area  $A$  was calculated using dimensions shown in Scheme 3-7. Since the area of the gel in contact with the graphite was part of a circle, a combination of equations was used to calculate the value of  $A$ .





**Scheme 3-7: (A) Schematic showing the position of the gel cylinder in respect to the graphite blocks, (B) Dimensions of the gel cylinder (C) Dimensions of the gel cylinder in contact with the graphite block (D) Area of the yellow sector is removed from the area of the blue triangle to get the area of the gel in contact (segment) with the graphite block.**

A combination of below equations was used; area of a triangle and area of a sector.

$$\text{Area of a sector (yellow)} = \frac{120}{360} \pi r^2 \quad (18)$$

In equation (2),  $r$  is the radius of the circle.

$$\text{Area of a sector} = \frac{120}{360} \pi \times (0.005)^2 = 2.62 \times 10^{-5} \text{ m}^2$$

$$\text{Area of a triangle (blue)} = \frac{1}{2} bh \quad (19)$$

In equation (3),  $b$  is the breadth of the triangle and  $h$  is the height respectively.

$$\text{Area of a triangle} = \frac{1}{2} \times 0.005 \text{ m} \times (2.89 \times 10^{-3} \text{ m}) = 7.23 \times 10^{-6} \text{ m}^2$$

$$\begin{aligned} \text{Since there are two triangles, the area is doubled} &= (2 \times 7.23 \times 10^{-6}) \\ &= 1.45 \times 10^{-5} \text{ m}^2 \end{aligned}$$

$$\text{Area of the segment} = \text{Area of sector} - \text{Area of triangle}$$

$$\text{Area of the segment} = (2.62 \times 10^{-5}) - (1.45 \times 10^{-5}) = 1.17 \times 10^{-5} \text{ m}^2$$

$$\begin{aligned} \text{Since there are two segments, the area is doubled} &= (2 \times 1.17 \times 10^{-5}) \\ &= 2.34 \times 10^{-5} \text{ m}^2 \end{aligned}$$

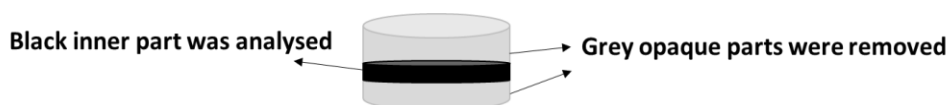
$$\text{Length in between electrodes} = 0.018 \text{ m}^2$$

Using equation (17), conductance measurements were converted to conductivity.

$$\frac{G \times l}{A} = \sigma$$

$$\frac{G \times 0.018 \text{ m}^2}{2.34 \times 10^{-5} \text{ m}^2} = \sigma$$

All the controls (no nanowires or nanoparticles) and samples were measured at minimum of 3 times and an average value was used for analysis.



**Scheme 3-8: Schematic showing the parts of GelAuNW in water that were analysed for conductivity**

For GelAuNW in water, the gel cylinders were cut to remove the opaque parts and only the darkly coloured middle portion of the GelAuNW was analysed for conductivity (Scheme 3-8).

**Table 3-2: Conductivity measurements of controls and GelAuNW in hexane and in water**

Name	Conductivity / $\text{Sm}^{-1}$	Volume of gel / ml	Gelator concentration / % w/v
Agarose in water	$5.39 \times 10^{-7}$	0.30	2
Agarose in hexane	$1.69 \times 10^{-7}$	0.30	2
GelAuNW in hexane	$1.11 \times 10^{-6}$	0.30	2
GelAuNW in water	$1.34 \times 10^{-4}$	0.30	2

The conductivity increases as you go down Table 3-2, GelAuNW in water and hexane have higher conductivity than all the other gels. GelAuNW in water has a relatively higher conductivity  $\sim 120$  times more than GelAuNW in hexane. This could be

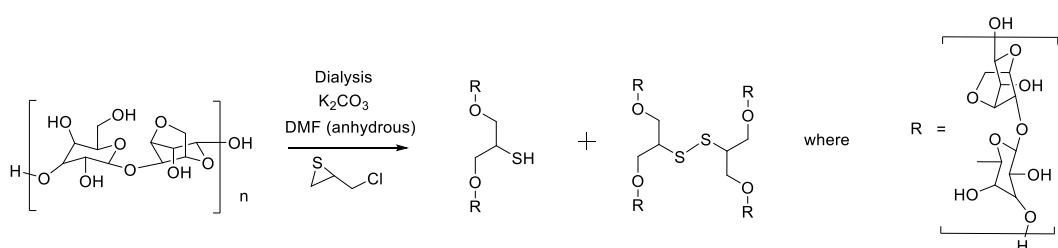
because the GelAuNW in hexane dries out very quickly making very little contact with the graphite block, whereas GelAuNW in water stays hydrated for longer making a good contact with the graphite block.

This proves the hypothesis that incorporation of nanostructures in gels make gels more conductive than the respective control. However, the instability of nanowires in the GelAuNW and their subsequent continual leaching makes them unsuitable for use in a bio-electrochemical system.

To improve the gold nanowire stability and to stop them leaching out of the gel, agarose gel structure can be modified to incorporate thiol groups as they are known to form Au-S bonds to stabilise gold nanostructures.<sup>181,392,393</sup>

### 3.3.3 Gold nanowires in thiolated agarose gels

A simple reaction was carried out in DMF using agarose, potassium carbonate and epithiochlorohydrin (Scheme 3-9).<sup>394</sup> The hydroxyl group of agarose was activated using potassium carbonate and reacted with epithiochlorohydrin for 12 hours at 85°C. The obtained product was dialysed for three days and lyophilised to obtain a dried yellow gel.



**Scheme 3-9: Functionalisation of agarose with thiol groups**

The dried gel obtained above was characterised by FTIR spectroscopy to identify the peak corresponding to a thiol group (Figure 3-14). FTIR spectrum of agarose compares well with literature values displaying the characteristic peaks for O-H stretch of the hydroxyl groups present within agarose, C-H stretches for CH and CH<sub>2</sub> groups present within agarose.<sup>317</sup> The C-O stretches were identified for the glycosidic linkage of the galactose units. The stretch at ~1659 cm<sup>-1</sup> was observed in the literature and also in the FTIR spectra provided by Sigma for unmodified agarose, the stretch is also observed for thiolated agarose and in both cases was attributed to bound water.<sup>314</sup> The gels were analysed in a freeze dried state so water should be minimal, but there could be residual water within the structure.

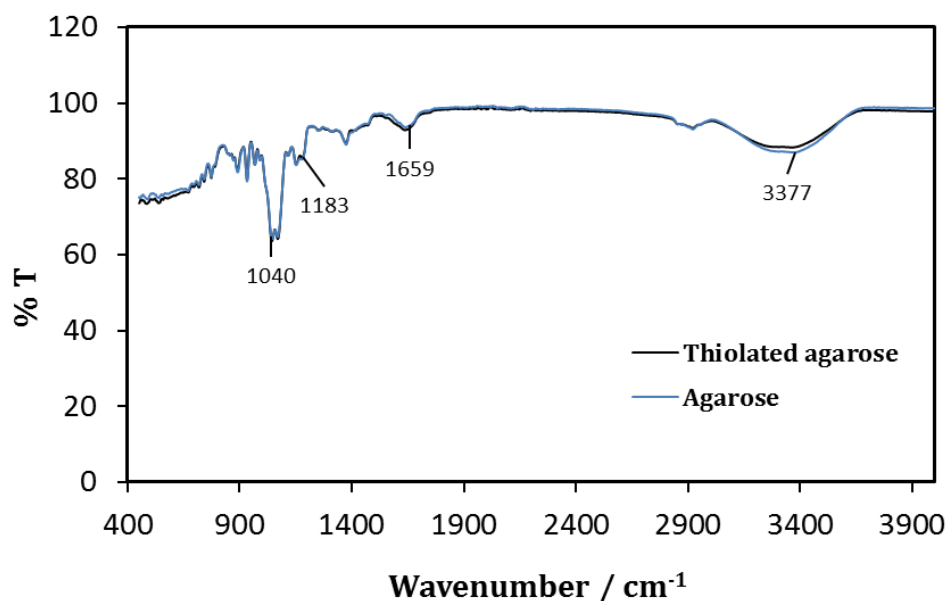


**Figure 3-14: FTIR spectrum of thiolated agarose (blue) and agarose (black)**

As both agarose and thiolated agarose are similar in structure, in their respective FTIR spectrums the peak positions and splitting patterns are almost identical, this could be because of very little thiol incorporation in agarose leading to undetectable peaks. This could be confirmed by elemental analysis of both agarose and thiolated agarose (Table 3-3). The elemental analysis confirms the percentage of sulphur incorporation into agarose, it equates to 1 sulphur group per 4 repeat units of agarose.

**Table 3-3: Showing the expected (exp) and observed (Obs) values of elemental analysis for agarose and thiolated agarose**

Name	C %		H %		S %		Rest %	
	<i>Exp</i>	<i>Obs</i>	<i>Exp</i>	<i>Obs</i>	<i>Exp</i>	<i>Obs</i>	<i>Exp</i>	<i>Obs</i>
<b>Agarose</b>	47.06	46.86	5.92	6.06	-	-	47.01	47.09
<b>Thiolated agarose</b>	45.45	44.20	6.10	6.09	8.09	2.31	40.36	49.72

The  $T_{gel}$  values of agarose and thiolated agarose were also recorded to understand if on thiolation the properties of the gel have changed compared to agarose. The gels were tested for their  $T_{gel}$ , using a temperature controlled oil bath (Table 3-4).

**Table 3-4:  $T_{gel}$  values of agarose and thiolated agarose**

Name	Gel concentration % (w/v)	Gel volume / ml	Temperature / °C
Agarose	2.88	0.3	97.8 - 100.1
Thiolated agarose	2.88	0.3	81.2 – 82.0

The  $T_{gel}$  value indicates the temperature at which a gel reverts to being a liquid. The  $T_{gel}$  of the thiolated agarose was  $\sim 18$  °C lower than agarose, indicating that thiolated agarose has physical properties different to agarose, further confirming that thiol incorporation was successful. In summary, elemental analysis and  $T_{gel}$  characterisations have confirmed the incorporation of thiol groups into agarose.

### ***3.3.3.1 Gold nanowire incorporation into thiolated agarose***

Gold nanowires were incorporated into thiolated agarose at a 2 % w/v concentration using a similar method as in section 3.3.2 where thiolated agarose (20mg) was heated to dissolve in water (1ml). However, on solvent replacement to more polar solvents such as acetone and water, the nanowires disintegrated into nanoparticles leading to the same coloured band in the middle of the gel cylinder and leaching of the colour into solvent. A single HR-TEM of the thiolated gels with gold nanowires was recorded in ethanol (Figure 3-15).

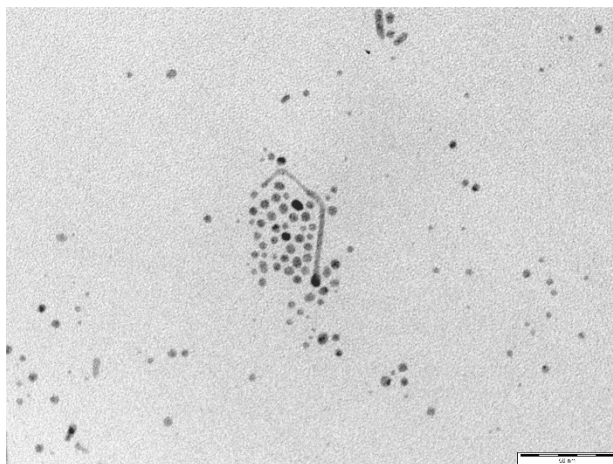


**Figure 3-15: HR-TEM image of gold nanoparticles in thiolated gel with gold nanowires in ethanol. Scale bar 50 nm.**

These thiolated gels with gold nanowires were not investigated further as on leaving the gels with nanowires in polar solvents for longer timescales, the gel completely lost colour. This was assumed to be due to the loss of nanowires. This led to the conclusion that the method of incorporation of gold nanowires had to be changed.

Electrodeposition can also be used to incorporate gold nanowires in agarose, this would ensure a direct incorporation of wires into the gel structure without the need for solvent replacement before or after nanowire incorporation. Using this method, a high concentration of gold nanoparticles could be incorporated into agarose at a relatively short time without the use of external reducing agents and purification process. It can also give a measure of the change in gels conductivity, as the quantity of gold nanoparticle incorporation increases because of the macrostructures that are formed on electrodeposition of gold. These are discussed in detail below.

### **3.4 Electrodeposition of gold nanowires in agarose gels**

#### **3.4.1 Gold nanowires in gels**

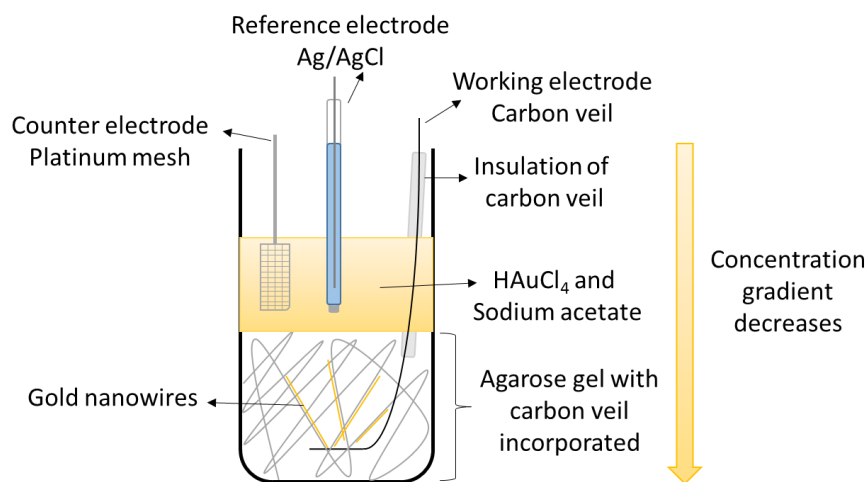
George and Vaidyan<sup>395,396</sup> have investigated the growth of silver dendrites and crystals in silica gel with particular emphasis on how the growth parameters effect the type of structures formed in gels using an electrolytic mechanism. Chakravorty *et al.*<sup>397</sup> have grown copper in silica gel using electrodeposition and have found that the applied voltage plays a major role in determining the type of structures formed and in their case lead to fractal growth of copper. Zou *et al.*<sup>398</sup> have electrodeposited

## Chapter 3: Gold nanowires in hydrogels

a thin layer of zinc dendrites of different morphologies in agar gel medium and have found that the gel medium plays a significant role in the type of morphology formed.

A similar method based on the above literature was chosen to electrodeposit gold nanostructures in an agarose gel medium. A three electrode electrochemical design with a reference electrode of silver / silver chloride, a working electrode of carbon veil cross linked by polyester and a counter electrode of a platinum mesh were used. By using a reference electrode, the potential of the working electrode can be maintained at a fixed value and would also allow for variation of potential if required.<sup>347</sup>

The idea was to use a design that would utilise the concentration gradient formed because of diffusion of the gold solution in an agarose gel, to preferentially electrodeposit gold nanowires in the direction of the gradient giving aligned fibers inside the agarose gel network (Scheme 3-10). The carbon veil was insulated using a two-part epoxy resin to prevent electrodeposition on the exposed part of the veil.



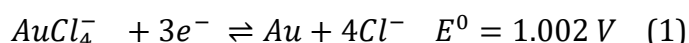
**Scheme 3-10: Schematic of three electrodes electrochemical design used to electrodeposit gold nanowires in agarose gel network**

### 3.4.2 Gold nanowires in agarose and thiolated gel

To increase the mechanical stability of the gel at high gold concentration and also to improve the gel's capability to support gold nanowire formation, a hybrid system containing a mixture of agarose and thiolated agarose (3.3.3) was used. An agarose and thiolated agarose gel at 0.5% w/v was prepared and poured on top of the partly insulated working electrode placed inside a sample vial and allowed to set at room temperature. An electrolyte containing chloroauric acid (~30 mM) and sodium

### Chapter 3: Gold nanowires in hydrogels

acetate trihydrate (100 mM) was added on top of the set gel and was diffused through this gel to generate a state of equilibrium within the interfaces, the reference and counter electrodes were placed in the electrolyte just on top of the gel. The electrodes were connected to a potentiostat to perform chronoamperometric measurements at a potential where  $\text{Au}^{3+}$  is reduced to  $\text{Au}^0$ , depending on the gold species present in solution, the reduction potential applied had to be varied. The reduction potentials of gold in chloroauric acid quoted vs SHE.<sup>399</sup>



In electrochemical experiments, mass transport, double layer capacitance, resistance and over potential influence the rate of deposition and also the structures formed during deposition.<sup>400</sup>

In general, the reduction potential of the metal is applied at an electrode but due to the factors mentioned above, a more negative (over potential) potential than the Nernst equilibrium or more positive (under potential) potential is applied. The applied potential controls the nucleation of the metal particles and their growth into 2D or 3D structures.<sup>401</sup>

The chronoamperometric experiment was run at a pH of 6-7 until a constant current was produced and a graph of current vs time was obtained (Figure 3-16).



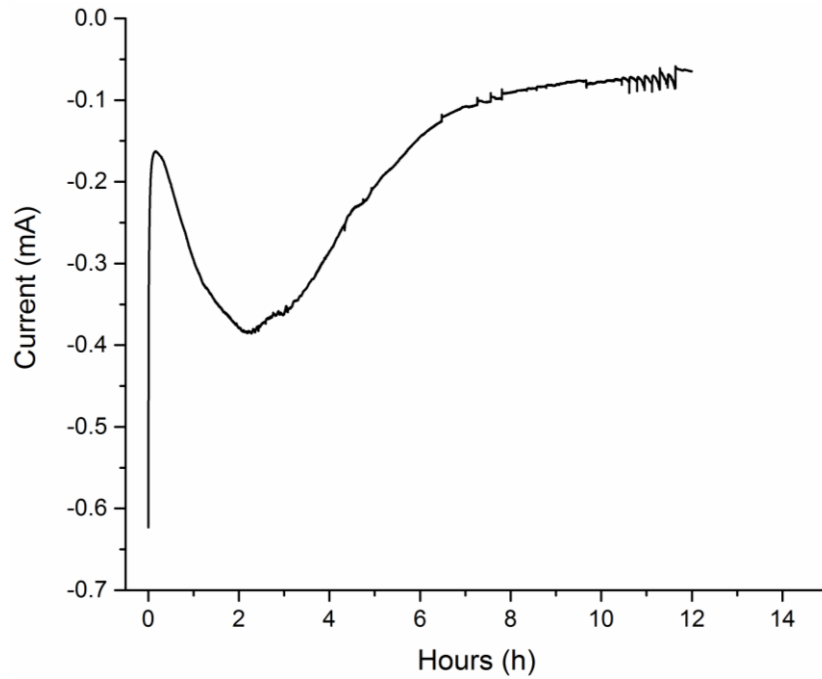


**Figure 3-16: Current vs time graph of electrodeposition in agarose and thiol gel at 0.5% w/v concentration**

The shape of the curve looks similar to the literature, where potentiostatic current-time plots of different growth models was considered. <sup>358,401,402</sup>

By eye the growth of macrostructures can be seen growing outwards from the veil and into the gel reaching the meniscus of the gel. (Figure 3-17).

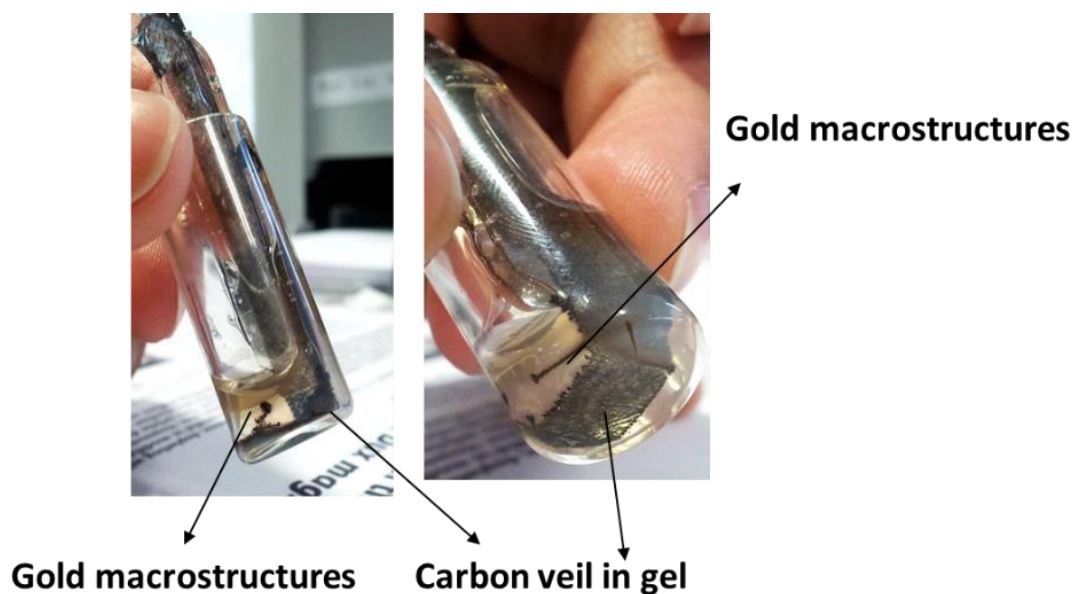


**Figure 3-17: Figures showing gold macrostructures growing inside agarose thiolated gel outwards from the working electrode carbon veil**

The gel and carbon veil were analysed by optical microscope to understand the morphology and the type of nanostructures formed inside the gel and on top of the veil. The carbon veil was extracted from underneath the gel and imaged using an optical microscope. The images are shown below (Figure 3-18), a control of just the veil without macrostructures was also done to compare it to the veil after the electrochemical experiment. Aggregated structures of gold can be seen coating the veil fibers.

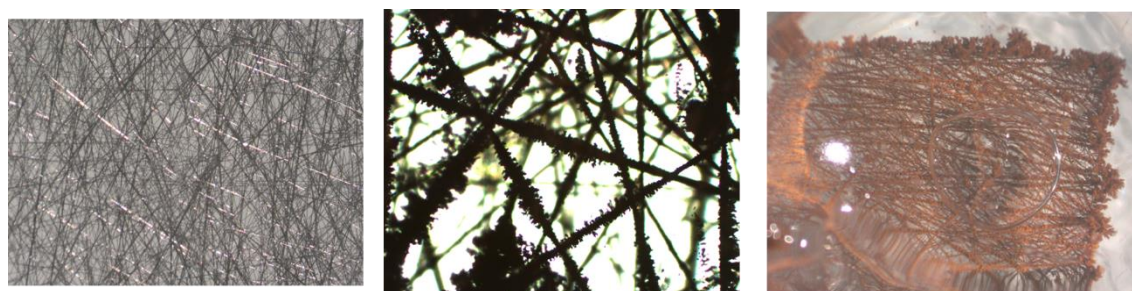


**Figure 3-18: Images of carbon veil before (left) and after (middle) the electrochemical experiment. Far right image shows the middle image at low magnification**

The gold macrostructures in the gel were analysed by HR-TEM to find a variety of morphologies within the gel (Figure 3-19). The images show some dendritic morphology (A) similar to the ones found by George and Vaidyan during their investigation of growth parameters on habit and morphology of silver crystals grown in gels.<sup>396</sup> The image (B) shows multiple nanoparticles inside the gel showing

a good distribution, it also shows the particles having a wide range of sizes that have small branches coming off them. The image (C) shows a trunk-like morphology completely made of gold nanoparticles, it was assumed that if the electrodeposition was continued, the trunk would have evolved into a dendritic structure.

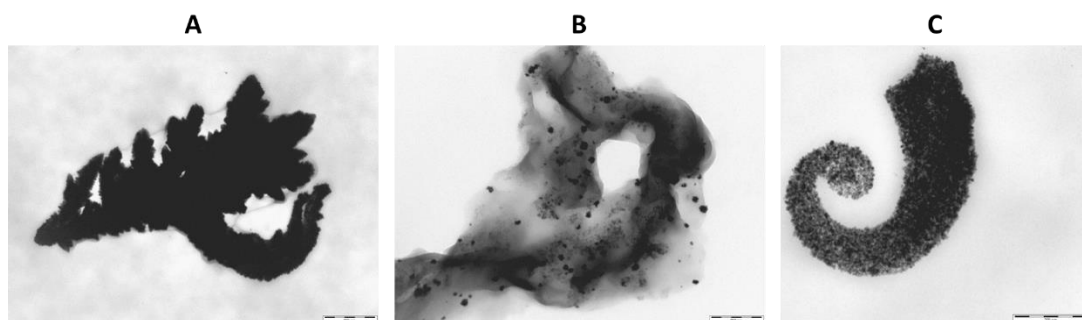


**Figure 3-19: HR-TEM images of the gold macrostructures formed during electrodeposition inside agarose and thiolated gel at 0.5% w/v concentration. (A) Shows a dendritic morphology, scale bar 500 nm (B) Shows a grey gel structure covered by black dots indicating gold nanoparticles, scale bar 500 nm (C) Shows a trunk like nanostructure formed inside the gel, scale bar 200 nm**

### 3.4.3 Gold quantification

It was important to determine the efficiency of gold deposition inside the gel; this can be calculated using Faraday's law.<sup>401</sup> The area under the curve of current vs time graph is equivalent to the charge passed; this was obtained by plotting the graph in Origin and using an analysis function to integrate the area under the curve. Since the experiment was exposed to air, an oxygen reduction reaction can also take place simultaneously to the gold reduction reaction. It was not possible to quantify the current produced because of just gold reduction, so the area under the curve representing the charge passed is a simplification. To improve the calculation, the constant current segment of the curve was disregarded.

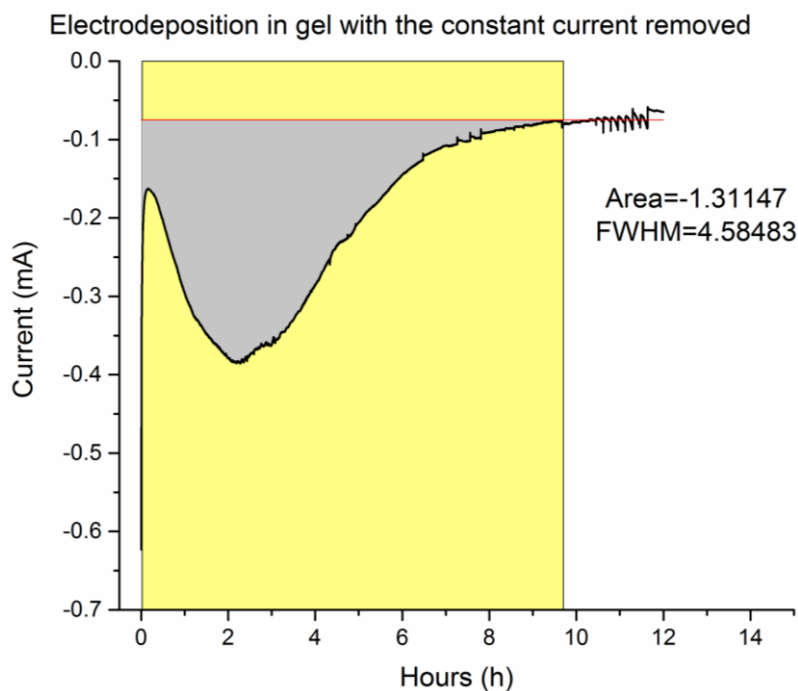


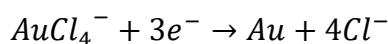
**Figure 3-20::** An image of the calculation of area under the curve using origin and the calculated area is highlighted in grey and the value is provided on the right hand side

The area under the curve is 1.3112 C.

$$\text{Current} \times \text{Time} = \text{Charge in coulombs}$$

$$1 \text{ mol of electrons} = 96,485 \text{ Coulombs}$$

$$\text{The number of moles of electrons} = \frac{1.3112}{96,485} = 0.0136 \text{ mmoles of electrons}$$



There is a requirement of 3 e<sup>-</sup> per mole of AuCl<sub>4</sub><sup>-</sup>. Therefore the

$$\text{Number of moles of Au} = \frac{0.0136}{3} = 0.00453 \text{ mmol of Au}$$

$$\text{Mass of Au deposited} = 0.00453 \text{ mmol} \times 196.97 \text{ gmol}^{-1}$$

$$\text{Mass of Au deposited} = 0.89 \text{ mg}$$

$$\% \text{ Current efficiency} = \frac{0.89 \text{ mg}}{5.77 \text{ mg}} \times 100 = 15.46 \%$$

Since the initial mass in the electrolyte was 5.77 mg, the deposition has an efficiency of ~ 15%. This is a very low efficiency, but as mentioned before the reason is that

the reduction is not specific to gold. In general if the constant current was assumed to be because of gold reduction then to completely deposit 5.77 mg, a charge of 8.52 C was needed which equates to about 22.43 hours as the reaction time. The consequent electrodeposition experiments were run for ~ 24 hours. Since the gold macro and nanostructures seem to be incorporated within the gel network these gels were tested for conductivity (Table 3-5). As expected the conductivity of the gels with gold dendrites is much higher than the respective controls, gels with no gold dendrites. Unfortunately, due to time constraints, the conductivity of plain agarose and thiolated agarose hybrid system was not recorded.

These gels can now be tested in a bio electrochemical system to see if the presence of the gold dendrites influences the current generated.

**Table 3-5: Conductivity data for gold nano and macro structures electrodeposited in agarose and thiolated gel at 0.5% w/v concentration**

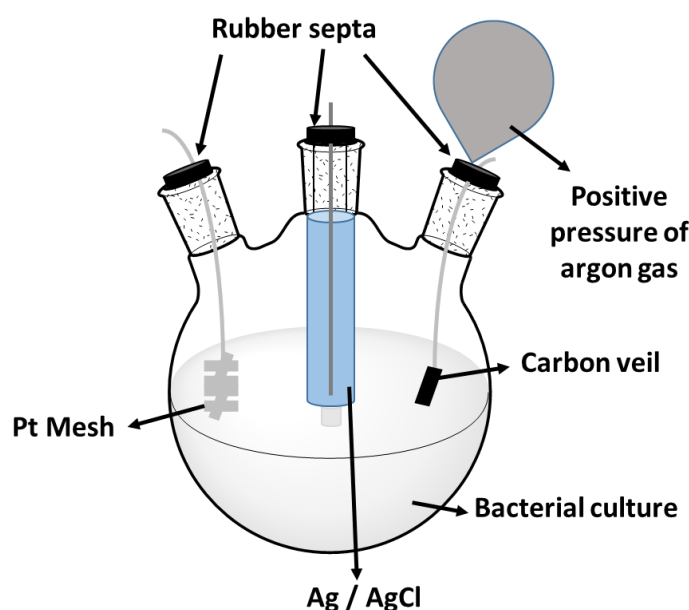
<b>Name</b>	<b>Repeats</b>	<b>Conductance / S</b>	<b>Conductivity / Sm<sup>-1</sup></b>
<b>Agarose only</b>	3		$5.40 \times 10^{-7}$
<b>Thiolated agarose only</b>	3		$1.90 \times 10^{-7}$
<b>Agarose and thiolated agarose with gold macrostructures</b>	1	$1.56 \times 10^{-3}$	
	2	$1.67 \times 10^{-3}$	
	3	$1.80 \times 10^{-3}$	
<b>Average</b>		$1.68 \times 10^{-3}$	$3.55 \times 10^{-3}$

These gels were tested in a bio electrochemical system to see if the presence of the gold dendrites influences the current generated.

#### 3.4.4 Electrochemical studies

The gels containing gold macrostructures were incorporated in a bio-electrochemical cell as a modified anode. The presence of the gold macrostructures was expected to improve current generation and electron transfer between So and

anode. A three electrode electrochemical design similar to Chapter 2 section 2.8 was used where the solution was a culture of *S. aureus* at an  $OD_{600}$  of 0.03 in minimal media that was purged with argon and sealed inside a three neck round bottomed flask. The reference electrode was Ag/AgCl, the counter electrode was a platinum mesh and the working electrode was the gel with gold macrostructures. The working electrode was prepared by carefully removing the insulated carbon veil with gel containing gold dendrites after electrodeposition and washing in water extensively to remove any electrolyte. The carbon veil was then sterilised in ethanol and used in the electrochemical design (Scheme 2-9).



**Scheme 3-11: Schematic of the three electrode electrochemical design used to record chronoamperometric data**

A chronoamperometric experiment was run for 27 h as per the limitation of the potentiostat to obtain a current vs time graph (Figure 3-21). The plot of the control with plain veil shows a similar shape to the plots before with the current initially increasing slowly and then rapidly with time. The current generated by the electrodeposited gel was higher than the plain carbon veil control, indicating that the presence of gold dendrites in the gel does improve the rate of electron transfer. However, the current generation seemed to reach a saturation point at about  $1.2 \mu\text{A}$  and does not increase any higher with time. This could be because the gold macrostructures might be disrupting *S. aureus* growth and biofilm formation hindering electron transfer.

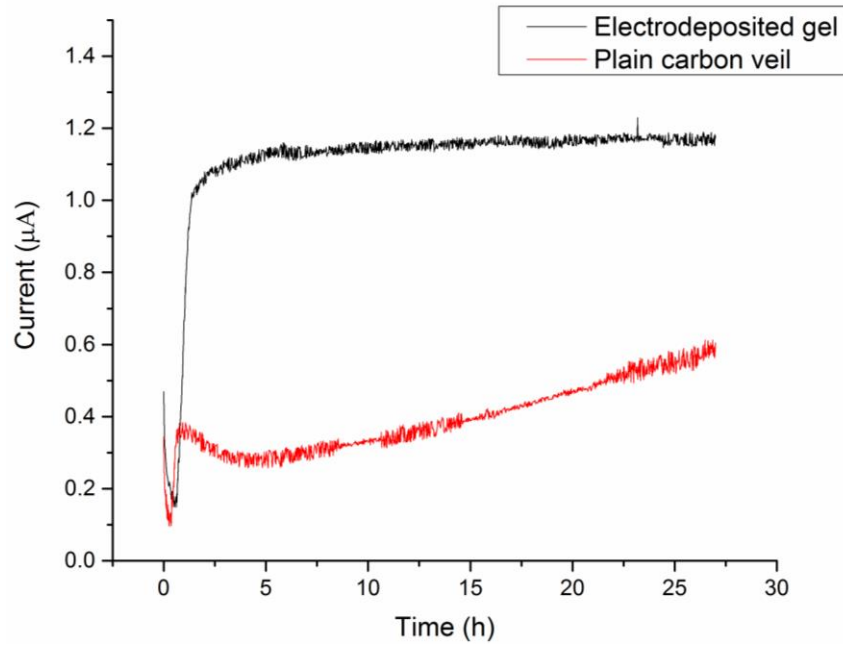


**Figure 3-21: Current vs time graph of electrodeposited gel used as the working electrode in an electrochemical experiment**

The areas of the carbon veil were the same in both cases, however since the gel was deposited on top of the veil, comparing current densities was not accurate. Since the current generation seemed to saturate with no further increase and growth of  $S_o$  seems to saturate as well, this gel with gold macrostructures was not pursued further.

### **3.5 Summary and conclusions**

Gold nanowires have been successfully incorporated into agarose gels using a 'novel' method of solvent replacement. The agarose gels with nanowires were stable in hexane as a solvent, but on replacing the solvent to water, the wires disintegrated into nanoparticles. The conductivity of the gels increased on nanowire incorporation, but due to instability in their structures and their leaching out of the gel completely, the idea was not continued further. Electrodeposition was used to incorporate gold macrostructures in an agarose and thiolated agarose hybrid gel system. Thiolated agarose was synthesised specifically to increase the agarose gel's capability to support gold nanowires. The electrodeposited gold macrostructures in the gel showed good conductivity and were tested in a bio-electrochemical cell. The presence of these gold macrostructures in the gel does seem to increase the current generated by improving the rate of electron transfer but the current generation saturated with time and did not increase further. This further proved that So growth was also affected since current generation is dependent on So growth. The gels with gold macrostructures are not a viable option to incorporate into a bio-electrochemical system.



## **Chapter 4: Gold**

**nanoparticle - decorated**

**So**

## 4 Introduction

The aim of this chapter, was to study the interaction of gold nanoparticles with *Shewanella oneidensis* MR-1 (*So*) and to use this interaction to improve electron transfer within a MFC. Improved electron transfer in a biofilm, has been shown to increase the current density and the power output of a MFC.<sup>124, 371</sup> There are many biological molecules present within a bacterial biofilm such as enzymes, EPS and some extracellular DNA. The presence of these biomolecules can hinder electron transfer process. By attaching gold nanoparticles to the surface of *So* their presence would enable the nanoparticles to act as electron relay units by acting as mediators.

### 4.1 Interaction of gold nanoparticles with bacteria

The synthesis of gold nanoparticles and their use to improve electron transfer in a bio-electrochemical system has been introduced in the main introduction **section 1.5**. The literature was reviewed to understand if nanoparticles can interact with bacteria without causing cell death<sup>403</sup> and also to investigate what determines these interactions of nanoparticles and bacteria.

#### 4.1.1 Cell structures of bacteria

Every bacterium's cell structure is specific to its species, however in general bacteria structures are classified according to the nature of their cell wall (Figure 4-1). There are two kinds of bacteria Gram positive (stains positive with Gram staining retaining the violet dye) and Gram negative (stains negative with Gram staining does not retain the dye).<sup>99</sup>

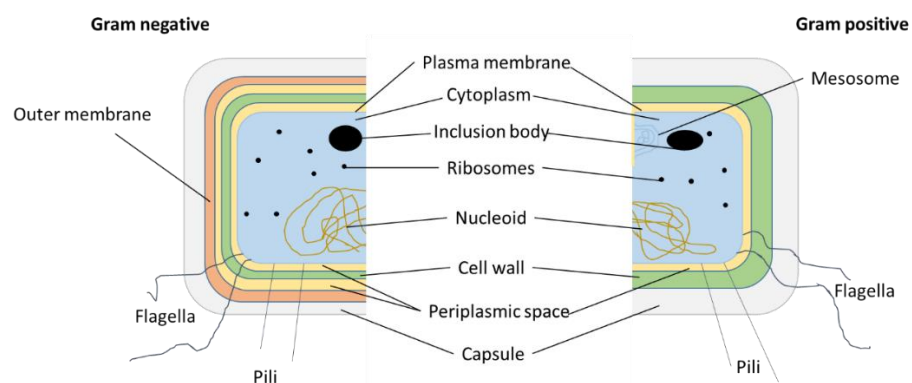
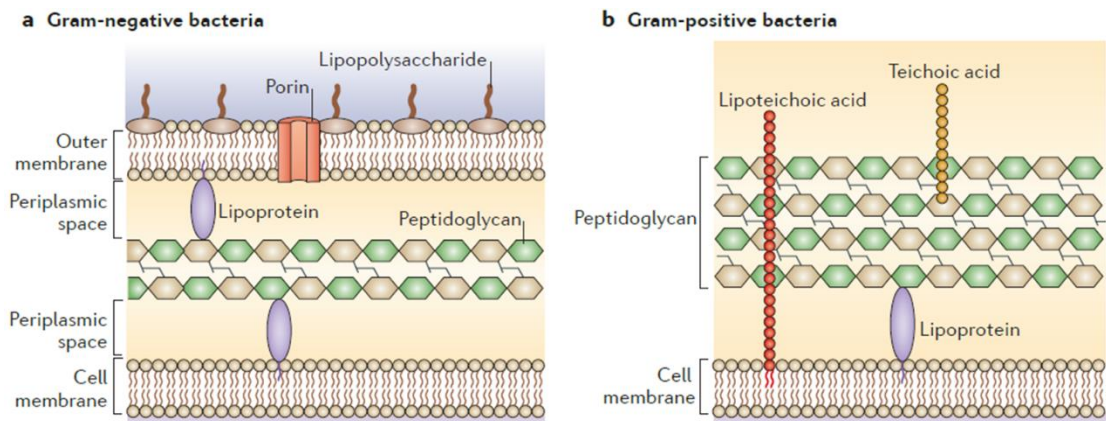


Figure 4-1: Cell structures of Gram negative and Gram positive bacteria. Adapted from ref <sup>404</sup>

Both Gram positive and negative bacteria have a plasma membrane followed by a cell wall and a capsule, the organelles present inside the cell are also similar. The plasma membrane contains phospholipids and is sometimes known as the inner membrane. The cell wall is composed of peptidoglycans (disaccharides and peptides) in both the Gram positive and negative cells. Gram positive cells have a thick peptidoglycan layer with teichoic acids (linear polymers made of polyglycerol, phosphates, sugars and amino acids) perpendicular to it. Teichoic acids distribute negative charge along the peptidoglycan wall. Gram negative bacteria have a very thin peptidoglycan layer followed by an outer membrane. The outer membrane is not present in Gram positive bacterial structure. The outer membrane contains lipopolysaccharides (LPS) and membrane proteins such as porins to transport nutrients across the LPS (Figure 4-2).<sup>100,404</sup>



**Figure 4-2: Images showing the difference in cell wall nature of Gram negative(left) and Gram positive (right) bacteria. Taken from ref <sup>405</sup>**

It is important to discover how these changes in cell wall nature influence a bacterium's interaction with nanoparticles.

#### 4.1.2 Biosynthesis of inorganic nanoparticles

Some bacteria that are capable of reducing metal salts to metal nanoparticles using their metabolism, such as *Shewanella oneidensis* MR-1 (So), *Escherichia coli* and *Lactobacillus* strains and they can biosynthesise metals such as gold, silver, uranium and chromium. <sup>229,230,232,262,264,406-408</sup> There are examples in literature of the production of inorganic nanoparticles by fungi, algae, plants and yeast as well. <sup>262,409</sup> The presence of nanoparticles can cause a change in the cell metabolism and understanding how this influences electron transfer and bacterial viability (ability to grow) is important.

Wu *et al.*<sup>236</sup> have conducted a simple experiment using wild type So and a mutant of So where the outer membrane proteins (OmcA and MtrC) responsible for electron transfer and metal reduction were deleted. They found that both the wild type So and mutant So were able to synthesise gold nanoparticles indicating that OmcA and MtrC are not the only outer membrane proteins responsible for metal reduction (Figure 4-3). The gold nanoparticles seem to be around the outer membrane of the So, no internalisation into the periplasmic space or the cytoplasm was observed.

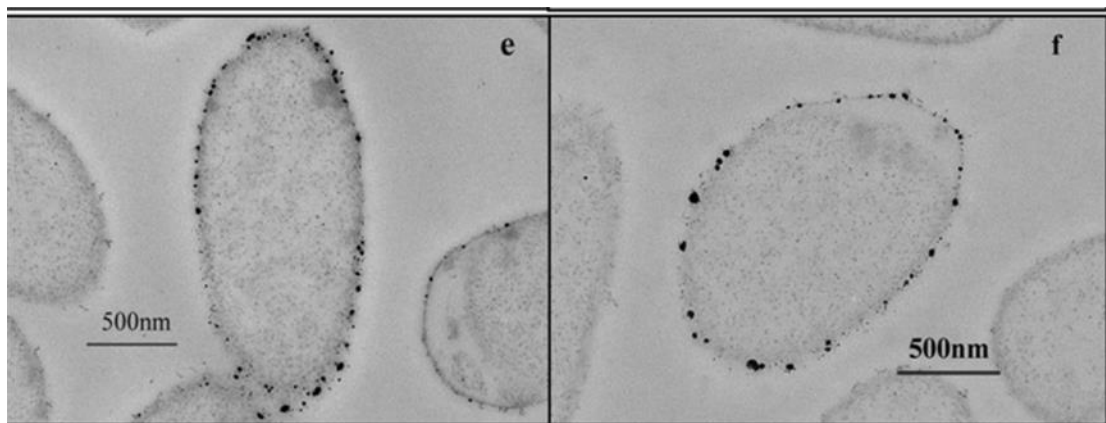


**Figure 4-3: Biosynthesised gold nanoparticles by wild type So (e) and mutant So (f). The black spots around the grey oval represent gold nanoparticles. Taken from ref <sup>236</sup>**

Cyclic voltammograms were recorded (-0.6 V to 0.4 V vs Ag / AgCl) for the strains by depositing them on a glassy carbon electrode (GCE), both strains displayed redox peaks relevant to the outer membrane proteins involved in electron transfer. But a reduction in redox peaks was observed for the Au synthesised - wild type So whereas Au synthesised - mutant So was able to produce a higher redox peak than wild So. This was attributed to the low gold nanoparticle loading improving the damaged electron transfer.

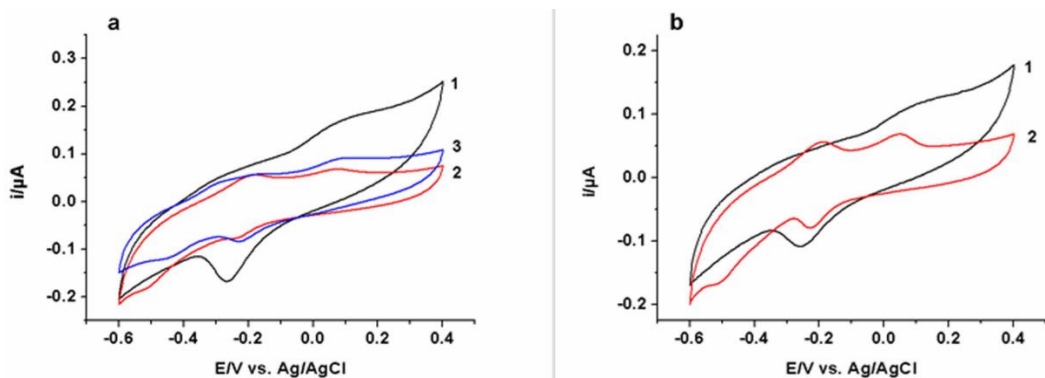


**Figure 4-4: Cyclic voltammograms for (a) (1) Au-free wild-type coated on a GC electrode; Au synthesised-wild type coated onto a GC electrode in the (2) absence and (3) presence of**

**lactate. (b) (1) Au-free mutant So and (2) Au synthesised-mutant So coated on a GC electrode. Taken from ref <sup>236</sup>**

The electron transfer capability of these nanoparticles was investigated by looking at lactate oxidation, on addition of lactate an increase in current was observed for both the Au-wild type and Au-mutant. The current increase was also rapid; this was not observed in the control experiment containing only the AuNPs on the electrode-no bacteria. This proved that the nanoparticles were somehow improving the oxidation of lactate by facilitating electron transfer by their presence on the cell membrane. However, no viability studies were conducted on the strains to check the growing ability of them after gold nanoparticle attachment.

This example proves that gold nanoparticles can improve electron transfer in So, but biosynthesised gold nanoparticles by So might partially hinder some electron transfer pathways.

#### **4.1.3 Pre-synthesised nanoparticles**

Pre-synthesised nanoparticles can be attached to bacteria and examples have been reported in literature. This will allow the bacterial electron transfer pathways to function without any hindrance.

##### ***4.1.3.1 Gold nanoparticles interaction with Gram positive bacteria***

Berry *et al.* have studied the interaction of *Bacillus cereus* (*B. cereus*) with lysine - protected gold nanospheres (diameter 30 nm)<sup>410</sup> and CTAB protected gold nanorods (diameter 25 nm) and nanospheres (diameter 45 nm).<sup>411</sup> In both cases a monolayer of particles and rods was formed on the bacterial surface, this was attributed to the electrostatic attraction between the positively charged gold nanoparticles and the negatively charged teichoic acids on the bacterial cell wall (Figure 4-5). Both systems were explored by current (I) vs voltage (V) studies to understand their conductance, showing a linear relationship. Gold nanorods proved to be ~4 orders more conductive than nanospheres.

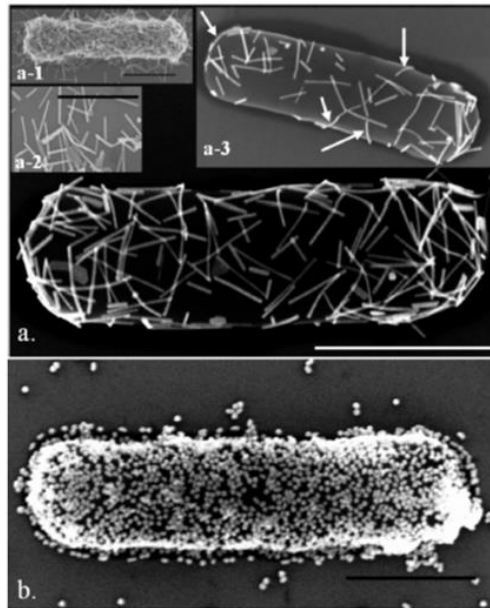


**Figure 4-5: CTAB protected gold nanorods and gold nanoparticles (right) deposited on *Bacillus cereus*. Scale bars are 1 $\mu$ m, adapted from ref <sup>411</sup>**

This example proves that pre-synthesised gold nanoparticles can be attached to bacterial surface using the charge on the gold nanoparticle and the bacterial surface leading to an increase in conductivity.

Shi *et al.* have reported the self-assisted assembly of gold nanoparticles by *Bacillus subtilis* (*B. subtilis*).<sup>408</sup> They were interested in studying how negatively charged citrate protected gold nanoparticles interact with Gram positive *B. subtilis* and found that bacteria connect end on end leading to a conductive gold nanoparticle coverage (Figure 4-6).

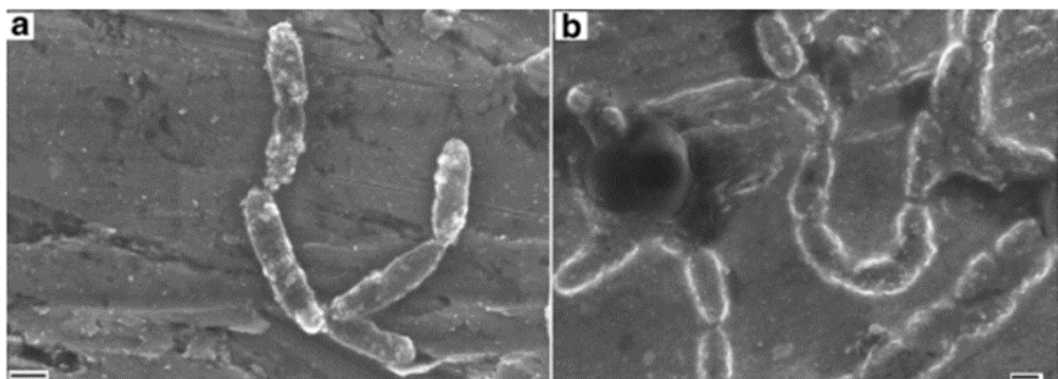


**Figure 4-6: End on end assembly of bacteria and coating by gold nanospheres (lighter spots on grey background) of the bacteria. Scale bar 1  $\mu$ m, adapted from ref <sup>408</sup>**

The main interaction between the nanoparticles and the bacteria was speculated to be not due to electrostatic interaction, but to the presence of sulphur residues on the bacterial surface, which stabilise the negatively charged citrate protected gold

nanoparticles. This is another example where charge on the nanoparticle influences their attachment to bacterial surface.

#### 4.1.3.2 Gold nanoparticles interaction with Gram negative bacteria

Two strains of bacteria *B. subtilis* (Gram positive) and *E. coli* (Gram negative) were tested with two different sizes of gold nanoparticles 6 (NP 1) and 2 (NP 2) nm protected by the same positively charged ligand (Figure 4-7) by Bunz *et al.*<sup>412</sup> The idea was to study how the size of gold nanoparticles impacts their interaction with two different bacteria (Gram positive and negative)

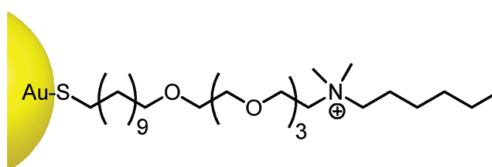


Figure 4-7: Ligand structure of NP 1 and NP 2

NP 1 aggregated and clustered around the surface of *B. subtilis* after 30 min incubation but no clustering was observed on the surface of *E. coli* (Figure 4-8). The aggregation of nanoparticles was attributed to surface proteins in both bacterial species. The main difference in both strains is the presence of teichoic acids on *B. subtilis* and the outer membrane proteins on *E. coli*.

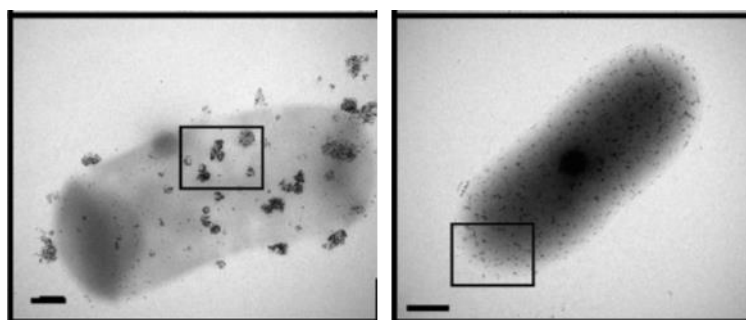


Figure 4-8: (Left) Aggregation and clustering of NP 1 (6nm) on surface of *B. subtilis* after 30 min incubation time (right) Aggregation of NP 1 (6nm) on the surface of *E. coli* after 30 min incubation time. Scale bar 200 nm, adapted from ref <sup>412</sup>.

NP 2 also interacted with *B. subtilis* and *E. coli*, with *B. subtilis* the NP 2 lysed the cells whereas *E. coli* showed increased blebbing and clustering of NP 2 on the bacterial surface but no lysis of cells (Figure 4-9). This could be because of the outer membrane presence in *E. coli* which has a Lipopolysaccharides (LPS), the nanoparticles could be interacting with the LPS or the other membrane proteins



## Chapter 4: Gold nanoparticles decorated So

present on the outer membrane. The outer membrane could also be responsible for the extra resistance of *E. coli* to the presence of nanoparticles.

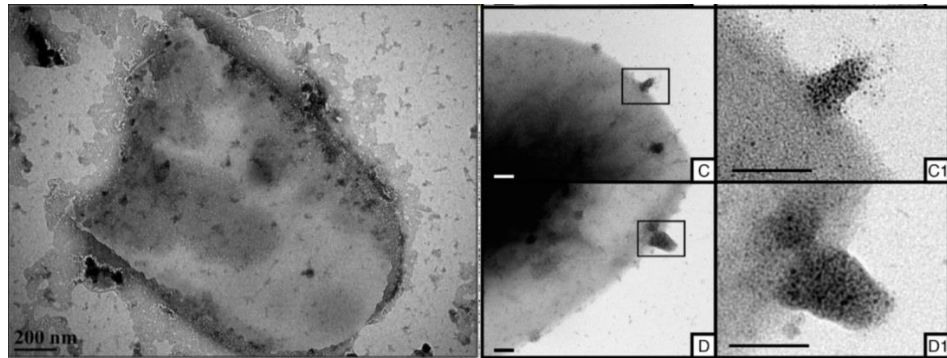


**Figure 4-9: *B. Subtilis* (left) lysed on exposure to NP 2, scale bar 200 nm. *E. Coli* (right) showing blebbing formation on exposure to NP 2, scale bar 50 nm. Adapted from ref <sup>412</sup>**

This proves that Gram negative bacteria are more resistant to cationic gold nanoparticles than Gram positive, the presence of the outer membrane seems to dictate the interaction between gold nanoparticles and Gram negative bacteria. It would be important to see if the same type of behaviour is observed for So when gold nanoparticle is attached.

Haynes *et al.* have also conducted a study of 3 different gold nanoparticles protected by 3 different types of ligands; anionic (MPA-AuNPs, ~4.5 nm in diameter), cationic (MPNH<sub>2</sub>-AuNPs, ~8.9 nm in diameter) and a cationic polyelectrolyte (PAH-AuNPs, ~4.5 nm in diameter) and interaction with *Shewanella oneidensis* MR-1 (So) (Gram negative) and *B. subtilis* (Gram positive) bacteria (Figure 4-10).<sup>413</sup>



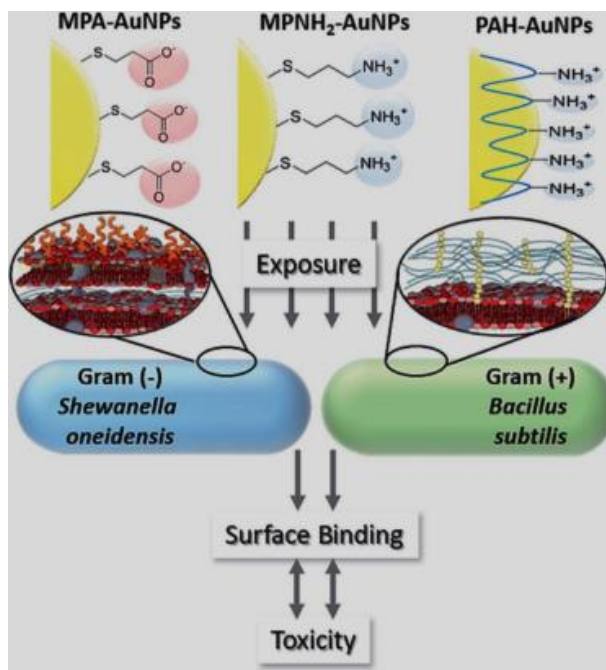


Figure 4-10: Schematic of the idea in literature. Adapted from ref <sup>413</sup>

Anionic gold nanoparticles MPA-AuNPs were the least associative with either *B. subtilis* or *So*. MPNH<sub>2</sub>-AuNPs and PAH-AuNPs both associated to *B. subtilis* and *So*, of both PAH-AuNPs associated more to *B. subtilis* than *So*.

The zeta potentials of the different gold nanoparticles were measured (Table 4-1), the association of the gold nanoparticles was found to be dependent on their surface charge, with the most associative having a higher zeta potential.

Table 4-1: Zeta potential measurements of the different charged gold nanoparticles. Adapted from ref <sup>413</sup>

Type of gold nanoparticle	$\zeta$ - potential value (H <sub>2</sub> O) / mV
MPA-AuNPs	-36.0 ± 1.4
MPNH <sub>2</sub> -AuNPs	26.7 ± 6.7
PAH-AuNPs	38.4 ± 1.8

MPNH<sub>2</sub>-AuNPs and PAH-AuNPs both have a positive zeta potential, but PAH-AuNPs has a much higher potential than MPNH<sub>2</sub>-AuNPs, this led to the PAH-AuNPs associating very strongly to *So* and causing cell lysis because of stronger electrostatic interactions between the PAH-AuNPs and bacterial membrane (Figure 4-11).

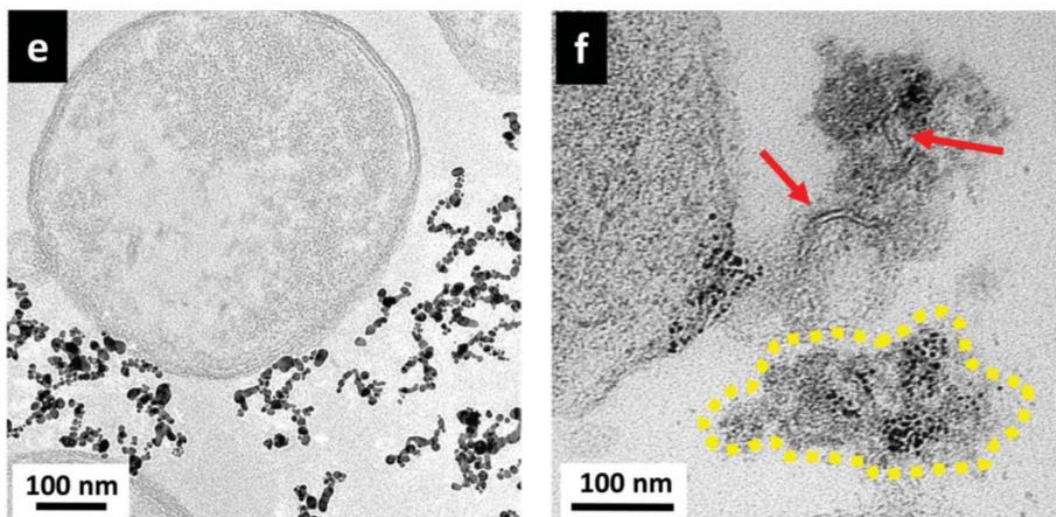


Figure 4-11: TEM images of MPNH<sub>2</sub>-AuNPs (e) and PAH-AuNPs (f) with So. Taken from ref <sup>413</sup>

This is the only example where So and its interaction with gold nanoparticles of different charges has been carried out with extensive viability studies. This study however, does not check for conductance or any electron transfer behaviour if applied in a bio-electrochemical system.

It is also important to note that in all cases of the literature, there was no internalisation of the gold nanospheres, nanoparticles or nanorods into the bacteria. Predominantly the nanoparticles were observed to associate with the outer membranes of Gram negative bacteria. From the literature is evident that pre-synthesised gold nanoparticles can be associated with So, but cationic gold nanoparticles of a small size (~2 - 8 nm) seem to be best suited for interaction. Cationic gold nanoparticles tend to aggregate and cluster on the surface of the So but depending on the zeta potential and charge density on the nanoparticles, the toxicity can be reduced.

#### 4.1.4 Aims of the chapter

The proposal was to identify a simple method for the incorporation of pre-synthesised gold nanoparticles into So. The AuNPs attached So were tested for their electrocatalytic ability in an electrochemical cell to check the effect on current generation.

## 4.2 Results and discussion

PAMAM G4 (NH<sub>2</sub> / SH) protected gold nanoparticles were chosen to be attached to So as they are positively charged, well characterised, provide control over particle

size, strong adhesion between ligand and gold nanoparticles and produce gold nanoparticles that are soluble in water.

#### 4.2.1 Synthesis of PAMAM G4 (NH<sub>2</sub> / SH) protected gold nanoparticles (DenAuNPs)

A PAMAM dendrimer is a poly(amido)amine molecule with terminal primary amine groups. The presence of amine groups at the ends makes them soluble in water and polar solvents. Dendrimers are highly branched flexible structures with a pre-defined cavity size. The terminal groups on dendrimers are multifunctional as they can be selectively modified to display specific groups, increasing the number and type of interactions as and when needed for a specific function such as catalysis and host-guest interactions.<sup>414</sup>

They are used in many applications from drug delivery, drug design to template synthesis. This makes the dendrimers very good ligands for functionalizing nanoparticles to make them biocompatible.<sup>415</sup> An illustration of a Generation 2 dendrimer is shown that reflects the size and complexity present within the dendrimers structure(Figure 4-12).

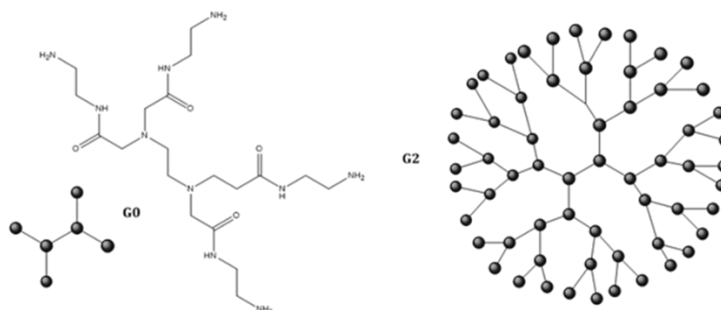
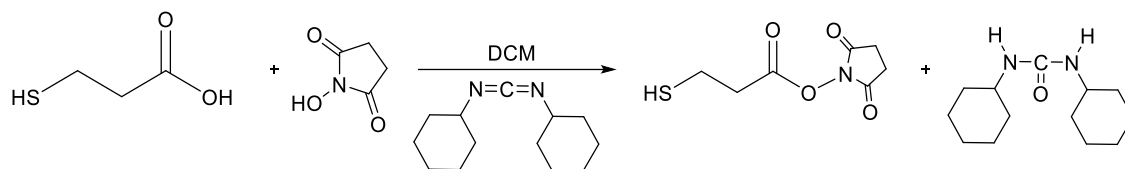


**Figure 4-12: PAMAM G2 dendrimer schematic. Each grey circle represents a nitrogen atom**

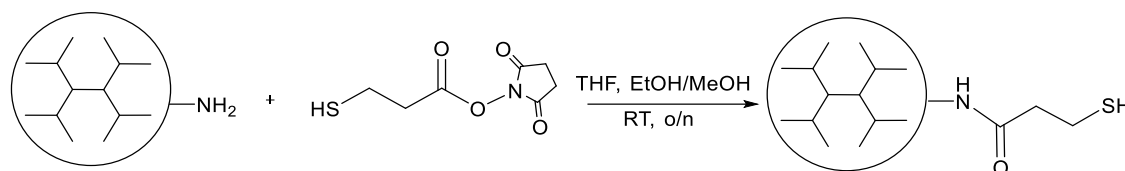
Dendrimers associate to the nanoparticle surface by a combination of Van der Waals and Au-N interactions which are labile in nature.<sup>416</sup> Selective thiolation of the primary amine groups to SH would increase the interaction with Au<sup>0</sup> by forming a strong S-Au<sup>0</sup> covalent bonds.<sup>181,346,393,417,418</sup> Thiolation of the dendrimer was achieved using 3-mercaptopropanoyl hydroxysuccinimide ester. It was synthesised following the literature procedure where mercaptopropionic acid and N-hydroxysuccinimide ester were reacted in the presence of carbodimide. The ester was purified and stored as stock solution in THF (Scheme 4-1).<sup>419</sup>

## Chapter 4: Gold nanoparticles decorated So



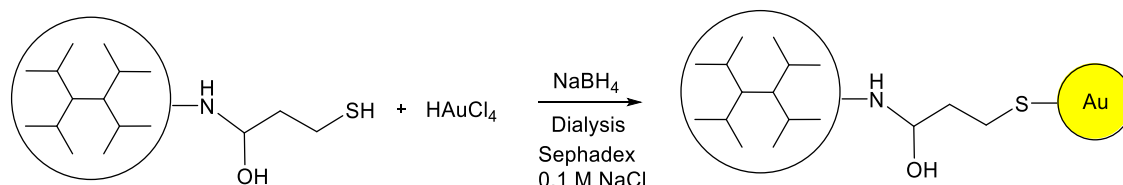
**Scheme 4-1: Synthesis of N-hydroxysuccinimide ester**

The PAMAM-G4 (NH<sub>2</sub>) was selectively thiolated using a procedure developed by Crooks and Chechik<sup>420</sup> which involved the addition of 3-mercaptopropanyl-N-hydroxysuccinimide ester to a solution of dendrimers, forming the 20% thiolated PAMAM-G4 (NH<sub>2</sub>/SH). The strong S-Au<sup>0</sup> covalent bond formed by the dendrimers would increase the nanoparticle stability to changes in pH (Scheme 4-2).



**Scheme 4-2: Synthesis of thiolated PAMAM G4 (NH<sub>2</sub>/SH) dendrimer**

This was further reacted with gold solution where the Au<sup>3+</sup> was reduced to Au<sup>0</sup> using excess sodium borohydride. The reaction solution changed colour from gold to black indicating nanoparticle formation, as reported in literature (Scheme 4-3).



**Scheme 4-3: Synthesis of PAMAM G4 (NH<sub>2</sub>/SH) protected gold nanoparticles (DenAuNPs)**

The particles were extensively dialysed and purified using gel permeation chromatography with Sephadex G-250. The obtained particles were stable in storage for 1-2 months without any aggregation.

### 4.2.2 Characterisation of DenAuNPs

DenAuNPs in solution, were characterised by UV-Vis spectroscopy (Figure 4-13). The spectrum shows a characteristic plasmon peak at ~ 535 nm specific to the gold nanoparticle shape and size. <sup>158,187,200</sup>

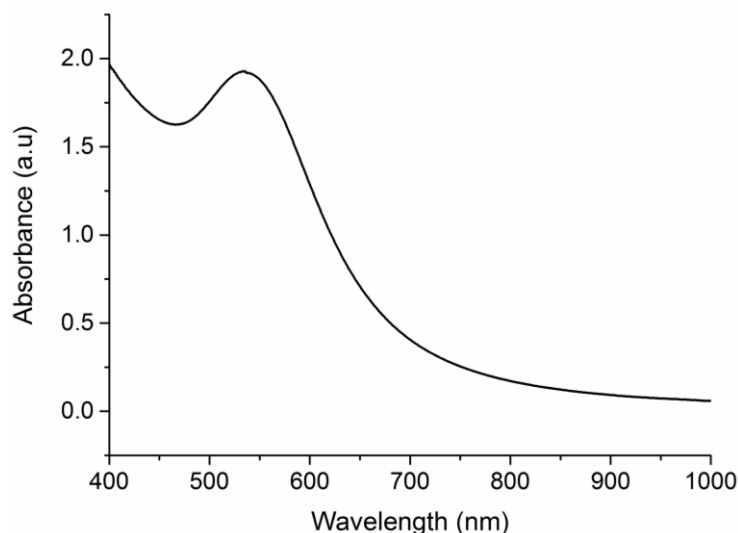


**Figure 4-13: UV-Vis spectrum of DenAuNPs in water**

DenAuNPs were analysed by zeta potential measurements (Figure 4-14) to determine their surface charge in water. The zeta potential was found to be 36.1 mV with a standard deviation of 7.59 mV, this was similar to the zeta potential of PAH-AuNPs (Table 4-1) synthesised by Haynes *et al.*<sup>413</sup>

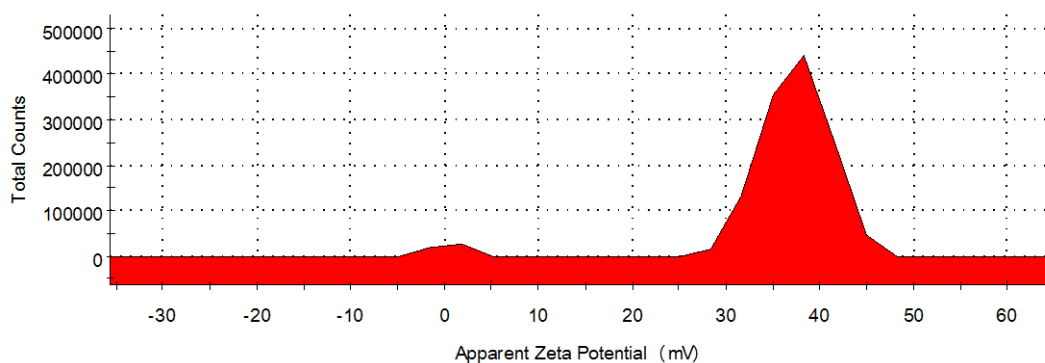


**Figure 4-14: Zeta potential distribution graph of PAMAM G4 (NH<sub>2</sub>/SH) protected gold nanoparticle**

DenAuNPs were also analysed by HR-TEM to determine their size and shape distributions, the images show a monodisperse distribution of particle sizes (Figure 4-15), the DenAuNPs seem well distributed with no aggregation.

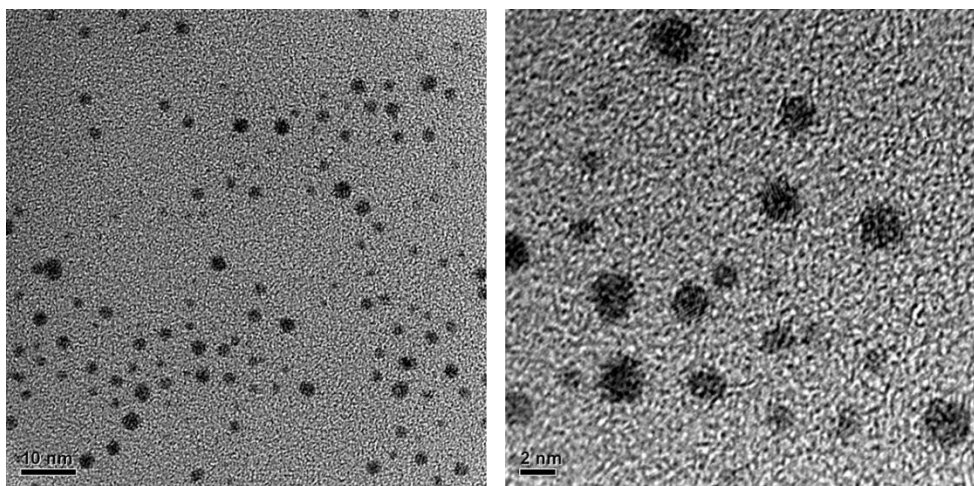


**Figure 4-15: HR-TEM images of DenAuNPs. Scale bar 10 and 2 nm respectively**

From Figure 4-15, 697 DenAuNPs (represent the sample) were analysed by Image J proGram to produce a histoGram showing the size distribution of the particles when (Figure 4-16). The average DenAuNPs size was determined to be  $\sim 2.3$  nm, this agrees well with literature and is suitable for attachment to So.

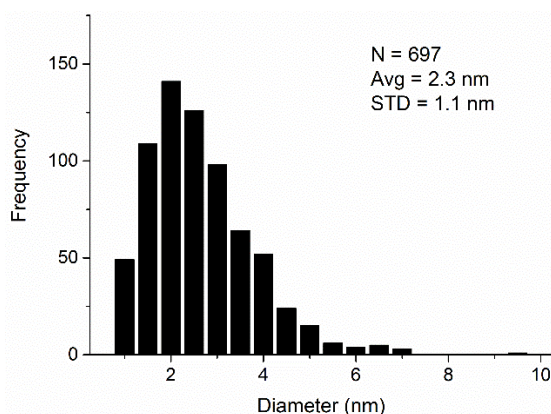


**Figure 4-16: HistoGram showing the size distribution of DenAuNPs**

A stock solution of DenAuNPs in water was digested by aqua regia to determine its gold concentration by ICP-MS and it was found to be  $\sim 0.31$  mg ml<sup>-1</sup>. To prepare a solution of DenAuNPs containing a higher concentration of gold, the stock solution was evaporated *in vacuo* to achieve a gold concentration of  $\sim 0.40$  mg ml<sup>-1</sup>.

#### 4.2.3 Incorporation of DenAuNPs into So

It was important to establish if DenAuNPs are stable in biological media such as Lysogeny broth (LB) and Phosphate Buffer Solutions (PBS) as they contain salts such as sodium chloride, disodium phosphate and potassium phosphate. Gold nanoparticles are known to aggregate and become unstable at high ionic strengths



if they are stabilised by electrostatic attractions by ligand exchange.<sup>188</sup> Since DenAuNPs are protected by thiol groups and primary amines a greater stability in both LB and PBS was expected as Au-S are resistant to ligand exchange.

A control experiment incorporating DenAuNPs into LB broth solution and PBS was conducted to check for any stability issues with the DenAuNPs. The gold nanoparticle solution 2.5 ml was mixed with 2.5ml LB broth and 2.5 ml PBS (0.01 M) in two separate containers respectively and incubated for 12 h. These solutions were analysed by HR-TEM to study the gold nanoparticles stability (Figure 4-17).

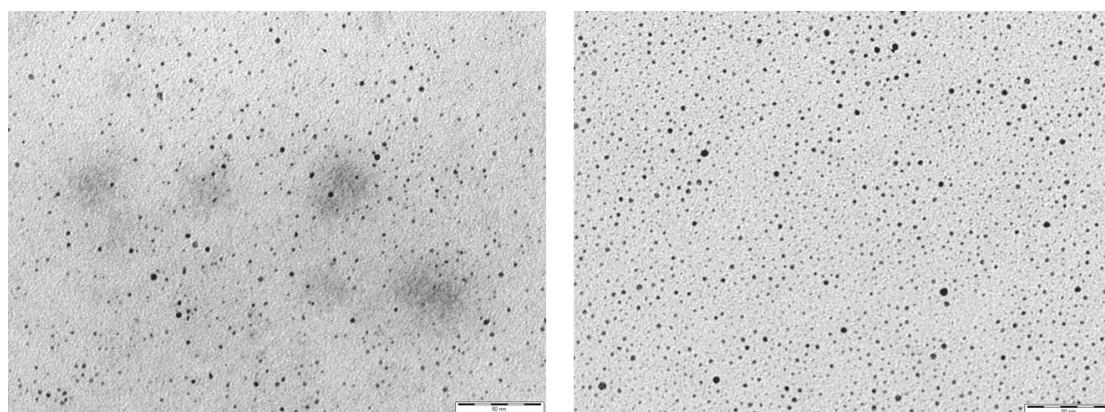


**Figure 4-17: TEM images of gold nanoparticles in LB broth (left) and PBS (right). Scale bar 50 nm respectively**

The images show DenAuNPs in both LB and PBS to be monodisperse with no aggregation or instability, this proves that DenAuNPs are suitable to be attached to So with good resistance to high ionic strengths. This also proves that DenAuNPs will be stable to changes in ionic strength over long term running in a bio-electrochemical system.

#### **4.2.3.1 First method of incorporation of DenAuNPs to *S. oneidensis***

Two different methods were used to incorporate DenAuNPs into So. The first was where So were grown *in situ* in the presence of the gold nanoparticles in an overnight culture at 25 °C with shaking at 180 rpm for 12 h. The growth time was similar to a normal liquid culture of So with no DenAuNPs, this incubation time was kept consistent to study the effect DenAuNPs on the viability of So.

The culture contained a mixture of 2.5 ml LB broth and 2.5 ml gold nanoparticle solution as there was very little growth of So (determined by OD<sub>600</sub> and the size of

## Chapter 4: Gold nanoparticles decorated So

pellet formed after centrifugation of 1 ml overnight liquid culture) observed when only DenAuNPs (5 ml) was used. The overall gold concentration was  $0.75 \text{ mg ml}^{-1}$  in the So liquid culture. 1 ml of the DenAuNPs + LB overnight culture solution was centrifuged to obtain a black pellet. A control culture with no gold nanoparticles was also grown, and pelleted to check the colour as if the pellet was not pink it would suggest the liquid cultures to be contaminated (Figure 4-18).

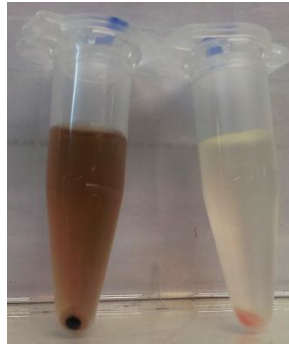


**Figure 4-18: Images of the pellets formed from overnight cultures grown with DenAuNPs (left) and without (right)**

The images show two different coloured pellets, one black indicative of DenAuNPs and pink indicative of only the So. Both pellets were resined and microtome for HR-TEM imaging (Figure 4-19).

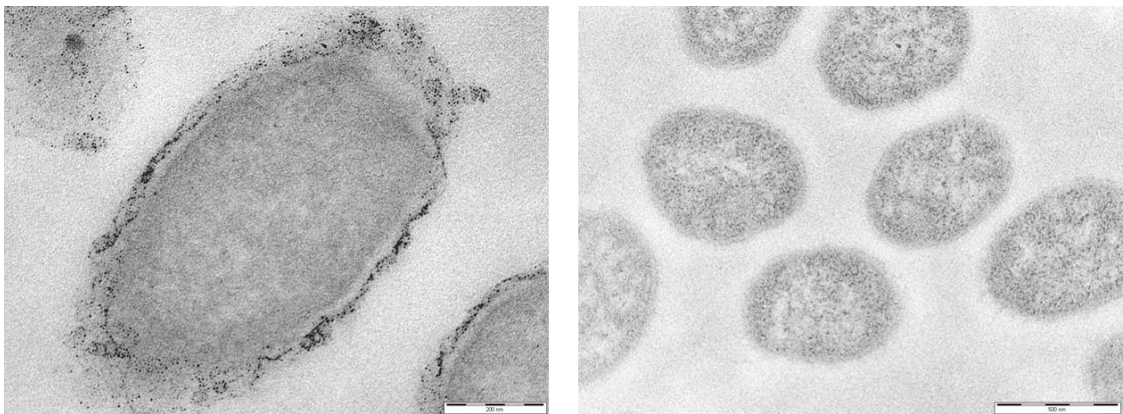


**Figure 4-19: HR-TEM imaging of So grown with DenAuNPs (left) and without (right). Scale bar 200 and 500 nm respectively.**

The TEM images show the gold nanoparticles surrounding the bacterial membrane, forming a shell around the bacteria but no DenAuNPs were found inside the So.



## Chapter 4: Gold nanoparticles decorated So

Haynes *et al.* <sup>413</sup> found a similar behaviour of PAH-AuNPs surrounding the membrane of So.

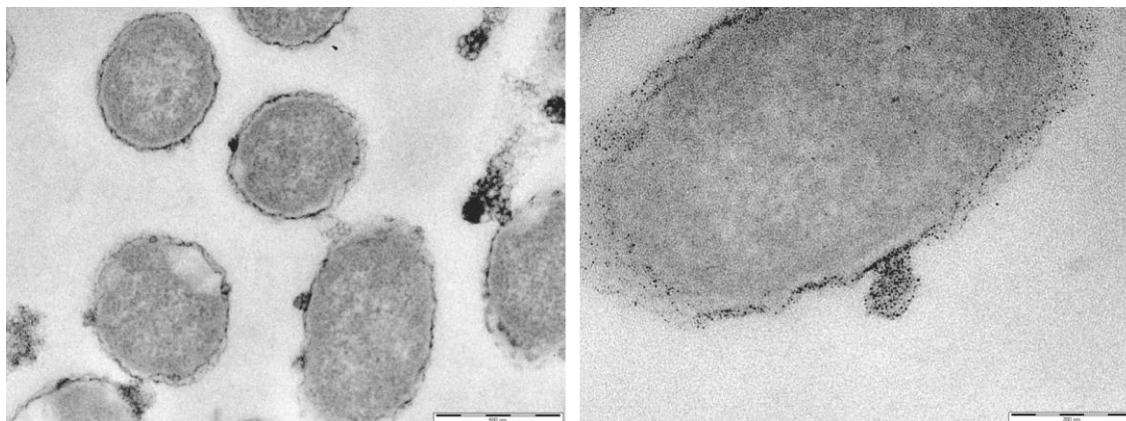


**Figure 4-20: TEM imaging of So grown with DenAuNPs, showing the concentrated regions of nanoparticles forming nodes on surface of bacteria. Scale bar 200 nm in both cases.**

Some of the So cells also show blebbing and clustering behaviour on the bacteria surface. This was similar to the blebbing behaviour observed by Bunz *et al.* <sup>412</sup> when *E. coli* were exposed to 2 nm sized gold nanoparticles protected by a cationic ligand, a nanoparticle similar to DenAuNPs.

The blebbing of DenAuNPs could be because of the Lipopolysaccharides (LPS) present in the outer membrane of So, the DenAuNPs could be interacting with the LPS or the other membrane proteins present on the outer membrane. The blebbing in *E. coli* was a cone shape whereas in So it was more rounded at the end, this could be because the height of LPS is different for every Gram negative bacterial species which could be dictating the shape of the blebbing. <sup>421</sup> It would be interesting to see the effect on blebbing when a higher gold concentration of DenAuNPs was used, as it would have more DenAuNPs per volume.

In a repeat experiment, a higher concentration of gold  $\sim 0.40 \text{ mg ml}^{-1}$  was used to investigate the effect on the DenAuNPs shell and their blebbing around the So (Figure 4-21).

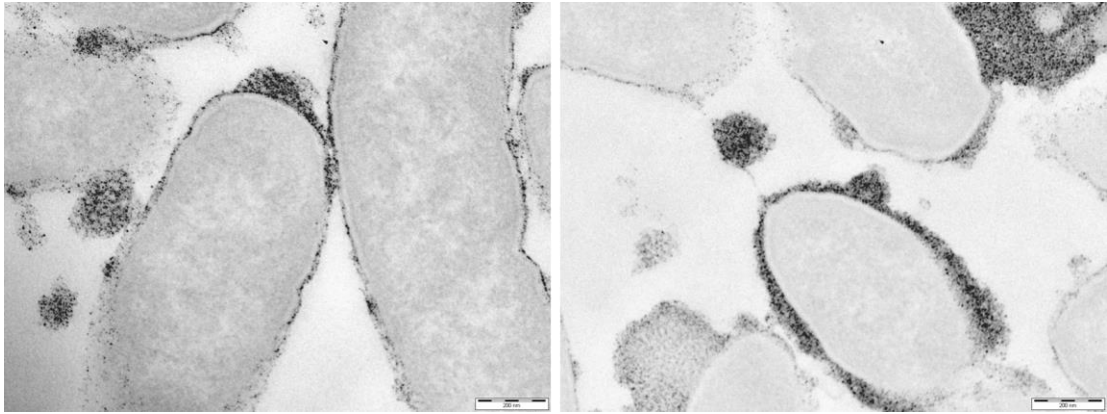


**Figure 4-21: TEM images at a slightly higher gold nanoparticle concentration and their attachment to *S. oneidensis* MR-1. Scale bar 200 nm in both cases.**

The shell around the So increased in thickness, and started forming a bridge between individual So cells linking them together (Figure 4-21). These could be the nanowires produced by So which are known to be extensions of the outer membrane electron transfer proteins of So itself (Figure 4-22).<sup>131,258,260</sup>

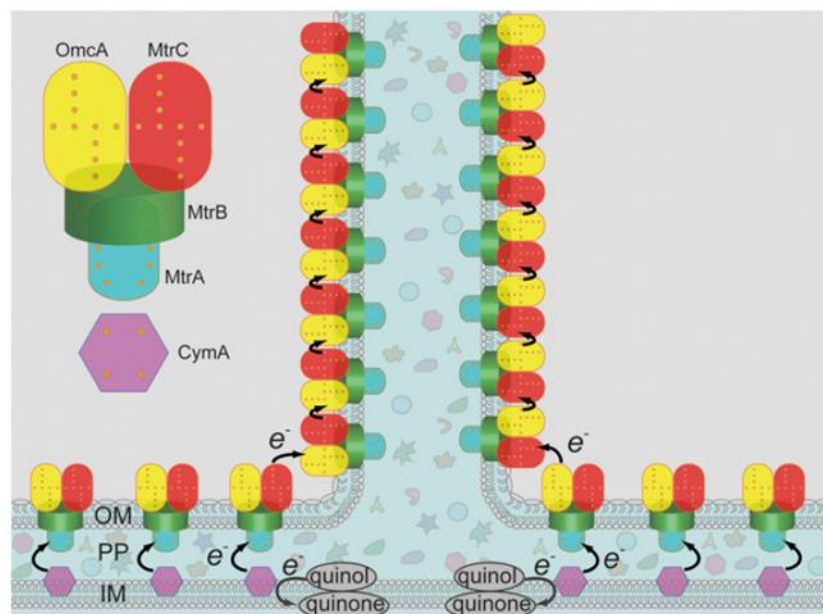


**Figure 4-22: Proposed structural model for So nanowires. Showing that the nanowires are outer membrane (OM) and periplasmic (PP) extensions including the multiheme cytochromes responsible for extracellular electron transport. Taken from ref<sup>131</sup>**

The linking of the So cells with DenAuNPs further proves that the interaction of DenAuNPs with So is related to the outer membrane structures of So. In all cases there was some lysis of cells, but not significant to impact growth. A second method was also pursued to attach DenAuNPs to So to investigate if the interaction between So and DenAuNPs would still be governed by LPS.

#### 4.2.3.2 Second method of incorporation of DenAuNPs to *S. oneidensis*

A second method of incorporation was also attempted, where the DenAuNPs were added to pre-grown liquid culture of *So*. The method consisted of pelleting a 1 ml *So* liquid culture and suspended it in a mixture of DenAuNPs (0.5 ml) and PBS (0.5 ml, 0.01M) and incubating it for 12h (keeping consistency for comparison). The resultant solution was pelleted and resined as before for TEM imaging (Figure 4-23).

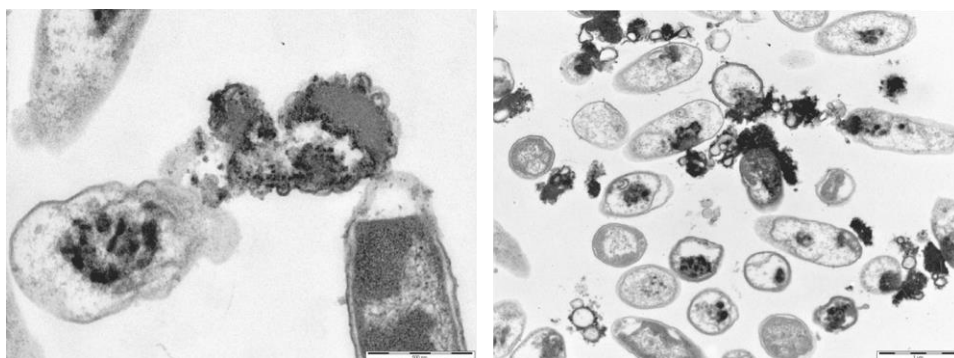


**Figure 4-23: TEM images of *So* cells on addition of DenAuNPs after growth. Scale bar 500nm and 1  $\mu$ m respectively.**

The gold content was measured to be  $\sim 0.15 \text{ mg ml}^{-1}$ . The images show most of the *So* cells undergoing lysis with the inner contents spilling outside the membrane. This is similar to the behaviour observed by Haynes *et al.*<sup>413</sup> when *So* were exposed to PAH-AuNPs. In most cases the gold nanoparticles seem to be interfering with the membrane disrupting it and causing its deformation as was also observed by Haynes *et al.*

This is a complete opposite observation of the first method's results, where the gold nanoparticles interact with bacterial cells and bridge cells causing very little cell death. The reason could be attributed to the addition of gold nanoparticles after growth of bacteria. In the first method of incorporation, the *So* have just started growing and are able to interact with DenAuNPs, whereas in the second method the *So* have probably grown are interacting with DenAuNPs. This was further investigated by varying the time the gold nanoparticles were incubated with the grown *So*. This was to identify a time dependent relationship between interaction of DenAuNPs with *So* membrane and its disruption. Two incubation times were attempted 1 and 4h. and both the samples were resined and analysed by HR-TEM to observe the difference (Figure 4-24, Figure 4-25).

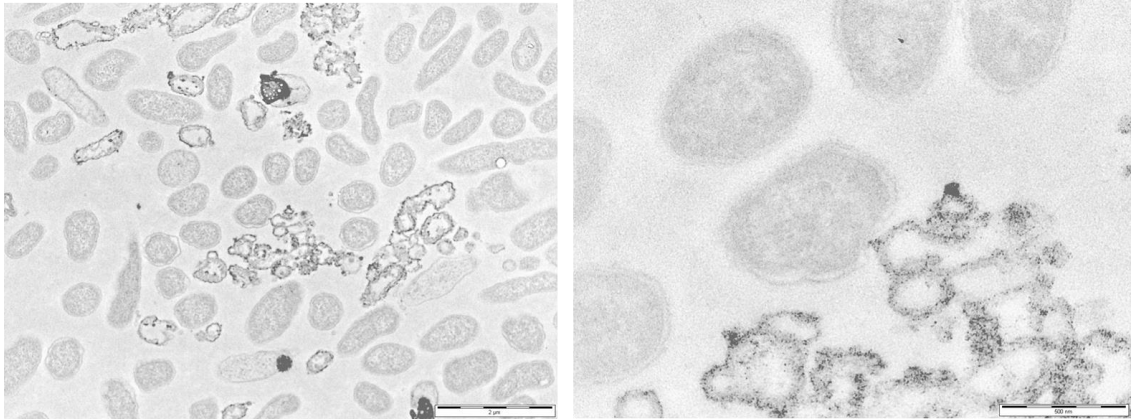


**Figure 4-24: HR-TEM images of So with DenAuNPs added after growth and incubated for 1 h.**

It was apparent that some So cell lysis has happened even at 1 h incubation time as the images show cells with ruptured membranes and the inner content spilling out.

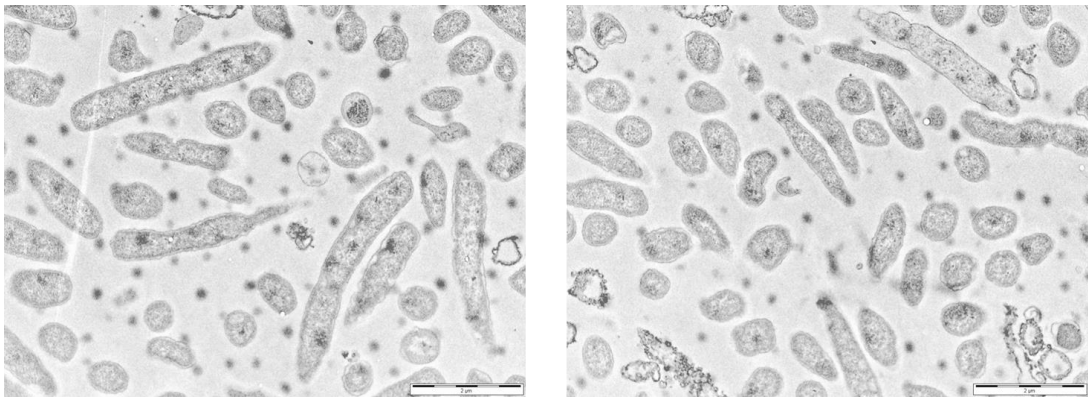


**Figure 4-25: HR-TEM imaging of So with DenAuNPs added after growth and incubated for 4 h**

For the incubation of 4h the same result was apparent, cell lysis and membrane deformation. There were no So cells with DenAuNPs attachment found in either incubation time. This could be because of a change in mechanism in which DenAuNPs associate with *in situ* growing culture of So and pre grown culture of So. It could be because in the *in situ* growth conditions the So cells are still metabolising at a fast rate and the DenAuNPs are able to take part in the electron transfer process of ATP synthesis. In the pre grown conditions So cells might be growing at a slower rate and DenAuNPs are unable to take part in electron transfer process and are attaching to So cells outer membranes that are already dying. This could be a reason as after 12h there are more number of dead or stationary bacteria that at 0 h. But this will not be investigated further in this project. Since this method proved to be

unsuccessful, the first method of growing So *in situ* in the presence of DenAuNPs was used throughout.

To prove that DenAuNPs are associating with the LPS using electrostatic interactions, negatively charged gold nanoparticles were also investigated for their attachment to So.

### **4.3 Citrate protected gold nanoparticles (CitAuNPs)**

#### **4.3.1 Synthesis of citrate protected gold nanoparticles (CitAuNPs)**

Negatively charged gold nanoparticles were synthesised using trisodium citrate as the protective ligand around the particles.

Trisodium citrate is a sodium salt soluble in water, which acts as both a reducing agent and a protecting ligand for the nanoparticles. This method was first pioneered by Turkevich<sup>161,179</sup> and further developed by G. Frens.<sup>180</sup> It involved a simple synthetic strategy consisting of the addition of citrate solution to a boiling solution of a gold salt (HAuCl<sub>4</sub>) to produce nanoparticles in a size range of (2-100 nm). The produced particles were soluble in water.

#### **4.3.2 Characterisation of citrate protected gold nanoparticles (CitAuNPs)**

The success of the reaction is inferred by a colour change of the solution from gold to purple. The particles were analysed by UV-Vis spectroscopy to find the plasmon resonance peak at ~ 550 nm (Figure 4-26).<sup>195,180</sup>

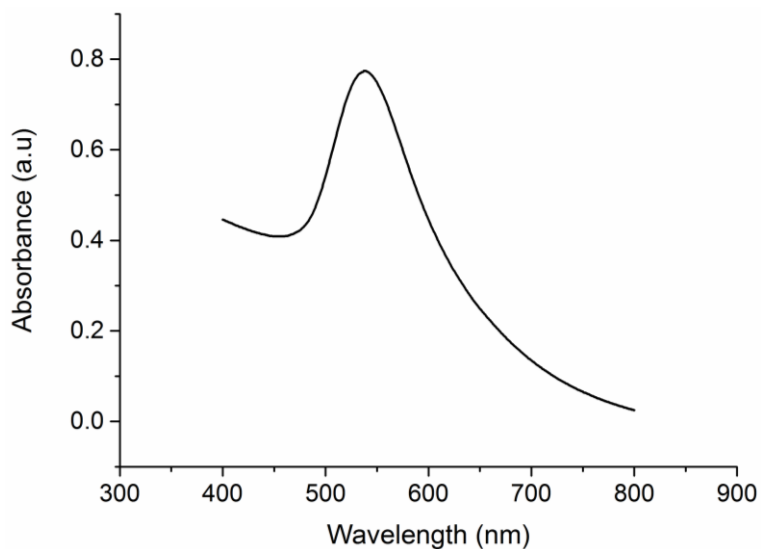


**Figure 4-26: UV-Vis spectrum of CitAuNPs**

The particles were also analysed by HR-TEM to determine the size and shape distribution of the CitAuNPs (Figure 4-27). The images show a mixture of spherical and triangular CitAuNPs but no aggregated CitAuNPs were found.

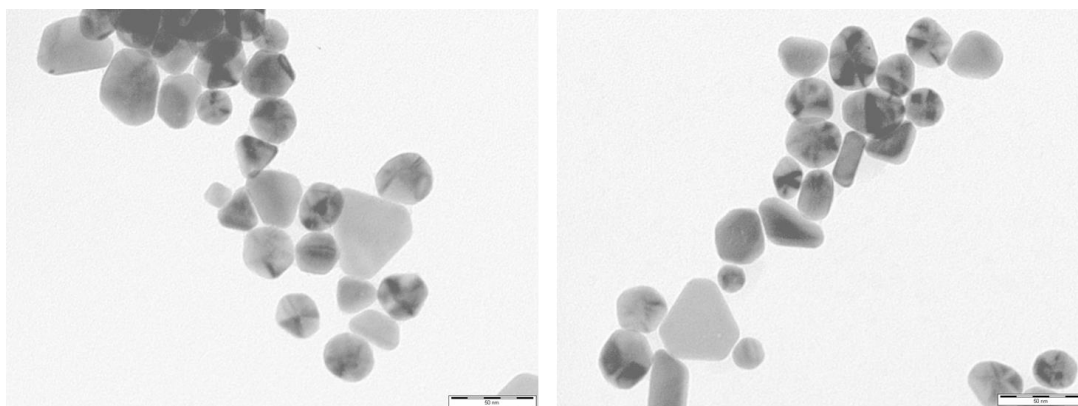


**Figure 4-27: HR-TEM images of CitAuNPs. Scale bar 50 nm in both cases.**

The HR-TEM images were used and 264 CitAuNPs (represent the sample) were analysed using Image J, to construct a histoGram showing the size distribution of CitAuNPs (Figure 4-28).

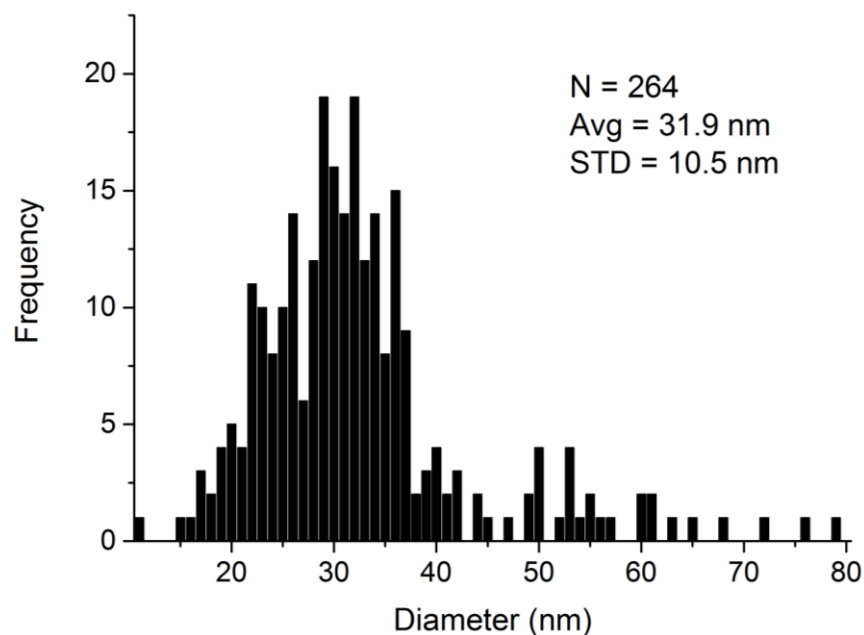


**Figure 4-28: Histogram showing the size distribution of CitAuNPs**

The histogram shows the average size of the CitAuNPs to be  $\sim 31.9$  nm with a standard deviation of 10.5 nm. These are a bigger size of gold nanoparticles than before (section 4.2.1). The charge on CitAuNPs was also confirmed using zeta potential measurements (Figure 4-29). The charge was found to be -30 mV with a standard deviation of 11.7 nm, this was similar to the MPA-AuNPs (Table 4-1) synthesised by Haynes *et al.*<sup>413</sup>

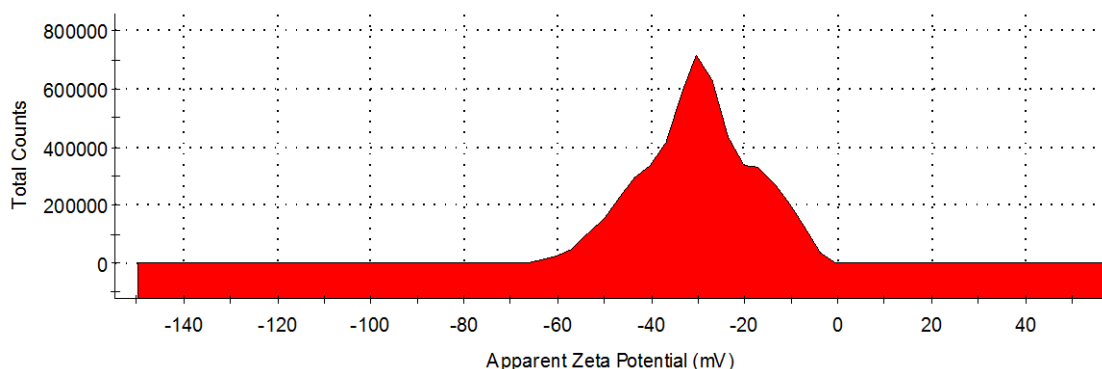


**Figure 4-29: Zeta potential graph of citrate protected gold nanoparticles**

### 4.3.3 Incorporation of CitAuNPs into So

CitAuNPs were incorporated into So using the first method (section 4.2.3.1). This was the method in which So were grown in the presence of the CitAuNPs. The overnight culture was centrifuged to obtain a purple colour pellet. The pellet was resined and analysed by HR -TEM (Figure 4-30).



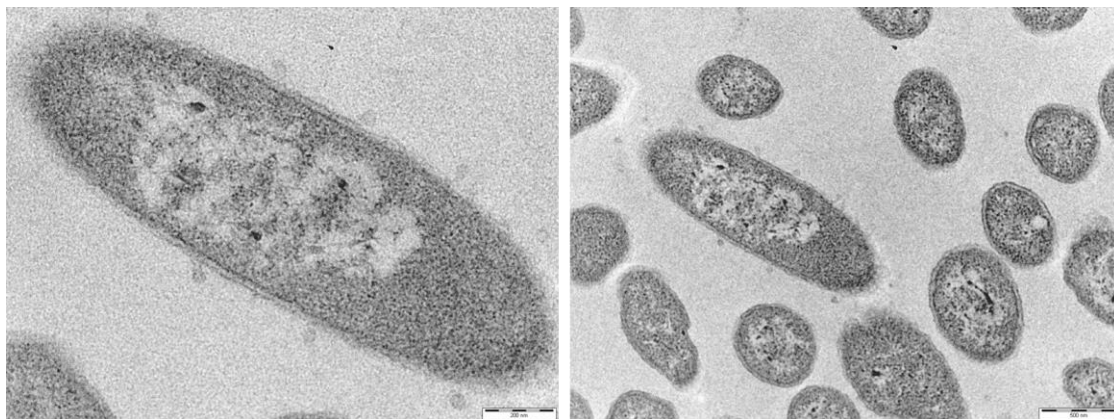


**Figure 4-30: HR-TEM images of So grown in the presence of CitAuNP**

The HR-TEM images show no CitAuNPs present within the So membrane or inside its organelles. There are no CitAuNPs present outside the cell. This was similar to the behaviour observed by Haynes *et al.*<sup>413</sup> when So were exposed to MPA-AuNPs, no association to cells. This is the opposite behaviour observed by Shi *et al.*<sup>408</sup> in the presence CitAuNPs and *B. subtilis* which was a Gram positive bacterium. Since Gram positive bacteria have amino acid and sugar residues on their cell wall surface, ligand exchange might be the reason for the CitAuNPs attachment to *B. subtilis*. Since Gram negative have a larger proportion of LPS attachment, the CitAuNPs could be repelled leading to no association.

These observations indicate that, a positive charge on gold nanoparticles is essential in forming an interaction between the So membrane and the gold nanoparticle. The presence of DenAuNPs on the surface of So was expected to create an electroactive biofilm with maximum electron transfer potential leading to higher current generation.

The So with associated DenAuNPs (4.2.3.1) was investigated in an electrochemical set up to identify if the attachment of DenAuNPs to So can improve the electron transfer from So to the anode.

#### **4.4 Electrochemical experiments**

A similar electrochemical experimental design as in Chapter-2 and Chapter -3 were used, where the experiments were conducted using a three electrode set up.<sup>347</sup> The reference electrode was Ag/AgCl, the counter electrode was a platinum mesh, the



working electrode was a strip of carbon veil of area  $\sim 1.2 \text{ cm}^2$  and the culture was DenAuNPs attached So.

#### 4.4.1 Chronoamperometric results

The chronoamperometric measurements were conducted for 27 h at 0.2 V vs Ag/AgCl.<sup>352</sup> Each of the experiment had the culture at an optical density OD<sub>600</sub> of 0.02 at a volume of 25 ml. A control with just So in minimal media was used as a comparison to check the influence on the current generated in the presence of DenAuNPs attached to So (Figure 4-31).

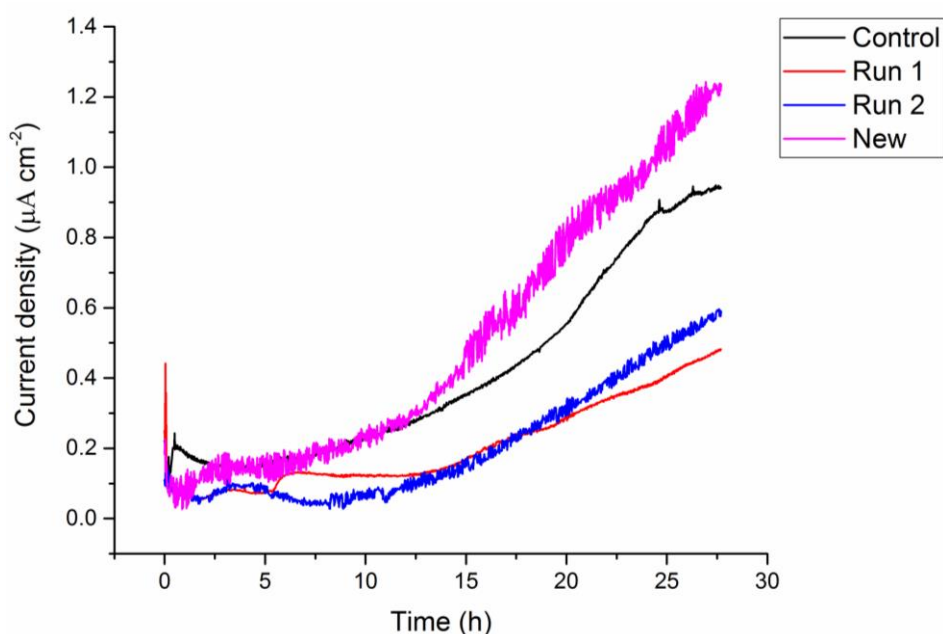


**Figure 4-31: Time vs Current density graph of DenAuNPs attached So. The run numbers (red and blue) indicate the number of repeats, control run (black) is with no DenAuNPs. New (pink) indicates the experiment with recently synthesised DenAuNPs.**

The current produced was normalised to the area of the strip as this was consistent throughout the experiments conducted in Figure 4-31. The curve shapes in Figure 4-31 are consistent with the results obtained with the other modified electrodes, where initially there is a lag in the increase in current followed by a rapid increase in current. This shape is also complementary to the growth of So as the current produced is dependent on So growth and biofilm formation on the working electrode. The shape follows the general trend of bacterial growth depicting the lag phase (initial acclimatisation to environment) and the exponential phase (rapid growth). The noise observed in data also correspond to curves where carbon veil

## Chapter 4: Gold nanoparticles decorated So

was used with no modification, this because of the carbon veils intrinsic structure. In some instances, instrumental noise seems to produce noise related data.

Since the runs were performed in a span of few weeks after the synthesis of DenAuNPs, a time dependent study was conducted using DenAuNPs that were synthesised recently with no time gap (Figure 4-31). It was seen that the recently synthesised DenAuNPs attached to So, do produce higher current than the control in a single run, but the increase was not significant. The increase in current for New compared to control was  $\sim 1.2$  times higher which was expected to be within experimental error. It could be because the DenAuNPs interfere with the growth of the bacteria, since current production is related to bacterial growth or it could also be due to disrupted biofilm formation on the carbon veil.<sup>422</sup>

To investigate the biofilm formation, one of the working electrodes from the chronoamperometric runs (after the experiment) was analysed using SEM (Figure 4-32).

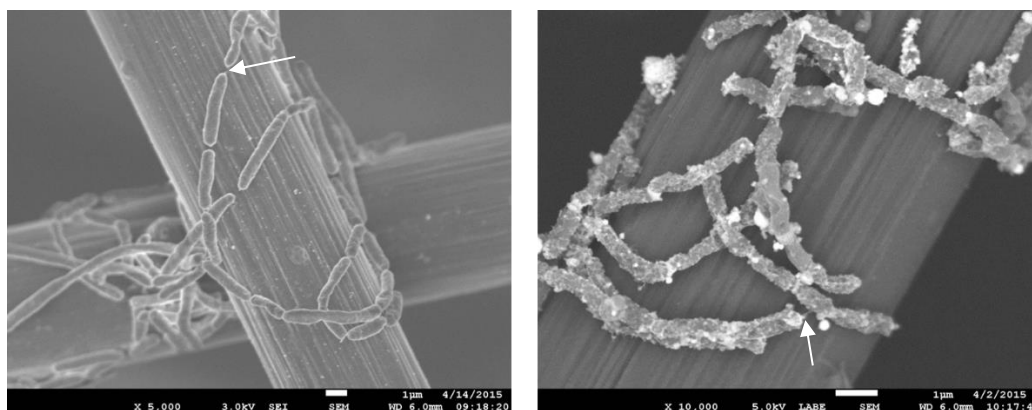


**Figure 4-32: Analysis of carbon veil after chronoamperometric measurement with DenAuNPs attached to So. Scale bar 1  $\mu\text{m}$  respectively. The pillars are the carbon veil fibers. Control with no DenAuNPs (left) and with DenAuNPs (right), the bright/white spots on the right image indicate DenAuNPs on So. White arrows indicate nanowires. recorded in LABE (Low angle back scattered electron images) mode**

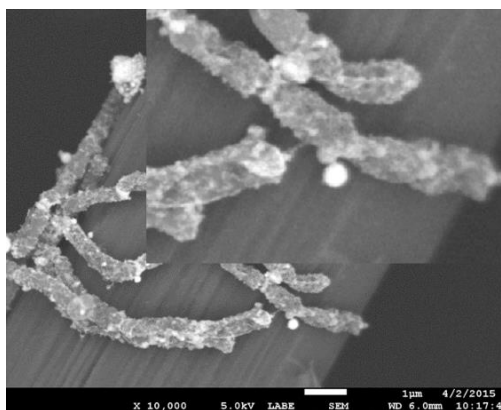


**Figure 4-33: SEM image with inset showing the nanowires of So recorded in LABE (Low angle back scattered electron images) mode with DenAuNPs**

The images look similar to the ones observed by Shi *et al.*<sup>408</sup> when negatively charged citrate protected gold nanoparticles were deposited on Gram positive *Bacillus subtilis*.

The Figure 4-32, shows So surface covered in DenAuNPs, this was not shown by the HR-TEM as they were prepared as slices giving a 2D representation. The images also show So connected together by nanowires covered by DenAuNPs (indicated by white arrows in Figure 4-32 and in inset Figure 4-33). The SEM's also give a good representation of the biofilm formation of So on carbon veil, both with and without DenAuNPs.

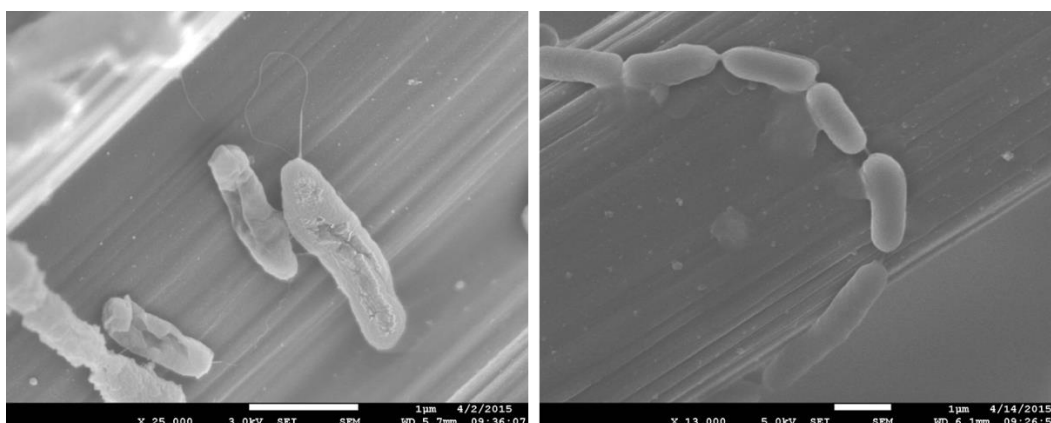


**Figure 4-34: SEM images of So with DenAuNPs (left) and without(right), these were recorded in SEI (secondary electron imaging) mode where DenAuNPs were not observed.**

Some of the SEM was recorded in SEI mode where nanoparticles are not recorded to understand how the So surface with and without DenAuNPs compares (Figure 4-34). It can be seen from the Figure 4-34, that the surface of So with DenAuNPs attached is much rougher and deformed than the So with no DenAuNPs. This further proves that the attachment of DenAuNPs disrupts the outer membranes of the So

cells. The reason for the decreased current production could be due to weak biofilm formation, as only a low density of bacteria were observed on the carbon veil once DenAuNPs were attached. The biofilm is prone disruption depending on the environmental conditions around the bacteria, the presence of DenAuNPs on bacterial surface could lead to a weaker biofilm that is easier to disperse (1.5.1). This could lead to hindered electron transfer process similar to Wu *et al.*<sup>236</sup> when So was used to synthesise gold nanoparticles.

#### 4.5 Overall comparison of electrochemical data

The current generated throughout this project using the different types of modified electrodes at 27 h were compared (Figure 4-35) to get an understanding of the most appropriate idea to be incorporated into a bio-electrochemical system. Figure 4-35 shows all the electrodes used in this project, Au dep gel refers to gel containing gold macrostructures, DenAuNPSo refers to DenAuNPs attached So. It was evident from looking at the histoGram, that of all the electrodes GelAuNP shows the highest current generation and Auveil is the second highest in current generation.

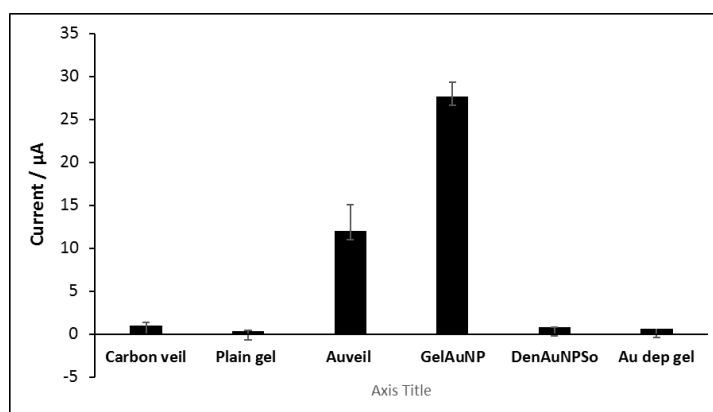


**Figure 4-35: Bar chart comparing the different electrodes in this project.**

In terms of incorporating modified electrodes in a bio-electrochemical system, GelAuNP was the best choice.

#### **4.6 Summary and conclusions**

Gold nanoparticles protected by PAMAM G4 (NH<sub>2</sub>/SH) were successfully synthesised with an average size of ~ 2.3 nm. These were attached to So using a new method of growing So in the presence of DenAuNPs, the viability of So with DenAuNPs attached was proved with the chronoamperometric measurements as current production is dependent on bacterial growth. The reason for DenAuNP's attachment to So surface was attributed to electrostatic interactions between the positively charged DenAuNPs and the negatively charged LPS of So, this was further proved when CitAuNPs did not associate to the surface of So.

DenAuNPs attached So were studied using chronoamperometric measurements, in a three electrode set up. The results showed a decreased current production compared to control with no DenAuNPs attachment. The increase in current was not significant leading to conclusion that the time gap was also not very significant.

**Chapter 5: Summary,  
conclusions and future  
work**

## 5 Summary, conclusions and future work

The aims of this project were to use gold nanoparticles to improve electron transfer from a bacterium to an anode in a bio-electrochemical system.

This was initially approached by synthesising MAgarose whose structure was thought to be partially hydrolysed agarose with some amine incorporation. Gold nanoparticles were incorporated into MAgarose using literature methods. This resulted in the production of GelAuNP which showed some promising conductivity data. The toxicity of gold nanoparticles' to *So* was also investigated and it was found that *So* were able to grow in the presence of gold nanoparticles and maintain their viability. The use of GelAuNP as an anode within a bio-electrochemical system containing *So* as the bacterial catalyst was investigated. The chronoamperometric data showed an enhancement in current by ~29 times compared to the plain carbon veil as a control. This enhancement was attributed to the GelAuNP having agarose as part of its makeup which would increase bacterial adhesion and maximise biofilm formation. The presence of gold nanoparticles in a porous framework as agarose also increases the electroactive surface area of the electrode.

In terms of future work, there are various avenues to explore with GelAuNP as an electrode that are worth pursuing. The use of GelAuNP as an electrode with different substrates (such as waste water, glucose and acetate), bacterium (*E. coli*, *B.subtilis* and *G. sulfurreducens*) and operational conditions (continuous flow, bigger culture volume and different potentials) would form a project in itself.

The second approach was incorporating gold nanowires in agarose gels, this was performed using a 'novel' solvent replacement method. The method involved the solvent replacement in an agarose gel from water to hexane. The nanowires were successfully incorporated into the gel matrix in hexane gels, but on solvent replacement back to water the nanowires disintegrated into nanoparticles and leached out of the gel. The leaching could not be prevented even on incorporation of gold anchoring groups such as sulfurs into the agarose gels. The conductivity of these gels with nanowires in hexane gels and on solvent replacement back to water gels was recorded using a 'custom made' graphite block electrodes. The conductivity of these hexane gels was lower than water gels, but still not as high as GelAuNP and

## Chapter 5: Conclusions and future work

their continual leaching of nanoparticles and wires makes them unsuitable for further applications.

An alternative method was also investigated to incorporate gold nanowires into gels by electrodeposition. The main disadvantage of this method is the production of macrostructures in the gel rather than nanowires. The resultant gel was tested for its conductivity and incorporated into the bio-electrochemical cell as an anode. However, it was noticed from the chronoamperometric data that the current generation reached a saturation point and did not increase over time. This could be because the biofilm of *S. aureus* has dispersed from the electrode or that *S. aureus* viability has stopped. In terms of future work for this avenue, an investigation into the amount of gold electrodeposited in gel to current response can be made. The gels after the chronoamperometric run could be analysed for the number of live and dead bacteria, this could provide a reason for the saturation of current over time.

The third approach involved the attachment of pre-synthesised gold nanoparticles protected by a thiol functionalised PAMAM dendrimer. The resulting DenAuNPs were attached to *S. aureus* by growing them in situ in the presence of DenAuNPs. The successful attachment was confirmed by HR-TEM images. These DenAuNPs attached *S. aureus* were incorporated in a bio-electrochemical cell and chronoamperometric data was recorded. However, the current generated was low compared to the respective control. This was attributed to a weak biofilm formation on the electrode because of the presence of DenAuNPs. The working electrode carbon veils from the chronoamperometric runs, were analysed by SEM and it was found that there was a smaller density of bacterial coverage in the presence of DenAuNPs than in their absence. In terms of future work, an investigation into the change in gold nanoparticle concentration and biofilm formation could be carried out. Once the optimal concentration of DenAuNPs to attach to *S. aureus* has been identified, chronoamperometric runs could be recorded.

An investigation into the reason for gold nanoparticles and *S. aureus* interaction could be carried out using gene deletion, protein deletion and other biological methods.



# **Chapter 6: Experimental part**

## 6 Experimental part

### 6.1 Materials and methods used for synthesis and characterisation

Materials and solvents were used as supplied by Sigma Aldrich, Alfa Aesar and Fluka without further purification. PAMAM G4 dendrimer was obtained from dendritech and was used without further purification. All the glassware used for nanoparticle synthesis were cleaned with aqua regia (HNO<sub>3</sub>: HCl, 1 : 3) and rinsed copiously with water. All the stock solutions and reactions were carried out in de-ionised water. All the compounds reported in Experimentals have been synthesised using literature methods or by their modification and have been cited respectively. <sup>1</sup>H NMR spectra were recorded on a JEOL EXC – 400 at 295 K. Chemical shifts ( $\delta$ ) were quoted in parts per million referenced to the residual proton signal of the solvent. Mass spectra were recorded on a Bruker microTOF electrospray mass spectrometer (ESI-MS). Elemental analyses were performed using an Exeter Analytical Inc. CE-400 analyser. Fourier transform infrared measurements were recorded on Perkin Elmer Spectrum Two. Ultraviolet-Visible spectroscopy was measured on Shimadzu UV-1800. Fluorescence measurements were recorded on Hitachi F-4500 Spectrophotometer. The gel transition temperatures ( $T_{gel}$ ) were measured on a Huber ministat cc2/230.

Viscosities were recorded on Brookfield rotational rheometer RVDV-II+Pro (cone and plate version) connected with a cryostat for the tempering of the samples (temperature accuracy  $\pm 1$  K). A Brookfield silicone fluid (97 mPa·s, 298 K) was used as a NIST-traceable viscosity standard. The viscosity measurements were performed at 303 K using a CP-40 cone spindle. All the viscosity measurements were carried out by Lucia 'Andrea at the University of York. Transmission electron microscopy images were recorded on FEI Tecnai 12 BioTWIN G2 transmission electron microscope with SIS CCD camera. For sect. 6.22 with So cells with and without DenAuNP, the suspensions were fixed in a solution of glutaraldehyde and treated with osmium tetroxide.<sup>423,424</sup> These were then washed, fixed in resin and microtome to get very thin sections that were analysed by TEM. All the bacterial imaging work for 6.22 was carried out by Anna Simon and all the TEM and SEM work was carried out by Meg Stark at the Imaging and cytometry lab in the Biology department at the University of York. The Scanning electron microscopy was

## Chapter 6: Experimental part

recorded on JEOL JSM-7600F field emission scanning electron microscope with Gatan Alto 2500 cryo-system or JEOL JSM-6490LV with Quorum Technologies PP2000 cryosystem. Confocal microscopy was carried out by the Imaging and cytometry lab in the Biology department at the University of York using Zeiss LSM 880. Zeta potential measurements were recorded for sect 6.20 and 6.21 on a Zetasizer Nano ZS90.

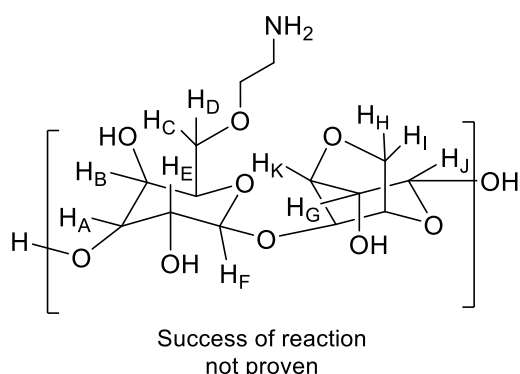
X-ray photoelectron spectroscopy was recorded by NEXUS facility at Newcastle University. K-Alpha or Theta Probe or Nova was used for the XPS analysis. Inductively coupled plasma mass spectrometry was performed by Emma Dux at the Bio-renewables development on Agilent 7700x. Electrochemical measurements were recorded on EmStat<sup>3</sup> and BASi-Epsilon. Conductance measurements were recorded on a Philips PW 9527. Resistance measurements were recorded on a Sealey MM20 digital multimeter.

All the glassware used for bacterial work was sterilised using autoclave Prestige Medical Classic 2100 standard or rinsed copiously in ethanol and dried. All the bacterial liquid cultures were grown using Gallenkamp orbital shaker incubator. All liquids were either autoclaved or passed through a microfilter of 0.2  $\mu\text{m}$  pore size to sterilise.

## Chapter – 1: GelAuNP

### 6.2 Gold nanoparticle incorporation <sup>300-302</sup>

Agarose or MAgarose (8.64 mg) was dissolved in 0.3 ml water with heating until a clear solution was obtained. The solution was poured into a 'bottomless' sample vial of dimension 0.5 mm  $\times$  0.5 mm to form a gel cylinder of concentration 2.88 % (w/v). A solution of HAuCl<sub>4</sub> (0.2 ml, 0.15 M) was added on top of the gel cylinder and allowed to diffuse into the gel overnight. The excess gold (III) chloride solution was removed and replaced by a solution of sodium borohydride (2 ml, 0.02 M) the following day. The sodium borohydride solution was replaced five times, using a freshly prepared solution of sodium borohydride each time to reduce all the gold (III) chloride solution in the gel. The gel was dialysed extensively with three changes of water for three days.

**6.3 Synthesis of MAgarose [1]** <sup>310-312</sup>

Agarose and 2-chloroethylamine hydrochloride were stored in a glove box and used throughout the project. Agarose (318 mg, 1.04 mmol, 1eq) was dissolved in dry DMF at 85 °C under an atmosphere of argon with vigorous stirring, until a clear solution was obtained. Potassium carbonate (215 mg, 1.56 mmol, 1.5 eq) was added to the mixture and stirred until the solution turned yellow. 2-chloroethylamine hydrochloride (180 mg, 1.56 mmol, 1.5 eq) was added to the mixture and reacted overnight at 85 °C under an argon atmosphere. The obtained product was quenched with hydrochloric acid (2M) to pH ~ 4, dialysed extensively for three days with three changes of water a day.

**Yield:** 0.199 g (55 %)

**<sup>1</sup>H NMR (DMSO-d<sub>6</sub>, 400 Hz):** δ 5.22 (s, H<sub>J</sub>, 1H), 5.07 (s, H<sub>F</sub>, 1H), 4.82 (s, H<sub>K</sub>, 1H), 4.65 (s, H<sub>E</sub>, 1H), 4.51 (s, H<sub>H</sub>, 1H), 4.35 (s, H<sub>I</sub>, 1H), 4.19 (s, H<sub>G</sub>, 1H), 3.76 (m, H<sub>C-D</sub>, 2H), 3.54 (s, NH<sub>2</sub>CH<sub>2</sub>, 2H), 2.50 (m, NH<sub>2</sub>CH<sub>2</sub>CH<sub>2</sub>, 2H).

**IR (solid state, ν<sub>max</sub>):** 3375 cm<sup>-1</sup> (O-H), 2974 cm<sup>-1</sup> (C-H), 1644 cm<sup>-1</sup> (Bound water), 1372 cm<sup>-1</sup> (C-H rock), 1068 cm<sup>-1</sup> (C-O)

**Elemental analysis:** Found % C 45.43, H 6.14, N 0; Calc % C 47.06, H 5.92, N 4.01. The discrepancy between the calculated values and the observed values for elemental analysis was attributed to the samples being hygroscopic. The absence of nitrogen indicates the failure of the reaction.

**T<sub>gel</sub> (water, 2.88 % w/v):** 80 – 83 °C

## 6.4 Fluorometric assay<sup>319,320</sup>

### 6.4.1 Calibration with ethanolamine

A stock solution at 0.03% (w/v) was prepared by dissolving fluorescamine (3 mg) in water (0.2 ml) and made up to 10 ml using DMSO. This stock solution was used for the fluorometric assay. A stock solution of DMSO with 2% water was prepared by adding water (0.4 ml) in a volumetric flask and making up to 20 ml using DMSO. A stock solution of ethanolamine (10 mM) was prepared by adding ethanolamine (6 µl) to a volumetric flask and making up to 10 ml with the stock solution of DMSO mentioned above. In general, ethanolamine at various concentrations was dissolved in known amounts of fluorescamine and DMSO with 2% water. The various volumes used are detailed in the table below (Table 6-1).

**Table 6-1: Volumes and concentrations used for calibration of amine to fluorescence**

<b>Concentration of ethanolamine / mM</b>	<b>Volume of ethanolamine solution /ml</b>	<b>Fluorescamine solution / ml</b>	<b>DMSO with 2% water / ml</b>	<b>Total volume /ml</b>
<b>0.10</b>	0.10	0.10	0.80	1.00
<b>0.20</b>	0.20	0.10	0.70	1.00
<b>0.30</b>	0.30	0.10	0.60	1.00
<b>0.40</b>	0.40	0.10	0.50	1.00
<b>0.50</b>	0.50	0.10	0.40	1.00

The fluorescence was recorded using quartz cuvettes. The concentration of ethanolamine in the total volume of 1ml was recalculated as a 1 in 10 dilution and plotted in the calibration curve.

### 6.4.2 Assay with agarose and MAgarose

A similar method as 6.4.1, was used by dissolving the respective amounts of gels in solutions, the quantities are detailed below (Table 6-2).

**Table 6-2: Quantities used for fluorometric assay of gels**

Name of gel	Weight of gel / mg	Fluorescamine / ml	DMSO with 2% water / ml	Total volume /ml
Agarose	2.98	0.10	0.90	1.00
MAgarose	1.55	0.10	0.90	1.00

## 6.5 $T_{gel}$ measurements

All the gels mentioned in a table below were heated to dissolve in water at a gel concentration of 2.88 % (w/v). The gels were allowed to set at room temperature in sample vials and the sample vials were placed in a temperature controlled oil bath. The temperature was set to ramp at 0.1 °C per second. The sample vials were inverted periodically till the gel reverted to liquid. The temperature was recorded once the gel started to melt and once it became a liquid.

**Table 6-3: The weights and volumes used for  $T_{gel}$  recording**

Name of the gel	Weight /mg	Water /ml	Total volume / ml
Agarose	8.40	0.30	0.30
MAgarose	8.40	0.30	0.30

## 6.6 Viscometry <sup>328,329</sup>

### 6.6.1 Viscosity average molecular weight determination

Five different concentrations of the agarose and MAgarose gel were dissolved in a solution of NaSCN (0.75 M) respectively as described below (Table 6-4). The volume of NaSCN was varied between samples, as some samples were too viscous to be handled for analysis.

**Table 6-4: Weights and volumes of agarose and MAgarose used for viscosity measurements**

Gelator	Weight / mg	Volume of NaSCN / ml	Concentration/ mg ml <sup>-1</sup>
Agarose	05.07	0.60	08.45
	07.63	0.60	12.72

	11.65	1.10	10.59
	16.32	1.10	14.84
	20.48	1.10	18.62
	11.73	0.60	19.55
	20.86	0.60	34.77
<b>M</b> Agarose	30.35	0.60	50.58
	39.06	0.60	65.10
	53.43	0.60	89.05

### 6.6.2 Control experiments

The gels from controlled experiments were also analysed in a similar method as 6.6.1. Some of these measurements were single measurements at the highest shear rate, no ramp was applied (highlighted in grey).

Name	% (v/v) Water	Weight / mg	Volume of NaSCN / ml	Concentration/ mg ml <sup>-1</sup>
<b>Hydrolysed Agarose</b>	0	11.48	0.60	19.13
<b>Ammonium chloride with known amount of water (2.5.7.2)</b>	0	11.63	0.60	19.38
	0.05	10.69	0.60	17.82
	0.10	11.53	0.60	19.21
	0.50	11.63	0.60	19.38
	1.00	11.29	0.60	18.82

## 6.7 Control experiments

### 6.7.1 Agarose hydrolysis

Agarose (60.50 mg) was added to anhydrous DMF (5 ml) at 85 °C. Once the solution turned clear potassium carbonate (41.10 mg, 1.5 eq) was added and left to react

overnight at 85 °C. The following day the reaction was removed and dialysed extensively for three days with three changes of water every day. Thus obtained gel was lyophilised and used without further purification.

**Yield:** 0.04358g (72 %)

### 6.7.2 Agarose with ammonium chloride and known amount of water

Agarose was added to anhydrous DMF (2 ml) at 85 °C. Once the solution turned clear potassium carbonate was added and once the solution turned yellow, ammonium chloride was added and left to react overnight at 85 °C (Table 6-5). The following day the reaction was quenched with HCl to pH ~ 4 and dialysed extensively for three days with three changes of water every day. Thus obtained gels were lyophilised and used without further purification.

**Table 6-5: Table detailing the reagents and quantities used for control experiments**

<b>Agarose / mg</b>	<b>Ammonium chloride / mg</b>	<b>Potassium carbonate / mg</b>	<b>% water (v/v)</b>	<b>DMF volume /ml</b>	<b>Yield / %</b>
<b>24.75</b>	06.47	16.73	0.00	2	76.60
<b>27.31</b>	07.11	18.50	0.05	2	78.90
<b>25.10</b>	06.52	16.90	0.10	2	96.50
<b>28.46</b>	07.43	19.20	0.50	2	85.00
<b>29.34</b>	07.48	19.80	1.00	2	68.75

### 6.8 ICP-MS sample preparation

The GelAuNP was placed in a quartz vial suitable for ICP-MS digestion and dried at room temperature for a week, until constant weight was recorded. The dried weight of the gel was recorded and the samples submitted for ICP-MS analysis. The samples were added to 4 mL analytical-grade concentrated nitric acid (70%) and 1 mL analytical grade hydrogen peroxide ( $\geq 30\%$ ) and heated to 200 °C for 20 minutes followed by heating to 230 °C for 15 minutes. Additionally 15 mL analytical grade hydrochloric acid (37%) was added and heated in a ramp to 200 °C over 20 mins, then a ramp to 230 °C over 15 minutes. The samples were diluted to 100 ml using deionised water and analysed.



## 6.9 XPS sample preparation

GelAuNP was dried at room temperature exposed to air and was placed on a sticky carbon background suitable for microscopic purposes. This was submitted to NEXUS for XPS analysis. The gel surface was divided into 3 segments and analysed by XPS.

## 6.10 Bacterial work<sup>80,99,101</sup>

All bacterial work was carried out in an Envair Class II laminar flow microbiological safety hood. *Shewanella oneidensis* MR-1 wild type cells were donated by University of Sheffield and were stored in a glycerol stock solution. Aseptic techniques were maintained throughout the time preparing and using bacterial materials to minimise contamination.

### 6.10.1 Stock solutions

All the solutions used in the bacterial growth were prepared as per the table below and sterilised in an autoclave. Deionised water was sterilised in an autoclave and used for subsequent dilutions.

**Table 6-6: Detailing the quantities and reagents used to make stock solutions**

<b>Name</b>	<b>Ingredient names</b>	<b>Per litre / g</b>
<b>LB broth</b>	Yeast extract	05
	Bacto - tryptone	10
	Sodium chloride	10
<b>LB agar</b>	Agar	15
<b>Calcium chloride</b>	Calcium chloride dihydrate	7.13
<b>Sodium Lactate</b>	Sodium lactate solution (60%)	666 ml
	Na <sub>2</sub> EDTA-2H <sub>2</sub> O	02.26
	MgSO <sub>4</sub> -7H <sub>2</sub> O	24.89
	MnSO <sub>4</sub> -4H <sub>2</sub> O	0.029
<b>Trace mineral solution</b>	NaCl	0.058
	FeCl <sub>2</sub>	0.068
	CoCl <sub>2</sub> -6H <sub>2</sub> O	0.065
	ZnSO <sub>4</sub> -7H <sub>2</sub> O	0.029
	CuSO <sub>4</sub> -5H <sub>2</sub> O	0.005

	H <sub>3</sub> BO <sub>3</sub>	0.350
	NaMoO <sub>4</sub>	0.080
	NiCl <sub>2</sub> -6H <sub>2</sub> O	0.119
	Na <sub>2</sub> SeO <sub>4</sub>	0.028
	K <sub>2</sub> HPO <sub>4</sub>	0.221
	KH <sub>2</sub> PO <sub>4</sub>	0.099
	NaHCO <sub>3</sub>	0.168
<b>Minimal media</b>	(NH <sub>4</sub> ) <sub>2</sub> SO <sub>4</sub>	1.189
	NaCl	7.305
	HEPES	1.192
	CaCl <sub>2</sub> stock	10 ml
	Trace mineral solution	10 ml
	Sodium lactate stock	4 ml
<b>Phosphate buffered saline</b>	NaCl	8
	KCl	0.2
	Na <sub>2</sub> HPO <sub>4</sub>	1.44
	KH <sub>2</sub> PO <sub>4</sub>	0.24

*Shewanella oneidensis* MR-1 (So) wild type cells were donated by University of Sheffield and were stored in a glycerol stock solution (section 6.10.6).

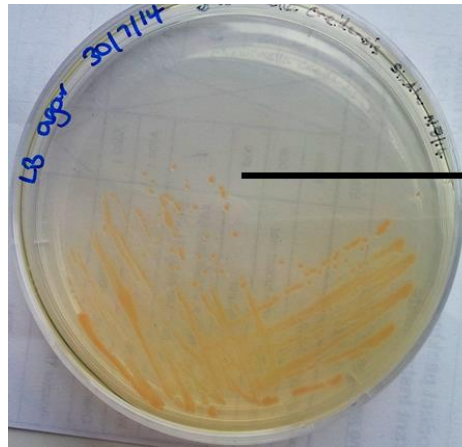
### 6.10.2 LB Broth

The above mentioned quantities (Table 6-6) were dissolved in 800 ml deionised water and the pH was adjusted to 7.5 with sodium hydroxide. The volume was made up to a litre using deionised water. This solution was used to grow liquid cultures of *Shewanella oneidensis* MR-1.

### 6.10.3 LB Agar

Agar (15 g) was dissolved in LB Broth (800 ml, 6.10.2) and heated in a microwave till a clear yellow solution was obtained. The volume was adjusted to a litre using deionised water and stored.

#### 6.10.4 Agar plate with So



**One pink spot  
represents a  
single colony of So**

Approximately 10 ml of hot LB Agar (section 6.10.3) was poured onto sterilised agar plate and allowed to cool for ~40 – 60 min to solidify. A flame sterilised metallic loop was dipped into the glycerol stock containing So and streaked across the LB agar plate to produce single colonies. The success of So growth was confirmed by the presence of pink colonies. These agar plates with So were stable to store at 2 °C without cell death for 1 .5 weeks.

#### 6.10.5 Liquid culture of So

5ml of LB broth (section 6.10.2) was poured into a centrifuge tube and a single colony from agar plate (section 6.10.4) was transferred using flame sterilised metallic loop into the LB Broth. The centrifuge tube containing the LB Broth was grown overnight at 30 °C with shaking at 180 rpm. The growth of So was confirmed the next day by a change in colour to pink and by an increase in turbidity of the solution. These liquid cultures were only stable for 24 hours.

#### 6.10.6 Glycerol stock of So

2ml of liquid culture of So (section 6.10.5) was centrifuged to obtain a pellet. The pellet was suspended in a (0.5 ml) 50% sterilised glycerol solution and stored at -80 °C.

#### 6.10.7 Minimal media

The reagents and quantities detailed in Table 6-6 were dissolved in deionised water (800 ml) and autoclaved, the volume was adjusted to 1000 ml using sterilised deionised water. The as prepared minimal media was only stable to store for one

## Chapter 6: Experimental part

week before sedimentation was observed. This solution was prepared as required and used immediately.

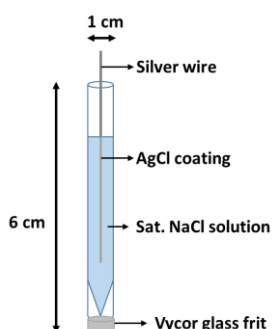
### 6.10.8 Toxicity study of *So* with gold nanoparticles

An LB agar plate was grown and 4 discs of ~ 1cm in diameter were cut out, leaving 4 holes in the LB agar plate. Separately, agarose (6 mg) was dissolved in 1.2 ml sterile deionised water with heating. The hot agarose solution was poured into 4 'bottomless sample vials' to make gel cylinders of volume 0.3 ml each. These gel cylinders were allowed to set and carefully removed. The gel cylinders were placed in chloroauric acid solution (30 mM) of four different volumes (1  $\mu$ l, 2  $\mu$ l, 10  $\mu$ l and 20  $\mu$ l). The solution was allowed to diffuse and replaced with an excess solution of sodium borohydride (10 ml, 20 mM). The gel cylinders were washed extensively with water to remove any excess unreacted gold or borohydride ions. This produced 4 agarose gel cylinders containing gold nanoparticles at different concentrations. These cylinders were placed in the LB agar plate that had holes cut into it.

1 ml of liquid culture containing *So* (section 6.10.5) was poured on top of the LB agar plate with gel cylinders containing gold nanoparticles and spread using a sterilised spreader. This plate was grown for three days at 30 °C.

## 6.11 Electrochemical experiments with *So*

### 6.11.1 Reference electrode



The reference electrode used for electrochemical experiments was designed and made 'in house' using a silver wire (1.0 mm diameter, 8 cm long). The silver wire was placed in a beaker containing HCl (50 ml, 1M) along with a platinum wire (0.2 mm in diameter, 4 cm in length). The reference electrode and the working electrode were the silver wire, while the platinum wire was the counter electrode. A potential of 1 V was applied until a grey matt coating of silver chloride was observed on top

## Chapter 6: Experimental part

of the wire and a constant current was recorded. A glass capillary of length 6 cm and diameter of 1 cm that narrows down to a very small opening at the end was designed to act as the reference electrode. A Vycor<sup>®</sup> porous glass frit was used to cover the narrow opening to allow flow of solutions and ions.

### 6.11.2 Preparation of working electrode

M Agarose (8.4 mg) was dissolved in water (0.3 ml) with heating to form a clear solution. This was poured into the 'bottomless sample vials' containing a strip of carbon veil (10 gm<sup>-2</sup>) and allowed to solidify at room temperature. Gold nanoparticles were incorporated by a similar method as in sect. 6.2. The GelAuNP with carbon veil was stored in water. The carbon veil (Optiveil<sup>™</sup>) was donated kindly by TFP.

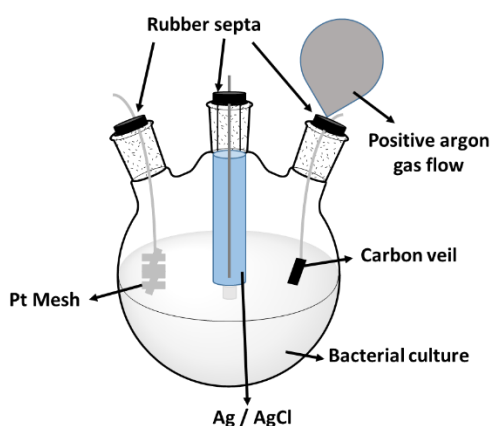
### 6.11.3 Counter electrode

The counter electrode used was purchased from GoodFellow and had the following dimensions 20 mm × 20 mm. The wires had a diameter of 0.06 mm.

### 6.11.4 Preparation of culture for electrochemical experiment

1 ml of the liquid culture of *So* (section 6.10.5) was centrifuged to obtain a pellet. The pellet was suspended in minimal media (1ml) and diluted to 5ml in minimal media. The OD<sub>600</sub> of this solution was recorded and diluted to obtain a solution with OD<sub>600</sub> 0.03 at 25 ml volume.

### 6.11.5 Preparing the electrochemical set up



The reference, working and counter electrodes were rinsed in ethanol and dried under laminar flow under a hood. The culture from section 6.11.4 was purged with argon to remove any oxygen present and poured into a three necked round

## Chapter 6: Experimental part

bottomed flask. The flask was also purged with argon and sealed with the three electrodes in the respective necks with rubber septa. An argon balloon was used to maintain a constant flow of argon throughout the length of the experiment. A potential of 0.2 V vs Ag/ AgCl was poised until the required amount of time depending on the experiment.

### 6.12 Electrodeposition experiment to produce Auveil

A reference electrode similar to section 6.11.1 was used but the length was 3 cm and the diameter 0.5 cm. The counter electrode was also a platinum mesh but the dimensions were 2 cm length and 0.5 cm wide, and wire diameter was 0.2 mm. The working electrode was also a carbon veil strip similar to section 6.11.2. The solution used for electrodeposition contained chloroauric acid (30 mM) and sodium acetate trihydrate (100 mM) in a total volume of 1 ml. All three electrodes were placed in a 2 ml sample vial and potential of -0.6 V vs Ag /AgCl was poised till the solution changed colour from yellow to clear and a constant current was recorded.

## Chapter – 2: GelAuNW

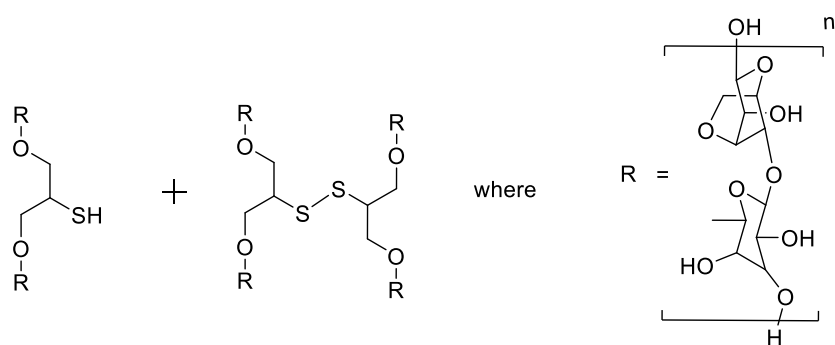
### 6.13 Gold nanowires and ribbons incorporated in agarose gel <sup>387</sup>

Agarose (31.25 mg) was dissolved in 1.56 ml water and heated to dissolve to form a gel at 0.2 % w/v concentration. 1 ml of this gel was transferred to a sample vial and allowed to set at room temperature. HAuCl<sub>4</sub> (30 mM, 17 µl) was diffused through this gel, followed by aspartic acid (0.1 M, 2.5 µl). The gel was left undisturbed for 48 hrs at room temperature to find a pink coloured gel.

**UV-Vis (gel):**  $\lambda_{\text{SPR}} \sim 550 \text{ nm}$

### 6.14 Gold nanowires in hexane solution <sup>204</sup>

HAuCl<sub>4</sub> (6 mg, 1eq, 0.0177 mmol) was added to hexane (5ml) containing oleylamine (200 µl, 34 eq, 0.608 mmol) and sonicated for 1 min. Triisopropylsilane (300 µl, 83 eq, 1.46 mmol) was added to the mixture and sonicated for a further 1 min and left at 30 °C for 4 h or 24 h depending on the experiment, with no stirring. A colour change from deep gold to dark purple to brown was observed.

**6.15 Synthesis of thiol functionalised agarose [2] <sup>394</sup>**

Agarose (321 mg, 1.05 mmol, 1eq) was dissolved in DMF at 85 °C under an atmosphere of nitrogen with vigorous stirring, until a clear solution was obtained. Potassium carbonate (145 mg, 1.05 mmol, 1 eq) was added to the mixture and stirred until the solution turned yellow in colour. Epithiochlorohydrin (114 mg, 1.05 mmol, 1 eq) was added to the mixture and reacted overnight at 85 °C under nitrogen atmosphere. The obtained product was dialysed extensively for five days with three changes of water a day and lyophilised to obtain a dry gel.

**Yield:** 0.295 g (91.77 %)

**IR (solid state,  $\nu_{\max}$ ):** 3375  $\text{cm}^{-1}$  (O-H), 2974  $\text{cm}^{-1}$  (C-H), 1644  $\text{cm}^{-1}$  (Bound water), 1372  $\text{cm}^{-1}$  (C-H rock), 1068  $\text{cm}^{-1}$  (C-O)

**Elemental analysis:** Found % C 44.20, H 6.09, S 2.31, Rest 49.72; Calc % C 46.15, H 5.53, S 8.09, Rest 40.36

The discrepancy between the calculated values and the observed values for elemental analysis was attributed to the samples being hygroscopic. It could also be because the actual structure of the gel is not known, there might be slight discrepancies between the calculated and the observed values.

**$T_{\text{gel}}$  (water, 2.88 % w/v):** 81 – 82 °C

**6.16 Electrodeposition of gold macrostructures****6.16.1 Preparation of working electrode**

A two-part epoxy resin was prepared by mixing the resin (1 ml, 1eq) and crosslinker (0.33 ml, 3eq) in a glass vial. A strip of carbon veil (1.2  $\text{cm}^2$ ) was placed on a PTFE sheet and the resin was poured on top and placed in a oven overnight at 60 °C. The

## Chapter 6: Experimental part

resultant resined carbon veil was used for the electrodeposition experiment. The two-part epoxy resin was purchased from Onecall.

Agarose (5 mg, 1 eq) was added to thiol functionalised agarose **[2]** (5 mg, 1 eq) and heated to dissolve in water (1ml) keeping the total volume as 1ml to achieve 0.5% w/v with respect to both gels. The dissolved gel solution (0.3 ml) was poured into a sample vial containing the resined carbon veil (similar to section 6.11.2). Once set, H<sub>2</sub>AuCl<sub>4</sub> (10  $\mu$ l, 100% w/v) and sodium acetate trihydrate (1ml, 0.1 M) was poured on top of the gel and allowed to diffuse through for 40 min.

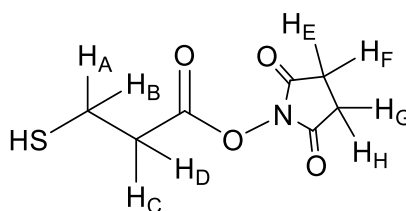
The same reference electrode and counter electrode as in section 6.12 were used. The solution used for electrodeposition was H<sub>2</sub>AuCl<sub>4</sub> (10  $\mu$ l, 30 mM) and sodium acetate trihydrate (1ml, 0.1 M) was poured on top of the gel and allowed to diffuse through for 40 min. A potential of -0.6 V vs Ag/ AgCl was poised for ~ 27 h or until constant current was recorded.

### 6.17 Electrochemical experiment with So

A similar method as in section 6.11.5 was used, with the working electrode being the gel with gold macrostructures from section 6.16. Everything else was the same in terms of reference electrode, counter electrode, potential and also the liquid culture.

## Chapter – 3: DenAuNP

### 6.18 Synthesis of 3-mercaptopropanoyl hydroxysuccinimide ester**[3]**<sup>419</sup>



N-Hydroxysuccinimide (1 g, 8.7 mmol, 1eq) was added to dry DCM (500 ml) with stirring followed by the addition of 3-mercaptopropionic acid (0.93 g, 8.7 mmol, 1 eq) and dicyclohexylcarbodiimide (1.97 g, 9.5 mmol, 1.09 eq). The reaction mixture was left to stir overnight. Solvent was removed *in vacuo* and the product was purified by column chromatography (EtOAc: Pet Ether, 50: 50) to obtain a white solid. The sample was stored as a stock solution (0.189 M) in dry THF.

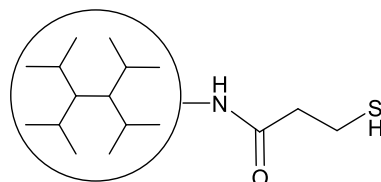


**Yield:** 1.15 g (65%)

**R<sub>f</sub>** = 0.58 (EtOAc/ Pet Ether (50: 50))

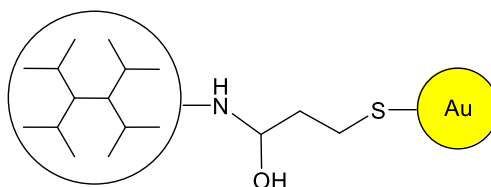
**<sup>1</sup>H NMR (CDCl<sub>3</sub>, 400 Hz):** δ 2.85-2.82 (t, *H<sub>C</sub>* and *H<sub>D</sub>*, *J* = 4 Hz 1H), 2.75-2.73 (m, *H<sub>A</sub>* and *H<sub>B</sub>*), 2.70 (s, *H<sub>E-HH</sub>*), 1.80-1.75 (t, *S<sub>H</sub>*, *J* = 8.5 Hz, 1H)

### 6.19 Synthesis of PAMAM G4 (NH<sub>2</sub>/SH)[4]<sup>420</sup>



PAMAM-G4 (NH<sub>2</sub>) (22.59 mg, 1.59 μmol, 1 eq per amino group) was diluted in 2 ml of methanol/ ethanol mixture (1:1) under an atmosphere of argon. 3-mercaptopropanyl-N-hydroxysuccinimide ester **[3]** (0.189 M, 20.3 μmol, 12.8 eq) was added to the mixture and stirred overnight under nitrogen. The obtained product was used with no further purification as per literature.

### 6.20 Synthesis of PAMAM-(NH<sub>2</sub>/SH) protected AuNP [DenAuNP]

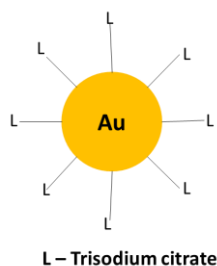


30 mM aq solution of hydrochloroauric acid (HAuCl<sub>4</sub>) (2 ml, 58.9 μmol, 40 eq) was added directly to a solution of PAMAM - G4 (SH) **[4]** (2 ml, 1.47 μmol, 1 eq) under stirring. 3.09 M aq sodium borohydride (1 ml, 2000 eq) was added dropwise with rigorous stirring. Reaction was stirred for further 10 min and dialysed to remove excess sodium borohydride. Particles were purified on a Sephadex G-150 column (eluent 0.1M NaCl) and dialysed. The gold concentration in the resultant solution of DenAuNP (30 ml) was determined by ICP-MS, as ~0.31 mg ml<sup>-1</sup>. For the higher concentration sample, the volume of DenAuNP was concentrated to 20 ml and analysed to find ~0.40 mg ml<sup>-1</sup>.

**UV-Vis (solution):** λ<sub>SPR</sub> - 535 nm

**Zeta potential (ζ):** 36.10 mV, standard deviation of 7.59 mV

## 6.21 Citrate protected gold nanoparticles [CitAuNP]<sup>180</sup>



HAuCl<sub>4</sub> (5 mg, 14.7 μmol) in 50 ml water was brought to reflux and trisodium citrate (7.5 mg, 25.5 μmol) was added and refluxed for further 10 min. A colour change to blue-violet was observed.

**UV-Vis (solution):**  $\lambda_{\text{SPR}}$  - 550 nm

**Zeta potential ( $\zeta$ ):** -30 mV , standard deviation of 11.7 mV

## 6.22 Attachment of gold nanoparticles to *So*

### 6.22.1 First method

A single colony from an LB Agar plate containing *So* was transferred using a flame sterilised metallic loop into a centrifuge tube containing LB (2.5 ml) and a solution of DenAuNP (gold concentration 0.31 mg/ml, 2.5ml). A change in turbidity indicated growth of *So*. A 1ml solution of the culture was centrifuged at 2000 rpm for 2 min to obtain a black coloured pellet. The pellet was washed twice with water and used without further purification.

### 6.22.2 Second method

A 1 ml solution of the liquid culture from section 6.10.5 was centrifuged at 2000 rpm for 2 min to obtain a pink coloured pellet. The pellet was washed twice with water and suspended in a solution of DenAuNP /CitAuNP (0.5 ml) and PBS (0.5 ml). This solution was incubated for 12 hours and analysed by TEM

## 6.23 Electrochemical experimental set up

The same method as in section 6.11.5 was used containing *So* with DenAuNP incorporated in the outer membranes. The liquid culture was diluted in minimal media to an OD<sub>600</sub> of 0.03.

## Appendices

### Appendix 1 : Chapter 2 - GelAuNP

#### 1.1 Removal of ionic species from gels using water

All the gels that were used for gold nanoparticle and gold nanowire incorporation were washed extensively in water to remove any residual ions.

Two agarose gel cylinders (20 mg and 5 mg) of different % w/v were prepared by dissolved in water (1ml each) by heating. An aliquot of the hot gel solution (0.30 ml) was added to a 'bottomless' sample vial and allowed to set at room temperature. The resultant gel cylinders were placed in a solution of brine (10 ml) for 2 hours. The conductance was recorded for the brine gels using the 'graphite block' design. Once the conductance was recorded, the brine gels were placed in water (500 ml) for a day and their conductance recorded the next day. The gels were washed in water and their conductance recorded after each wash, this was repeated three times for each gel.

**Table 6-7: Conductivity values of brine gels with consecutive water washing**

Conductivity / $\text{Sm}^{-1}$				
Gel concentration / % w/v	0 wash	1st wash	2nd wash	3rd wash
0.50	1.42E-01	5.35E-05	4.4310 <sup>-5</sup>	3.8810 <sup>-5</sup>
2.00	1.33E-01	4.1110 <sup>-4</sup>	6.8710 <sup>-6</sup>	6.4510 <sup>-6</sup>

The conductivity of the 2<sup>nd</sup> wash was very close to experimental error for 2 %w/v indicating that there is no conductivity due to ionic movement in any of the gels measured in this project.

## 1.2 Conductivity data for all the gels

	Resistance / $\Omega$	Resistivity / $\Omega \text{ m}^{-1}$	Conductivity / $\text{S.m}^{-1}$	Average Conductivity / $\text{S.m}^{-1}$	Standard deviation / $\text{S.m}^{-1}$
<b>GelAuNP</b>	3.10E+02	6.82E+02	1.47E-03	1.27E-03	2.06E-04
	3.50E+02	7.70E+02	1.30E-03		
	3.80E+02	8.36E+02	1.20E-03		
	3.73E+02	8.21E+02	1.22E-03		
	3.05E+02	6.71E+02	1.49E-03		
	4.89E+02	1.08E+03	9.30E-04		
<b>Agarose</b>	4.86E+06	1.82E+06	5.49E-07	5.40E-07	7.93E-09
	5.00E+06	1.88E+06	5.33E-07		
	4.96E+06	1.86E+06	5.38E-07		
<b>MAgarose</b>	4.65E+06	1.74E+06	5.73E-07	5.76E-07	4.29E-08
	4.99E+06	1.87E+06	5.34E-07		
	4.30E+06	1.61E+06	6.20E-07		
<b>Agarose AuNPs</b>	1.57E+05	5.90E+04	1.70E-05	1.68E-05	1.95E-07
	1.59E+05	5.97E+04	1.68E-05		
	1.61E+05	6.04E+04	1.66E-05		
<b>Thiolated agarose</b>	1.39E+07	5.19E+06	1.93E-07		
	1.43E+07	5.36E+06	1.87E-07		
	1.40E+07	5.24E+06	1.91E-07		

### 1.3 Electrochemical data

All the experiments with no So for all the different electrodes

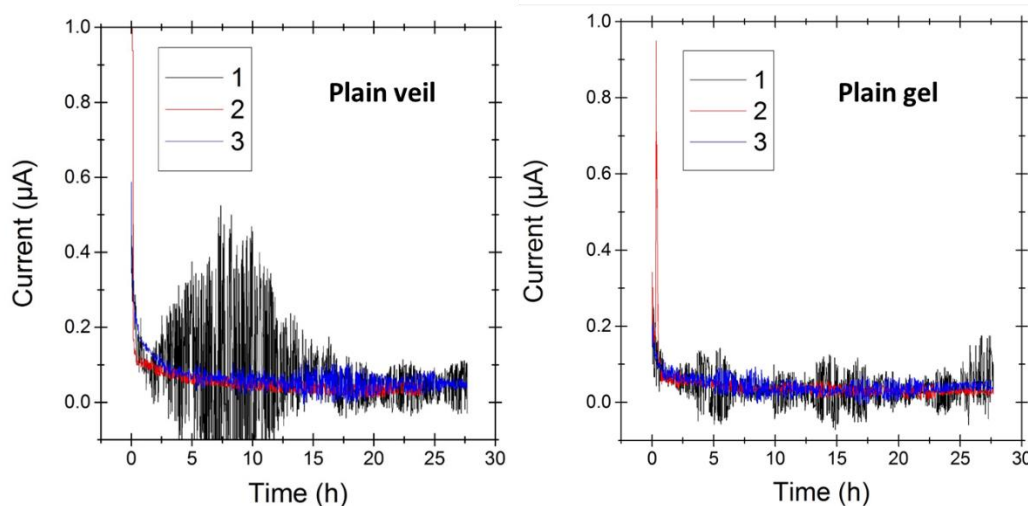


Figure 6-1: Current vs time plots of plain veil (left) and plain gel (right) no So

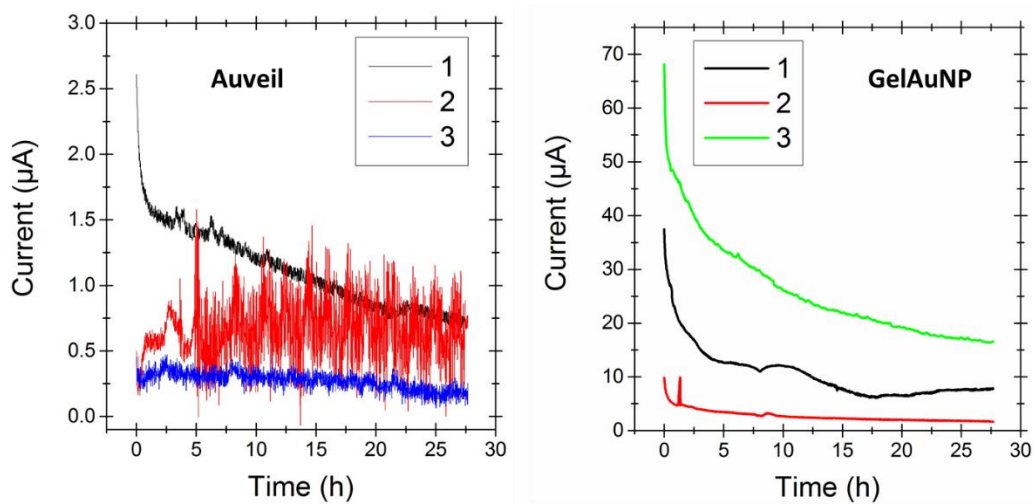


Figure 6-2: Current vs time plots of Auveil (left) and GelAuNP (right) no So

All experiments with So for all the different electrodes

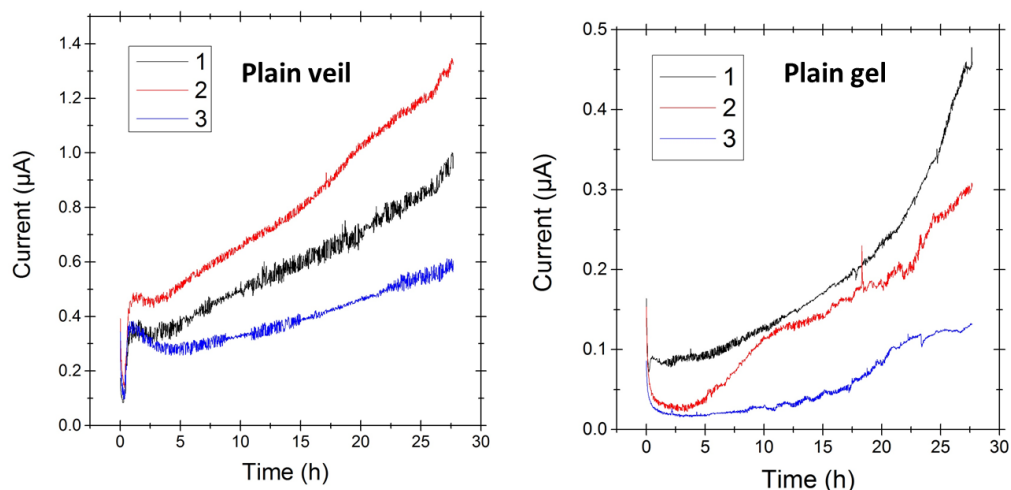


Figure 6-3: Current vs time plot of plain veil (left) and plain gel (right) with So

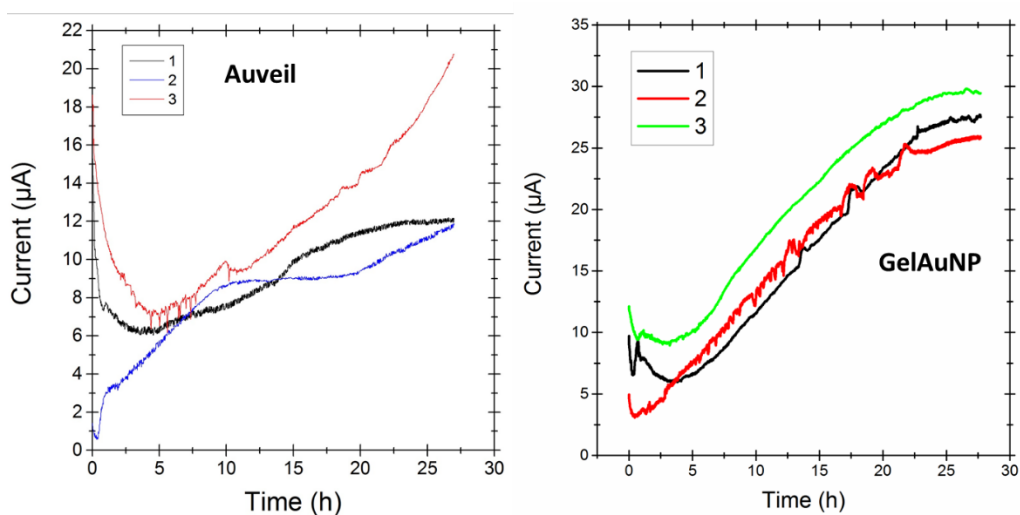


Figure 6-4: Current vs time plot of Auveil (left) and GelAuNP (right) with So

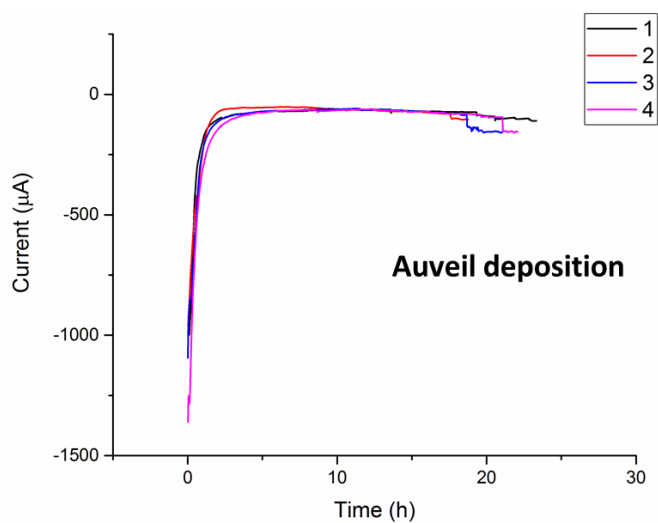
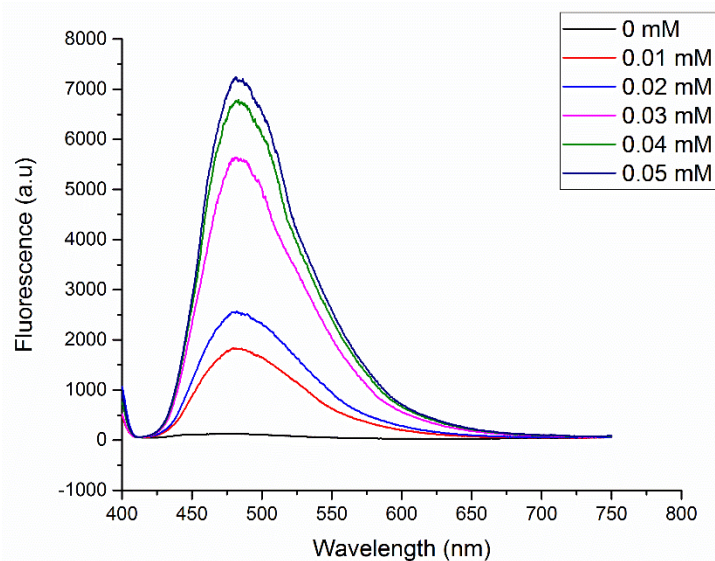


Figure 6-5: Current vs time plot of electrodeposition of gold on plain veil

## 1.4 Fluorometric data



**Figure 6-6: Fluorescence spectrum showing the fluorescence at different amine concentrations**

**Table 6-8: Concentration of amine and the respective fluorescence values at 475 nm used for calibration plot**

<b>Concentration of ethanolamine/ mM</b>	<b>Fluorescence @ 475 nm / a.u</b>
<b>0.00</b>	0081
<b>0.01</b>	1730
<b>0.02</b>	2406
<b>0.03</b>	5218
<b>0.04</b>	6319
<b>0.05</b>	6898

## 1.5 Viscosity data

**Table 6-9: Viscosity data for agarose at various concentrations**

<b>Agarose</b>				
<b>Concentration / g ml<sup>-1</sup></b>	<b>Viscosity/cP</b>	<b>Relative viscosity/cP</b>	<b>Specific Viscosity / ml g<sup>-1</sup></b>	<b>Inherent Viscosity / ml g<sup>-1</sup></b>
<b>8.45E-03</b>	1.70E+01	2.20E+01	2.10E+01	3.66E+02
<b>1.86E-02</b>	8.32E+01	1.08E+02	1.07E+02	2.52E+02
<b>1.06E-02</b>	3.00E+01	3.89E+01	3.79E+01	3.45E+02

<b>1.46E-02</b>	3.90E+01	5.05E+01	4.95E+01	2.69E+02
<b>1.27E-02</b>	3.16E+01	4.10E+01	4.00E+01	2.92E+02

**Table 6-10: Viscosity data for MAgarose at various concentrations**

<b>Aminated</b>				
<b>Concentration / g ml<sup>-1</sup></b>	Viscosity/cP	Relative viscosity/cP	Specific Viscosity / ml g <sup>-1</sup>	Inherent Viscosity / ml g <sup>-1</sup>
<b>1.96E-02</b>	3.42E+00	4.44E+00	3.44E+00	7.62E+01
<b>3.47E-02</b>	9.39E+00	1.22E+01	1.12E+01	7.20E+01
<b>6.51E-02</b>	8.07E+01	1.05E+02	1.04E+02	6.58E+01
<b>8.90E-02</b>	1.04E+02	1.35E+02	1.34E+02	5.57E+01
<b>5.00E-02</b>	1.93E+01	2.51E+01	2.41E+01	6.45E+01



## 1.7 HR-TEM images

### 1.7.1 Agarose with gold nanoparticles

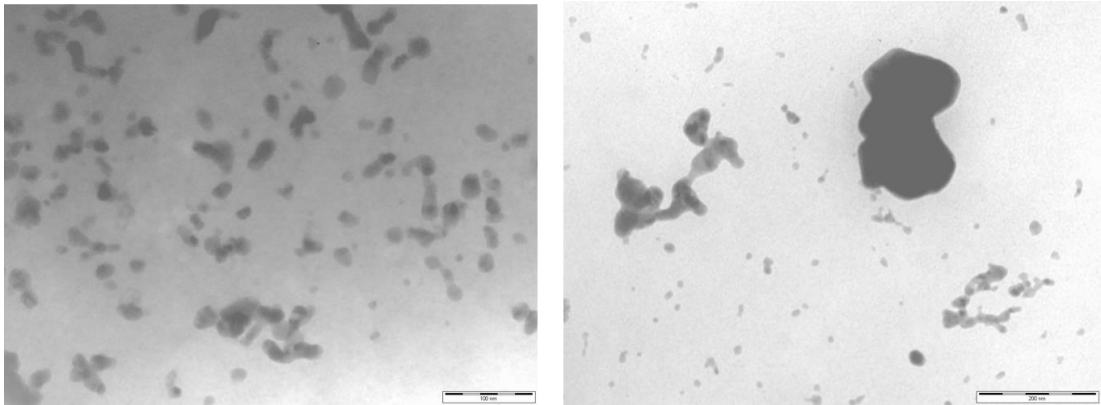


Figure 6-7: HR-TEM images of agarose with gold nanoparticles. Scale bar 100 and 200 nm

### 1.7.2 MAgarose with gold nanoparticles

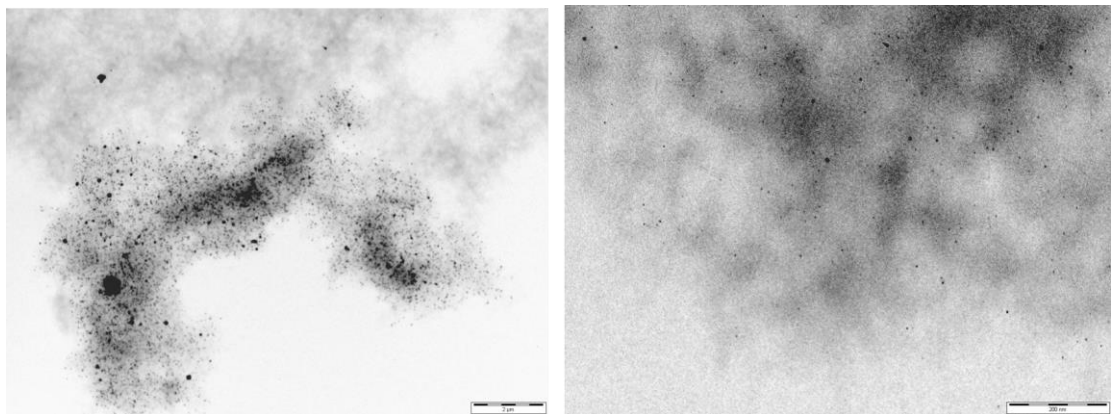


Figure 6-8: HR-TEM image of bottom of GelAuNP. Scale bar 2 μm and 200 nm.

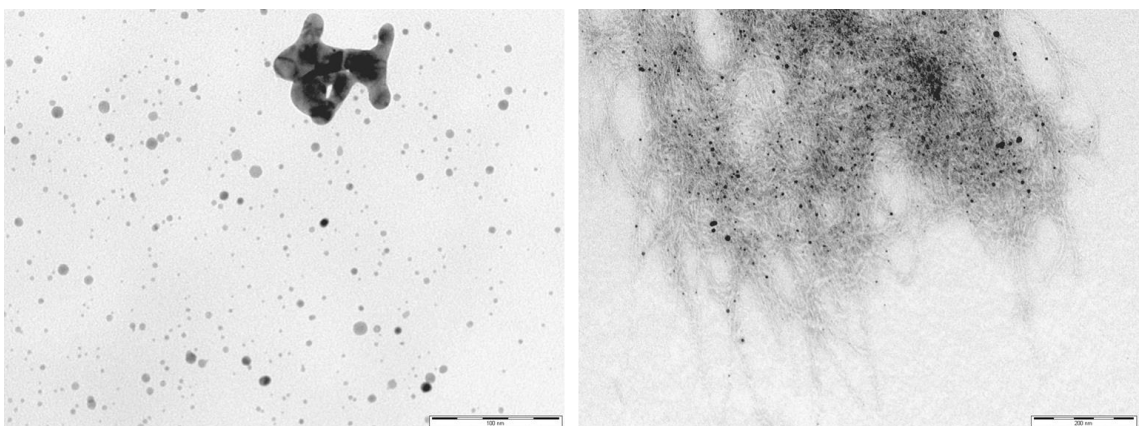


Figure 6-9: HR-TEM images of top of GelAuNP. the right image has been stained with uranyl acetate to identify gel fibres. Scale bar 100 and 200 nm

### 1.7.3 Image J processing of HR-TEM images

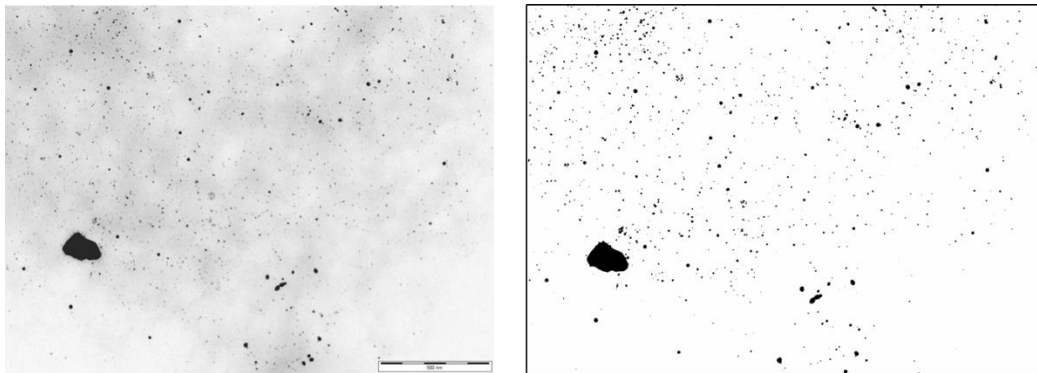


Figure 6-10: Image J processing of counting particles automatically. (left) Original HR-TEM image, (right) Processed image by Image J

### 1.8 XPS spectra

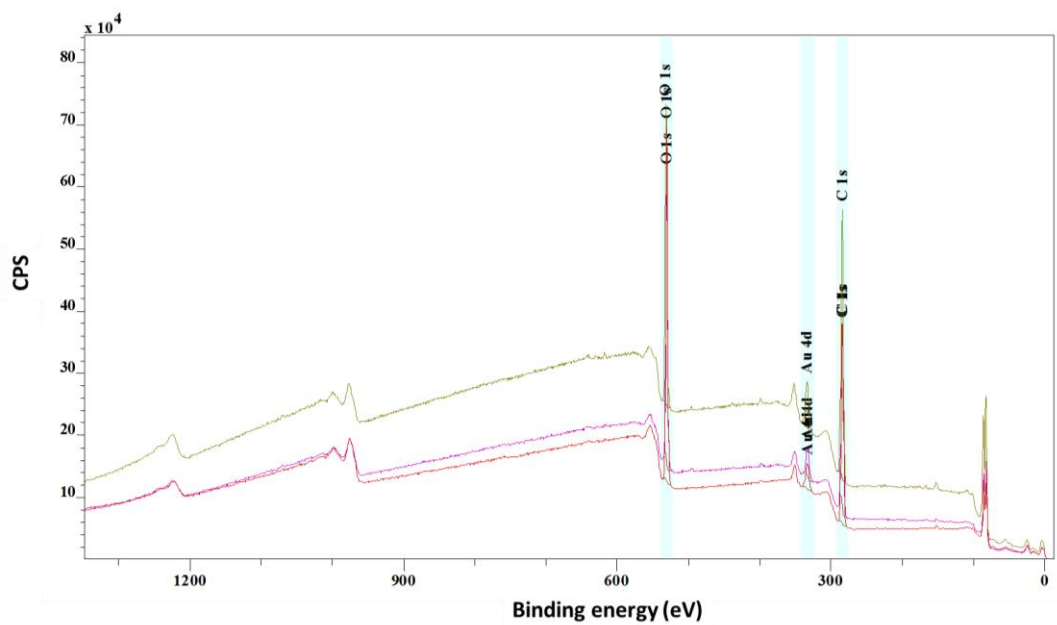
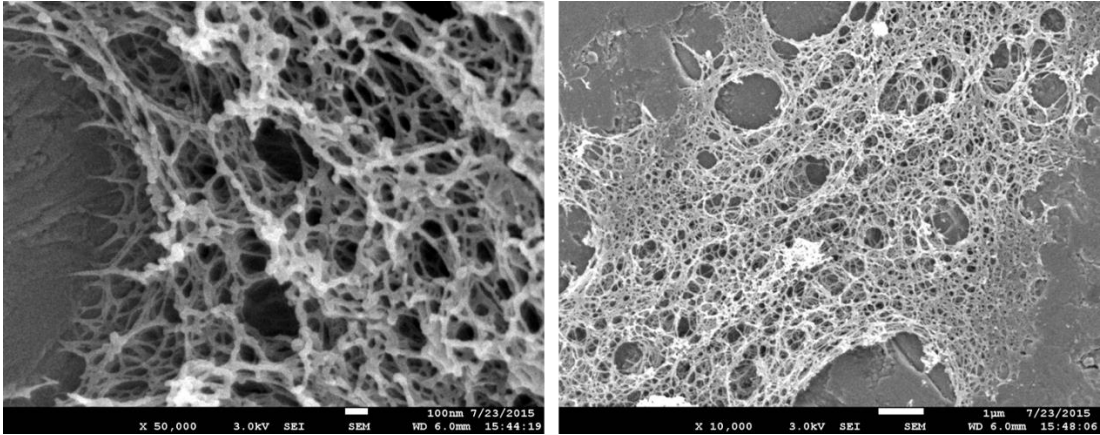


Figure 6-11: An overlay of all the XPS spectra of GelAuNP

**1.9 SEM images**

**1.9.1 Agarose**



**Figure 6-12: SEM images of agarose**

**1.9.2 MAgarose**

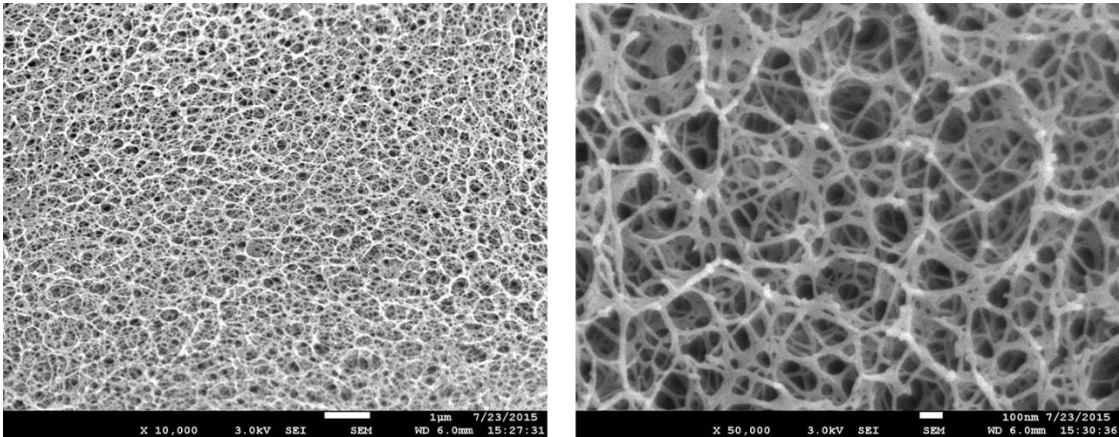


**Figure 6-13: SEM images of MAgarose**

### 1.10 Confocal data for long term GelAuNP with So

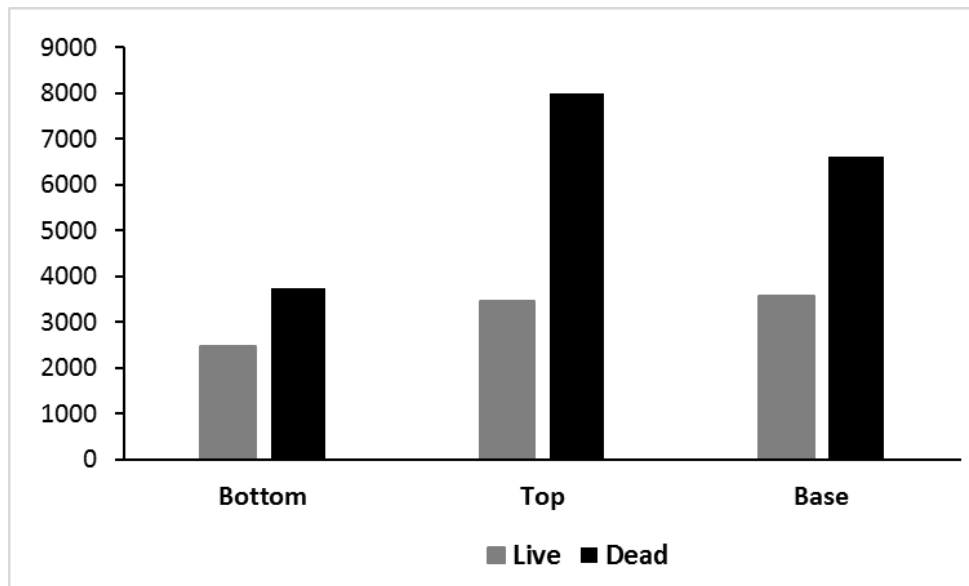


Figure 6-14: Bar chart of live and dead bacteria for the long term chronoamperometric experiment with GelAuNP

## Appendix 2 : Chapter 3 – GelAuNW

### 2.1 TEM images

#### 2.1.2 Aspartic acid and agarose nanoribbons

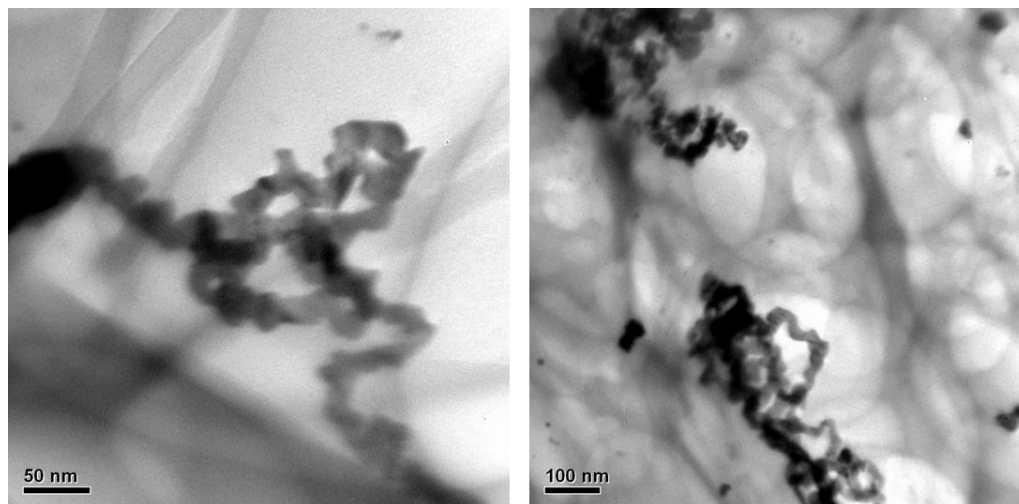


Figure 6-15: TEM images of nanoribbons in agarose

#### 2.1.3 Gold nanowires in hexane

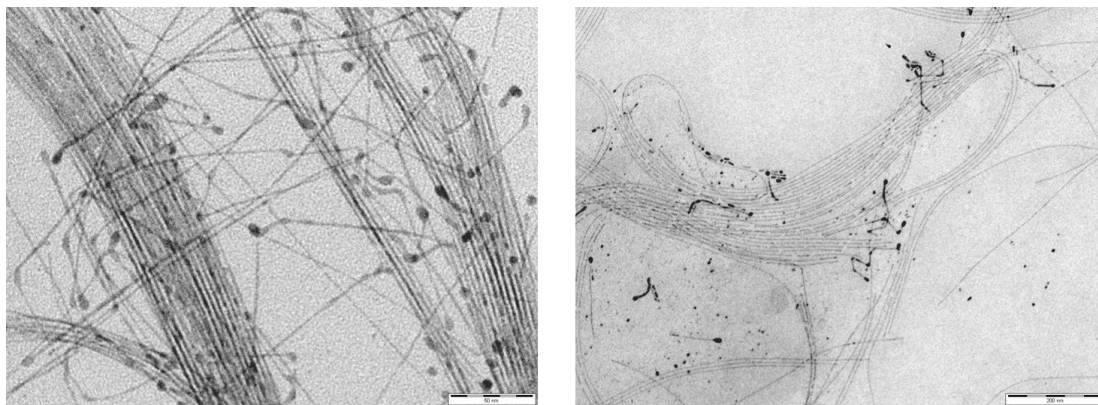


Figure 6-16: HR-TEM images of gold nanowires in hexane. Scale bars 50 and 100nm

#### 2.1.4 Gold nanowires in hexane gel

## 2.3 SEM images

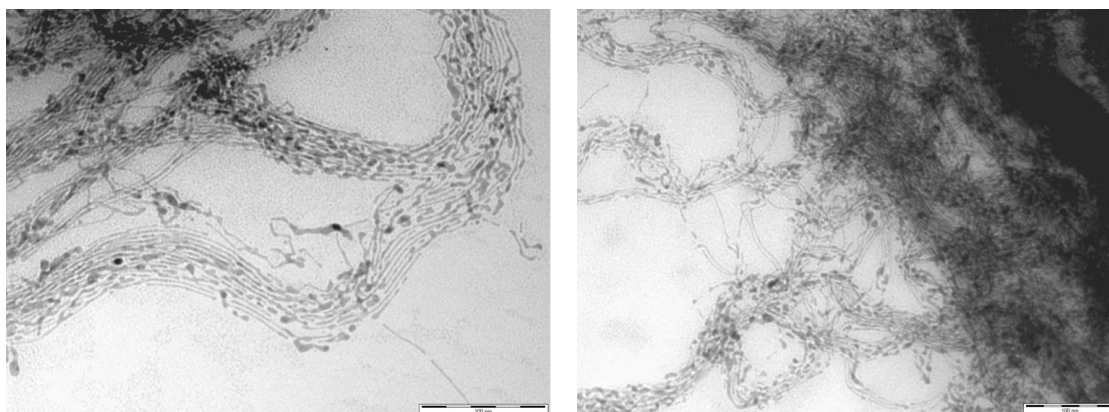
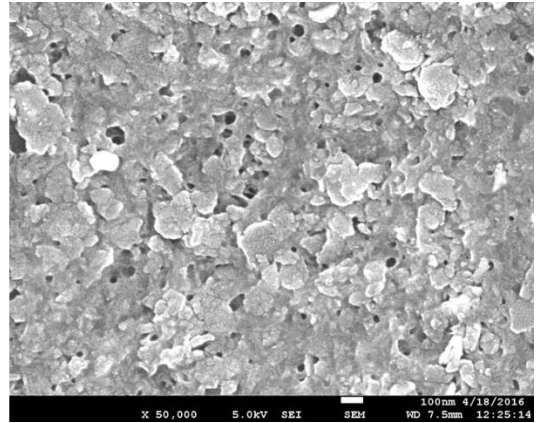
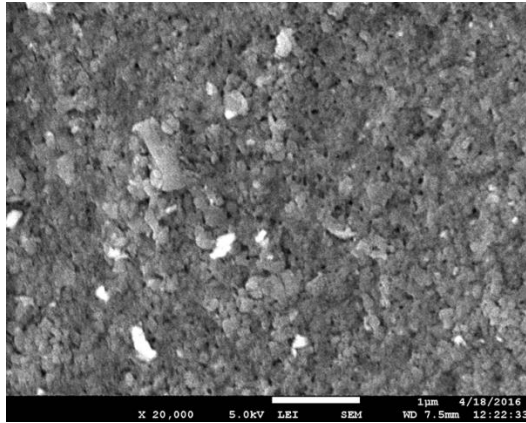


Figure 6-17: HR-TEM images of gold nanowires in hexane gel. Scale bars 100nm respectively

## 2.2 Conductivity data for all the gels

Table 6-11: Conductivity values for all the gels

Gels	Conductance / S	Conductivity/ S m <sup>-1</sup>	Average Conductivity/ S m <sup>-1</sup>
Plain hexane gel	8.30E-08	1.77E-07	1.69E-07
	8.00E-08	1.70E-07	
	7.50E-08	1.60E-07	
Hexane gel with AuNW (no washing)	7.37E-07	1.57E-06	1.11E-06
	7.62E-07	1.62E-06	
	6.52E-08	1.39E-07	
Gold nanowire gel after washing in water twice	1.95E-05	4.14E-05	
Gold nanowire complete washed	5.01E-05	1.07E-04	1.34E-04
	7.00E-05	1.49E-04	
	6.92E-05	1.47E-04	



**Figure 6-18: SEM images of agarose in hexane**

## Appendix 3 : Chapter 4 – DenAuNPs

### 3.1 HR-TEM images

#### 3.1.1 First method of incorporation

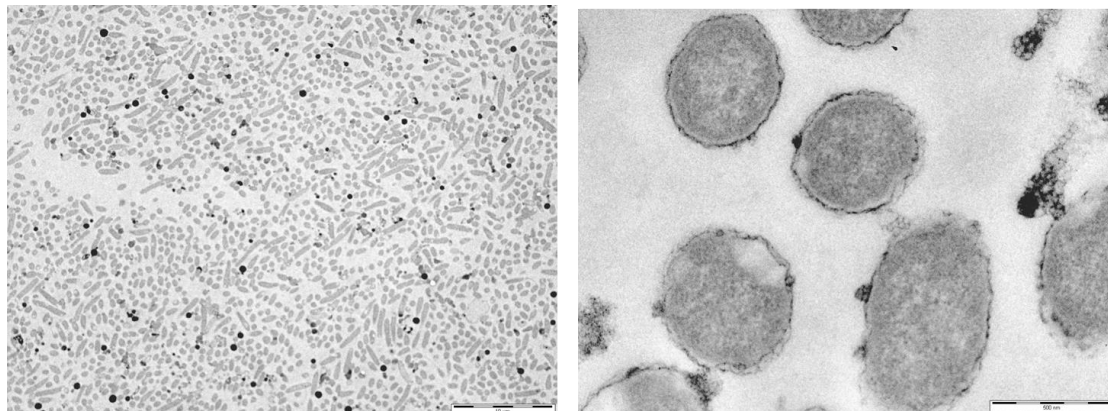


Figure 6-19: HR-TEM images of DenAuNPs attached to So. Scale bars 10μm and 500 nm.

#### 3.1.2 Second method of incorporation

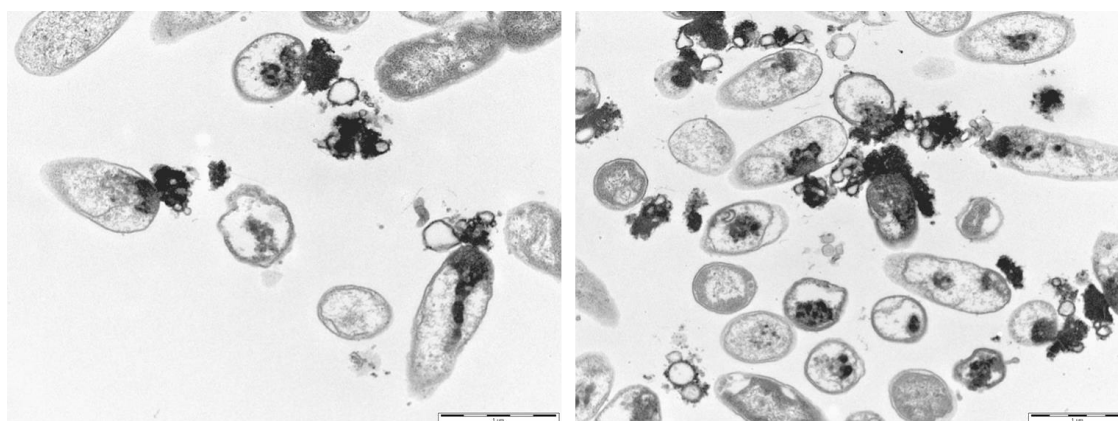


Figure 6-20: HR-TEM images of DenAuNPs attached to So after growth. Scale bar 1μm



## 3.2 SEM images

### 3.2.1 So in media

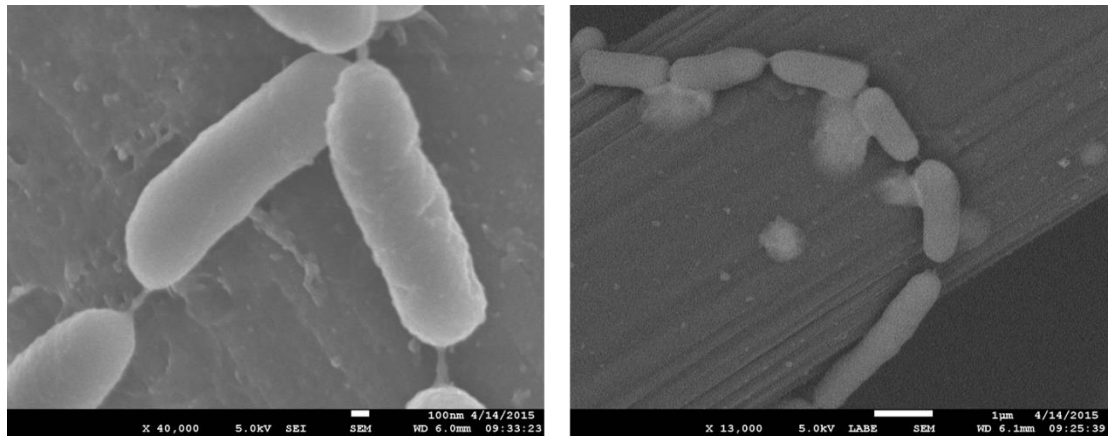


Figure 6-21: SEM images of So on carbon veil in media, no DenAuNPs

### 3.2.2 So with DenAuNPs

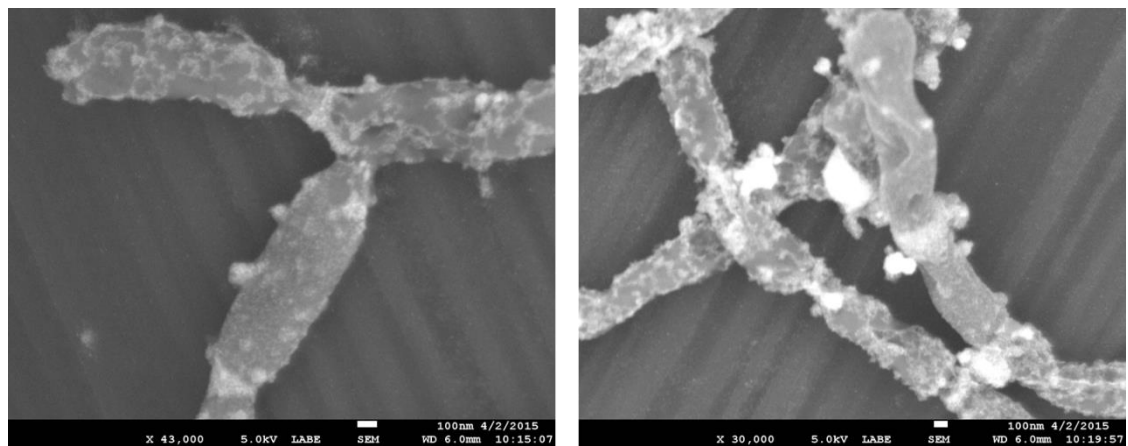


Figure 6-22: SEM images of DenAuNPs attached to So on carbon veil in media

### 3.3 Overall comparison of electrodes

Table 6-12: The average current generated at 27 h for all electrodes with So

<b>Electrode material</b>	<b>Current at 27h / μA</b>	<b>Standard deviation</b>
<b>Carbon veil</b>	9.73E-01	3.60E-01
<b>Plain gel</b>	2.97E-01	1.62E-01
<b>Auveil</b>	1.20E+01	3.07E+00
<b>GelAuNP</b>	2.76E+01	1.74E+00
<b>DenAuNPSo</b>	7.70E-01	7.58E-02
<b>Au dep gel</b>	6.04E-01	0.00E+00

## Abbreviations

°C degrees Celsius

μA Microampere

2D 2 – dimensional

3D 3-dimensional

AC Alternating current

AuNW Gold nanowires

Auveil Electrodeposited gold on plain carbon veil

Btu British thermal unit

C mol<sup>-1</sup> Coulombs per mole

CNT Carbon nanotube

cP centipoise

CTAB Cetyl trimethylammonium bromide

Cyt Cytochrome

DenAuNP PAMAM G4 (NH<sub>2</sub>/SH) protected gold nanoparticles

depAu Electrodeposited gold macrostructures in agarose and thiolated agarose gel

DLS Dynamic light scattering

DMF Dimethylformamide

DMSO Dimethylsulfoxide

DNA Deoxyribonucleic acid

FAD Reduced Flavin adenine dinucleotide

FADH<sub>2</sub> Oxidised Flavin adenine dinucleotide

GCE Glassy carbon electrode

GelAuNP MAgarose with gold nanoparticles incorporated

h hours

ICP-MS Inductively coupled mass spectroscopy

J Joules

K Kelvin

K<sub>2</sub>CO<sub>3</sub> Potassium carbonate

LB Luria-Bertani / lysogeny borth

mA Milliampere

mAm<sup>-2</sup> Milliampere per meter squared

MFC Microbial Fuel Cell

mg milligrams

mM millimolar

MPA 3-mercaptopropionic acid

MPNH<sub>2</sub> 3-mercaptopropylamine

mWm<sup>-2</sup> Milliwatts per meter squared

NAD<sup>+</sup> Oxidised Nicotinamide adenine dinucleotide

NADH Reduced Nicotinamide adenine dinucleotide

nm nanometre

NMR Nuclear magnetic resonance

NP nanoparticle

OD<sub>600</sub> optical density at 600 nm

PAH poly(allylamine hydrochloride)

PAMAM Polyamidoamine

pH  $-\log [H^+]$

ppm parts per million

PTFE Polytetrafluoroethylene

rpm rotations per minute

SEM Scanning electron microscopy

SHE Standard hydrogen electrode

So *Shewanella oneidensis* MR-1

TEM Transmission electron microscopy

T<sub>gel</sub> gel transition temperature

UK United Kingdom

V Volts

vs versus

w/v weight over volume

XPS X-ray photoelectron spectroscopy

XRD X-ray diffraction

$\pi$  pi

## References

- 1 B. O. Okesola, S. K. Suravaram, A. Parkin and D. K. Smith, *Angew. Chemie - Int. Ed.*, 2016, **55**, 183–187.
- 2 L. E. Doman, *International Energy Outlook 2013*, 2013.
- 3 I. E. Agency, *Key World Energy Statistics 2013*, France, 2013.
- 4 DEFRA, *Defra*, 2012, 49.
- 5 V. G. Gude, *J. Clean. Prod.*, 2016, **122**, 287–307.
- 6 R. A. Bullen, T. C. Arnot, J. B. Lakeman and F. C. Walsh, *Biosens. Bioelectron.*, 2006, **21**, 2015–2045.
- 7 F. Davis and S. P. J. Higson, *Biosens. Bioelectron.*, 2007, **22**, 1224–1235.
- 8 G. A. Justin, Y. Zhang, M. Sun and R. Scabassi, *Proc. Annu. Int. Conf. IEEE Eng. Med. Biol. Soc.*, 2004, **26**, 4096–4099.
- 9 C. H. Shaw, J. F. Castner and L. B. Wingard JR, *Enzyme Microb. Technol.*, 1982, **4**, 97–105.
- 10 J. R. Rao, G. J. Richter, F. Von Sturm and E. Weidlich, *Bioelectrochemistry Bioenerg.*, 1976, **3**, 139–150.
- 11 I. Ivanov, T. Vidaković-Koch and K. Sundmacher, *Energies*, 2010, **3**, 803–846.
- 12 D. Leech, P. Kavanagh and W. Schuhmann, *Electrochim. Acta*, 2012, **84**, 223–234.
- 13 S. C. Barton, J. Gallaway and P. Atanassov, *Chem. Rev.*, 2004, **104**, 4867–86.
- 14 A. Karimi, A. Othman, A. Uzunoglu, L. Stanciu and S. Andreescu, *Nanoscale*, 2015, 6909–6923.
- 15 M. C. Potter, *Proc. R. Soc. Chem.*, 1911, **84**, 260–276.
- 16 H. J. Conn, V. Burke, B. Cohen, E.-B. F. Genung, I. C. Hall and W. L. Kulp, *J. Bacteriol.*, 1930, **XXI**, 18–19.

- 17 A. Parkash, *J. Microb. Biochem. Technol.*, 2016, **8**, 247–255.
- 18 Z. Du, H. Li and T. Gu, *Biotechnol. Adv.*, 2007, **25**, 464–82.
- 19 M. Winter and R. J. Brodd, *Chem. Rev.*, 2004, **104**, 4245–69.
- 20 L. Huang, J. M. Regan and X. Quan, *Bioresour. Technol.*, 2011, **102**, 316–23.
- 21 J. K. Jang, J. Kan, O. Bretschger, Y. A. Gorby, L. Hsu, B. H. Kim and K. H. Nealson, *J. Microbiol. Biotechnol.*, 2013, **23**, 1765–1773.
- 22 Y. Zhang and I. Angelidaki, *Biotechnol. Bioeng.*, 2011, **108**, 2339–2347.
- 23 C. J. Murphy and J. M. Buriak, *Chem. Mater.*, 2015, **27**, 4911–4913.
- 24 D. L. Cologgi, S. Lampa-Pastirk, A. M. Speers, S. D. Kelly and G. Reguera, *Proc. Natl. Acad. Sci. U. S. A.*, 2011, **108**, 15248–15252.
- 25 G. M. Gadd, *FEMS Microbiol. Lett.*, 1992, **79**, 197–203.
- 26 J. M. Tront, J. D. Fortner, M. Plötze, J. B. Hughes and A. M. Puzrin, *Biotechnol. Lett.*, 2008, **30**, 1385–1390.
- 27 J. M. Morris and S. Jin, *J. Environ. Sci. Health. A. Tox. Hazard. Subst. Environ. Eng.*, 2008, **43**, 18–23.
- 28 M. Danish Khan, H. Abdulateif, I. M. Ismail, S. Sabir and M. Zain Khan, *PLoS One*, 2015, **10**.
- 29 H. Wang and Z. J. Ren, *Water Res.*, 2014, **66**, 219–232.
- 30 Y. V. Nancharaiah, S. Venkata Mohan and P. N. L. Lens, *Bioresour. Technol.*, 2015, **195**, 102–114.
- 31 M. Zhou, H. Wang, D. J. Hassett and T. Gu, *J. Chem. Technol. Biotechnol.*, 2013, **88**, 508–518.
- 32 L.-L. Wan, X.-J. Li, G.-L. Zang, X. Wang, Y.-Y. Zhang and Q.-X. Zhou, *RSC Adv.*, 2015, **5**, 82276–82281.
- 33 G. K. Rader and B. E. Logan, *Int. J. Hydrogen Energy*, 2010, **35**, 8848–8854.

- 34 J. Babauta, R. Renslow, Z. Lewandowski and H. Beyenal, *Biofouling*, 2012, **8**, 789–812.
- 35 J. Y. Nam and B. E. Logan, *Int. J. Hydrogen Energy*, 2011, **36**, 15105–15110.
- 36 G. Kyazze, A. Popov, R. Dinsdale, S. Esteves, F. Hawkes, G. Premier and A. Guwy, *Int. J. Hydrogen Energy*, 2010, **35**, 7716–7722.
- 37 L. Lu, N. Q. Ren, X. Zhao, H. A. Wang, D. Wu and D. F. Xing, *Energy Environ. Sci.*, 2011, **4**, 1329–1336.
- 38 S. Cheng and B. E. Logan, *Proc. Natl. Acad. Sci. U. S. A.*, 2007, **104**, 18871–3.
- 39 L. T. Angenent, K. Karim, M. H. Al-Dahhan, B. A. Wrenn and R. Domínguez-Espinosa, *Trends Biotechnol.*, 2004, **22**, 477–485.
- 40 L. M. Tender, C. E. Reimers, H. a Stecher, D. E. Holmes, D. R. Bond, D. a Lowy, K. Pilobello, S. J. Fertig and D. R. Lovley, *Nat. Biotechnol.*, 2002, **20**, 821–5.
- 41 Y. Wang, J. Hu, L. Wang, D. Shan, X. Wang, X. Mao, Y. Zhang, L. Xing and D. Wang, *RSC Adv.*, 2016, **6**, 80079–80085.
- 42 L. Hsu, B. Chadwick, J. Kagan, R. Thacher, A. Wotawa-Bergen and K. Richter, *RSC Adv.*, 2013, **3**, 15947.
- 43 A. Zabihallahpoor, M. Rahimnejad and F. Talebnia, *RSC Adv.*, 2015, **5**, 94171–94183.
- 44 D. Bin Wang, T. S. Song, T. Guo, Q. Zeng and J. Xie, *Int. J. Hydrogen Energy*, 2014, **39**, 13224–13230.
- 45 T. Ewing, P. T. Ha, J. T. Babauta, N. T. Tang, D. Heo and H. Beyenal, *J. Power Sources*, 2014, **272**, 311–319.
- 46 C. E. Reimers, L. M. Tender, S. Fertig and W. Wang, *Environ. Sci. Technol.*, 2001, **35**, 192–195.
- 47 J. J. Guzman, K. G. Cooke, M. O. Gay, S. E. Radachowsky, P. R. Girguis



- and M. A. Chiu, *Proc. SPIE Defense, Secur. Sens.*, 2010, 76662M-76662M-12.
- 48 L. M. Tender, S. a. Gray, E. Groveman, D. a. Lowy, P. Kauffman, J. Melhado, R. C. Tyce, D. Flynn, R. Petrecca and J. Dobarro, *J. Power Sources*, 2008, **179**, 571-575.
- 49 L. T. Angenent, K. Karim, M. H. Al-Dahhan, B. a Wrenn and R. Domínguez-Espinosa, *Trends Biotechnol.*, 2004, **22**, 477-85.
- 50 J. Choi and Y. Ahn, *J. Environ. Manage.*, 2013, **130**, 146-52.
- 51 W.-W. Li, H.-Q. Yu and Z. He, *Energy Environ. Sci.*, 2014, **7**, 911.
- 52 W. Yang, H. Han, M. Zhou and J. Yang, *RSC Adv.*, 2015, **5**, 49513-49520.
- 53 C. A. Mart, M. A. Rodrigo, I. Sire and O. Scialdone, *Chem. Rev.*, 2015, **115**, 13362-13407.
- 54 Q. Zhang, J. Hu and D. J. Lee, *Bioresour. Technol.*, 2015, **217**, 121-128.
- 55 P. Pandey, V. N. Shinde, R. L. Deopurkar, S. P. Kale, S. A. Patil and D. Pant, *Appl. Energy*, 2016, **168**, 706-723.
- 56 P. T. Ha, T. K. Lee, B. E. Rittmann, J. Park and I. S. Chang, *Environ. Sci. Technol.*, 2012, **46**, 3022-3030.
- 57 X. Xie, M. Ye, P.-C. Hsu, N. Liu, C. S. Criddle and Y. Cui, *Proc. Natl. Acad. Sci. U. S. A.*, 2013, **110**, 15925-30.
- 58 C. I. Torres, *Curr. Opin. Biotechnol.*, 2014, **27**, 107-114.
- 59 V. B. Oliveira, M. Simões, L. F. Melo and A. M. F. R. Pinto, *Biochem. Eng. J.*, 2013, **73**, 53-64.
- 60 J. Kim, H. Jia and P. Wang, *Biotechnol. Adv.*, 2006, **24**, 296-308.
- 61 J. R. G. K. B. E. Logan, B. Hamelers, R. Rozendal, U. Schroder and and K. R. S. Freguia, P. Aelterman, W. Verstraete, *Environ. Sci. Technol.*, 2006, **40**, 5181-5192.

- 62 H. Rismani-Yazdi, S. M. Carver, A. D. Christy and O. H. Tuovinen, *J. Power Sources*, 2008, **180**, 683–694.
- 63 F. Zhao, R. C. T. Slade and J. R. Varcoe, *Chem. Soc. Rev.*, 2009, **38**, 1926–39.
- 64 M. A. C. Brett and A. M. O. and Brett, *Electroanalysis*, Oxford University Press, New York, 1998.
- 65 V. J. Watson and B. E. Logan, *Electrochem. Commun.*, 2011, **13**, 54–56.
- 66 S. Haddadi, G. R. Nabi-Bidhendi and N. Mehrdadi, *J. Environ. Chem. Eng.*, 2014, **2**, 612–618.
- 67 S. T. Read, P. Dutta, P. L. Bond, J. Keller and K. Rabaey, *BMC Microbiol.*, 2010, **10**, 98.
- 68 A. E. Franks and K. P. Nevin, *Energies*, 2010, **3**, 899–919.
- 69 B. Dawoud, E. Amer and D. Gross, *Int. J. energy Res.*, 2007, **31**, 135–147.
- 70 Y. Fan, E. Sharbrough and H. Liu, *Environ. Sci. Technol.*, 2008, **42**, 8101–8107.
- 71 K. Rabaey, J. Rodríguez, L. L. Blackall, J. Keller, P. Gross, D. Batstone, W. Verstraete and K. H. Nealson, *ISME J.*, 2007, **1**, 9–18.
- 72 S. Cheng and B. E. Logan, *Bioresour. Technol.*, 2011, **102**, 4468–4473.
- 73 H.-S. Lee, P. Parameswaran, A. Kato-Marcus, C. I. Torres and B. E. Rittmann, *Water Res.*, 2008, **42**, 1501–10.
- 74 Y. R. J. Thomas, M. Picot, A. Carer, O. Berder, O. Sentieys and F. Barrière, *J. Power Sources*, 2013, **241**, 703–708.
- 75 J. M. Logan, Bruce E., Regan, *Environ. Sci. Technol.*, 2006, **40**, 5172–5180.
- 76 I. A. Ieropoulos, J. Greenman, C. Melhuish and J. Hart, *Enzyme*

- Microb. Technol.*, 2005, **37**, 238–245.
- 77 V. J. Watson and B. E. Logan, *Biotechnol. Bioeng.*, 2010, **105**, 489–498.
- 78 D. F. Juang, P. C. Yang, H. Y. Chou and L. J. Chiu, *Biotechnol. Lett.*, 2011, **33**, 2147–2160.
- 79 D. Pant, G. Van Bogaert, L. Diels and K. Vanbroekhoven, *Bioresour. Technol.*, 2010, **101**, 1533–43.
- 80 J. Monod, *Annu. Rev. Microbiol.*, 1949, **3**, 371–394.
- 81 C. Rao and D. Trivedi, *Coord. Chem. Rev.*, 2005, **249**, 613–631.
- 82 A. Baudler, I. Schmidt, M. Langner, A. Greiner and U. Schröder, *Energy Environ. Sci.*, 2015, **8**, 2048–2055.
- 83 M. Zhou, M. Chi, J. Luo, H. He and T. Jin, *J. Power Sources*, 2011, **196**, 4427–4435.
- 84 F. Cœuret, E. O. Vilar and E. B. Cavalcanti, *J. Appl. Electrochem.*, 2002, **32**, 1175–1182.
- 85 Mustakeem, *Mater. Renew. Sustain. Energy*, 2015, **4**, 1–11.
- 86 J. Wei, P. Liang and X. Huang, *Bioresour. Technol.*, 2011, **102**, 9335–44.
- 87 V. G. Debabov, *Mikrobiologiya*, 2008, **77**, 149–157.
- 88 D. R. Lovley, *Annu. Rev. Microbiol.*, 2012, **66**, 391–409.
- 89 Z. A. W. and M. F. M. D. Ravinder Kumar, Lakhveer Singh, *Int. J. energy Res.*, 2007, **31**, 135–147.
- 90 B. E. Logan, *Nat. Rev. Microbiol.*, 2009, **7**, 375–81.
- 91 S. Oh and B. Min, *Environ. Sci. Technol.*, 2004, **38**, 4900–4904.
- 92 H. Liu, S. Cheng and B. E. Logan, *Environ. Sci. Technol.*, 2005, **39**, 5488–5493.
- 93 S. E. Oh and B. E. Logan, *Appl. Microbiol. Biotechnol.*, 2006, **70**, 162–169.

- 94 F. Harnisch and U. Schröder, *Chem. Soc. Rev.*, 2010, **39**, 4433–4448.
- 95 U. Schröder, *Phys. Chem. Chem. Phys.*, 2007, **9**, 2619–29.
- 96 U. De Geneve, E. Polytechnique, F. De Lausanne, T. Chemical and E. Potential, *J. Chem. Educ.*, 1994, **71**, 493–494.
- 97 A. Arevalo and G. Pastor, *J. Chem. Educ.*, 1985, **62**, 882–884.
- 98 F. J. Vidal-iglesias, J. Solla-gullo, A. Rodes, E. Herrero and A. Aldaz, *J. Chem. Educ.*, 2012, **89**, 936–939.
- 99 G. Toole and S. Toole, *Understanding biology for advanced level*, Stanley Thornes, Cheltenham, 3rd edn., 1995.
- 100 M. T. Cabeen and C. Jacobs-Wagner, *Nat. Rev. Microbiol.*, 2005, **3**, 601–610.
- 101 D. Hames and N. Hooper, *Biochemistry*, Taylor & Francis Group, New York and London, 4th edn., 2011, vol. 4.
- 102 T. J. Silhavy, D. Kahne and S. Walker, *Cold Spring Harb. Perspect. Biol.*, 2010, **2**, 1–17.
- 103 O. Schaetzle, F. Barrière and K. Baronian, *Energy Environ. Sci.*, 2008, **1**, 607.
- 104 G. E. Pinchuk, O. V. Geydebrekht, E. a. Hill, J. L. Reed, A. E. Konopka, A. S. Beliaev and J. K. Fredrickson, *Appl. Environ. Microbiol.*, 2011, **77**, 8234–8240.
- 105 Y. J. Tang, A. L. Meadows, J. Kirby and J. D. Keasling, *J. Bacteriol.*, 2007, **189**, 894–901.
- 106 J. M. Berg, J. L. Tymoczko and L. Stryer, *Biochemistry*, W H Freeman, New York, 5th edn., 2002.
- 107 B. A. Haddock and C. W. Jones, *Bacteriol. Rev.*, 1977, **41**, 47.
- 108 A. Bruce, A. Johnson, J. Lewis, M. Raff, K. Roberts and P. Walter, *Molecular Biology of the Cell*, Garland Science, New York, 4th edn., 2002.

- 109 R. A. Marcus and N. Sutin, *Biochim. Biophys. Acta*, 1985, **811**, 265–322.
- 110 R. A. Marcus, *Rev. Mod. Phys.*, 1992, 599.
- 111 K. Guo, A. PrévotEAU, S. a Patil and K. Rabaey, *Curr. Opin. Biotechnol.*, 2015, **33**, 149–156.
- 112 X. Xie, C. Criddle and Y. Cui, *Energy Environ. Sci.*, 2015, **8**, 3418–3441.
- 113 J. . Davis and H. F. J. Yarbrough, *Science (80-. )*, 1962, **137**, 615–616.
- 114 K. Rabaey, N. Boon, M. Höfte and W. Verstraete, *Environ. Sci. Technol.*, 2005, **39**, 3401–8.
- 115 D. K. Newman and R. Kolter, *Nature*, 2000, **405**, 94–7.
- 116 D. R. Lovley, *Nat. Rev. Microbiol.*, 2006, **4**, 497–508.
- 117 N. S. Malvankar and D. R. Lovley, *Curr. Opin. Biotechnol.*, 2014, **27**, 88–95.
- 118 B. E. Logan and J. M. Regan, *Trends Microbiol.*, 2006, **14**, 512–518.
- 119 J. W. Costerton, *Int. J. Antimicrob. Agents*, 1999, **11**, 217–221.
- 120 M. Crouzet, C. Le Senechal, V. S. Brözel, P. Costaglioli, C. Barthe, M. Bonneu, B. Garbay and S. Vilain, *BMC Microbiol.*, 2014, **14**, 1–12.
- 121 M. Kostakioti, M. Hadjifrangiskou and S. J. Hultgren, *Cold Spring Harb. Perspect. Med.*, 2013, **3**, 1–23.
- 122 T. Das, P. K. Sharma, H. J. Busscher, H. C. Van Der Mei and B. P. Krom, *Appl. Environ. Microbiol.*, 2010, **76**, 3405–3408.
- 123 A. P. Borole, G. Reguera, B. Ringeisen, Z.-W. Wang, Y. Feng and B. H. Kim, *Energy Environ. Sci.*, 2011, **4**, 4813.
- 124 N. S. Malvankar, M. T. Tuominen and D. R. Lovley, *Energy Environ. Sci.*, 2012, **5**, 5790.
- 125 K. M. Thormann, R. M. Saville, S. Shukla, A. Dale, A. M. Spormann, M. Saville and D. A. Pelletier, *J. Bacteriol.*, 2004, **186**, 8096–8104.

- 126 Y. Qiao, S.-J. Bao and C. M. Li, *Energy Environ. Sci.*, 2010, **3**, 544.
- 127 V. Flexer, J. Chen, B. C. Donose, P. Sherrell, G. G. Wallace and J. Keller, *Energy Environ. Sci.*, 2013, **6**, 1291.
- 128 H. M. Jensen, A. E. Albers, K. R. Malley, Y. Y. Londer, B. E. Cohen, B. a Helms, P. Weigele, J. T. Groves and C. M. Ajo-Franklin, *Proc. Natl. Acad. Sci. U. S. A.*, 2010, **107**, 19213–8.
- 129 M. J. Marshall, A. S. Beliaev, A. C. Dohnalkova, D. W. Kennedy, L. Shi, Z. Wang, M. I. Boyanov, B. Lai, K. M. Kemner, J. S. McLean, S. B. Reed, D. E. Culley, V. L. Bailey, C. J. Simonson, D. a. Saffarini, M. F. Romine, J. M. Zachara and J. K. Fredrickson, *PLoS Biol.*, 2006, **4**, 1324–1333.
- 130 M. Breuer, K. M. Rosso, J. Blumberger and J. N. Butt, *J. R. Soc. Interface*, 2015, **12**, 1–27.
- 131 S. Pirbadian, S. E. Barchinger, K. M. Leung, H. S. Byun, Y. Jangir, R. a. Bouhenni, S. B. Reed, M. F. Romine, D. a. Saffarini, L. Shi, Y. a. Gorby, J. H. Golbeck and M. Y. El-Naggar, *Proc. Natl. Acad. Sci.*, 2014, **111**.
- 132 K. Kondo, A. Okamoto, K. Hashimoto and R. Nakamura, *Langmuir*, 2015, 7427–7434.
- 133 L. Peng, S.-J. You and J.-Y. Wang, *Biosens. Bioelectron.*, 2010, **25**, 1248–51.
- 134 L. Yang, S. Wang, S. Peng, H. Jiang, Y. Zhang, W. Deng, Y. Tan, M. Ma and Q. Xie, *Chem. - A Eur. J.*, 2015, **21**, 10634–10638.
- 135 P. Gangadharan, I. M. Nambi, J. Senthilnathan and P. V. M., *RSC Adv.*, 2016, **6**, 68827–68834.
- 136 H. Ren, H. Tian, C. L. Gardner, T.-L. Ren and J. Chae, *Nanoscale*, 2016, **8**, 3539–3547.
- 137 C. E. Zhao, J. Wu, S. Kjelleberg, J. S. C. Loo and Q. Zhang, *Small*, 2015, **11**, 3440–3443.
- 138 X. Tang, H. Li, Z. Du, W. Wang and H. Y. Ng, *RSC Adv.*, 2015, **5**,

50968–50974.

- 139 R. W. Murray, *Chem. Rev.*, 2008, **108**, 2688–2720.
- 140 B. H. Weller, *Adv. Mater.*, 1993, **5**, 88–95.
- 141 A. Henglein, *Chem. Rev.*, 1989, **89**, 1861–1873.
- 142 J. Kiwi and M. Gratzel, *J. Am. Chem. Soc.*, 1979, **101**, 7214–7217.
- 143 A. Henglein, *J. Phys. Chem.*, 1979, **2**, 2209–2216.
- 144 X. Zhang, H. Liu, J. Wang, G. Ren, B. Xie, H. Liu, Y. Zhu and L. Jiang, *Nanoscale*, 2015, **7**, 18763–18769.
- 145 L. Deng, S. Guo, Z. Liu, M. Zhou, D. Li, L. Liu, G. Li, E. Wang and S. Dong, *Chem. Commun.*, 2010, **46**, 7172–7174.
- 146 C. Zhao, P. Gai, R. Song, J. Zhang and J.-J. Zhu, *Anal. Methods*, 2015, **7**, 4640–4644.
- 147 Y. Fan, S. Xu, R. Schaller, J. Jiao, F. Chaplen and H. Liu, *Biosens. Bioelectron.*, 2011, **26**, 1908–12.
- 148 F. A. a Alatraktchi, Y. Zhang and I. Angelidaki, *Appl. Energy*, 2014, **116**, 216–222.
- 149 P. Zhao, N. Li and D. Astruc, *Coord. Chem. Rev.*, 2013, **257**, 638–665.
- 150 V. A. Online, D. Fragouli, R. Ruffilli and A. Athanassiou, *RSC Adv.*, 2014, **4**, 20449–20453.
- 151 M. E. Garcia, L. A. Baker and R. M. Crooks, *Anal. Chem.*, 1999, **71**, 256–8.
- 152 N. R. Jana, L. Gearheart and C. J. Murphy, *J. Phys. Chem. B*, 2001, **105**, 4065–4067.
- 153 O. Deschaume, B. De Roo, M. J. Van Bael, J. Locquet, C. Van Haesendonck and C. Bartic, *Chem. Mater.*, 2014.
- 154 S. Diegoli, A. L. Manciuola, S. Begum, I. P. Jones, J. R. Lead and J. a Preece, *Sci. Total Environ.*, 2008, **402**, 51–61.
- 155 D. T. Nguyen, D.-J. Kim, M. G. So and K.-S. Kim, *Adv. Powder Technol.*,

- 2010, **21**, 111–118.
- 156 L. Huang, Y. Zhang, Z. Guo and N. Gu, *Chinese Sci. Bull.*, 2009, **54**, 1626–1629.
- 157 M.-C. Daniel, M. E. Grow, H. Pan, M. Bednarek, W. E. Ghann, K. Zabetakis and J. Cornish, *New J. Chem.*, 2011, **35**, 2366.
- 158 M. Iqbal, G. Usanase, K. Oulmi, F. Aberkane, T. Bendaikha, H. Fessi, N. Zine, G. Agusti, E. S. Errachid and A. Elaissari, *Mater. Res. Bull.*, 2016, **79**, 97–104.
- 159 K. Vasilev, T. Zhu, M. Wilms, G. Gillies, I. Lieberwirth, S. Mittler, W. Knoll and M. Kreiter, *Langmuir*, 2005, **21**, 12399–12403.
- 160 P. Huang, Z. Li, J. Lin and D. Cui, *J. Phys. Conf. Ser.*, 2009, **188**, 12031.
- 161 J. Turkevich, *Gold Bull.*, 1985, **18**, 125–131.
- 162 R. P. Ramasamy and S. M. Maliyekkal, *New J. Chem.*, 2014, **38**, 63–69.
- 163 Z. Guo, X. Fan, L. Liu, Z. Bian, C. Gu, Y. Zhang, N. Gu, D. Yang and J. Zhang, *J. Colloid Interface Sci.*, 2010, **348**, 29–36.
- 164 J.-C. Parisien-La Salle, 2012.
- 165 F. Schulz, T. Homolka, N. G. Bastús, V. F. Puentes, H. Weller, T. Vossmeier and V. Puentes, *Langmuir*, 2014.
- 166 L. Ding, C. Hao, Y. Xue and H. Ju, *Biomacromolecules*, 2007, **8**, 1341–6.
- 167 D. K. Smith and B. A. Korgel, *Langmuir*, 2008, **24**, 644–9.
- 168 R. G. Acres, V. Feyer, N. Tsud, E. Carlino and K. C. Prince, *J. Phys. Chem. C*, 2014, **118**, 10481–10487.
- 169 P. Pyykkö, *Angew. Chem. Int. Ed. Engl.*, 2004, **43**, 4412–56.
- 170 L. Gou and C. J. Murphy, *Chem Mater*, 2005, **17**, 3668–3672.
- 171 S. R. Makhsin, K. A. Razak, R. Noordin, N. D. Zakaria and T. S. Chun, *Nanotechnology*, 2012, **23**, 495719.



- 172 N. Li, P. Zhao and D. Astruc, *Angew. Chemie - Int. Ed.*, 2014, **53**, 1756–1789.
- 173 X. Huang, S. Neretina and M. A. El-Sayed, *Adv. Mater.*, 2009, **21**, 4880–4910.
- 174 W. W. Weare, S. M. Reed, M. G. Warner and J. E. Hutchison, *J. Am. Chem. Soc.*, 2000, **122**, 12890–12891.
- 175 G. a. Rance, D. H. Marsh and A. N. Khlobystov, *Chem. Phys. Lett.*, 2008, **460**, 230–236.
- 176 M.-H. Park, Y. Ofir, B. Samanta and V. M. Rotello, *Adv. Mater.*, 2009, **21**, 2323–2327.
- 177 T. Pellegrino, S. Kudera, T. Liedl, A. M. Javier, L. Manna and W. J. Parak, *Small*, 2005, **1**, 48–63.
- 178 M. Faraday, *Philos. Trans. R. Soc. London*, 1857, **147**, 145–181.
- 179 J. Turkevich, P. C. Stevenson and A. J. Hillier, *Disc. Farad. Soc.*, 1951, **55–75**.
- 180 G. Frens, *Nat. Phys. Sci.*, 1973, **241**, 20–22.
- 181 M. Brust, M. Walker, D. Bethell, D. J. Schiffrin and R. Whyman, *J. Chem. Soc. Chem. Commun.*, 1994, 801–802.
- 182 E. Katz and I. Willner, *Angew. Chem. Int. Ed. Engl.*, 2004, **43**, 6042–108.
- 183 K. G. Thomas and P. V Kamat, 2003, **36**, 888–898.
- 184 X. Xu, Y. Chen, H. Wei, B. Xia, F. Liu and N. Li, *Anal. Chem.*, 2012, **84**, 9721–8.
- 185 P.-H. Chan, S.-Y. Wong, S.-H. Lin and Y.-C. Chen, *Rapid Commun. Mass Spectrom.*, 2013, **27**, 2143–8.
- 186 A. M. El Badawy, T. P. Luxton, R. G. Silva, K. G. Scheckel, M. T. Suidan and T. M. Tolaymat, *Environ. Sci. Technol.*, 2010, **44**, 1260–6.
- 187 S. K. Ghosh and T. Pal, *Chem. Rev.*, 2007, **107**, 4797–862.

- 188 R. Pamies, J. G. H. Cifre, V. F. Espín, M. Collado-González, F. G. D. Baños and J. G. Torre, *J. Nanoparticle Res.*, 2014, **16**, 2376.
- 189 P. Mulvaney, in *Nanoscale materials in Chemistry*, ed. J. K. Klabunde, John Wiley & Sons, 2001, vol. 3, pp. 121–167.
- 190 Y. Ju-Nam and J. R. Lead, *Sci. Total Environ.*, 2008, **400**, 396–414.
- 191 R. A. Sperling, 2008.
- 192 D. J. Lewis, T. M. Day, J. V MacPherson and Z. Pikramenou, *Chem. Commun.*, 2006, 1433–5.
- 193 K. E. Fong and L.-Y. L. Yung, *Nanoscale*, 2013, **5**, 12043–71.
- 194 S. Eustis and M. A. El-Sayed, *Chem. Soc. Rev.*, 2006, **35**, 209–17.
- 195 P. N. Njoki, I.-I. S. Lim, D. Mott, H.-Y. Park, B. Khan, S. Mishra, R. Sujakumar, J. Luo and C.-J. Zhong, *J. Phys. Chem. C*, 2007, **111**, 14664–14669.
- 196 V. Sharma, K. Park and M. Srinivasarao, *Mater. Sci. Eng. R Reports*, 2009, **65**, 1–38.
- 197 S. Link and M. a. El-Sayed, *Int. Rev. Phys. Chem.*, 2000, **19**, 409–453.
- 198 L. Vigderman and E. R. Zubarev, 2012.
- 199 I. Ojea-Jiménez and V. Puentes, *J. Am. Chem. Soc.*, 2009, **131**, 13320–7.
- 200 W. Haiss, N. T. K. Thanh, J. Aveyard and D. G. Fernig, *Anal. Chem.*, 2007, **79**, 4215–21.
- 201 J. Wirth, F. Garwe, R. Meyer, a Csáki, O. Stranik and W. Fritzsche, *Nano Lett.*, 2014, **14**, 3809–3816.
- 202 X. Ma, Y. Xia, L. Ni, L. Song and Z. Wang, *Spectrochim. Acta - Part A Mol. Biomol. Spectrosc.*, 2014, **121**, 657–661.
- 203 Z. Wang, S. Zong, J. Yang, C. Song, J. Li and Y. Cui, *Biosens. Bioelectron.*, 2010, **26**, 241–7.
- 204 H. Feng, Y. Yang, Y. You, G. Li, J. Guo, T. Yu, Z. Shen, T. Wu and B.

- Xing, *Chem. Commun. (Camb)*, 2009, 1984–1986.
- 205 K. R. Brown, L. A. Lyon, A. P. Fox, B. D. Reiss and M. J. Natan, *Chem. Mater.*, 2000, **313**, 314–323.
- 206 M. P. Casaletto, A. Longo, A. Martorana, A. and Prestianni and A. . Venezia, *Surf. Interface Anal.*, 2006, **38**, 215–218.
- 207 E. D. and Park and J. S. Lee, *J. Catal.*, 1999, **186**, 1–11.
- 208 S. Gonzalez, 2014.
- 209 S. Koepl, N. Ghielmetti, W. Caseri and R. Spolenak, *J. Nanoparticle Res.*, 2013, **15**, 1471.
- 210 T. Romaskevicius, M. Sedlevicius, S. Budriene, A. Ramanavicius, N. Ryskevicius, S. Miasojedovas and A. Ramanaviciene, *Macromol. Chem. Phys.*, 2011, **212**, 2291–2299.
- 211 N. German, A. Ramanavicius and A. Ramanaviciene, *Sensors Actuators, B Chem.*, 2014, **203**, 25–34.
- 212 A. Y. Chen, Z. Deng, A. N. Billings, U. O. S. Seker, M. Y. Lu, R. J. Citorik, B. Zakeri and T. K. Lu, *Nat. Mater.*, 2014, **13**, 515–23.
- 213 T. Jing, T. Xiao-Chun and Z. F.-Q. Y.-Q. L. Jian-Hang, *Acta Phys. - Chim. Sin.*, 2011, **27**, 641–646.
- 214 S. R. Nambiar, P. K. Aneesh and T. P. Rao, *J. Electroanal. Chem.*, 2014, **722–723**, 60–67.
- 215 D. A. Walker and V. K. Gupta, *Nanotechnology*, 2008, **19**, 435603.
- 216 H. M. Zakaria, A. Shah, M. Konieczny, J. a Hoffmann, a J. Nijdam and M. E. Reeves, *Langmuir*, 2013.
- 217 P. a Hassan, S. Rana and G. Verma, *Langmuir*, 2014.
- 218 S. Du, K. Kendall, P. Toloueinia, Y. Mehrabadi, G. Gupta and J. Newton, *J. Nanoparticle Res.*, 2012, **14**.
- 219 X. Xu, J. Jia, X. Yang and S. Dong, *Langmuir*, 2010, **26**, 7627–7631.
- 220 L. Fairbrother, B. Etschmann, J. Brugger, J. Shapter, G. Southam and

- F. Reith, *Environ. Sci. Technol.*, 2013, **47**, 2628–35.
- 221 R. Jin, S. Sun, Y. Yang, Y. Xing, D. Yu, X. Yu and S. Song, *Dalton Trans.*, 2013, **42**, 7888–7893.
- 222 S. T. Camli, F. Buyukserin, C. T. Yavuz and M. S. Yavuz, *Mater. Chem. Phys.*, 2012, **134**, 1153–1159.
- 223 P. R. Chandran, M. Naseer, N. Udupa and N. Sandhyarani, *Nanotechnology*, 2012, **23**, 15602.
- 224 A. M. Alkilany, S. R. Abulateefeh, K. Mills, A. Bani Yaseen, M. Hamaly, H. Alkhatib, K. Aiedeh and J. W. Stone, *Langmuir*, 2014.
- 225 E. Oh, J. B. Delehanty, K. E. Sapsford, K. Susumu, R. Goswami, J. B. Blanco-canosa, P. E. Dawson, J. Granek, M. Shoff, Q. Zhang, P. L. Goering, A. Huston and I. L. Medintz, *J. Am. Chem. Soc.*, 2011, **5**, 6434–6448.
- 226 H. Urakami, J. Hentschel, K. Seetho, H. Zeng, K. Chawla and Z. Guan, *Biomacromolecules*, 2013.
- 227 A. K. Suresh, D. a Pelletier, W. Wang, M. L. Broich, J.-W. Moon, B. Gu, D. P. Allison, D. C. Joy, T. J. Phelps and M. J. Doktycz, *Acta Biomater.*, 2011, **7**, 2148–2152.
- 228 G. Plascencia-Villa, D. Bahena, A. R. Rodríguez, A. Ponce and M. José-Yacamán, *Metallomics*, 2013, **5**, 242–50.
- 229 L. Du, H. Jiang, X. Liu and E. Wang, *Electrochem. commun.*, 2007, **9**, 1165–1170.
- 230 S. De Corte, T. Hennebel, S. Verschuere, C. Cuvelier, W. Verstraete and N. Boon, *J. Chem. Technol. Biotechnol.*, 2011, **86**, 547–553.
- 231 M.-C. Daniel and D. Astruc, *Chem. Rev.*, 2004, **104**, 293–346.
- 232 Y. Konishi, T. Tsukiyama, T. Tachimi, N. Saitoh, T. Nomura and S. Nagamine, *Electrochim. Acta*, 2007, **53**, 186–192.
- 233 R. A. Blaik, E. Lan, Y. Huang and B. Dunn, *ACS Nano*, 2016, **10**, 324–

332.

- 234 B. Radha, M. Arif, R. Datta, T. K. Kundu and G. U. Kulkarni, *Nano Res.*, 2010, **3**, 738–747.
- 235 L. a Dykman and N. G. Khlebtsov, *Chem. Rev.*, 2013.
- 236 R. Wu, L. Cui, L. Chen, C. Wang, C. Cao, G. Sheng, H. Yu and F. Zhao, *Sci. Rep.*, 2013, **3**, 3307, pp 7.
- 237 H. Shu, L. Cao, G. Chang, H. He, Y. Zhang and Y. He, *Electrochim. Acta*, 2014, **132**, 524–532.
- 238 H. Liu, F. Favier, K. Ng, M. . Zach and R. . Penner, *Electrochim. Acta*, 2001, **47**, 671–677.
- 239 J.-M. Moon and A. Wei, *J. Phys. Chem. B*, 2005, **109**, 23336–23341.
- 240 G. Sai-Anand, A. I. Gopalan, S.-W. Kang and K.-P. Lee, *IEEE Electron Device Lett.*, 2013, **34**, 1065–1067.
- 241 S. Manivannan and R. Ramaraj, *J. Nanoparticle Res.*, 2013, **15**, 1978.
- 242 Y. Xiao, F. Patolsky, E. Katz, J. F. Hainfeld and I. Willner, *Science (80-. )*, 2003, **299**, 1877–1881.
- 243 D. R. Lovley, *Annu. Rev. Microbiol.*, 1993, **47**, 263–290.
- 244 J. E. Champine, B. Underhill, J. M. Johnston, W. W. Lilly and S. Goodwin, *Anaerobe*, 2000, **6**, 187–196.
- 245 J. F. Heidelberg, I. T. Paulsen, K. E. Nelson, E. J. Gaidos, W. C. Nelson, T. D. Read, J. a Eisen, R. Seshadri, N. Ward, B. Methe, R. a Clayton, T. Meyer, A. Tsapin, J. Scott, M. Beanan, L. Brinkac, S. Daugherty, R. T. DeBoy, R. J. Dodson, a S. Durkin, D. H. Haft, J. F. Kolonay, R. Madupu, J. D. Peterson, L. a Umayam, O. White, A. M. Wolf, J. Vamathevan, J. Weidman, M. Impraim, K. Lee, K. Berry, C. Lee, J. Mueller, H. Khouri, J. Gill, T. R. Utterback, L. a McDonald, T. V Feldblyum, H. O. Smith, J. C. Venter, K. H. Nealson and C. M. Fraser, *Nat. Biotechnol.*, 2002, **20**, 1118–1123.

- 246 Y. Furukawa and J. R. Dale, *Geochem. Trans.*, 2013, **14**, 3.
- 247 G. M. Gadd, *Curr. Opin. Biotechnol.*, 2000, **11**, 271–279.
- 248 O. Bretschger, A. Obratzsova, C. a. Sturm, S. C. In, Y. a. Gorby, S. B. Reed, D. E. Culley, C. L. Reardon, S. Barua, M. F. Romine, J. Zhou, A. S. Beliaev, R. Bouhenni, D. Saffarini, F. Mansfeld, B. H. Kim, J. K. Fredrickson and K. H. Nealson, *Appl. Environ. Microbiol.*, 2007, **73**, 7003–7012.
- 249 S. M. Belchik, D. W. Kennedy, A. C. Dohnalkova, Y. Wang, P. C. Sevinc, H. Wu, Y. Lin, H. P. Lu, J. K. Fredrickson and L. Shi, *Appl. Environ. Microbiol.*, 2011, **77**, 4035–4041.
- 250 C. K. Ng, T. K. Cai Tan, H. Song and B. Cao, *RSC Adv.*, 2013, **3**, 22498.
- 251 G. J. Newton, S. Mori, R. Nakamura, K. Hashimoto and K. Watanabe, *Appl. Environ. Microbiol.*, 2009, **75**, 7674–7681.
- 252 S. Pirbadian and M. Y. El-Naggar, *Phys. Chem. Chem. Phys.*, 2012, **14**, 13802.
- 253 J. S. McLean, P. D. Majors, C. L. Reardon, C. L. Bilskis, S. B. Reed, M. F. Romine and J. K. Fredrickson, *J. Microbiol. Methods*, 2008, **74**, 47–56.
- 254 X. Jiang, J. Hu, L. a Fitzgerald, J. C. Biffinger, P. Xie, B. R. Ringeisen and C. M. Lieber, *Proc. Natl. Acad. Sci. U. S. A.*, 2010, **107**, 16806–10.
- 255 L. Shi, D. J. Richardson, Z. Wang, S. N. Kerisit, K. M. Rosso, J. M. Zachara and J. K. Fredrickson, *Environ. Microbiol. Rep.*, 2009, **1**, 220–227.
- 256 N. J. Kotloski and J. a Gralnick, *MBio*, 2013, **4**, 1–4.
- 257 E. Marsili, D. B. Baron, I. D. Shikhare, D. Coursolle, J. a Gralnick and D. R. Bond, *Proc. Natl. Acad. Sci. U. S. A.*, 2008, **105**, 3968–3973.
- 258 Y. A. Gorby, S. Yanina, J. S. McLean, K. M. Rosso, D. Moyles, A. Dohnalkova, T. J. Beveridge, I. S. Chang, B. H. Kim, K. S. Kim, D. E.

- Culley, S. B. Reed, M. F. Romine, D. A. Saffarini, E. A. Hill, L. Shi, D. A. Elias, D. W. Kennedy, G. Pinchuk, K. Watanabe, S. Ishii, B. Logan, K. H. Nealson and J. K. Fredrickson, *Proc. Natl. Acad. Sci. U. S. A.*, 2006, **103**, 11358–63.
- 259 E. D. Brutinel and J. a. Gralnick, *Appl. Microbiol. Biotechnol.*, 2012, **93**, 41–48.
- 260 M. Y. El-Naggar, G. Wanger, K. M. Leung, T. D. Yuzvinsky, G. Southam, J. Yang, W. M. Lau, K. H. Nealson and Y. A. Gorby, *Proc. Natl. Acad. Sci. U. S. A.*, 2010, **107**, 18127–31.
- 261 M. Breuer, K. M. Rosso, J. Blumberger and J. N. Butt, *Interface*, 2015, **12**, 20141117.
- 262 N. Krumov, I. Perner-Nochta, S. Oder, V. Gotcheva, A. Angelov and C. Posten, *Chem. Eng. Technol.*, 2009, **32**, 1026–1035.
- 263 S. Mann, *Nature*, 1992, **357**, 358–360.
- 264 Y. Konishi, T. Tsukiyama, K. Ohno, N. Saitoh, T. Nomura and S. Nagamine, *Hydrometallurgy*, 2006, **81**, 24–29.
- 265 R. G. Beveridge, T J and Murray, *J. Bacteriol.*, 1980, **141**, 876–887.
- 266 D. J. Abdallah and R. G. Weiss, *Adv. Mater.*, 2000, **12**, 1237–1247.
- 267 D. K. Smith, *Nat. Chem.*, 2010, **2**, 162–3.
- 268 W. Richtering and B. R. Saunders, *Soft Matter*, 2014, **10**, 3695–3702.
- 269 T. Coviello, P. Matricardi, C. Marianecchi and F. Alhaique, *J. Control. Release*, 2007, **119**, 5–24.
- 270 M. Hamidi, A. Azadi and P. Rafiei, *Adv. Drug Deliv. Rev.*, 2008, **60**, 1638–49.
- 271 J. a. Hunt, R. Chen, T. van Veen and N. Bryan, *J. Mater. Chem. B*, 2014, **2**, 5319.
- 272 A. Guiseppi-Elie, *Biomaterials*, 2010, **31**, 2701–16.

- 273 J. Hur, K. Im, S. W. Kim, J. Kim, D. Y. Chung, T. H. Kim, K. H. Jo, J. H. Hahn, Z. Bao, S. Hwang and N. Park, *ACS Nano*, 2014, **8**, 10066–10076.
- 274 R. Fuhrer, E. K. Athanassiou, N. A. Luechinger and W. J. Stark, *Small*, 2009, **5**, 383–388.
- 275 S. Ahadian, J. Ramón-Azcón, M. Estili, X. Liang, S. Ostrovidov, H. Shiku, M. Ramalingam, K. Nakajima, Y. Sakka, H. Bae, T. Matsue and A. Khademhosseini, *Sci. Rep.*, 2014, **4**, 4271.
- 276 D. Y. Lewitus, J. Landers, J. Branch, K. L. Smith, G. Callegari, J. Kohn and A. V Neimark, *Adv. Funct. Mater.*, 2011, **21**, 2624–2632.
- 277 A. K. Gaharwar, N. A. Peppas and A. Khademhosseini, *Biotechnol. Bioeng.*, 2014, **111**, 441–453.
- 278 P. Schexnailder and G. Schmidt, *Colloid Polym. Sci.*, 2008, **287**, 1–11.
- 279 K. Kostarelos, M. Prato, E. Va, S. Merino and C. Martí, *ACS Nano*, 2015, **9**, 4686–4697.
- 280 A. Chakrabarty, U. Maitra and A. D. Das, *J. Mater. Chem.*, 2012, **22**, 18268.
- 281 R. N. Mitra and P. K. Das, *J. Phys. Chem. C*, 2008, **112**, 8159–8166.
- 282 D. Das, T. Kar and P. K. Das, *Soft Matter*, 2012, **8**, 2348.
- 283 C. Stoffelen, J. Voskuhl, P. Jonkheijm and J. Huskens, *Angew. Chemie Int. Ed.*, 2014, **53**, 1–6.
- 284 I. Odriozola, N. Ormategui, I. Loinaz, J. a. Pomposo and H. J. Grande, *Macromol. Symp.*, 2008, **266**, 96–100.
- 285 I. Odriozola, I. Loinaz, J. A. Pomposo and H. J. Grande, *J. Mater. Chem.*, 2007, **17**, 4843.
- 286 I. Odriozola, P. Casuso, I. Loinaz, G. Cabañero and H. J. Grande, *Org. Biomol. Chem.*, 2011, **9**, 5059–5061.



- 287 P. Thoniyot, M. J. Tan, A. A. Karim, D. J. Young and X. J. Loh, *Adv. Sci.*, 2015, **2**, 1400010.
- 288 A. Y.-Y. Tam and V. W.-W. Yam, *Chem. Soc. Rev.*, 2013, **42**, 1540–67.
- 289 X. W. Liu, Y. X. Huang, X. F. Sun, G. P. Sheng, F. Zhao, S. G. Wang and H. Q. Yu, *ACS Appl. Mater. Interfaces*, 2014, **6**, 8158–8164.
- 290 Y. Zhao, B. Liu, L. Pan and G. Yu, *Energy Environ. Sci.*, 2013, **6**, 2856.
- 291 C. Yang, H. Wei, L. Guan, J. Guo, Y. Wang, X. Yan, X. Zhang, S. Wei and Z. Guo, *J. Mater. Chem. A*, 2015, **3**, 14929–14941.
- 292 M. Cametti and Z. Džolić, *Chem. Commun.*, 2014, **50**, 8273–8286.
- 293 S. Arnott, A. Fulmer, W. E. Scott, I. C. Dea, R. Moorhouse and D. a Rees, *J. Mol. Biol.*, 1974, **90**, 269–284.
- 294 M. R. Letherby and D. a. Young, *J. Chem. Soc. Faraday Trans. 1*, 1981, **77**, 1953.
- 295 P. Serwer, *Electrophoresis*, 1983, **4**, 375–382.
- 296 Y. Luo and M. S. Shoichet, *Biomacromolecules*, 2004, **5**, 2315–23.
- 297 J. Hur, K. Im, S. W. Kim, J. Kim, D.-Y. Chung, T.-H. Kim, K. H. Jo, J. H. Hahn, Z. Bao, S. Hwang and N. Park, *ACS Nano*, 2014, **8**, 10066–10076.
- 298 X. Wang, D. R. G. Mitchell, K. Prince, A. J. Atanacio and R. A. Caruso, *Chem. Mater.*, 2008, **20**, 3917–3926.
- 299 X. Wang, C. E. Egan, M. Zhou, K. Prince, D. R. G. Mitchell and R. a Caruso, *Chem. Commun.*, 2007, 3060–3062.
- 300 E. Faoucher, P. Nativo, K. Black, J. B. Claridge, M. Gass, S. Romani, A. L. Bleloch and M. Brust, *Chem. Commun.*, 2009, 6661–6663.
- 301 Y. Murali Mohan, K. Lee, T. Premkumar and K. E. Geckeler, *Polymer*, 2007, **48**, 158–164.
- 302 Y. M. Mohan, T. Premkumar, K. Lee and K. E. Geckeler, *Macromol. Rapid Commun.*, 2006, **27**, 1346–1354.

- 303 M. K. Jaiswal, J. R. Xavier, J. K. Carrow, P. Desai, D. Alge and A. K. Gaharwar, *ACS Nano*, 2016, **10**, 246–256.
- 304 J. D. S. Newman and G. J. Blanchard, *Langmuir*, 2006, **22**, 5882–5887.
- 305 X. Lu, H.-Y. Tuan, B. A. Korgel and Y. Xia, *Chemistry (Easton)*, 2008, **14**, 1584–1591.
- 306 M. Aslam, L. Fu, M. Su, K. Vijayamohanan and V. P. Dravid, *J. Mater. Chem.*, 2004, **14**, 1795.
- 307 S. H. Lee, K. H. Bae, S. H. Kim, K. R. Lee and T. G. Park, *Int. J. Pharm.*, 2008, **364**, 94–101.
- 308 R. a Sperling and W. J. Parak, *Philos. Trans. A. Math. Phys. Eng. Sci.*, 2010, **368**, 1333–83.
- 309 C. Subramaniam, R. T. Tom and T. Pradeep, *J. Nanoparticle Res.*, 2005, **7**, 209–217.
- 310 U. Schuchardt, R. Sercheli and R. Matheus, *J. Braz. Chem. Soc.*, 1998, **9**, 199–210.
- 311 M. Kazemi, Z. Noori, H. Kohzadi, M. Sayadi and A. Kazemi, *Iran. Chem. Commun.*, 2013, **98**, 43–50.
- 312 Z. Yang, J. Kang, H. Kim, A. Park and H. S. Kim, *Bull. Korean Chem. Society*, 2009, **30**, 1463–1469.
- 313 Y. Xie, X. Liu and Q. Chen, *Carbohydr. Polym.*, 2007, **69**, 142–147.
- 314 G. K. Mehta, S. Kondaveeti and A. K. Siddhanta, *Polym. Chem.*, 2011, **2**, 2334.
- 315 Z. M. Enikeeva, *Chem. Nat. Compd.*, 1998, **34**, 699–705.
- 316 H. Y. Kim, A. Talukdar and M. Cushman, *Org. Lett.*, 2006, **8**, 1085–1087.
- 317 S. Yixue, C. Bin, G. Yuan, W. Chaoxi, Z. Lingmin, C. Peng, W. Xiaoying and S. Tang, *Carbohydr. Polym.*, 2013, **92**, 2245–2251.

- 318 R. B. Garcia, R. R. L. Vidal and M. Rinaudo, *Polímeros*, 2000, **10**, 155–161.
- 319 S. De Bernardo, M. Weigele, V. Toome, K. Manhart, W. Leimgruber, P. Böhlen, S. Stein and S. Udenfriend, *Arch. Biochem. Biophys.*, 1974, **163**, 390–399.
- 320 J. V Castell, M. Cervera and R. Marco, *Anal. Biochem.*, 1979, **99**, 379–391.
- 321 P. Sidney, K. Bohlen and S. Udenfriend, *Arch. Biochem. Biophys.*, 1974, **161**, 161–163.
- 322 C. Rochas and M. Lahaye, *Carbohydr. Polym.*, 1989, **10**, 289–298.
- 323 S. K. H. Gulrez, S. Al-Assaf and G. O. Phillips, in *Progress in Molecular and Environmental Bioengineering*, 2003, vol. 51, pp. 117–150.
- 324 A. R. Y. R.-M. María Guadalupe Neira-Velásquez, María Teresa Rodríguez-Hernández, Ernesto Hernández-Hernández, *Handb. Polym. Synth. Charact. Process.*, 2013, 355–366.
- 325 P. W. Allen, *Techniques of polymer characterisation*, Butterworth & Co, Great Britain, First, 1959.
- 326 J. M. G. Cowie and V. Arrighi, *Polymers: Chemistry and Physics of Modern Materials*, Taylor & Francis Group, Florida, 3rd edn., 2008.
- 327 P. J. Flory, *Principles of Polymer Chemistry*, Cornell University Press, London, 1953.
- 328 H. L. Wagner, *J. Phys. Chem. Ref. data*, 1985, **14**, 611–616.
- 329 M. A. Masuelli, L. De Membranas, I. D. F. Aplicada, F. De Química and B. Farmacia, *J. Polym. Biopolym. Phys. Chem.*, 2014, **2**, 37–43.
- 330 M. H. Kwaambwa, J. W. Goodwin, R. W. Hughes and P. A. Reynolds, *Colloids Surfaces A Physicochem. Eng. Asp.*, 2007, **294**, 14–19.
- 331 L. Huggins, *J. Am. Chem. Soc.*, 1942, **64**, 2716–2718.
- 332 E. Kraemer, *Ind. Eng. Chem.*, 1938, **30**, 1200–1203.

- 333 R. Pamies, J. G. Hernández Cifre, M. del Carmen López Martínez and J. García de la Torre, *Colloid Polym. Sci.*, 2008, **286**, 1223–1231.
- 334 A. P. Mahapatra, R. K. Samal, R. N. Samal and G. S. Roy, *Phys. Chem. Liq.*, 2001, **39**, 169–181.
- 335 M. V. S. Rao, *Polymer*, 1993, **34**, 592–596.
- 336 I. L. Mello, M. C. Delpech, F. M. B. Coutinho and F. F. M. Albino, *J. Braz. Chem. Soc.*, 2006, **17**, 194–199.
- 337 M. Watase and K. Nishinari, *Rheol. Acta*, 1983, **22**, 580–587.
- 338 J. M. Garcia-Ruiz, M. L. Novella, R. Moreno and J. A. Gavira, *J. Cryst. Growth*, 2001, **232**, 165–172.
- 339 E. R. Morris, A. N. Cutler, S. B. Ross-Murphy, D. A. Rees and J. Price, *Carbohydr. Polym.*, 1981, **1**, 5–21.
- 340 R. Meena, A. K. Siddhanta, K. Prasad, B. K. Ramavat, K. Eswaran, S. Thiruppathi, M. Ganesan, V. A. Mantri and P. V. S. Rao, *Carbohydr. Polym.*, 2007, **69**, 179–188.
- 341 K. Prasad, A. M. Goswami, R. Meena, B. K. Ramavat, P. K. Ghosh and A. K. Siddhanta, *Indian J. Mar. Sci.*, 2006, **35**, 268–274.
- 342 Hickson, T. G. I And and A. Polson, *Biochim. Biophys. Acta*, 1968, **165**, 43–58.
- 343 J. Praiboon, A. Chirapart, Y. Akakabe, O. Bhumibhamon and T. Kajiwarra, *ScienceAsia*, 2006, **32(s1)**, 11–17.
- 344 S. Waki, J. D. Harvey and a R. Bellamy, *Biopolymers*, 1982, **21**, 1909–1926.
- 345 A. Y. Klyushin, T. C. R. Rocha, M. Hävecker, A. Knop-Gericke and R. Schlögl, *Phys. Chem. Chem. Phys.*, 2014, **16**, 7881–7886.
- 346 M. J. Hostetler, J. E. Wingate, C.-J. Zhong, J. E. Harris, R. W. Vachet, M. R. Clark, J. D. Londono, S. J. Green, J. J. Stokes, G. D. Wignall, G. L. Glish, M. D. Porter, N. D. Evans and R. W. Murray, *Langmuir*, 1998,

- 14**, 17–30.
- 347 M. Rimboud, D. Pocaznoi, B. Erable and a Bergel, *Phys. Chem. Chem. Phys.*, 2014, **16**, 16349–16366.
- 348 C. Ding, H. Liu, M. Lv, T. Zhao, Y. Zhu and L. Jiang, *Nanoscale*, 2014, **6**, 7866–7871.
- 349 A. a. Carmona-Martínez, F. Harnisch, U. Kuhlicke, T. R. Neu and U. Schröder, *Bioelectrochemistry*, 2013, **93**, 23–29.
- 350 S. Khilari, S. Pandit, J. L. Varanasi, D. Das and D. Pradhan, *ACS Appl. Mater. Interfaces*, 2015, **7**, 20657–20666.
- 351 J. M. Tiedje, *Nat. Biotechnol.*, 2002, **20**, 1093–1094.
- 352 J. N. Roy, K. E. Garcia, H. R. Luckarift, a. Falase, J. Cornejo, S. Babanova, a. J. Schuler, G. R. Johnson and P. B. Atanassov, *J. Electrochem. Soc.*, 2013, **160**, H866–H871.
- 353 M. Lu, S. Chan, S. Babanova and O. Bretschger, *Biotechnol. Bioeng.*, 2016, **9999**, 1–10.
- 354 M. A. Rosenbaum, H. Y. Bar, Q. K. Beg, D. Segre, J. Booth, M. A. Cotta and L. T. Angenent, *PLoS One*, 2012, **7**, e30827.
- 355 N. G. Tsierkezos, *J. Solution Chem.*, 2007, **36**, 289–302.
- 356 R. G. Crompton and C. E. Banks, *Understanding Voltammetry*, Imperial College Press, 2nd edn., 2011.
- 357 G. C. L. Robert R. Gagne , Carl A. Koval, *Inorg. Chem.*, 1980, **19**, 2854–2855.
- 358 F. Haniyeh, a Abdollah and D. Abolghasem, *Mater. Sci. Appl.*, 2013, **4**, 667–678.
- 359 R. Yoho, S. C. Popat, L. Rago, A. Guisasola and C. I. Torres, *Langmuir*, 2015, **31**, 12552–12559.
- 360 M. Sun, F. Zhang, Z. H. Tong, G. P. Sheng, Y. Z. Chen, Y. Zhao, Y. P. Chen, S. Y. Zhou, G. Liu, Y. C. Tian and H. Q. Yu, *Biosens. Bioelectron.*,

- 2010, **26**, 338–343.
- 361 K. Critchley, B. P. Khanal, M. Górzny, L. Vigderman, S. D. Evans, E. R. Zubarev and N. A. Kotov, *Adv. Mater.*, 2010, **22**, 2338–2342.
- 362 B. J. Muster, G. T. Kim, V. Krstic, J. G. Park, Y. W. Park and S. Roth, *Adv. Mater.*, 2000, **12**, 420–424.
- 363 E. C. Walter, K. Ng, M. P. Zach, R. M. Penner and F. Favier, *Microelectron. Eng.*, 2002, **61–62**, 555–561.
- 364 T. Ahuja and D. Kumar, *Sensors Actuators, B Chem.*, 2009, **136**, 275–286.
- 365 N. K. Guimard, N. Gomez and C. E. Schmidt, *Prog. Polym. Sci.*, 2007, **32**, 876–921.
- 366 X. Lu, W. Zhang, C. Wang, T. Wen and Y. Wei, *Prog. Polym. Sci.*, 2011, **36**, 671–712.
- 367 H. P. Wu, J. F. Liu, X. J. Wu, M. Y. Ge, Y. W. Wang, G. Q. Zhang and J. Z. Jiang, *Int. J. Adhes. Adhes.*, 2006, **26**, 617–621.
- 368 Y. H. Wang, N. N. Xiong, H. Xie, Y. Z. Zhao and J. Li, *J. Mater. Sci. Mater. Electron.*, 2014, **26**, 621–629.
- 369 X. Li and X. Xiang, *Rare Met.*, 2016, 0–4.
- 370 G. Reguera, K. P. Nevin, J. S. Nicoll, S. F. Covalla, T. L. Woodard and D. R. Lovley, *Appl. Environ. Microbiol.*, 2006, **72**, 7345–8.
- 371 S. M. Strycharz-Glaven, R. M. Snider, A. Guiseppi-Elie and L. M. Tender, *Energy Environ. Sci.*, 2011, **4**, 4366.
- 372 A. Standing, S. Assali, L. Gao, M. A. Verheijen, D. van Dam, Y. Cui, P. H. L. Notten, J. E. M. Haverkort and E. P. A. M. Bakkers, *Nat. Commun.*, 2015, **6**, 7824.
- 373 A. R. Patel and A. V. Rao, *Bull. Mater. Sci.*, 1982, **4**, 527–548.
- 374 M. J. Ashley, M. N. O'Brien, K. R. Hedderick, J. A. Mason, M. B. Ross and C. A. Mirkin, *J. Am. Chem. Soc.*, 2016, 8–11.

- 375 S. V. N. T. Kuchibhatla, A. S. Karakoti, D. Bera and S. Seal, *Prog. Mater. Sci.*, 2007, **52**, 699–913.
- 376 Z. Miao, D. Xu, J. Ouyang, G. Guo and X. Zhao, *Nano Lett.*, 2002, **2**, 717–720.
- 377 S. Bhattacharyya, S. K. Saha and D. Chakravorty, *Appl. Phys. Lett.*, 2000, **77**, 3770–3772.
- 378 A. Huczko, *Appl. Phys. A-Materials Sci. Process.*, 2000, **376**, 365–376.
- 379 M. Lai and D. J. Riley, *J. Colloid Interface Sci.*, 2008, **323**, 203–212.
- 380 G. Cao and D. Liu, *Adv. Colloid Interface Sci.*, 2008, **136**, 45–64.
- 381 B. Jin, H. Bang and K. S. Suslick, *Adv. Funct. Mater.*, 2010, **22**, 1039–1059.
- 382 W. R. Small and V. N. Paunov, *J. Mater. Chem.*, 2008, **18**, 2082.
- 383 S. M. Jung, H. Y. Jung, W. Fang, M. S. Dresselhaus and J. Kong, *Nano Lett.*, 2014, **14**, 1810–1817.
- 384 H. Kitching, M. J. Shiers, A. J. Kenyon and I. P. Parkin, *J. Mater. Chem. A*, 2013, **1**, 6985.
- 385 Z. Yi, X. Xu, K. Zhang, X. Tan, X. Li, J. Luo, X. Ye, W. Wu, J. Wu, Y. Yi and Y. Tang, *Mater. Chem. Phys.*, 2013, **139**, 794–801.
- 386 M. Le Thai, G. T. Chandran, R. K. Dutta, X. Li and R. M. Penner, *ACS Energy Lett.*, 2016, **1**, 57–63.
- 387 Y. N. Tan, J. Y. Lee and D. I. C. Wang, *J. Phys. Chem. C*, 2008, **112**, 5463–5470.
- 388 D. Azulai, E. Cohen and G. Markovich, *Nano Lett.*, 2012, **12**, 5552–8.
- 389 N. Pazos-Pérez, D. Baranov, S. Irsen, M. Hilgendorff, L. M. Liz-Marzán and M. Giersig, *Langmuir*, 2008, **24**, 9855–9860.
- 390 F. Kim, K. Sohn, J. Wu and J. Huang, *J. Am. Chem. Soc.*, 2008, **130**,

- 14442–14443.
- 391 Y.-N. Wang, W.-T. Wei, C.-W. Yang and M. H. Huang, *Langmuir*, 2013.
- 392 J. Gao, X. Huang, H. Liu, F. Zan and J. Ren, *Langmuir*, 2012, **28**, 4464–4471.
- 393 S. R. K. Perala and S. Kumar, *Langmuir*, 2013, **29**, 9863–9873.
- 394 H.-J. Cho, M.-J. Jung, S. Woo, J. Kim, E.-S. Lee, Y. Kwon and Y. Na, *Bioorg. Med. Chem.*, 2010, **18**, 1010–1017.
- 395 M. T. G. and V. K. Vaidyan, *J. Cryst. Growth*, 1981, **53**, 300–304.
- 396 M. T. George and V. K. Vaidyan, *J. Appl. Electrochem.*, 1982, **12**, 359–367.
- 397 S. Roy, D. Chakravorty and S. Bansyopadhyay, *Solid State Commun.*, 1996, **99**, 835–838.
- 398 Y.-F. Tu, X.-H. Chao, J.-P. Sang, S.-Y. Huang and X.-W. Zou, *Phys. A Stat. Mech. its Appl.*, 2008, **387**, 4007–4014.
- 399 W. M. Haynes, *CRC Handbook of Chemistry and Physics*, 2014.
- 400 L. Guo and P. C. Searson, *Electrochim. Acta*, 2010, **55**, 4086–4091.
- 401 M. Paunovic and M. Schlesinger, *Fundamentals of Electrochemical Deposition*, 2006, vol. 5.
- 402 M. E. Hyde and R. G. Compton, *J. Electroanal. Chem.*, 2003, **549**, 1–12.
- 403 M. J. Hajipour, K. M. Fromm, A. Akbar Ashkarran, D. Jimenez de Aberasturi, I. R. de Larramendi, T. Rojo, V. Serpooshan, W. J. Parak and M. Mahmoudi, *Trends Biotechnol.*, 2012, **30**, 499–511.
- 404 S. Baron, Ed., *Medical Microbiology*, Univ of Texas Medical Branch, Galveston, 4th edn., 1996.
- 405 L. Brown, J. M. Wolf, R. Prados-Rosales and A. Casadevall, *Nat. Rev. Microbiol.*, 2015, **13**, 620–30.



- 406 K. N. Thakkar, S. S. Mhatre and R. Y. Parikh, *Nanomedicine Nanotechnology, Biol. Med.*, 2010, **6**, 257–262.
- 407 K. B. Narayanan and N. Sakthivel, *Adv. Colloid Interface Sci.*, 2010, **156**, 1–13.
- 408 Y. He, J. Yuan, F. Su, X. Xing and G. Shi, *J. Phys. Chem. B*, 2006, **110**, 17813–17818.
- 409 N. Pantidos and L. E. Horsfall, *J. Nanomed. Nanotechnol.*, 2014, **5**, 10.
- 410 V. Berry, S. Rangaswamy and R. F. Saraf, *Nano Lett.*, 2004, **4**, 939–942.
- 411 V. Berry, A. Gole, S. Kundu, C. J. Murphy and R. F. Saraf, *J. Am. Chem. Soc.*, 2005, **127**, 17600–17601.
- 412 S. C. Hayden, G. Zhao, K. Saha, R. L. Phillips, X. Li, O. R. Miranda, V. M. Rotello, M. A. El-Sayed, I. Schmidt-Krey and U. H. F. Bunz, *J. Am. Chem. Soc.*, 2012, **134**, 6920–3.
- 413 Z. V. Feng, I. L. Gunsolus, T. a. Qiu, K. R. Hurley, L. H. Nyberg, H. Frew, K. P. Johnson, A. M. Vartanian, L. M. Jacob, S. E. Lohse, M. D. Torelli, R. J. Hamers, C. J. Murphy and C. L. Haynes, *Chem. Sci.*, 2015, **6**, 5186–5196.
- 414 B. Klajnert and M. Bryszewska, *Acta Biochim. Pol.*, 2001, **48**, 199–208.
- 415 G. Navarro and C. Tros de Ilarduya, *Nanomedicine*, 2009, **5**, 287–97.
- 416 D. V. Leff, L. Brandt and J. R. Heath, *Langmuir*, 1996, **12**, 4723–4730.
- 417 D. V. Leff, P. C. Ohara, J. R. Heath and W. M. Gelbart, *J. Phys. Chem.*, 1995, **99**, 7036–7041.
- 418 S. R. K. Perala and S. Kumar, *Langmuir*, 2013, **29**, 14756–62.

- 419 S. Connolly, S. N. Rao and D. Fitzmaurice, *J. Phys. Chem. B*, 2000, **104**, 4765–4776.
- 420 V. Chechik and R. M. Crooks, *Langmuir*, 1999, 6364–6369.
- 421 K. H. Jacobson, I. L. Gunsolus, T. R. Kuech, J. M. Troiano, E. S. Melby, S. E. Lohse, D. Hu, W. B. Chrisler, C. J. Murphy, G. Orr, F. M. Geiger, C. L. Haynes and J. A. Pedersen, *Environ. Sci. Technol.*, 2015, **49**, 10642–10650.
- 422 J. S. Mclean, G. Wanger, Y. a. Gorby, M. Wainstein, J. Mcquaid, S. I. Ishii, O. Bretschger, H. Beyenal and K. H. Nealson, *Environ. Sci. Technol.*, 2010, **44**, 2721–2727.
- 423 M. a. Maurer-Jones, I. L. Gunsolus, B. M. Meyer, C. J. Christenson and C. L. Haynes, *Anal. Chem.*, 2013, **85**, 5810–5818.
- 424 T. L. Daulton, B. J. Little, K. Lowe and J. Jones-Meehan, *J. Microbiol. Methods*, 2002, **50**, 39–54.